Flame Aegis: An Urban Firefighting UAV

Final Report

AE3200: Design Synthesis Exercise

Group 05

Delft University of Technology

TU Delft

Flame Aegis: An Urban Firefighting UAV

Final Report

by

DSE Group 05

Student Name	Student Number
Andres Rafael Garaiman	5685443
Eduard Teodor Iacob	5742781
Ștefan Ion	5738547
Hugo Madrid Gutierrez	5740703
Arun Osman	5801117
Alexandra Pereira Matias Teles Teixeira	5753198
Radu Ioan Pop	5716527
Gijs Reurekas	5782155
Vlad Mihail Stoica	5734142
Laura Cristina Tanasiciuc	5677807

Supervisors:	Dr. Daniele Ragni and Brian Püroja
Coaches:	Tom Konijn and Abdelrahman Elshaer
Faculty:	Faculty of Aerospace Engineering, Delft
Date:	June 24, 2025

Executive Overview

Given the scarcity of available space for building in the Netherlands, more and more high-rise buildings are being built across the country. However, traditional firefighting methods like aerial fire trucks have difficulties reaching the higher floors of these buildings, especially in busy, urban environments. This is why Gezamenlijke Brandweer is looking for an innovative solution to deal with these high-rise fires.

The aim of this report is to present a firefighting UAV capable of tackling these challenges. The Flame Aegis drone will be an untethered UAV, carrying at least 40 liters of water, spraying it at a distance of at least 6 meters at a flow rate of at least 150 L/min. Furthermore, the drone will feature a water-release system and will be foldable for easy transport to the scene inside a VW Crafter.

The most important findings of this report are summarized in this Executive Overview. This is structured in sections, which correspond to individual chapters. However, not all chapters are present. More specifically, only Chapters 4–11 are summarized, as they capture the core design decisions. The remaining chapters address broader topics like risk, sustainability, or project management and are therefore not repeated here, as they do not directly affect the technical configuration of the UAV.

Conceptual Design Review

Chapter 4 tackles the first key design decision: the overall UAV configuration. After constructing a design option tree and performing a trade-off analysis, the X8 coaxial octocopter configuration is selected. This provides the best performance-to-weight ratio while accounting for redundancy and folding capabilities.

Operations and Mission Logistics

In Chapter 5, logistical concepts, the flow of the firefighting mission, as well as a typical sortie of the UAV, are detailed. These are aspects that not only help in the preliminary sizing of certain subsystems but also drive the design towards the client's needs.

In addition, relevant simulations for determining the drag coefficient of the UAV during the mission were performed, using SimScale, an online CFD software using OpenFOAM in the backend. A simplified model of the drone was considered, yielding a 0.62 preliminary drag coefficient. This was used as an upper limit consideration for the actual design of the UAV.

Furthermore, the temperatures experienced by the UAV were estimated, considering 2 cases: spraying the water through a window and on a roof. Considering an operational limit of 50 ° C, a distance of 3.5 m is needed from the window, while for the roof fire, a 3 m height and 4.3 m horizontal distance are required.

Propulsion Subsystem

Chapter 6 starts with defining the thrust-to-weight ratios used for sizing the propulsion subsystem. The final values were chosen as 2.1 for the peak thrust-to-weight ratio, while the average thrust-to-weight ratio is 1.15. Using these values, the 3 main components of the propulsion subsystem can be selected: the motors, the electronic speed controllers, and the propellers.

Starting with the motors, eight brushless, low KV motors, providing an individual thrust of 40kg and a total thrust of 320 kg, were chosen. In an X8 configuration, the rotation of diagonally placed motors matches, whereas the rotation of coaxial motors is opposite for torque cancellation purposes. Next, for the electronic speed controllers, eight 32-bit ESCs were selected, offering better cooling and redundancy. Finally, the propellers were chosen as having a fixed pitch, being foldable, and made out of CFRP. Furthermore, they have two blades for lower drag and blade interference.

Power Subsystem

In Chapter 7, a detailed trade-off analysis leads to the selection of solid-state batteries with NMC cathodes and silicon anodes, chosen for their energy density, safety, and cycle life. A hybrid configuration (2S4P) was implemented to meet both peak power and endurance demands. The total energy storage capacity is 9.34 kWh, complying with the estimated mission need of 8.31 kWh, accounting for a 90% depth of discharge.

Two types of Power Distribution Boards (PDBs) are used to supply power at high and low voltages, ensuring compatibility with both propulsion and control subsystems. The selected batteries allow for full recharge in 30 minutes and can be removed and replaced without shutting down the system within 60 seconds.

Control Subsystem

In Chapter 8, the control subsystem is detailed from a hardware perspective, by selecting off-the-shelf components, as well as from a software perspective, analyzing the functions that need to be accomplished by the UAV.

Hardware benefits from redundancy on multiple levels (4 IMUs, 2 microcontrollers, 2 power connections of the FMU) with a modular design and military-grade components included in the form of the flight controller. Special for the design is an array of 9 RADAR sensors that prevent any collision: 8 sensors point horizontally, covering 344 out of 360°, with the 9th working in radio-altimeter mode. The drone was found to be controllable with any one engine inoperative and in some cases with 2 or more engines inoperative.

Payload Subsystem

Chapter 9 outlines the design of the payload subsystem, which features the firefighting capabilities of the UAV. The heart of this subsystem is a 54.6-liter HDPE water tank, chosen for its low weight, durability, and corrosion resistance. The tank is designed with a circular 'mushroom' shape to optimize the volume within the dimensional constraints set by EU regulations.

Two centrifugal pumps were selected, each capable of delivering 75 L/min at 5 psi, allowing for an overall flow rate of 150 L/min. These pumps are mounted directly beneath the tank in a parallel configuration, allowing for independent operation and avoiding flow interference. Each pump connects to a 70 cm aluminium pipe, which contains a nozzle at the end. This nozzle is conically contracting, tapering from 3.8 cm to 1.4 cm at a 10° angle, designed through iterative analysis to achieve an effective reach of 7.15 m, measured from the pump.

Another important part of this subsystem is the water release system, featuring a hinged door at the bottom of the tank, held closed by a solenoid door lock through a preloaded spring. A rubber gasket is installed between the tank and the door, making sure no leakage is present. Finally, the camera gimble contains both a visual and thermal camera, while the visual and acoustic signaling includes 4 lights, one for each arm, and 4 buzzers, delivering up to 80 dB.

Structure Subsystem

Chapter 10 presents the structural configuration of the UAV, developed for strength, modularity, and minimal weight. A combination of carbon fiber reinforced polymer (CFRP) and aluminum alloys 7075-T6 and 6063-T6 is employed, each selected for specific mechanical and operational requirements.

The primary load-bearing elements, including the top and bottom plates and the foldable arms, are constructed from aluminium and CFRP, respectively. Additionally, the landing legs are also made from CFRP. This material offers an exceptional stiffness-to-weight ratio, thermal stability, and fatigue resistance, which is critical to support propulsion loads and maintain structural integrity during flight.

Secondary structural components are made from aluminum 6063-T6 and 7075-T6 alloys known for their excellent strength, corrosion resistance, and manufacturability. It is used for structural brackets,

mounting reinforcements, and plates. These aluminum parts are designed to handle localized mechanical loads, support payload integration, and absorb ground impact forces during landing.

Subsystem Integration and Review

Chapter 11 confirms the compatibility of the UAV's major subsystems, ensuring the design choices integrate into an operationally viable product. A detailed N2 diagram highlights key interdependencies, particularly between Payload–Structure, Payload–Power, Propulsion–Structure, and Propulsion–Power.

Final engineering budgets are consolidated, with a total system mass of 107.1 kg (excluding water), leaving an allowance of approximately 42.9 kg under the 150 kg MTOW limit. To remain compliant with regulations while fulfilling firefighting needs, the water payload was adjusted to 40 L following stakeholder discussions. Cost and power consumption remain well within the project's constraints, confirming the feasibility of the configuration. The full budgets can be seen in Table 1:

Table 1: Final Engineering Budgets

Subsystem	**Mass [kg]**	**Cost [€]**	**Power Required [W]**
Propulsion	29.36	9727.20	68000.00
Power	29.89	18876.64	-
Control	9.88	7592.75	40.00
Payload	10.14	2004.56	320.72
Structure	27.83	700.00	-
Total	**107.1**	**38901.15**	**68360.71**

Furthermore, a design sensitivity analysis is performed to evaluate the impact of alternative configurations such as fewer, larger motors; a fully aluminum frame; reduced thrust-to-weight ratio; and increased arm length. While some alternatives showed potential gains in cost or endurance, they often compromised safety, structural simplicity, or redundancy, reinforcing the current design as the most balanced and regulation-compliant choice.

The final UAV layout can be seen in Figure 1 and 2, in both the unfolded and folded cases. As can be seen in these figures, the dimensions are within the EU regulations, while the folded configuration allows the transport of the UAV in a VW Crafter. Note that the nozzles are included in the same position in the folded view to avoid a possible tip-over.

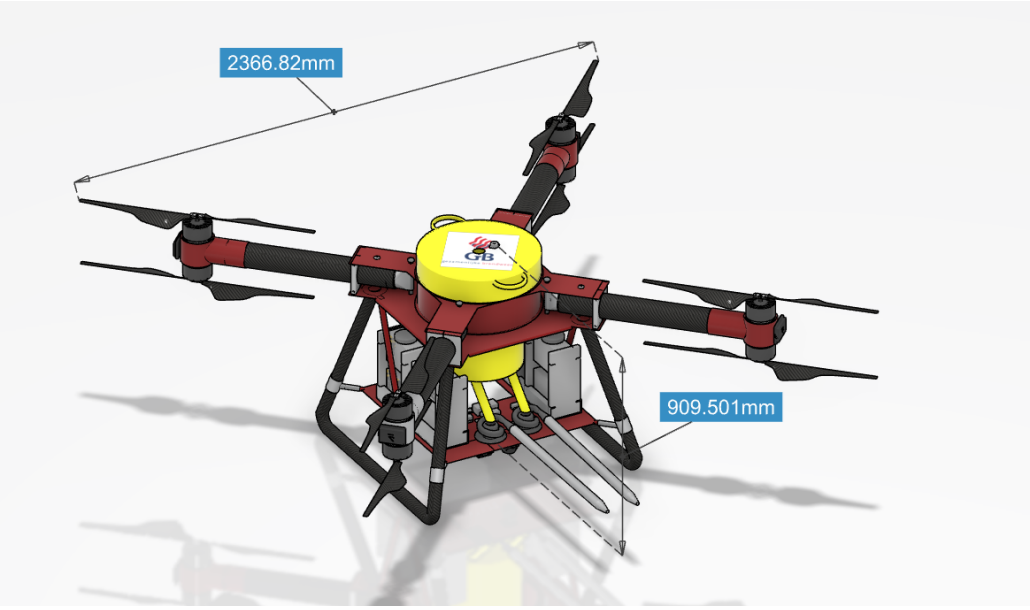

Figure 1: UAV Layout – Unfolded Configuration

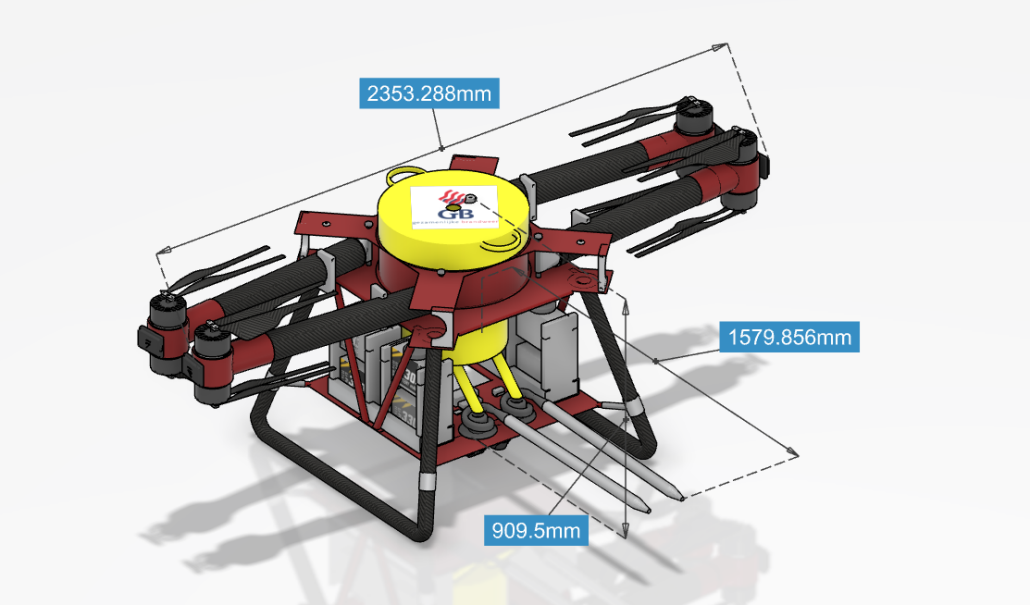

Figure 2: UAV Layout – Folded Configuration

Contents

1. Introduction

In recent years, the number of tall residential buildings in the Netherlands has been steadily increasing, as part of the country's efforts to provide more housing in cities where space is limited [1]. However, this also creates new challenges for the Dutch Fire Brigade. Fires in high-rise buildings are more difficult to reach and dangerous to fight. Fire trucks can only reach up to 30 meters, which is often not enough. Additionally, modern building features, such as solar panels on roofs and large batteries installed inside apartments, introduce new risks. These can make fires harder to control and more dangerous to reach for firefighters.

Currently, drones used in firefighting are often tethered to the ground or not allowed to fly under European regulations. Many of them cannot carry enough water or reach the necessary height. To address this problem, the Gezamenlijke Brandweer (Dutch Fire Brigade) has requested the design of a firefighting drone that can operate untethered at high altitudes, carry at least 50 liters of water, and spray it at a rate of 150 liters per minute. The drone must also be easy to transport, quick to deploy, and able to perform maneuvers in windy conditions.

This report presents the final design of such a drone, named Flame Aegis, developed during a 10-week Design Synthesis Exercise (DSE) by a team of ten Aerospace Engineering students at TU Delft. The project builds on previous reports, which explored mission needs, performed trade-off studies, and defined a preliminary concept. The final design is based on an X8 coaxial octocopter configuration, chosen for its strong lifting capacity, safety, and compact size. The drone is untethered, fully electric, and can be deployed quickly from a fire brigade van to assist in emergencies.

The report is organized as follows. The system requirements and functional decomposition of the UAV are described in Chapter 2. A detailed analysis of the market and involved stakeholders is given in Chapter 3. The trade-off study and concept selection process are explained in Chapter 4. The operational mission profile is presented in Chapter 5. The propulsion and power subsystems are detailed in Chapter 6 and Chapter 7, respectively. The control subsystem development is covered in Chapter 8, followed by the payload subsystem in Chapter 9, and the structural design in Chapter 10.

Subsystem integration and interface management are addressed in Chapter 11, while risk assessment and mitigation strategies are presented in Chapter 12. The production plan is showcased in Chapter 13. Sustainability considerations are described in Chapter 14, and the UAV's RAMS (Reliability, Availability, Maintainability, and Safety) characteristics are detailed in Chapter 15. Verification and validation procedures are included in Chapter 16, along with a requirement compliance check in Chapter 17. The cost breakdown structure is shown in Chapter 18, and the design logic of the project is concluded in Chapter 19. In the end, the conclusions and recommendations are formulated in Chapter 20.

[1] https://www.ad.nl/wonen/wonen-op-grote-hoogte-groeispurt-wolkenkrabbers-in-nederland~a5e41543/ [Date Accessed: 24/06/2025]

2. System Requirements and Functional Analysis

2.1. Subsystem Definitions

In order to make the requirement analysis and functional decomposition more relevant, the UAV system was split into several subsystems. These subsystems are:

- **Power**: This subsystem includes any batteries as well as the main power distribution components, such as power distribution boards;
- **Propulsion and Aerodynamic Performance**: It includes the motors themselves and any other propulsive mechanisms or aerodynamic components;
- **Payload**: The fire retardant tank, along with any related sub-components such as the pumping system and water dispensing mechanisms, forms this subsystem. The rest is represented by the camera array(s) and the signaling system, which includes lights and buzzers;
- **Control**: It includes an autopilot module, antennas, sensors for the inertial reference system (GPS, accelerometer, gyroscope, barometer, magnetometer), a ground controller + receiver for ground input, collision avoidance sensors;
- **Structure**: It represents the structure of the UAV: the main body, the engine covers or arms, shielding, harnessing, or any other structural components, along with the interfaces between them or between the structure and other subsystems.

2.2. Functional Decomposition

As a prerequisite to the analysis of requirements, it is necessary to establish what the product will do during its lifetime. For this, a Functional Breakdown Structure (FBS) and a Functional Flow Diagram (FFD) were created.

The FBS is an "AND" tree, meaning that each parent function is the sum of its children. The functions are, at the highest level, split based on the lifetime phases of the drone. Each function was assigned a unique identifier, and the lowest-level functions in each branch were attributed to one of the subsystems of the drone. The FBS can be visualized on the following page.

While the FBS is useful for discovering functions of the drone and its subsystems, it does not show any temporal relation between the functions. Therefore, the FFD was created to complement it. The same functions that appear in the FBS are used for the FFD, while the flow of functions is indicated by solid arrows pointing from one function to another. This flow can also include conditional statements, such as "AND" or "OR" statements. Moreover, dashed arrows are used to reference higher-level functions when the flow transitions to a lower level. The FFD follows right after the FBS.

Functional Breakdown Structure

Development & Production

- Manufacture Drone **F.1**
  - Order Necessary Materials **F.1.1 | S&M**
  - Acquire Necessary Equipment **F.1.2 | S&M**
  - Follow Production Plan **F.1.3**
    - Analyze Sketches **F.1.3.1 | S&M**
    - Turn Raw Materials into Parts **F.1.3.2 | S&M**
    - Combine Parts into Assemblies **F.1.3.3 | S&M**
    - Assemble Final Product **F.1.3.4 | S&M**
- Certify Drone **F.2**
  - Perform Development Tests **F.2.1**
    - Perform Individual Subsystem Tests **F.2.1.1 | -**
    - Perform Subsystem Integration Tests **F.2.1.2 | -**
  - Perform Qualification Tests **F.2.2**
  - Perform Acceptance Tests **F.2.3**
  - Assess Sustainability Impact **F.2.4**
  - Validate Product **F.2.5**

Operational Phase

- Deploy **F.3**
  - Transport **F.3.1**
    - Transport Drone **F.3.1.1**
      - Load/Unload from Van Bed **F.3.1.1.1 | S&M**
      - Harness the Drone **F.3.1.1.2 | S&M**
    - Transport Support Equipment **F.3.1.2 | C&O**
  - Start Up **F.3.2**
    - Turn On Systems **F.3.2.1**
      - Connect Battery Power **F.3.2.1.1 | ELP**
      - Turn on Electronics **F.3.2.1.2 | ELP**
    - Initialize Systems **F.3.2.2**
      - Calibrate Instruments **F.3.2.2.1 | P&L**
      - Perform Self-Tests **F.3.2.2.2 | ELP**
      - Activate Acoustic and Visual Signals **F.3.2.2.3 | P&L**
- Maintain Drone **F.5**
  - Maintain Software **F.5.1**
    - Update Software **F.5.1.1 | C&O**
    - Clear memory **F.5.1.2 | C&O**
  - Maintain Hardware **F.5.2**
    - Replace Parts **F.5.2.1 | S&M**
    - Service Parts **F.5.2.2 | S&M**

- Perform Mission **F.4**
  - Fly **F.4.1**
    - Take-Off **F.4.1.1**
      - Power Up **F.4.1.1.1 | ELP**
      - Determine Lift Force **F.4.1.1.2**
        - Sense Altitude Change **F.4.1.1.2.1 | C&O**
        - Determine Weight **F.4.1.1.2.2 | C&O**
    - Maneuver **F.4.1.2**
      - Control Attitude **F.4.1.2.2**
        - Determine Desired Attitude **F.4.1.2.2.1 | C&O**
        - Measure Current Attitude **F.4.1.2.2.2 | C&O**
        - Compare Desired and Current Attitude **F.4.1.2.2.3 | C&O**
        - Compute Control Angles **F.4.1.2.2.4 | C&O**
      - Control Speed **F.4.1.2.3**
        - Determine Desired Speed **F.4.1.2.3.1 | C&O**
        - Measure Current Speed **F.4.1.2.3.2 | C&O**
        - Compare Desired and Current Speed **F.4.1.2.3.3 | C&O**
        - Compute Required Thrust **F.4.1.2.3.4 | C&O**
      - Control Altitude **F.4.1.2.4**
        - Determine Desired Altitude **F.4.1.2.4.1 | C&O**
        - Measure Current Altitude **F.4.1.2.4.2 | C&O**
        - Compare Desired and Current Altitude **F.4.1.2.4.3 | C&O**
        - Compute Required Lift **F.4.1.2.4.4 | C&O**
    - Stabilize **F.4.1.3**
      - Sense Motion **F.4.1.3.1**
        - Measure Current Attitude **F.4.1.3.1.1 | C&O**
        - Measure Angluar Rates **F.4.1.3.1.2 | C&O**
        - Identify Deviation From Reference Condition **F.6.1.3.1.3 | C&O**
      - Perform Stabilization **F.4.1.3.3**
        - Compute Stability Corrections **F.4.1.3.3.1 | C&O**
        - Prioritize Control Signals **F.4.1.3.3.2 | C&O**
    - Generate Control Forces **F.4.1.4**
      - Calculate Required Forces **F.4.1.4.1 | C&O**
      - Determine Current Forces **F.4.1.4.2 | C&O**
      - Compare Desired and Current Forces **F.4.1.4.3 | C&O**
      - Change Aerodynamic & Propulsive Forces **F.4.1.4.4 | A&P**
    - Land **F.4.1.5**
      - Detect Ground Contact **F.4.1.5.1 | C&O**
      - Power-Down **F.4.1.5.2**
        - Cut Propulsion **F.4.1.5.2.1 | A&P**
        - Cut Power **F.4.1.5.2.2 | ELP**
  - Supress Fire **F.4.2**
    - Detect Seat of the Fire **F.4.2.1**
      - Inspect Heat Sources **F.4.2.1.1 | P&L**
      - Determine Point with Maximum Heat Release Rate **F.4.2.1.2 | P&L**
      - Scout for Embers **F.4.2.1.3 | P&L**
    - Attack Fire **F.4.2.2**
      - Choose Adequate Attack Position **F.4.2.2.1 | C&O**
      - Fix Attack Attitude **F.4.2.2.2 | C&O**
      - Maintain Attack Attitude **F.4.2.2.3 | C&O**
      - Release Water **F.4.2.2.4 | P&L**
  - Perform Turnaround Routine **F.4.3**
    - Refill Water **F.4.3.1 | P&L**
    - Replenish Energy **F.4.3.2 | ELP**
    - Inspect for Damage **F.4.3.3**
  - Monitor Status **F.4.4**
    - Gather Telemetry Data **F.4.4.1**
      - Record Telemetry Parameters **F.4.4.1.1 | P&L**
      - Store Telemetry Data Onboard **F.4.4.1.2 | P&L**
      - Transmit Telemetry Data to Ground Segment **F.4.4.1.3 | P&L**
    - Check for Obstacles **F.4.4.2**
      - Scan Environment **F.4.4.2.1 | P&L**
      - Recognize Obstacles **F.4.4.2.2 | C&O**
    - Check for Faults **F.4.4.3**
      - Monitor Hardware Status **F.4.4.3.1 | C&O**
      - Monitor Software Status **F.4.4.3.2 | C&O**
    - Manage Faults **F.4.4.4**
      - Transmit Warning **F.4.4.4.1 | C&O**
      - Initiate Emergency Landing Procedures **F.4.4.4.2 | C&O**

End-of-Life Management

- Dispose at End-of-Life **F.6**
  - Dismantle Drone **F.6.1 | S&M**
  - Repurpose Components **F.6.2 | S&M**
  - Recycle Materials **F.6.3 | S&M**

Legend

- 1st Level Function **IDENTIFIER (ID)**
  - 2nd Level Function **ID | SUBSYSTEM**
    - 3rd Level Function **ID | SUBSYSTEM**
      - 4th Level Function **ID | SUBSYSTEM**
        - 5th Level Function **ID | SUBSYSTEM**

Subsystem Legend

ELP - Electrical Power
A&P - Aerodynamic Performance and Propulsion
P&L - Payload and Logistics
S&M - Structures and Materials
C&O - Control and Operations

Functional Flow Diagram

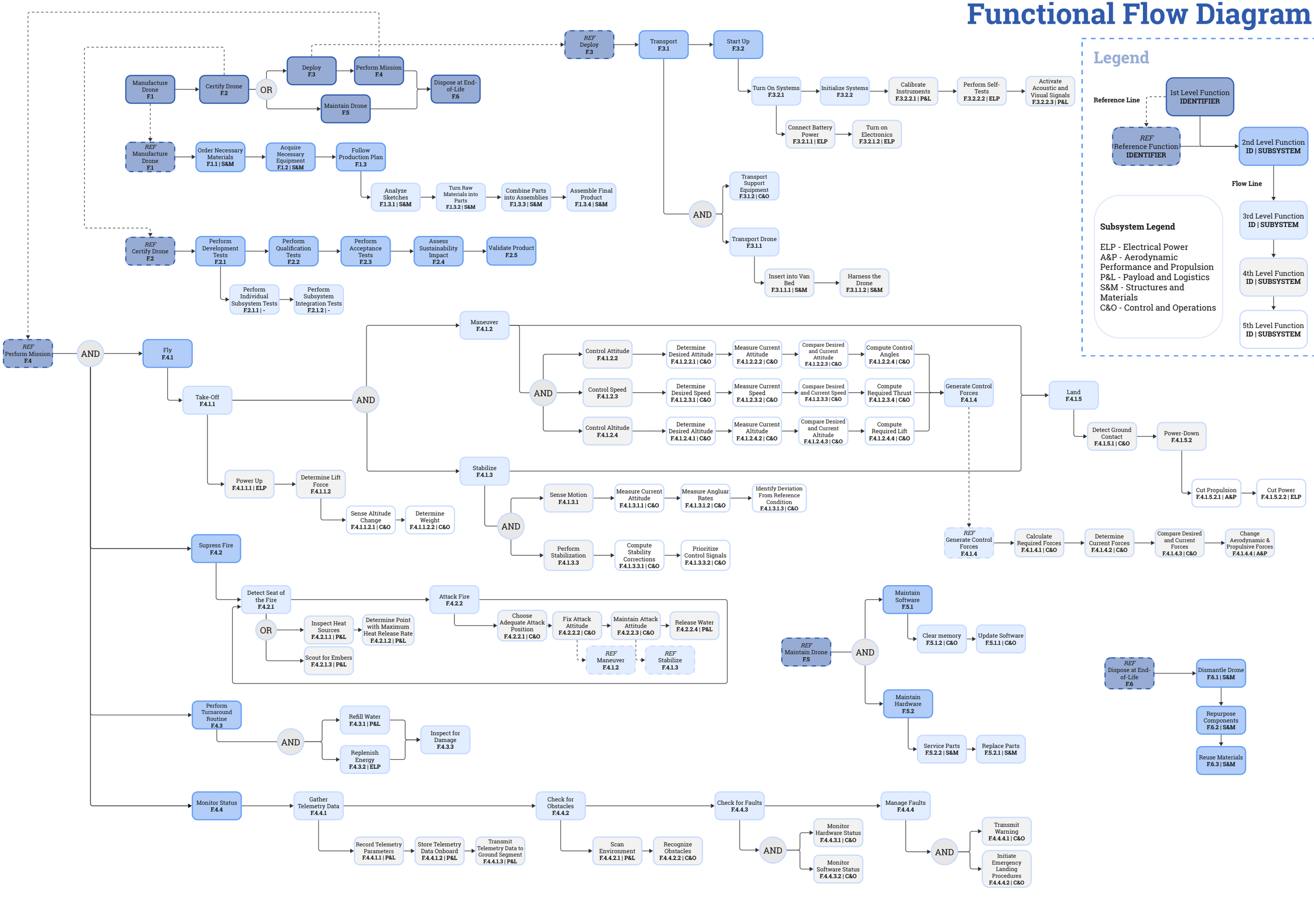

2.3. Requirement Analysis

A certain set of requirements was given to initiate this project. These requirements are divided into the technical part of the mission, specific subsystems, and the logistics, cost, safety, legal, and sustainability constraints that the mission has to follow. Further distinction is made by the split of stakeholders, mission, and system requirements. The system requirements are derived from the mission and stakeholder requirements. The stakeholders that influence the requirements are the Gezamenlijke Brandweer and the Dutch Government, responsible for establishing the regulations. In addition to the initially defined requirements, measures to mitigate risks and contingency plans lead to other requirements, as will be thoroughly explained in Chapter 12.

The stakeholder and mission requirements are given in Table 2.1, with the system requirements given in Table 2.2. These are categorized by their type: STK for stakeholder, MIS for mission, and SYS for system requirements. Then, to ensure that the requirement is descriptive enough, acronyms related to a specific subsystem are added: FF for firefighting, COM for guidance and communication, PROP for propulsion, CTRL for controllability, POW for power, STRUC for structures, LOG for logistics, COST for cost, SAF for safety, LEG for legal, SUS for sustainability, and RISK for risk-associated requirements. For the mission and stakeholder requirements, the requirement type is also defined, namely key, driving, and killer. Note the numbering convention: the requirements are numbered based on a requirement discovery tree in the baseline report preceding this document [1]. The other types of requirements are numbered based on the order they are presented in their respective section.

Table 2.1: Stakeholder and Mission Requirements

Requirement Code	Requirement	Requirement Type
REQ-STK-1.1.1	The extinguishing mechanism shall have a minimum flow rate of 150 L/min.	Key
REQ-STK-1.1.2	The minimum amount of water transported shall be 50 L.	Key
REQ-STK-1.3.1	The UAV shall be able to fly at least 70 m from the ground.	Key
REQ-STK-2.1.1	The UAV dimensions during transport shall not exceed 1.38 x 3.00 x 1.63 m (w/l/h).	Key
REQ-STK-2.4.1	The Maximum Take-Off Weight of the UAV shall be less than 150 kg.	Key
REQ-STK-2.4.2	The maximum span of the UAV when operating shall be 3.0 x 3.0 m.	Key
REQ-STK-2.5.1	The use of sustainable materials shall be maximized.	-
REQ-MIS-FF-1.1.3	The throw length of the water jet shall be at least 6 m.	Driving
REQ-MIS-CTRL-1.4.1	The UAV shall fly in windy conditions up to 6 bft.	Driving
REQ-MIS-POW-1.5.1	Hover endurance for one flight shall be at least 15 min.	Driving
REQ-MIS-LOG-2.1.4	The drone shall have a 5 min turnaround time.	Driving
REQ-MIS-SAF-2.3.3	The UAV shall have fault-tolerant control to land safely when one engine is inoperative.	Key
REQ-MIS-SAF-2.3.4	The UAV shall autonomously land at the nearest clearing if signal loss occurs.	Driving
REQ-MIS-SAF-2.3.1	The UAV shall have a redundant collision avoidance system operable in smoke and high temperatures.	Driving
REQ-MIS-SAF-2.3.2	The UAV shall be equipped with visual and acoustic signals.	Key
REQ-MIS-COM-1.2.1	The UAV shall carry at least one thermal camera and 1 visual light camera.	Key
REQ-MIS-SUS-2.5.2	The UAV shall operate using battery power.	Driving
REQ-MIS-FF-1.1.4	The payload mechanism shall be able to drop water while hovering above the target area.	Driving
REQ-MIS-COST-2.2.1	The cost of a single vehicle shall not exceed 75,000 EUR.	Key

Table 2.2: System Requirements

Requirement Code	Requirement	Requirement Type
REQ-SYS-COM-1.2.2	The delay between control command and drone movement shall be less than 200 ms.	-
REQ-SYS-PROP-1.3.2	The drone shall produce a thrust in excess of 30.9 kN.	-
REQ-SYS-PROP-1.3.3	The drone shall have a climb rate of at least 1 m/s.	-
REQ-SYS-CTRL-1.4.2	The drone shall be able to adjust to weight loss.	-
REQ-SYS-POW-1.5.2	The drone shall have an energy storage of at least 9.23 kWh.	-
REQ-SYS-STRUC-1.6.1	The drone structure shall withstand temperatures of at least 50 $°C$.	-
REQ-SYS-STRUC-1.6.2	The drone structure shall carry the propulsive forces of the motors.	-
REQ-SYS-LOG-2.1.2	The onboard computer of the UAV shall log and store flight data.	-
REQ-SYS-LOG-2.1.3	The deployment of the drone shall take less than 10 minutes.	-
REQ-SYS-LOG-2.1.5	The battery recharge time shall be maximum 30 minutes.	-
REQ-SYS-LOG-2.1.6	The UAV system shall be operated by fewer than 3 people.	-
REQ-SYS-SAFE-2.3.5	The UAV shall detect battery overheating and notify the operator in that case.	-
REQ-SYS-LEG-2.4.4	The drone shall not reach an altitude above 120 m. [1]	-
REQ-SYS-LEG-2.4.5	The drone shall stay within the line of sight of the operator. [1]	-
REQ-SYS-LEG-2.4.6	The UAV shall be at a maximum distance from the operator of 500 [m]. [1]	-
REQ-SYS-SUS-2.5.3	At EOL, the UAV shall have a high degree of recyclability.	-

[1] `https://wetten.overheid.nl/BWBR0036568/2017-10-07` [Date Accessed: 01/05/2025]

3. Market Analysis

High-rise fires present significant risks due to the rapid spread of flames, with fire size doubling approximately every 30 seconds [2]. This is why a quick intervention with a firefighting UAV is crucial to provide a knock-down effect on the fire. Furthermore, traditional firefighting methods face notable limitations in combating fires above certain elevations. While the highest turntable ladder for firefighting in the world can reach up to 68 meters [1], comparable vehicles in the Netherlands are limited to a maximum operational height of 32 meters [2].

Most of the existing UAV solutions rely on tethered hoses connected to ground-based water sources, significantly restricting their mobility and operational flexibility [3]. In the context of high-rise fires, where speed, agility, and access to elevated fire zones are critical, such tethered systems impose severe limitations.

This market analysis evaluates these challenges and explores the opportunity for developing a UAV capable of carrying its own water payload. This concept was developed in direct consultation with the Gezamenlijke Brandweer in the Netherlands, through stakeholder/customer meetings, specifically to address their operational needs and to enhance firefighting capabilities for buildings beyond the reach of conventional ground-based equipment.

3.1. Stakeholder Analysis

The first step of the market analysis is identifying and analyzing all the stakeholders involved. This is done by constructing Table 3.1, which indicates the interest and influence of each stakeholder.

Table 3.1: Stakeholder Interest-Influence Analysis

Stakeholder	**Interest**	**Influence**
Dutch Fire Brigade (Gezamenlijke Brandweer)	High	High
Operation Team	High	High
Maintenance Providers	High	High
UAV Operators	High	Low
Local Communities, Civilians	High	Low
Manufacturers (Suppliers)	Low	High
Dutch Government	Low	High
EU Regulatory Body (EASA, IL&T)	Low	High
Humanity	Low	Low
Other Emergency Services (Ambulances)	Low	Low
Asian Market (Competitors)	Low	Low

To improve visualization, the stakeholders can be plotted into an interest-influence graph. At the top right, the stakeholders with the highest interest and influence are displayed.

[1] `https://www.magirusgroup.com/de/en/products/turntable-ladders/m68l/` [Date Accessed: 28/04/2025]

[2] `https://www.gabijdebrandweer.nl/hoogtevreestest/` [Date Accessed: 28/04/2025]

[3] https://www.topskyeqpt.com/lt-uavfw-hose-mooring-type-fire-extinguishing-uav-product/ [Date Accessed: 28/04/2025]

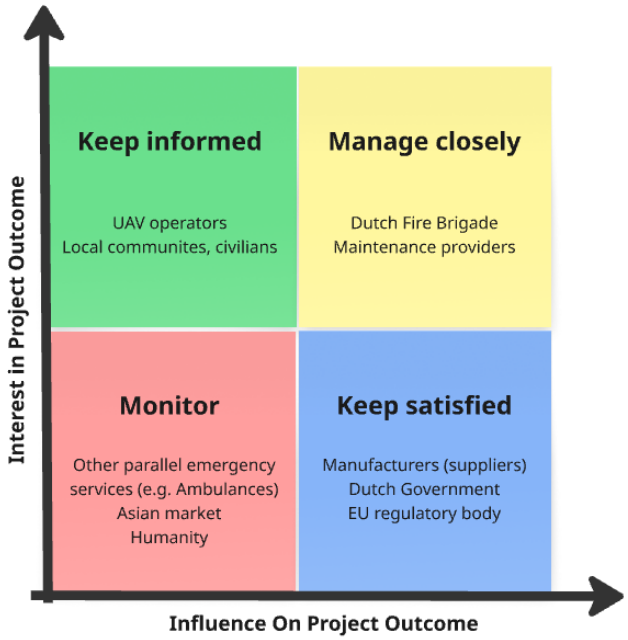

Figure 3.1: Interest-influence Graph for Stakeholders

From Figure 3.1, the key stakeholders can be identified. These are the stakeholders that have the highest interest in the project as well as the highest influence. For this project, the key stakeholders would therefore be:

- Project Owner: Gezamenlijke Brandweer (Dutch Fire Brigade)
- Maintenance Team

The project owner is a key stakeholder since they can directly influence how the project develops through the user requirements. The project owner is the Dutch Fire Brigade, which will change the batteries and refill the tanks when on site. Moreover, their interest level is very high since they requested the project. The maintenance team is needed to ensure that the team is always on standby. They will provide hardware and software maintenance such as part inspections, replacing damaged parts, and running software diagnostics and updates.

The stakeholders that need to be kept satisfied are the manufacturers and the regulatory bodies. Manufacturers must be consulted to ensure that the UAV can be produced using available technologies. Furthermore, the Dutch Government and the EU regulatory body will limit the design flexibility through regulations, but this is not specific to this project, but rather applied to all UAVs. Hence, regulations like weight constraints or size can steer the project.

In addition, there are stakeholders that have a high level of interest in the project but little influence on it, and these would only have to be informed. For example, the UAV operators have a high level of interest since they will be the ones who are flying the drone, so any problems will affect them directly and the success of their given mission. On the other hand, they have little influence since they are most likely external operators. The local communities will also be kept informed, but they have no decision-making power.

The last type of stakeholders is the ones that need to be monitored. These have no interest/influence on the project, but might provide innovative ideas. This group includes other emergency services, the Asian market, and humanity as a whole.

3.2. Market Overview

The market overview identifies the main competitors, as well as the market gaps and the potential of creating a new design.

Existing Solutions

The current market for firefighting drones can be categorized into four primary groups. Ground-tethered drones, such as the LT-UAVFW [4], which utilize hoses connected to ground water or electricity supplies. These systems are heavy, limited in mobility, and constrained by hose length. Grenade systems offer lightweight solutions, though they are only capable of extinguishing small fires. Thermal and imaging drones, like the Skydio X10 [5], focus solely on situational awareness without active suppression capabilities. The last category includes the untethered options; however, they face complex logistical challenges and considerable regulatory problems, such as the EHang 216F, which has a length of 7.33 m [6]. The main competitor options are summarized in Table 3.2:

Table 3.2: Competitor Options Overview

Competitor	Description
LT-UAVFW (China) [4]	Tethered UAV, requiring a water hose from the fire truck during operations, but EU-compliant: MTOW of 120 kg and within the 3 x 3 m limits.
EHang 216F (China) [6]	Autonomous drone, 150 L foam payload, significant size (length of 7.33 m), faces considerable regulatory challenges in Europe.
F50-LS (EagleFly) [7]	Carries substantial payload (14 tons/hour, 780 L/min), highly powerful but not agile, connected to a hose.

Unfortunately, no cost analysis could be performed due to data unavailability, as all the previously presented concepts do not have set purchase prices or are only at the conceptual stage.

Market Gaps

The market analysis reveals several gaps. Current drone solutions experience limited mobility because they are primarily attached to the ground. In addition, they either have insufficient flow rates (>150 L/min) or are not EU compliant (MTOW >150 kg or a length larger than 3 m). Therefore, an untethered drone that can carry heavy payloads with fire-suppressing capabilities and an adequate flow rate is currently not on the market.

3.3. Competitiveness and SWOT Analysis

To determine the position in the market of the design created, a SWOT analysis was performed. By doing so, the competitiveness of the design created can be identified.

Strengths:

- **Follows regulations and relatively small during transport:** Compliance with EU regulations (≤ 150 kg, 3.00 x 3.00 m in operation) could rapidly establish market dominance in Europe. Since drones from China do not comply with these. It is relatively small during transport (1.38 x 3.00 x 1.63 m), so it fits inside a Volkswagen Crafter.
- **Quick Deployment:** Easily deployed from standard fire brigade vehicles since the drone is mission-ready once deployed, unlike some other design alternatives. This means that the drone is untethered, it has removable batteries, and can achieve a turnaround time under 5 minutes, including water refilling.
- **Advanced Stability and Control:** Improved stability systems (gyroscopic stabilization, advanced autopilot) to handle increased payload and bad weather. The UAV is also able to land autonomously in case of signal loss.

[4] `https://www.topskyeqpt.com/lt-uavfw-hose-mooring-type-fire-extinguishing-uav-product/` [Date Accessed: 28/04/2025]

[5] `https://www.skydio.com/x10` [Date Accessed: 28/04/2025]

[6] `https://www.ehang.com/ehang216f/` [Date Accessed: 28/04/2025]

- **Flexible Payload:** Future adaptability to multiple extinguishing agents (foam, chemical powder) could greatly expand market appeal.
- **High Water Pressure:** Most drones found on the market have large water tanks for agricultural purposes, so the water flow rate and distance they can reach are much lower. A lower flow rate would decrease the effectiveness in suppressing the fire, which is critical for the mission type [8].

Weaknesses:

- **Limited Water:** Carrying a tank of water means no constant water source, which is not optimal for longer missions, as it will imply a shorter mission time. The payload is, therefore, also limited.
- **Short battery life:** Since the system is power-intensive, the batteries have to be replaced more often, increasing the downtime.
- **Wind limitations:** If the wind conditions exceed 6 bft, the drone will not be able to operate safely. Therefore, if the wind is too strong, the mission shall be canceled.

Opportunities:

- **Large budgets:** The Dutch government is the third most spending country in the EU for firefighting per inhabitant, so the budget is quite large, allowing for innovation [9].
- **Expanding market:** Increase in high-rise buildings creates growing demand for such UAV solutions since they are hard for firemen to reach (in time).
- **Future changes:** In the near future, there is a potential relaxation of UAV airspace regulations, which could mean a larger market and therefore an increased demand.
- **Few legal drones:** For Europe, few UAVs are legally operable and therefore this UAV would fill that spot.
- **New markets:** Nearby countries could adopt this drone, so there are many potential customers.

Threats:

- **Alternative fire suppressing methods:** Drone which can carry bombs filled with water-gel based extinguishing agent [10] or dry powder extinguishing agent [11] rather than a water tank and a nozzle. Since these might deliver more fire suppressant per weight, and with a less complex system.
- **Multiple purpose drones:** Modular drones [11] which can do similar actions but can also be used for other things like search and rescue or attaching a hose.

All in all, the UAV would be a competitive product, since there are no untethered options with a large water tank (> 50 L) and high water flow (> 150 L/min), while adhering to EU regulations (MTOW < 150 kg and dimensions < 3.00 x 3.00 [m] in operation). Due to the user requirements, the drone must carry a large tank filled with water, so other alternative fire suppressing methods cannot be utilized freely. Moreover, the user requirements require the folded drone to fit within certain dimensions, so the drone is also limited in size. This is not a huge problem since the current regulations are similar, meaning the drone is still competitive in terms of capabilities relative to its size. Also, having a smaller drone would make it more portable, which could make it more competitive in the market.

From this analysis, the following requirements can be derived for the UAV design:

- **REQ-STK-MKT-1** The drone shall be untethered, operating without any physical ground connection.

[8] https://ag.dji.com/t50 [Date Accessed: 01/05/2025]

[9] https://ec.europa.eu/eurostat/web/products-eurostat-news/-/edn-20190504-1 [Date Accessed: 28/04/2025]

[10] https://spideruav.com/product/industrial-drone/h200-firefighting/ [Date Accessed: 28/04/2025]

[11] https://www.hongfeidrone.com/hzh-y50-delivery-drone-50-kg-payload-for-efficient-transportation-short-description-product/ [Date Accessed: 28/04/2025]

- **REQ-STK-MKT-2** The drone shall have a modular payload allowing changes depending on the situation.
- **REQ-STK-MKT-3** The UAV shall have a status display to indicate when a refill or battery replacement is required.
- **REQ-STK-MKT-4** The UAV shall run a self-diagnostic before beginning a mission.

3.4. Trade-off Analysis

Currently, the drone is quite competitive for this specific market, but some small changes can be made to make it more competitive. Its weaknesses have been mentioned previously, so these should be solved with minor changes.

Table 3.3: Improvement Ideas and Associated Cost

Improvement	Cost
Higher energy density batteries	Higher cost or increased weight
Larger water tank	Very large weight increase
Stronger pump	Higher cost and increased weight
Longer propellers	Small weight increase and slightly higher cost

From Table 3.3 it can be seen that some changes are simpler to fix than others. The batteries could be swapped with ones that have a higher energy density, for example, silicon anode batteries. This would mean that they would be lighter, but the cost of these would increase greatly. On the other hand, larger batteries could be used while keeping the same energy density; this would be cheaper, but the weight would increase, so further design changes would be required. Therefore, if there is a budget and thrust margin, this change could be implemented. By doing so, the mission endurance would increase, decreasing the total downtime. Moreover, this would mean that more power is available for the subsystems; therefore, more power could be used for power-requiring payload, like for example a stronger pump or a better set of cameras. Therefore, this would be a viable option if more budget were available.

Another option is using a larger water tank ($>$ 50 [L]). With such a change, more water could be carried by the drone, allowing it to increase its fire-suppressing capabilities. Moreover, this means increasing the payload weight, so if the payload is changed, it can now carry heavier ones. But to carry a larger payload, multiple design changes would be required. The design iterative process would have to be repeated for larger motors and possibly larger propellers, which would increase the total take-off weight. This, in turn, could mean that the drone no longer meets the regulations. Since these changes would no longer be minor, this option has been rejected, even though it could become more attractive for other customers.

The pumps could also be changed for stronger ones, since then the flow rate would increase. By increasing the flow rate, the UAV's fire suppression capabilities can also be improved, making it more attractive as a product. To upgrade the pumps, stronger ones would be required; this would mean more cost and more weight. Since this change wouldn't be extreme, stronger pumps could be an alteration made to the system to make it more competitive.

Longer propellers could also be used, assuming that these could be changed without having to change the dimensions of other subsystems, like the motors or the dimensions of the whole drone. Moreover, if, after the change, the drone does not follow the regulations, this change could not be made without further changes. Having larger propellers would provide more thrust provided which could lead to larger batteries but also a larger payload. Therefore, if this change could be implemented, it would have few negative implications, making it a viable option.

4. Conceptual Design Review

Prior to the detailed design, a preliminary design was first established in preceding reports [1, 3]. The search for the most suitable configuration was done by the consideration of all possible design options, after which an extensive trade-off analysis revealed the most promising concept.

4.1. Design Options

After considering various options, the functional analysis of the mission highlighted the feasibility of each. The three best candidates were found to be

- **Pentacopter** - A departure from traditional multi-copter UAV configurations. The design presents a primary rotor in the center of the aluminium body and four smaller rotors attached to the body through arms. As the drone is designed around the primary rotor, failure of this rotor will likely lead to a hard emergency landing, as the drone is expected to be unable to fly normally without its main rotor.
- **Hexa X** - Owing to its compromise between simplicity, lifting capability, and more compact size, the Hexa X configuration can more often be found on the market.
- **X8** - The X8 configuration, although rarer, can also be found on the drone market. It is part of the octocopter family, and it consists of the central body and four arms, where each arm has two motors in a coaxial configuration with two propellers spinning in opposite directions, providing a large amount of thrust and OEI redundancy. In comparison with the standard configuration octocopter, the overall design is simpler from a structural perspective, while more attention must be paid to the integration of the motors, to ensure that the effects of vibrations are minimized.

4.2. Trade-Off

To further proceed with the design, a trade-off was performed. The selected trade-off criteria are

- payload/weight ratio;
- fault tolerance (risk level);
- cost;
- thrust/weight ratio;
- operational efficiency;
- sustainability.

The reason for this selection is that they are derived directly from the main stakeholder needs to successfully perform the firefighting mission. The weight of each criterion is guided by the stakeholder requirements. The relative importance to the customer is defined for each stakeholder requirement on a 1-5 scale [4].

To assess the criteria weights as objectively as possible, Quality Function Deployment (QFD), introduced first in the Japanese car industry to help translate customer needs into requirements, will be used [5]. In this method, each trade-off criterion is assigned a correlation/coupling score on a 0-1-3-9 scale with the stakeholder requirements. The large difference between possible coupling scores is meant to showcase the most important consequences of direct relationships between what the customer wants and what was valued in the design options trade-off. The specific reasoning for these scores is explained in Table 4.2. The relative importance to the customer and the criteria scores were multiplied and then summed. The total of each criterion was divided by the total points so the criterion's weight (%) could be obtained [5]. The highest results are marked in green, while the lowest are marked red.

Table 4.1 presents the configuration trade-off between the Pentacopter, Hexa X, and X8, based on the previously defined criteria and their respective weights. Each criterion was evaluated on a scale from 1 to 3. For each criterion, green means good, yellow means acceptable, and red means poor. The total weighted score is compared to determine the selected design. The result of the presented trade-off shows that the best design to pursue for the mission needs is the X8.

Table 4.1: Configuration Trade-off

FIREFIGHTING UAV CONFIGURATION TRADE-OFF			
Design / Criteria	**Pentacopter**	**Hexa X**	**X8**
Payload/Weight Ratio (19.3%)	3 - Compact design, larger central rotor + 4 arms offers good structural efficiency. [6]	2 - 6 arms increase structural weight, no significant payload advantage. [7]	3 - Coaxial design provides higher thrust with fewer structural elements.
Fault Tolerance (24.6%)	1 - Main rotor failure is critical, very limited emergency recovery options.	3 - In case of OEI, 5 others with many degrees of freedom available (for example, opposite motor can be stopped).	2 - Coaxial rotors can compensate for thrust when losing the other, and the rest can reduce thrust level, but for torque considerations, this option can be more complicated. [8]
Cost (14.5%)	1 - Unconventional design and limited commercial availability, may incur higher development and maintenance costs. [6]	2 - Common in market, competitive pricing.	2 - Solutions using this configuration that would fit the budget exist on market [1].
Thrust/Weight Ratio (17.1%)	2 - Main larger rotor provides larger thrust while the 4 arms can be shorter, more compact.	2 - Feasible, many designs available on market.	3 - Has a large number of rotors and engines for a structure equivalent to a quad, with just 4 arms.
Operational Efficiency (14.5%)	2 - Compact but central rotor can complicate maintenance/refill.	1 - Many arms require folding and more handling time.	2 - Only 4 arms, easier ground handling, might require folding.
Sustainability (10.1%)	1 - Higher composite material usage for four arms plus reinforced central-rotor support increases embodied energy and complicates end-of-life recycling.	2 - Higher material use due to larger frame. [7]	3 - Good ratio of flight capabilities to amount of material used in manufacturing. [9]
Weighted Score (Total)	1.7	2.1	2.5

[1] `https://ag.dji.com/t50` [Date Accessed: 19/05/2025]

Table 4.2: Criteria Weights

Relative importance to customer	Stakeholder Requirements	Payload/weight ratio	Fault tolerance / Risk level	Cost	Thrust/weight ratio	Operational efficiency	Sustainability
3	**Transportability**	0: not related	1: transportability measures (like foldability) can introduce more failure points in operation	1: more space needed for transportation increases the cost	0: not related	9: direct coupling	3: fit as many products (drone + related equipment) as possible during transportation without using many resources
5	**Safety, minimum risk**	0: not related	9: direct couple	3: risks affecting the product's components lead to a higher cost for replacement	3: influences maneouvrability, safe flying	1: the faster the ground operations, the more prone to errors, introduces some risk	1: sustainability imposes protection of the environment
5	**Firefighting Performance**	9: mission aims to carry maximum payload possible	9: high danger mission environment makes fault tolerance critical for success	3: better performance implies higher cost to develop the product	9: determines speed of ascent/descent, agility, helps minimize turnaround	3: mission efficiency depends on the product's capabilities	1: sustainability can restrict options
2	**Cost-effectiveness**	3: carry maximum payload at minimum cost	3: contingency plans for risks increase the cost	9: direct coupling	3: more powerful motors are more expensive	3: higher efficiency implies higher costs	3: higher cost for a sustainable design
1	**Environmental impact**	1: high efficiency design in terms of payload capability uses resources more effectively	9: mission failure and UAV crash damage the environment	3: lower environmental impact might imply higher cost	0: not related	1: more efficient operations in terms of time could imply more resources needed	9: direct coupling
4	**Payload weight and total weight**	9: direct couple	1: might be harder to handle OEI situations if payload is high compared to the total mass	3: cost-effectiveness if more payload is carried	3: more thrust allows carrying more payload	3: more effective mission if more payload available	3: carrying more payload with less resources
Sum		88	112	66	78	66	40
Weights (%)		19.3	24.5	14.5	17.1	14.5	10.1

Trade-off Sensitivity Analysis

A sensitivity test has also been performed on the trade-off table. To perform this sensitivity analysis, the values assigned to the relative importance to the customer, the criteria weights, and the trade-off scores were slightly changed to assess whether the trade-off is properly conducted. The difference in the final score for the first and second winners of the trade-off was computed to asses whether the result differs significantly due to slight changes. A small difference in final score means that the second-best option might become the first-best option. Therefore, these cases had to be identified.

A complete sensitivity analysis was conducted to evaluate the robustness of the top two design choices, including the following key steps:

- Adjusting customer weightings by ±1 to test their impact on results;
- Removing trade-off criteria and redistributing weights — this caused larger shifts in scores but did not change the winning design, so these cases are excluded;
- Varying weights by a factor of 3 using the 0-1-3-9 scale — this still did not affect the outcome;
- Altering individual trade-off scores by ±1 on a 1–3 scale — this led to the smallest changes in weighted sums.

The smallest score difference between the top two options, the X8 and Hexa X, is 0.118, indicating both are closely matched and suitable. This aligns with their popularity in the market. The detailed trade-off helped identify the X8 as the best choice, and sensitivity analysis confirmed its validity, as small changes in the criteria did not affect the outcome.

4.3. Preliminary Design

Conceptual subsystem trade-offs have been performed after finalizing the X8 configuration. The winners of the subsystem trade-offs were merged into a preliminary UAV concept. However, as the approach to conceptual design in this project is bottom-up rather than top-down, compatibility between subsystems was a concern that must be addressed. Furthermore, the level of detail in the design was still low, but a first sizing process of the UAV provided useful insights.

The initial thrust requirement was set as 333 kg of lift, given a target weight of 150 kg. The coaxial interference, specific to the X8 configuration, was taken into account here. Market analysis showed that the increment in thrust between motors is significant. Choosing another motor for each small change of thrust required for a specific iteration is thus not a feasible process, so it was decided that the motor should be designed to fulfill the maximum thrust from the beginning of the design process.

The power and energy requirements followed directly after an initial estimation of the average power consumption. Solid-state batteries were found to be optimal. For the payload subsystem, only a water tank and pumps were considered, given their large dimensions and/or weight. While the water tank was to be custom-made, designed to optimize the weight while accommodating all other components of the UAV, the pump is an off-the-shelf product. The structure of the drone was simplified by considering only the loading in the arms. Hence, this will be the focus of the detailed design.

The mass budget of the preliminary design revealed that the structure has a very tight margin. Without new design iterations, the maximum take of weight of 150 kg will be exceeded. As a result, modifications to the conceptual design are introduced during the final phase to ensure feasibility.

5. Operations and Mission Logistics

The support logistics for the UAV's mission are important to discuss before going further with the design process, since they may determine required system characteristics that influence the design. These logistics are derived from the Functional Flow Diagram and the Functional Breakdown Structure of the UAV system, which describe its operations.

5.1. Logistic Concept Description

As a first step, the supporting logistic concepts can be described. They are split into four categories:

- Supporting Employees (SE): all the Gezamenlijke Brandweer Employees involved in the UAV's mission. They can either come into contact with the UAV directly or be decision-makers, determining its deployment and mission.
- Supporting Hardware (MH): all the equipment used to support the UAV's mission.
- Support Infrastructure (SI): support facilities during the UAV's operational life.
- Standard Procedures (SP): a set of pre-established procedures that the operators are required to follow during the UAV's operation.

The identified logistic concepts are laid out in the Logistic Concept Diagram, visible on the following page.

5.2. Logistic Process Flow

The Logistic Concept Diagram, while useful, does not illustrate the logistic flow. Therefore, a Logistic Process Flow Diagram was also constructed and can be seen on the following page as well. The diagram illustrates all the activities undertaken during the UAV's operational life, either directly related to the mission or for support/maintenance, and can be considered an extension of the Functional Flow Diagram of the UAV System. Note that each activity is linked to one/more logistic concept(s) through the identifiers defined in the list above.

In the Logistic Process Flow Diagram, each box represents a process. They are connected such that the temporal flow of these processes is illustrated. These processes are either in series or parallel. Moreover, under each process, the logistics concepts related to the process are enumerated, which provides the connection between the two Logistic Diagrams. The Standard Procedures, defined in the Logistic Concept Diagram, are highlighted in yellow.

5.3. UAV Sortie Profile

During the mission, the UAV will undergo multiple sorties to tackle the fire. For the sizing of the subsystems and design iterations, it is important to devise a standard sortie of the UAV and design for it. The customer requirements only establish the minimum endurance of the UAV. Aside from this, however, it must climb to the altitude at which the fire is located, maneuver, and descend back to the operator. Therefore, at this stage in the design, the following phases of a sortie were considered:

1. Take-off and climb to desired altitude;
2. Maneuver to the designated fire extinguishing spot;
3. Start fire suppression operations;
4. Maneuver to the deployment zone;
5. Descend and land.

Each of these phases is related to certain requirements, so they must be elaborated upon further. Owing to the fact that the UAV is expected to move from the deployment zone to the fire extinguishing spot roughly along the same course, as well as ascend in descend in the same manner, these phases can be combined when discussed.

Logistic Concept Diagram

Gezamenlijke Brandweer Employees

- SE-1 Emergency Dispatch
- SE-3 Ground Operator (Pilot)
- SE-2 Group Coordinator
- SE-4 Turn-around Crew / Mechanic

Mission Hardware Components

- MH-1 Fire Engine
- MH-2 VW Crafter Van
- MH-3 Van (Un)Loading System
- MH-4 UAV
- MH-5 Camera and Telemetry Tablet
- MH-6 RC Controller
- MH-7 Spare batteries + Charger
- MH-8 Separate C-Hose Branch
- MH-9 Ground Water Pump (Lower Pressure)
- MH-10 Ground Water Tank

Standard Procedures

- SP-1 Periodic Maintenance Schedule
- SP-3 Turnaround Procedure
- SP-2 Pre-Flight Check
- SP-4 Post-Mission Maintenance Procedure

Support Infrastructure

- SI-1 Charging and Storage Station
- SI-3 Service Station
- SI-2 Flight Data Log Server

Logistic Process Flow

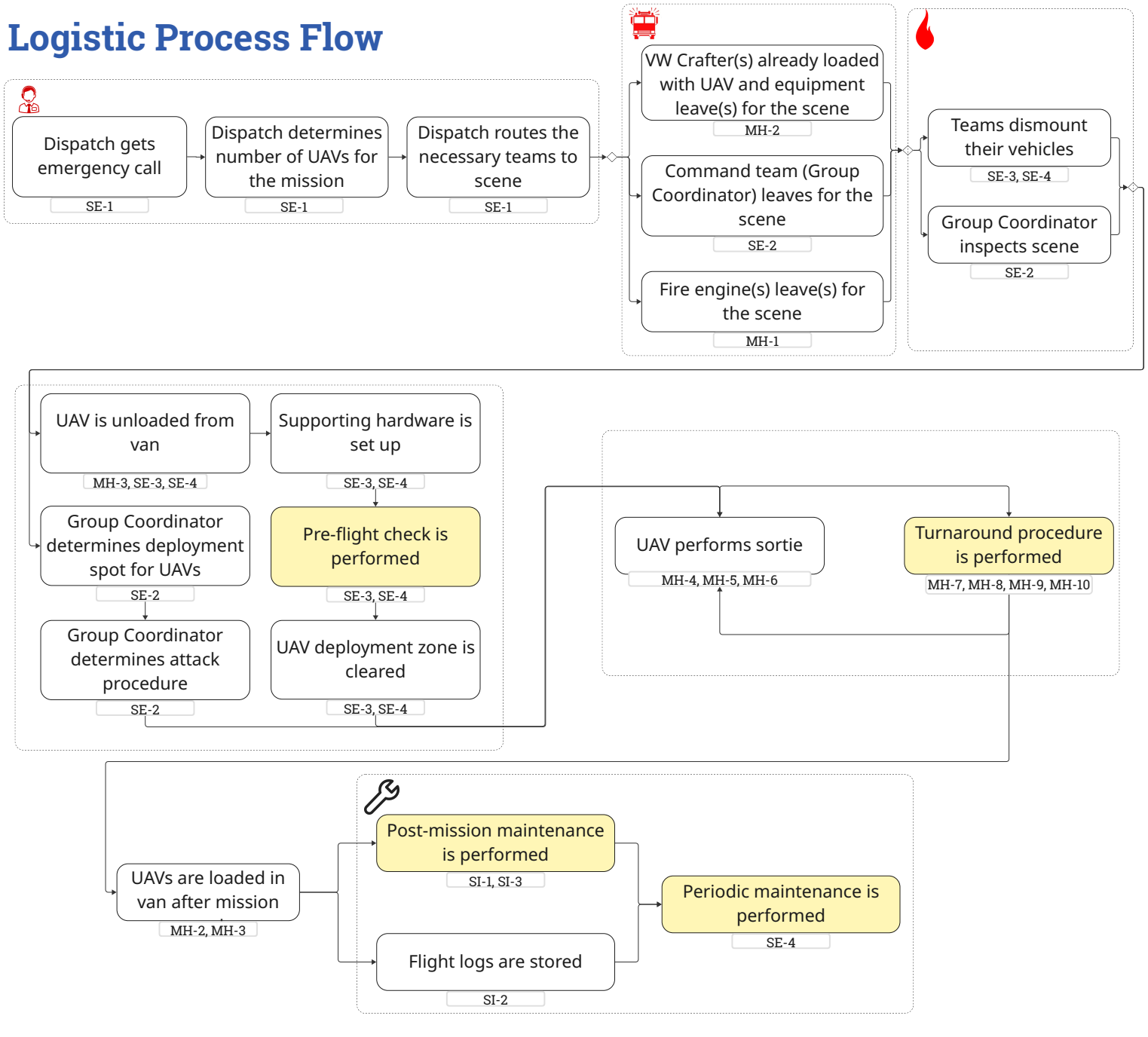

5.3.1. Take-off and Climb, Descending and Landing

The first phase of the sortie, the take-off and climb to altitude, is significant for both the total thrust and hence power consumption, especially since this phase will normally occur at full payload. In the UAV's case, climb performance is determined by the climb rate. The height at which the UAV has to climb also affects the energy consumed. As per customer requirements as well as regulations, the UAV must be able to climb to an altitude of at least 70 meters and is not allowed to climb to over 120 meters. For a conservative estimate of the energy consumption during a climb, the worst-case scenario was assumed, in which the UAV must climb to 120 meters.

Moreover, as the UAV participates in emergency operations, a high climb rate is required in order to climb to the altitude of the fire as high as possible. This is also beneficial for a second reason: preliminary analysis shows that ascending at higher speeds leads to a smaller energy consumption. The analysis is done for an ascent rate range between 0.5 m/s and 17 m/s.

It must also be mentioned that the drone will be hovered briefly after takeoff before ascending to the desired altitude to stabilize the drone [1]. Moreover, this allows the assessment of the environment before following with the mission. This maneuver will reduce the risk of flying since it allows checking that the drone responds as desired to the inputs. Since the hovering would be at about one meter from the ground and for about 10 seconds, it has not been accounted for in the climb profile.

The induced velocity during vertical climb is an important factor in estimating power requirements. It is calculated using Equation 5.1, which is derived from momentum theory for axial flight, assuming steady vertical climb [10].

$$v_i = -\frac{V_c}{2} + \sqrt{\left(\frac{V_c}{2}\right)^2 + \frac{T}{2\rho A}} \tag{5.1}$$

where v_i is the induced velocity, V_c is the vertical climb rate, T is the required thrust, ρ is the air density, and A is the rotor disk area [m^2]. This formula accounts for both the climb velocity as well as the additional flow that is induced by the rotor. Once the induced velocity is known, the instantaneous power can be estimated by $P = T \cdot v_i$, and the energy consumption follows as the integral of this power over time.

Figure 5.1 highlights that after approximately 3 m/s of vertical ascent speed, there is a diminishing return of the saved energy. For the sake of controllability and to prevent high current draws, 3 m/s is chosen as the ascent rate.

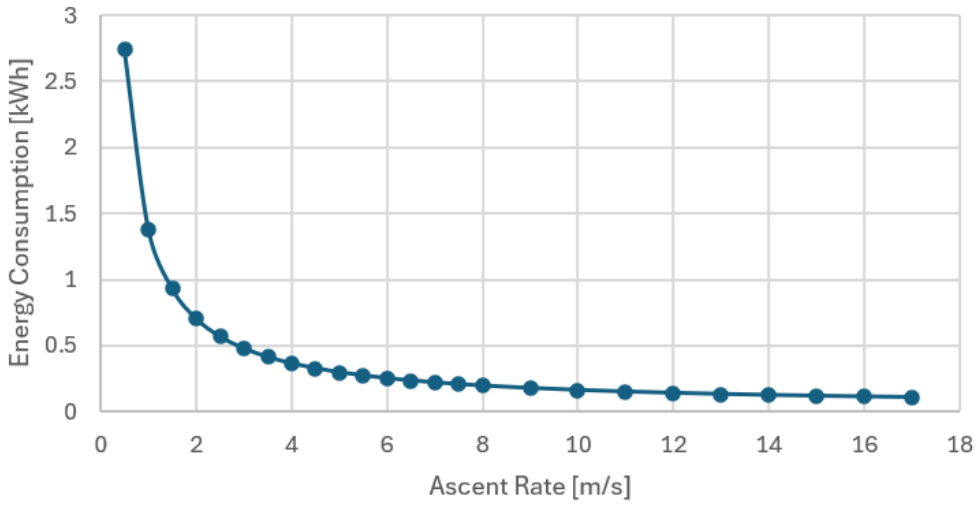

Figure 5.1: Energy Consumption at Various Ascent Rates

[1] https://uavcoach.com/how-to-fly-a-quadcopter-guide/#guide-3 [Date Accessed:11/06/2025]

This being considered, a climb profile was determined that consists of the following distinct stages:

- A constant vertical acceleration, of 1.5 m / s^2, for approximately 2 seconds. This leads to a climb rate of 3 m/s;
- A constant climb rate of 3 m/s, for approximately 38 seconds;
- A constant vertical deceleration, of 1.5 m / s^2, for approximately 2 seconds.

This climb profile leads to a total climb time of 42 seconds to 120 meters. The acceleration, rate of climb, and height were simulated in Python, and the climb profile was plotted, as visualized in Figure 5.2.

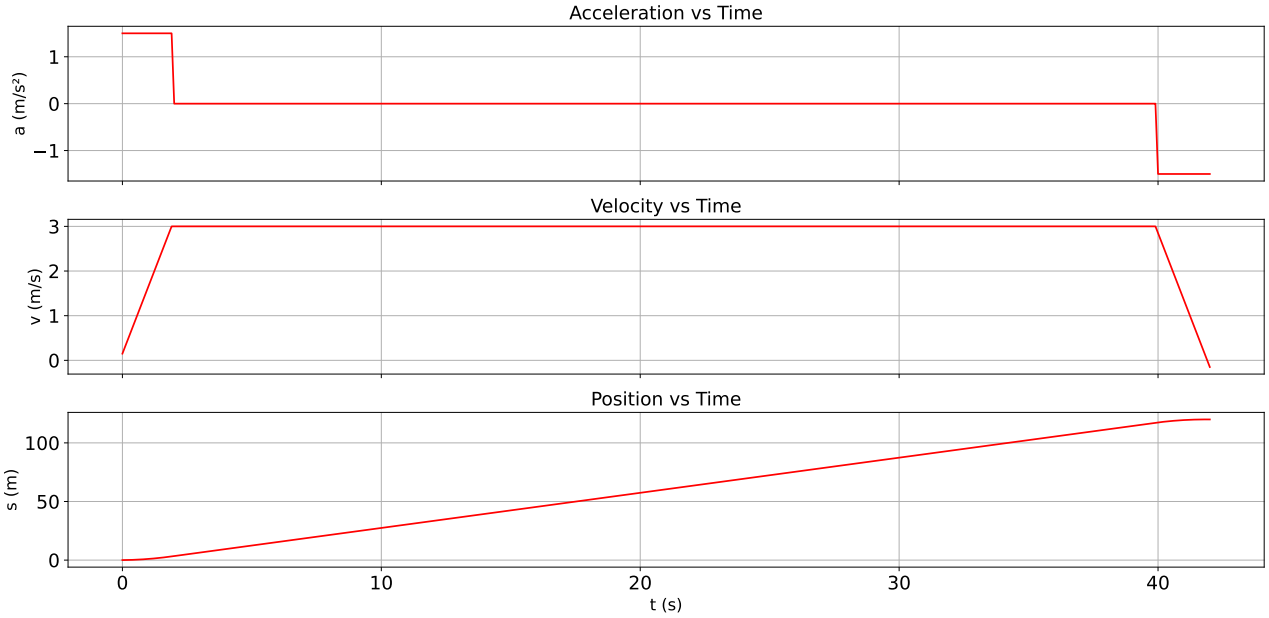

Figure 5.2: UAV Climb Profile during mission following customer requirements and considering energy consumption

5.3.2. Maneuvering Between Deployment Zone and Fire Suppression Spot, Drag Estimation

It is difficult to compile and detail a path for the UAV during a sortie, because every mission will be different. At this stage in the design, however, assumptions about general aspects of a sortie can be made to help in estimations and the sizing of the power and propulsion subsystems.

Firstly, it is established from customer requirements that the UAV shall have a minimum endurance of 15 minutes. This can be directly translated into an energy requirement once the mass of the UAV and the propulsion system are known. At the same time, energy consumed for extra maneuvers around obstacles, the effects of wind, and horizontal acceleration or deceleration motions might also need to be considered when determining how much energy is consumed during a sortie.

Since the UAV depends on a fire engine for water refilling, it is reasonable to assume that the deployment zone of the UAV will be in proximity to where the rest of the fire apparatuses are stationed. At the same time, because the UAV is a supporting element of a firefighting mission, with the role of containing the fire until it is reached by firefighters, it can be assumed that the fire apparatuses are deployed in a perimeter close to the affected building, such that it can also be reached with hoses or cranes. These assumptions, combined, lead to the inference that the time to maneuver to the fire suppression spot is not significant. Therefore, unlike the ascent and descent, separate energy calculations for these phases were deemed not necessary, instead being covered through a safety factor and a conservative estimate of the power required, as explained in Chapter 7. By also considering this, a horizontal maneuvering speed of 3 m/s was considered sufficient for the mission and targeted for both controllability and operational efficacy reasons.

Taking these aspects into account, there remains one challenge that occurs while the UAV is maneuvering, namely the influence of wind gusts and drag in general. This was investigated with SimScale, an online CFD software using OpenFOAM in the backend. Three simplified 3D models of the UAV were tested, inspired by the overall dimensions determined in the previous design phases [3], each with increasing fidelity to the real shape. The models chosen are a cube with a reference frontal area of 0.49 m^2, illustrated in Figure 5.3a, a cylinder with a reference area of 0.69 m^2 and a reference length of 2.69 m, shown in Figure 5.3c, and a cylinder with spherical caps, illustrated in Figure 5.3e.

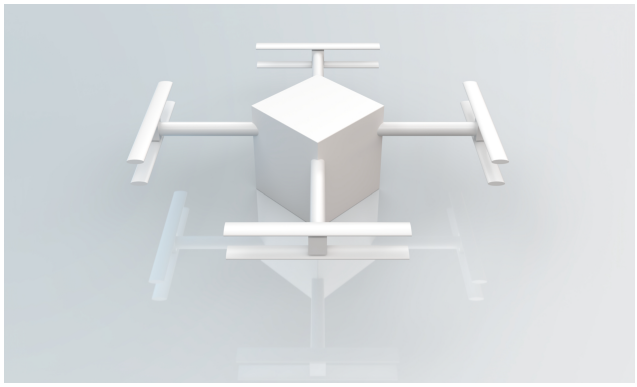

(a) Simplified Model 1

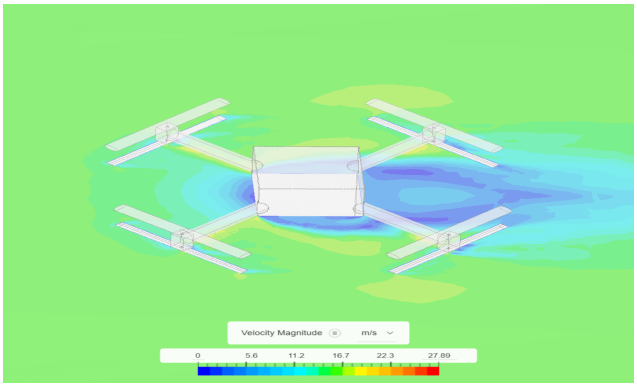

(b) Flow Field - Model 1

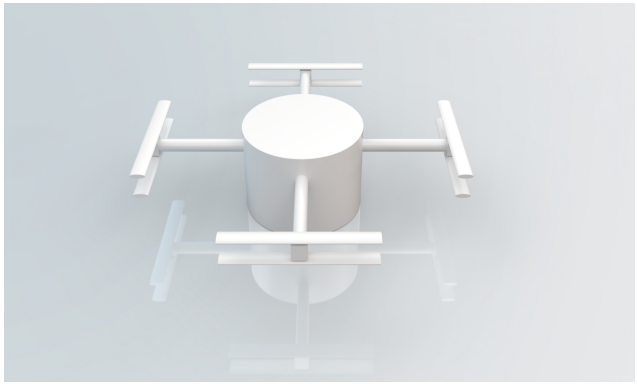

(c) Simplified Model 2

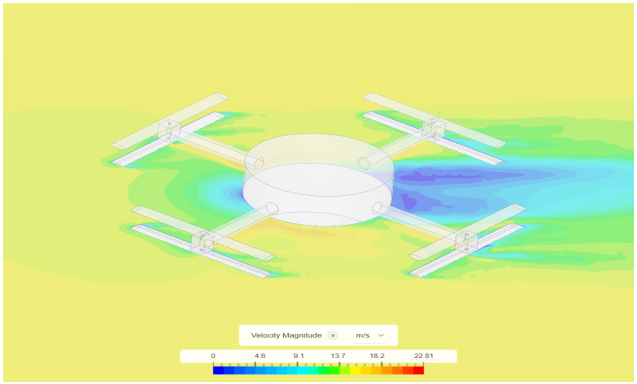

(d) Flow Field - Model 2

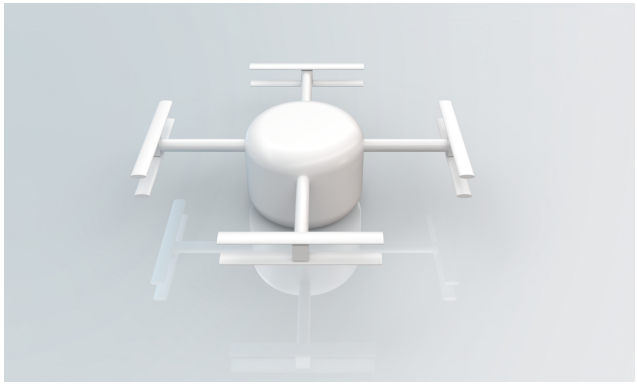

(e) Simplified Model 3

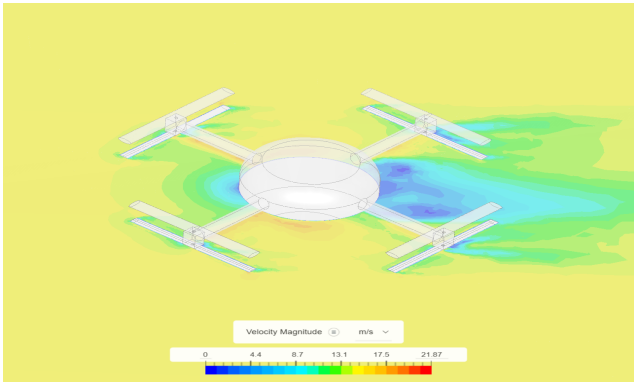

(f) Flow Field - Model 3

Figure 5.3: Side-by-side comparison of UAV simplified models (left) and their CFD velocity magnitude plots (right)

Within an incompressible regime simulation, a flow volume representing a cubic shape of side length 11.4 m is created around the UAV. The size was chosen considering that the diagonal length (rotor to rotor) of the drone is, preliminarily, around 2.7 m, so the flow volume was sized to be roughly 6 times longer diagonally, leading to a diagonal length of 16 m, which corresponds to the aforementioned side length.

In all simulations, some common parameters are used, including populating the flow volume with air with a density of 1.196 kg/m^3, and setting up the following boundary conditions:

- Velocity inlet on one face of the flow volume, normal to one side face of the UAV - the airspeed was set to 15 m/s as a worst case scenario based on the desired 3 m/s forward velocity and the wind resistance requirement (REQ-MIS-CTRL-1.4.1) of 6 bft $\approx$ 12 m/s;
- The other 5 faces are set with a custom boundary condition on ambient atmospheric pressure, equal to 1 atm;
- The drone surfaces are set with wall, no-slip boundary conditions.

The simulation was run for 1000 iterations, and convergence was achieved for all calculated coefficients and forces. In Figure 5.3b, Figure 5.3d, and Figure 5.3f, a plane cut containing the velocity magnitude of the flow field can be observed for the three models.

The obtained drag forces and coefficients are presented in Table 5.1, outlining the decrease of the drag coefficient when refining the shape. The third model's drag coefficient of 0.62 is already a good value that is close in magnitude to similar-shaped UAVs studied in literature [11]. This analysis is done to emphasize that the actual UAV model will not have a higher drag coefficient; thus, the estimated drag value serves as a conservative upper bound. For future work, a more in-depth aerodynamics analysis will have to be performed on the actual model.

Table 5.1: Drag Force and Coefficient

Model	**Model 1**	**Model 2**	**Model 3**
Drag Force [N]	103	83.82	56.61
Drag Coefficient	1.56	0.90	0.62

Taking these cases into consideration, a preliminary estimation for the drag and wind influence on the UAV can be obtained. This will be used as a disturbance input in the control and stability model described at the subsystem level in the coming chapters. This simplified analysis can be augmented during further design steps and prototyping to include the rotational effect of the propellers and the final 3D model of the UAV instead of simpler shapes.

5.3.3. Suppressing the Fire - Temperature Analysis

The most important factor to consider during this phase is the position of the UAV relative to the fire, as this greatly influences the safety of operations. In order to determine the safety distance that the UAV has to keep from the fire, a temperature analysis was performed. Two operational situations were considered for analysis: extinguishing a fire located inside the building through the window or extinguishing a fire on the roof of a high-rise building.

The temperature distribution in this analysis is derived from convective plume modeling. Radiative heat transfer — which may also impact UAV thermal loads — is not explicitly included in this model and could be addressed in future work or accounted for in more conservative distance estimates. For a pool fire, the increase in temperature as a function of height z above the center of the fire can be defined using Equation 5.3 [12], with respect to the origin of the fire source computed in Equation 5.2 [12].

$$z_0 = 0.083\dot{Q}^{\frac{2}{3}} - 1.02D, \tag{5.2}$$

where $\dot{Q}$ is the total heat release rate and D is the fire source diameter.

$$\Delta T(z,0) = 9.1\left(\frac{T_\infty}{g c_p^2 \rho_\infty^2}\right)^{\frac{1}{3}} Q_c^{\frac{2}{3}}(z - z_0)^{-\frac{5}{3}}, \tag{5.3}$$

where T_∞ is the atmospheric temperature, p_∞ is the atmospheric density, C_p is the specific heat capacity, Q_c is the convective heat release defined as 70% of the total heat release rate.

The total temperature along the z-axis is added up in Equation 5.4.

$$T(z,0) = T_\infty + \Delta T(z,0) \tag{5.4}$$

Radially, the increase in temperature as a function of height z and radius r is computed as indicated in Equation 5.5 [12].

$$\Delta T(z,r) = T(z,0) \cdot \exp\left(-\beta \cdot \left(\frac{r}{b(z)}\right)^2\right), \tag{5.5}$$

where β is an empirical constant approximated with one and $b(z)$ is the plume radius approximated with D/2 based on a cylindrical shape estimation.

The total temperature at a height z and radius r with respect to the fire source is computed in Equation 5.6.

$$T(z,r) = T_\infty + \Delta T(z,r) \tag{5.6}$$

The resulting temperatures are analyzed using a temperature map in order to determine operational procedures, more exactly, the minimum distance between the UAV and the fire, to meet the temperature conditions for all the subsystems.

The first situation considered is the fire inside the building with an open window. The UAV is situated outside the building and extinguishes the fire by aiming at the window. For a fire power density of 0.25 MW/m^2 [13] and a room of 40 m^2, the 3D temperature map is shown in Figure 5.4 and the 2D temperature map at z=0m is shown in Figure 5.5. To maintain a maximum temperature of 323 K, the UAV has to keep a horizontal distance of at least 3.5 m.

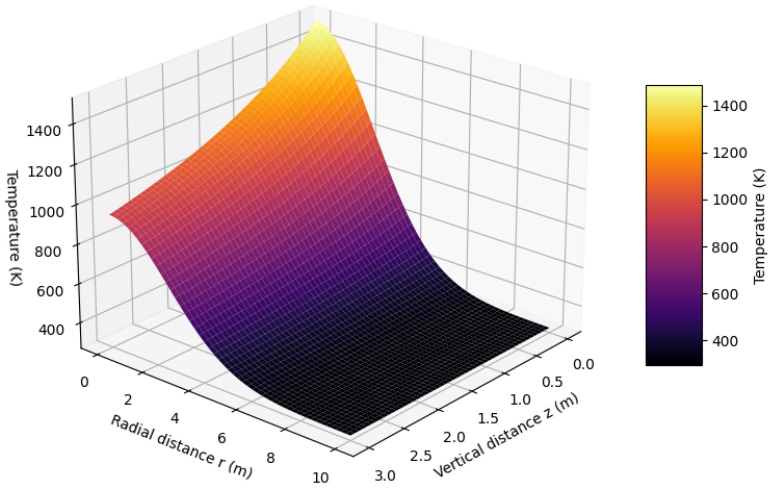

Figure 5.4: 3D Temperature Map for a Room Fire Situation

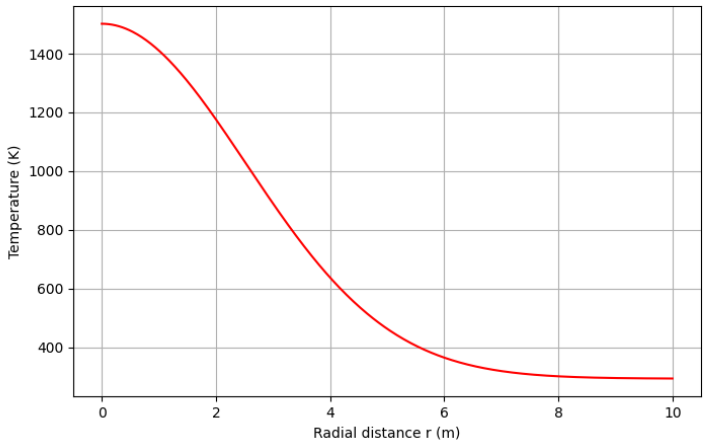

Figure 5.5: 2D Temperature Map for a Room Fire Situation

The second situation considered is the rooftop fire. For a fire power density of $0.2MW/m^2$ [13] based on open-air conditions and a fire area of 100 m^2, the 3D temperature map is illustrated in and the 2D temperature map at z = 3 m is illustrated in Figure 5.7. To maintain a maximum temperature of 323K, the UAV has to keep a horizontal distance of at least 3 m in height from the roof and 4.3 m in horizontal distance away from the edge of the fire.

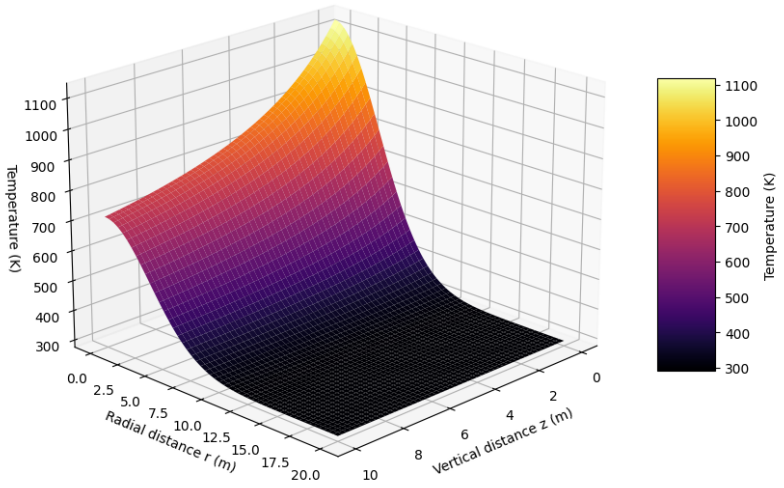

Figure 5.6: 3D Temperature Map for a Rooftop Fire Situation

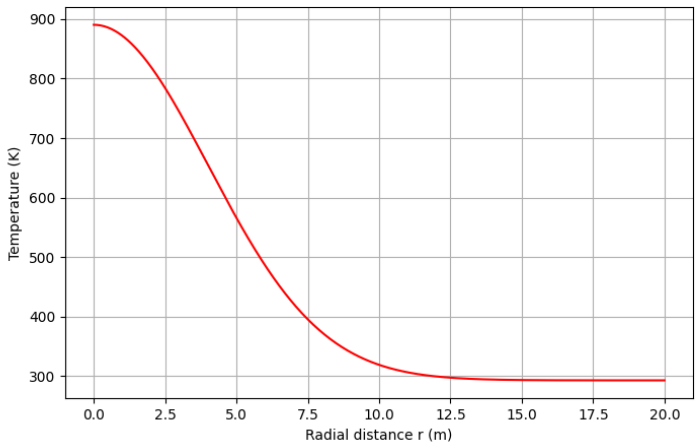

Figure 5.7: 2D Temperature Map for a Rooftop Fire Situation

5.4. Turnaround Procedure and Deployment

A stage of the mission that also warrants further discussion is the turnaround procedure, as REQ-MIS-LOG-2.1.4 directly addresses it. The turnaround is one of the standard procedures and should be conducted by the operators in the same manner after every sortie, in order to streamline operations. This procedure is intended to be performed mainly by the turnaround mechanic, with the help of the UAV operator in certain cases specified further. While it is recommended to perform activities in the sequence specified below, they can be parallelized to an extent. Three main activities were considered to be part of the turnaround:

1. Replacing the water tank;

   The empty water tank is disconnected and lifted out of the UAV by the turnaround mechanic, with a full one to be put back in. Because a full tank will weigh slightly over 50 kg, installing the new tank was considered to be a two-person job. Therefore, the operator is also required to play a part in this step.

   Connecting the water tank to the pump hoses and checking that it is properly installed requires an amount of time, but considering that the full tank is brought inside the deployment zone beforehand, it was estimated that this step of the turnaround would take no more than two minutes.

2. Replacing the batteries, if energy is below 30%;

   This step can be performed entirely by the turnaround mechanic. There are eight batteries to be replaced, in packs of 2 batteries. The step involves disconnecting the battery cables, sliding out the old batteries, sliding in the new ones, and reconnecting the cables.

   While the new batteries should be brought close to the landing spot, there are still 8 disconnect / connect movements done by a mechanic, which brings the estimate of the time required for this step to **three minutes**. It must also be stressed in this case that one sortie might take much less than the 15 minutes the UAV is required to hover, so it is possible that the batteries will have enough charge left to perform another sortie without replacement.

3. Checking the structural integrity of the UAV;

   This step is intended to be conducted in parallel to the battery replacement: while the turnaround mechanic is replacing the batteries, a quick inspection of the propellers, arms, landing legs, and body must be performed by the operator to detect any easily visible cracks and defects. Because this step is done in parallel, it does not require any extra time.

   A more extensive structural integrity check for the legs and main structure is, however, required if the UAV performs a hard landing. For design purposes, a hard landing was defined as equivalent to the fully loaded UAV falling freely from 0.5 m.

Putting the steps together, the time required to perform the turnaround is estimated as five minutes, as required by the customer. However, it must be stressed that these are only initial estimations based on the design, and to determine the actual time, tests must be performed together with an operator/turnaround mechanic crew during the advanced design and certification phases.

As for the deployment of the UAV, it can be considered akin to the turnaround procedure, with the extra step that the UAV must be unfolded and set up. As the deployment spot is established by the group coordinator, the van with the UAV can be brought into the deployment zone, and the zone itself can be marked with tape or cones, such that it is delimited from the rest of the firefighting operations. By transporting it without batteries installed or water in the tank, the UAV can be lifted from the van by the operator and turnaround mechanic: without water and batteries, it is expected to weigh around 60 kg and can be lifted by grabbing the arms.

The steps required in addition to those mentioned for the turnaround procedure are:

- Unfolding the UAV: the unfolding is done manually by the turnaround mechanic. This step is not expected to take more than two minutes;
- Powering up the UAV: after the batteries are installed, the operator can turn on the system and wait for the software to boot and self-diagnose. The booting time was estimated at around one minute;
- Selecting the deployment spot position on the GPS system: this is a mandatory step that allows the UAV to return autonomously to the deployment spot. While the operator will navigate through the interface of the software, this is not expected to take more than **one minute**.

With these in mind, the deployment of the UAV is expected to take five minutes more than just a standard turnaround, bringing the time to nine minutes.

6. Propulsion Subsystem

The propulsion subsystem design aims to select a set of motors and propellers capable of providing the required thrust capabilities for this mission, and ESCs are meant to establish the connection with the power subsystem.

6.1. Requirements Assessment

Based on the mission and system requirements defined in the baseline report [1], propulsion subsystem requirements are defined below:

- **REQ-SUBSYS-PROP-1**: The propulsion system shall provide a peak thrust-to-weight ratio of 2.1.
- **REQ-SUBSYS-PROP-2**: Each motor shall provide a peak thrust of at least 39.4 kg.
- **REQ-SUBSYS-PROP-3**: Each motor shall provide a hover thrust of 21.6 kg.
- **REQ-SUBSYS-PROP-4**: The motors shall be compatible with the size of the propellers (as specified in their technical sheet).
- **REQ-SUBSYS-PROP-5**: The 8 rotors shall form counter-rotating coaxial pairs.
- **REQ-SUBSYS-PROP-6**: The 4 pairs of rotors shall ensure the torque balance and symmetry.
- **REQ-SUBSYS-PROP-7**: The propellers shall not flutter at the peak rpm of the motors.
- **REQ-SUBSYS-PROP-8**: The propellers shall be made out of a high-temperature resistant material.
- **REQ-SUBSYS-PROP-9**: The ESC rated current shall be at least as high as the rated current of the motors.
- **REQ-SUBSYS-PROP-10**: The ESC and motor rated voltages shall be compatible with the voltage provided by the batteries.

The compliance matrix is correspondingly shown at the end of the chapter, filled in with supporting justifications for the current or planned fulfillment of each requirement. The *check* column indicates the compliance as:

✔: Complied with
✗: Not complied with
P: Pending, still to be verified.

6.2. Thrust-to-Weight Ratio

To start the design, a maximum thrust-to-weight ratio has to be defined. Based on literature, the minimum desired ratio is 2 [14].

The ratio is obtained by accounting for multiple factors, such as the maximum wind resistance, the efficiency loss on the lower rotors due to coaxial interference. When a maneuver is desired, the T/W ratio needs to be even higher to allow the ability to make maneuvers beyond the hovering mode . The shift in the center of gravity while emptying the water tank, as well as wind disturbances, also have to be considered.

The X8 configuration requires an increase in power for each coaxial set of rotors due to the interference. The maximum ratio of induced power for a coaxial rotor pair versus the induced power of two separate rotors is given by Equation 6.1 [10]. Note that this is an application of Equation 6.2, which is the induced rotor power. The analysis shows that the ratio will be a maximum $\sqrt{2}$, because a zero finite spacing is considered. However, a more detailed analysis showed that the ratio becomes 1.28 for a nonzero finite spacing [10]. Experiments mainly show a ratio of 1.16. To be conservative, a k_{int} of 1.28 is taken.

$$k_{\text{int}} = \frac{(P_i)_e}{P_i} = \frac{(2T)^{\frac{3}{2}}}{\sqrt{2\rho A}} \cdot \frac{\sqrt{2\rho A}}{2T^{\frac{3}{2}}} = \frac{2^{\frac{3}{2}}}{2} = \sqrt{2} \tag{6.1}$$

Momentum theory shows that rotor power is related to its thrust by Equation 6.2, assuming quasi-steady 1-D flow. This shows that power is related to thrust as $P \propto T^{\frac{3}{2}}$, or corollary, $T \propto P^{\frac{2}{3}}$ [10]. The coaxial factor is therefore found as $1.28^{\frac{2}{3}} = 1.18$.

$$P_{\text{i}} = \sqrt{\frac{T^3}{2\rho A}} \tag{6.2}$$

where P_i is the induced power [W], T is the required thrust [N], ρ is the air density [kg/m^3], A is the rotor disk area [m^2].

Initially, the peak thrust-to-weight ratio was set to 2.22 and the average thrust-to-weight was 1.35. The suitable components were selected in [3]. Due to MTOW considerations and the aim of increasing the payload capabilities, the average thrust-to-weight ratio had to be decreased. As a conservative estimate, an average operational value of T/W = 1.15 is chosen, meaning the drone needs to provide power for an average thrust of 172.5 kg, based on the maximum take-off weight of 150 kg. Note that after delivery of the payload, this weight drops to 100 kg, effectively reducing the power requirements, explaining the conservative nature of the estimation. The initial product specifications and the iterated ones are presented for each subsystem in the following sections, as well as the advantages of performing these changes.

6.3. Component Selection

Based on the established requirements, the system's components are selected based on trade-offs performed in [3].

Motor

The motor is selected to be brushless, as it has greater efficiency, longer lifespan and reduced maintenance compared to the brushed option. Then, low-KV windings are opted for because they are correlated with a higher thrust level, needed for the heavy payload capabilities.

Based on the found off-the-shelf motors, it was observed that the increase in thrust between available products is significant and affects the thrust-to-weight ratio too much. Choosing another motor for each small change of thrust needed during an iteration is not a feasible process, so it is decided that the motor should be designed to fulfill the maximum thrust from the beginning of the design process.

Considering a maximum take-off weight of 150 kg and a peak thrust-to-weight ratio of 2.22 defined in [3], the maximum thrust the design considers is 333 kg. Given that the drone has eight rotors, each motor requires a maximum thrust of at least 41.63 kg. Aiming to fulfill the thrust requirements and stay within weight and cost limits, the selected motor is illustrated in and its specifications are presented in Table 6.1.

Due to MTOW limitations followed by the decrease of the peak thrust-to-weight ratio aimed for, the new peak thrust-to-weight ratio of 2.10 leads to a total maximum thrust of 315 kg and a total thrust per motor of at least 39.4 kg. The specifications of the newly selected motor are outlined in Table 6.2. As the aim of this iteration is to decrease the weight of the UAV, it can be seen that the eight motors weigh 3 kg less than the previously selected ones.

Figure 6.1: Motor - Furious Motor

Table 6.1: Initial Motor Specifications for Furious Motor Model [1]

Specification	Value
Dimensions	⌀120 × 90 mm
KV	78 RPM/V (customizable)
Max. Thrust	42 kg
Max. Torque	18 N · m
Max. RPM	4770 RPM
Suggested ESC	24S, 150 A
Suggested Propeller	36″
Max. Current	136 A
Max. Voltage	88.8 V (24 S)
Max. Power	9 kW
Hall Sensor	Optional
Weight	2.78 kg
Cost [21/05/2025]	€ 304

Table 6.2: Iterated Motor Specifications for Furious Motor Model [2]

Specification	Value
Dimensions	⌀120 × 70 mm
KV	80 RPM/V (customizable)
Max. Thrust	40 kg
Max. Torque	16 N · m
Max. RPM	6400 RPM
Suggested ESC	24S, 150 A
Suggested Propeller	36″
Max. Current	112 A
Max. Voltage	88.8 V (24 S)
Max. Power	8.5 kW
Hall Sensor	Optional
Weight	2.4 kg
Cost [03/06/2025]	€ 300

Figure 6.2 indicates the rotation direction of the motors. The rotation of diagonally placed motors in an X-plane matches and the rotation of coaxial motors is opposite, due to torque cancellation purposes.

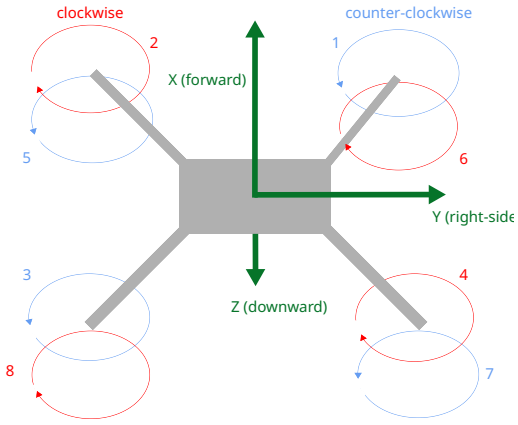

Figure 6.2: Motor Direction Configuration Chosen

[1] https://furiousmotor.com/products/zero-g-120-90 [Date Accessed: 20/05/2025]
[2] https://furiousmotor.com/products/zero-g-120-70 [Date Accessed: 04/06/2025]

Electronic Speed Controller

Firstly, two 4-in-1 ESCs were considered, as a 4-in-1 ESC packs four channels in one unit, saving wiring and weight. However, it concentrates heat and it might get overloaded by the current draw of 4 larger motors, so the final choice consists of 8 single-channel ESCs, offering easier cooling and redundancy. 32-bit speed controllers were selected, which provide faster, more precise PWM updates than legacy 8-bit units, important for smooth thrust control under dynamic loads.

Compatible ESCs were selected as found in the specifications of the motors, in order to match the voltage level and to ensure the ESCs can withstand higher currents than the maximum level the motors can draw. It is shown in Figure 6.3 and its details can be found in Table 6.3.

Figure 6.3: ESC - Furious Motor

Table 6.3: ESC Specifications for Furious Motor Model [3]

Specification	Value
Dimensions	$148 \times 66.6 \times 47$ mm
Voltage Range	44.4V–88.8V
Continuous Current	240 A
Max. Current	300 A
Switching Frequency	50–400 Hz
Effective Throttle	900–2000 μs
Ingress Protection	Optional
Mode	BLDC
Electrical Advance	15°
Weight	810 g
Working Temperature	−20°C to 65°C
Cost [21/05/2025]	€ 397.5

Propeller

The propeller is designed to have fixed pitch, to be foldable and to be made out of CFRP. Given the requirement of a maximum 150 kg MTOW and the requirement for peak thrust-to-weight ratio, it is clear that as much thrust as possible has to be obtained from the rotors such that the UAV can perform properly in emergencies. The thrust performance importance in reaching the fire location and ensuring safety, even when losing a motor, is essential when choosing the number of blades for the propeller. Additionaly, the blade diameter influences the transportability of the drone and the number of blades per propeller can also imply different levels of manufacturing complexity and cost. The chosen design consists of two blades, because it leads to minimal drag and blade interference

[3] `https://furiousmotor.com/products/maven-24s-150a?` [Date Accessed: 20/05/2025]

in terms of efficiency and power consumption considerations, it is the easiest to fold and easiest to manufacture compared to 3- or 4-blade configurations.

The propeller is selected based on the specified diameter for the thrust tests performed on the selected motor. Since the recommended propellers from the same manufacturer are not foldable, it was chosen to opt for an alternative product with similar dimensions, illustrated in Figure 6.4a, but also with an incorporated folding mechanism, as shown in Figure 6.4b. The specifications can be seen in Table 6.4.

(a) Unfolded Propeller

(b) Folded Propeller

Figure 6.4: Propeller - T-Motor

Table 6.4: Foldable Propeller Specifications from T-MOTOR [4]

Specification	Value
Dimensions	919.5 × 299.7 mm
T-MOTOR Series	Foldable
Weight (Single Blade)	230 g
Material	CF + Epoxy
Thrust Limitation	45 kg
Ambient Temperature	−40°C to 65°C
Optimum RPM	1900–3200 RPM
Storage Temperature	−10°C to 50°C
Storage Humidity	< 85%
Surface Treatment	Glossy
Cost [21/05/2025]	€ 411.5

6.4. Propulsion Subsystem Budgeting

The propulsion subsystem budget is presented in Table 6.5.

Table 6.5: Propulsion Budgets

Component	Mass [kg]	Cost [€]	Power Required [W]
Motor (8x)	2.40	300.00	8500
ESC (8x)	0.81	450.00	–
Propeller (8x, 2 blades)	0.46	465.90	–
Total	29.36	9727.20	68000.00

[4] `https://store.tmotor.com/product/folding-carbon-fiber-36_2x11_8-prop.html` [Date Accessed: 20/05/2025]

Table 6.6: Compliance Matrix Propulsion System

Identifier	Requirement Description	Check	Justification	Method	Reference
REQ-SUBSYS-PROP-1	The propulsion system shall provide a peak thrust-to-weight ratio of 2.1.	**P**	The total peak thrust provided by the motors will be assessed during a test.	Demonstration	Section 6.3
REQ-SUBSYS-PROP-2	Each motor shall provide a peak thrust of at least 39.4 kg.	**P**	The peak thrust of the motor is 40 kg according to the datasheet and it will go through testing procedures.	Demonstration	Table 6.1
REQ-SUBSYS-PROP-3	Each motor shall provide a hover thrust of 21.6 kg	**P**	The hover thrust of the motor will be tested at the average power setting for compliance with the calculated energy budget.	Test	Section 6.3, Table 6.1
REQ-SUBSYS-PROP-4	The motors shall be compatible with the size of the propellers.	✔	The propeller blades have been checked against the recommendations in the technical data sheet of the motor. Their compatibility was also checked in the datasheets.	Inspection	Table 6.1
REQ-SUBSYS-PROP-5	The 8 rotors shall form counter-rotating coaxial pairs.	✔	The rotors' coaxial configuration and rotation has been checked in the CAD drawings. The rotation can also be further demonstrated during direction testing.	Demonstration, Inspection	Figure 6.2
REQ-SUBSYS-PROP-6	The 4 pairs of rotors shall ensure torque balance and symmetry.	**P**	Flight testing controllability and hover stability will be checked. Also OEI scenarios will be simulated by switching the correct motors off and assessing flight capabilities	Demonstration, Test	Section 6.3
REQ-SUBSYS-PROP-7	The propellers shall not flutter at the peak rpm of the motors.	✔	A modal analysis has been performed in CATIA to check that when the motors work at their peak rpm, the first natural frequency of the propellers is higher, so there is no resonance.	Analysis	Section 6.3
REQ-SUBSYS-PROP-8	The propellers shall be made out of a high-temperature resistant material.	✔	The material's maximum operating temperature (65°C) has been checked against the mission's maximum operating temperature, (50°C).	Inspection	Table 6.4
REQ-SUBSYS-PROP-9	The ESC current rating shall be at least as high as the rated current of the motors.	✔	The current rating has been checked in the ESC data sheet. The selected ESC is designed for 240 A continuous current and 300 A maximum current, which is higher than the motor's compatibility suggestion with 150 A.	Analysis	Table 6.3, Table 6.1
REQ-SUBSYS-PROP-10	The ESC and motor voltages ratings shall be compatible with the voltage provided by the batteries.	✔	The voltage ratings compatibility has been checked in the respective data sheets. The motor's maximum voltage is 88.8V, The ESC voltage range is 44.4V-88.8V and the batteries provide 24S.	Analysis	Table 6.1, Table 6.3, Table 7.3

7. Power Subsystem

The power subsystem mainly consists of the batteries, as well as the Power Distribution Board (PDB) that used for routing power and regulating voltages, and wiring between components. At this stage of the design, only the battery choice is discussed, as its mass is the most critical for the design.

7.1. Requirements Assessment

The electrical power system shall perform functions as specified in the baseline report [1]. Requirements are established to conceptualize the system later on. Redundancy, performance, electrical, and thermal constraints are all taken into account. The specified values are based on mission and conceptual design requirements, which are found further in this chapter. For instance, the the required energy is set by the mission profile and estimated power consumption of the propulsion system.

- **REQ-SUBSYS-PWR-1**: The power system shall have redundant power paths between the battery and the other critical subsystems, such as the ESC.
- **REQ-SUBSYS-PWR-2**: Failure of a singular battery cell shall not result in a complete loss of power.
- **REQ-SUBSYS-PWR-3**: The battery system shall be continuously monitored during missions and reported to the drone operator.
- **REQ-SUBSYS-PWR-4**: The battery charging time to nominal voltage shall be maximum 30 minutes.
- **REQ-SUBSYS-PWR-5**: The battery shall store a minimum of 9.23 kWh of energy.
- **REQ-SUBSYS-PWR-6**: The batteries shall be replaced within 60 seconds.
- **REQ-SUBSYS-PWR-7**: The battery charging system shall comply with the current fire truck connections.
- **REQ-SUBSYS-PWR-8**: The maximum current through the battery connections shall not exceed 263 A.
- **REQ-SUBSYS-PWR-9**: The battery operating temperature shall remain between $-40°C$ and $60°C$.

The compliance matrix is correspondingly shown at the end of the chapter, filled in with supporting justifications for the current or planned fulfilment of each requirement.

7.2. Power System Configuration

The power system is mainly driven by the power demand of the motors, hence this will be the focus of the sizing. Before sizing, however, the configuration and type of batteries should be considered. These are selected based on design option trees and trade-offs performed in [3].

Operational Battery Configuration

The operational battery configuration encompasses both the arrangement of modules and operational considerations, namely the rechargeability and modularity of the power system. From the initial mission requirements in Table 2.1, it directly follows that the battery shall be both rechargeable and replaceable (REQ-MIS-LOG-2.1.4, REQ-SYS-LOG-2.1.5). These requirements are justified by the sustainable impracticality of using non-rechargeable batteries and the need for a short turnaround time.

While initially series and parallel arrangements seem to have their advantages, their drawbacks quickly become apparent. A series configuration introduces a single point of failure, lacking redundancy as required by REQ-SUBSYS-PWR-2. While a parallel connection does provide this redundancy, the

voltage requirements cannot be met. This implies the use unrealistic gauge sizes, which eliminates the purely parallel approach. Leftover is a hybrid arrangement, which is feasible since it provides both redundancy and sufficient capacity.

Battery Chemical Composition

Several factors have been taken into account during the sizing process, each having varying impact on the design decision. For instance, weight and safety were deemed vital for the design whereas sustainability and the maximum discharge rate were less driving. The importance of cost effectiveness and cycle life was considered moderate.

A decision was made to select solid-state batteries over lithium-ion alternatives because of their slightly higher energy density and improved safety characteristics, despite their higher cost. Batteries consist of an anode and a cathode. A silicon anode was chosen since it has a very high energy density, while also being quite safe and performing moderately on sustainability. For the cathode, Nickel Manganese Cobalt (NMC) was selected because of its relatively high cycle life and low cost, although it does pose certain safety risks that will need to be addressed later. Furthermore, NMC is more readily available on the market when combined with a silicon anode, making it a more practical choice than other alternatives. The final configuration therefore consists of a solid state battery with a silicon anode and NMC cathode.

7.3. Power System Sizing

The specifications of the motors reveal the necessary information to size the power system. To determine what the characteristics shall be, two cases need to be investigated:

1. **Maximum Power Conditions:** This condition directly sets the requirement for the maximum power that the battery can deliver. The requirements are defined by using the maximum T/W ratio of 2.10 and taking into account the required motor power. The maximum discharge current of the battery should not be exceeded.
2. **Average Power Conditions:** Although the maximum T/W ratio dictates the maximum discharge current, the continuous discharge current should also be considered. The average T/W ratio defines the required power and hence discharge rate at which the battery generally operates. The battery cannot be discharged continuously above its continuous discharge limit and should therefore remain below. As explained in Section 6.2, the average thrust-to-weight ratio was quantified to be 1.15.

The power estimation is done considering a relevant solid state battery catalog[1]. Initially, a cell voltage of 3.7 V is used to find the required cells in series to step up the voltage. Then, based on the voltage and needed power, a current rating is determined. The capacity [Ah] and continuous/maximum discharge current of a cell are then set, directly yielding the required parallel strings.

For scenario 1, the maximum power of an engine is 8.5 kW (Table 6.2), hence 68 kW for all eight engines. For scenario 2, the relation $P \propto T^{\frac{3}{2}}$ from Equation 6.2 can again be applied to find the average power requirement per motor. Moreover, a maximum per-motor thrust of 40 kg and target weight of 150 kg were also taken from Table 6.2.

$$P_{\text{avg}} = P_{\text{max}} \left(\frac{T_{\text{avg}}}{T_{\text{max}}} \right)^{\frac{3}{2}} = P_{\text{max}} \left(\frac{T/W_{\text{avg}} \cdot W}{T_{\text{max}} \cdot n_{\text{motors}}} \right)^{\frac{3}{2}} = 8500 \cdot \left(\frac{1.15 \cdot 150}{40 \cdot 8} \right)^{\frac{3}{2}} = 3.36 \text{ kW} \tag{7.1}$$

Therefore, from Equation 7.1 a total power demand of 26.88 kW was found. These power numbers cannot be interpreted yet as they must first be related to the corresponding discharge current. The motor operates at a maximum voltage of 24S (88.8 V) and the aim is to minimize power losses, hence

[1] https://www.grepow.com/nmc811-battery/350wh-kg-semi-solid-state-high-energy-density-battery.html[Data Accessed: 19/05/2025]

the battery should operate at a voltage close to this value. The battery database[2] shows that 88.8 V is directly in line with the necessary voltage and now allows calculating the current ratings. For scenarios 1 and 2, the total currents yielded 766 A and 303 A, respectively. For the battery packs in mind, the maximum and continuous discharge rates are 263 A and 78.9 A, respectively. The minimum required number of parallel strings is then three for the maximum scenario, while it is four for the average power consumption, highlighting that the average condition dictates the required capacity.

Grepow[3] offers a semi-solid state high-nickel NMC cathode with a silicon-carbon anode. According to the website, this battery offers over 1200 charge cycles before degrading to 80% [15]. It also provides rapid 2C charging, meaning it can get fully charged in 30 minutes, and it needs to be in a temperature range of -40°C to 60°C for peak performance and safety. The TARBG3526312S10X solid-state battery is found to be most suitable with the requirements, as will be explained in Figure 7.3. It is visualized in Figure 7.1 and the characteristics can be found in Table 7.1.

Figure 7.1: Grepow TARBG3526312S10X battery

Optimization

Before the preceding computations, a propulsive force of 42 kg was considered, which led to increased power requirements. However, this analysis reveals that the battery system mass can significantly drop for only a small decrement in thrust. The iteration also alleviates the cost budget, highlighted by the comparison between Table 7.1 and Table 7.2, where the latter was the corresponding initial battery. The new battery reduces the mass by almost 900 g per battery. Moreover, it takes a smaller volume and has a price drop of 21%. It should also be noted that this change has incurred several other changes, as the capacity is now lower and thereby the discharge rate. Although the maximum discharge current value has decreased, no problems arise since only the average demand was limiting. The continuous discharge rate maintains relatively constant, which allows for the implementation of the new battery.

Table 7.3 and Table 7.4 contain the characteristics of both the new and old system, respectively. The C-rate is determined by Equation 7.2, where I is the current [A], and C is the capacity [Ah]. The discharge time follows from the reciprocal of the C-rate.

$$\text{C-rate} = \frac{I}{C} \tag{7.2}$$

The per-system differences follow the same trend as the comparison of individual batteries. Notably, the same hybrid composition is kept because a 2S3P configuration would not allow a distributed connection of 8 motors, limited by the current and unequal power consumption. Furthermore, the decrease in capacity does not cause performance limits regarding endurance, as the estimated average power consumption is simultaneously lowered. Following up on the comparison of discharge rate of

[2] `https://www.grepow.com/semi-solid-state-battery/350wh-kg-series-high-energy-density-battery-pack.html` [Date Accessed: 19/05/2025]

[3] `https://www.grepow.com/semi-solid-state-battery/350wh-kg-series-high-energy-density-battery-pack.html` [Date Accessed: 19/05/2025]

the individual batteries, both the continuous but mainly the maximum system C-rate have increased. Hence, the new system is more effectively using the available battery performance. The most important change is the reduction of 8.9 kg mass.

Table 7.1: New Solid-State Battery Specifications [15]

Specification	Value
Model No.	TARBG3526312S10X
Dimensions	$129.7 \times 76.5 \times 197$ mm
Nominal Voltage	44.4 V
Cells in Series	12 S
Cells in Parallel	1 P
Capacity	26.3 Ah
Energy	1167.72 Wh
Energy Density	326.68 Wh/kg
Weight	3.574 kg
Const. Discharge (3C)	78.9 A
Max Discharge (10C)	263 A
Charge Rate	2 C
Cost [11/06/2025]	€394.38

Table 7.2: Old Solid-State Battery Specifications [15]

Specification	Value
Model No.	TARBG3533K12S10X
Dimensions	$127.1 \times 89.5 \times 212$ mm
Nominal Voltage	44.4 V
Cells in Series	12 S
Cells in Parallel	1 P
Capacity	33 Ah
Energy	1465 Wh
Energy Density	329.81 Wh/kg
Weight	4.443 kg
Const. Discharge (3C)	99 A
Max Discharge (10C)	330 A
Charge Rate	2 C
Cost [21/05/2025]	€499.50

Table 7.3: New Power System Specifications

Specification	Value
Nominal Voltage	88.8 V
Batteries in Series	2 S
Batteries in Parallel	4 P
Capacity	9.34 kWh
Capacity (Ah)	105.2 Ah
Cont. Discharge Current	75.7 A
Continuous System C-rate	2.877 /hr
Max Discharge Current	766 A
Max System C-rate	7.28 /hr
Mass	28.6 kg
Cost [21/05/2025]	€3155.04

Table 7.4: Old Power System Specifications

Specification	Value
Nominal Voltage	88.8 V
Batteries in Series	2 S
Batteries in Parallel	4 P
Capacity	11.72 kWh
Capacity (Ah)	132 Ah
Cont. Discharge Current	379 A
Continuous System C-rate	2.873 /hr
Max Discharge Current	810 A
Max System C-rate	6.14 /hr
Mass	35.5 kg
Cost [21/05/2025]	€3996.03

Power Distribution Board (PDB)

To send power from the batteries to other components, it must go through a Power Distribution Board (PDB). A very high voltage and high current PDB is required to deliver sufficient power to the ESCs and hence the motors. The PDB-1000 from Avizar [4], visualized in Figure 7.2 allows for this delivery. This PDB from the batteries will also provide power to the pump or the auto pilot board through electric converters. It costs €349,- and weighs 300 g. The four pairs of batteries would thus require a total cost and mass of €1,396,- and 1200 g, respectively.

[4] https://www.ercmarket.com/UAVSYS-1200amp-power-distribution-board-pdb-for-industrial-uav/#tab_images[Date Accessed:13/06/2025]

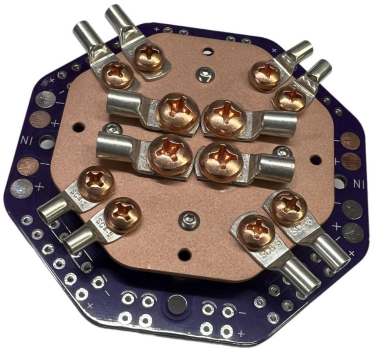

Figure 7.2: PDB-1000 from Avizar

In addition, to distribute power to the RADAR sensors a lower voltage and lower current carrying PDB is needed. This would be the SVPDB-8S from Mateksys [5] and can be seen in Figure 7.3. It costs €7.04 [13/06/2025], weighs 50 g and will be connected to five RADAR sensors.

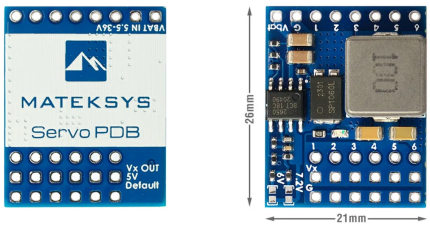

Figure 7.3: SVPDB-8S from Mateksys

Charging Procedure

Since the batteries charge at a rate of 2C, it would take them 30 minutes to fully recharge, computed by Equation 7.2. Assuming a per-mission time of 15 minutes, two spare battery packs would be needed for unlimited turn-arounds. However, since one battery pack could become defective, a spare battery pack is also accounted for. For this reason, four battery packs, each composed of eight batteries, each are considered. This yields a total cost of €12,620.16 for a set of 32 batteries, meaning a reduction of more than €3,000 with the new system.

The corresponding battery charger[6], depicted in Figure 7.4, can charge two batteries at a time, meaning 8 on-site chargers are required to maintain the availability of the system. This means €4,846.4 [17/06/2025] of costs for the chargers. The specifications are provided in Table 7.5. It must also be mentioned that the battery charger model remains unchanged compared to the initial setup as it is compatible with both batteries.

[5] https://www.unmannedtechshop.co.uk/product/matek-servo-pdb-with-4a-bec-5-5-36v-to-5-8-2v/[Date Accessed:13/06/2025]

[6] https://genstattu.com/tattu-dual-channelsmart-charger-60a-3200w-for-6s-14s-lipo-tattu-smart-battery/ [Date Accessed: 19/05/2025]

Figure 7.4: Grepow TA3200 charger

Table 7.5: Battery charger Specifications [15]

Specification	Value
Model No.	Grepow TA3200
Dimensions	$276 \times 154 \times 216$ mm
Charging Current	60 A
AC Input	100–240 V
Max Output Power	AC 100–110 V
Weight	6000 g
Cost	€ 605.80 [17/06/2025]

Power Subsystem Verification

A verification should be conducted on whether the specifications actually adhere to the requirements. This is mainly done by looking at the voltage and C-rate in Table 7.3. The voltage does meet the necessary motor requirements. Also, the average C-rate is found to be 2.877 /hr, which complies with the battery limit of 3 /hr. The maximum current per parallel string is thus $\frac{1}{4} \cdot 2.877$ /hr$\cdot 105.2$ Ah $= 75.7$ A, which stays correctly below the maximum motor current of 136 A. Furthermore, it can be seen that the maximum C-rate of 7.28 /hr also stays below the maximum C-rate that the battery system can deliver (10C).

It should only still be checked whether the battery has enough energy storage. For this, a rough estimate of the total energy consumption can be used based on the mission profile defined in Chapter 5. The most energy-intensive case is the hovering phase of 15 minutes or $t_{\text{hover}} = 900$ s. When assuming the average power of 26.88 kW, an estimate for the hover energy is found as Equation 7.3.

$$E = P_{\text{avg}} \cdot t_{\text{hover}} = 26880 \text{ W} \cdot 900 \text{ s} = 6.72 \text{ kWh} \tag{7.3}$$

Being conservative and considering that the rest of the mission is performed at full power, i.e. 72 kW. The total time of the ascent and descent phases is 84 seconds. Thus, the energy used during these maneuvers is given by:

$$E = 68000 \text{ W} \cdot 84 \text{ s} = 1.59 \text{ kWh}.$$

The energy consumption of the other systems is negligible compared to the hovering power; for instance, a pump of 2 kW for 30 seconds yields only 0.0167 kWh. Summing the relevant energy contributions yields a total of 8.31 kWh. Considering a depth of discharge (DoD) of 90%[7], the total

[7] https://www.teslaestorage.eu/en/battery-depth-of-discharge-dod-and-its-impact-on-lifespanhlbka-vybitia-baterie-a-jej-vplyv-na-zivotnost/ [Date Accessed: 21/05/2025]

battery capacity shall be at least 9.23 kWh. As can be seen in Table 7.3, this is sufficient. The estimate is conservative as the drone will likely not operate at maximum power for such a long period, while it also loses weight (water) during the flight. Hence, the energy requirement is, in reality, alleviated.

Although the power system sizing is mainly dependent on the motors, it is still an integral part of the control system as well. More specifically, the power system ensures that power is distributed over the important flight control components, while the control system sends signals utilizing this power. Therefore, the electrical diagram of the power system will be displayed in Chapter 8. Table 7.7 shows the compliance matrix of the system requirements. At this stage, most but not all requirements have been verified. The operational procedures still need to be verified by means of demonstration, checked as pending (P). The justifications, methods, and references are also found in the table.

7.4. Power Subsystem Budgeting

The power subsystem budget is presented in Table 7.6.

Table 7.6: Power Budgets

Component	Mass [kg]	Cost [€]	Power Required [W]
Battery (x8)	3.57	394.38	N/A
Spare Battery (x24)	N/A	394.38	N/A
PDB HV (x4)	0.300	349.00	N/A
PDB LV (x2)	0.050	7.04	N/A
Charger (x8)	N/A	605.80	N/A
Total	29.89	18876.64	N/A

Table 7.7: Compliance Matrix Power System

Identifier	Requirement Description	Check	Justification	Method	Reference
REQ-SUBSYS-PWR-1	The power system shall have redundant power paths between the battery and the other critical subsystems, such as the ESC.	✔	In the electrical diagram it was inspected wether redundant paths are present. The diagram shows that four independent battery strings directed to two ECS's each. Similarly, there are two separate power inputs to the flight controller.	Inspection	Section 8.6
REQ-SUBSYS-PWR-2	Failure of a singular battery cell shall not result in a complete loss of power.	✔	The electrical diagram shows that the failure of one cell, hence one battery back, only results in 25% loss of power. Three other battery packs are still available in this scenario.	Analysis	Section 8.6
REQ-SUBSYS-PWR-3	The battery system shall be continuously monitored during missions and reported to the drone operator.	✗	Current, the mass budget does not allow the addition of additional electronic units.	-	-
REQ-SUBSYS-PWR-4	The battery charging time to nominal voltage shall be maximum 30 minutes.	✔	The battery charging characteristics specify a charge rate of 2C, equivalent to 30 minutes. A demonstration will also be done to further verify this.	Demonstration, Inspection	Table 7.1
REQ-SUBSYS-PWR-5	The battery shall store a minimum of 9.23 kWh of energy.	✔	The battery characteristics show a per-battery capacity of 1.17 kWh, thus summing to 9.36 kWh for 8 batteries.	Inspection	Table 7.1
REQ-SUBSYS-PWR-6	The batteries shall be replaced within 60 seconds.	✔	This will be demonstrated by a trained operator.	Analysis, Demonstration	Section 5.4
REQ-SUBSYS-PWR-7	The battery charging system shall comply with the current fire truck connections.	✔	The standard fire trucks are equipped with a 230 VAC Dynawatt Unit. This corresponds with the charger working range of 100-240 V. A demonstration will also be performed.	Demonstration, Inspection	SFS International[8]
REQ-SUBSYS-PWR-8	The maximum current through the battery connections shall not exceed 263 A.	✔	The power system analysis showed that the maximum current drawn from two motors is 191.5 A. The power draw of other electronics are significantly smaller, meaning the total sum will not exceed 263 A. A controlled test will also be done.	Test, Analysis	Section 7.3, Table 8.2
REQ-SUBSYS-PWR-9	The battery operating temperature shall remain within −40°C and 60°C.	✔	The temperature analysis showed an operation at maximum 60 degrees. Also, the batteries will not discharge at their maximum C-Rate, effectively reducing the temperature. The temperature will also be measured during a test.	Test, Analysis	Figure 5.4, Table 7.3

[8] `https://www.sfsinternational.nl/verhuur/voertuigen` [Date Accessed: 16/06/2025]

8. Control Subsystem

The control subsystem encompasses hardware components, namely the autopilot and accompanying sensors, as well as software, represented by the in-flight control law, sensor drivers and algorithms for emergency procedures and autonomous operations.

8.1. Requirements Assessment

The requirements for the control subsystem stem from stability and control concerns, but also from considerations related to the communication between the operator and the UAV, as well as autonomous capabilities and features requested by the Gezamenlijke Brandweer. The requirements are derived from subsystem requirements:

- **REQ-SUBSYS-CTRL-1**: The control subsystem shall keep the UAV stable when expelling fire retardant.
- **REQ-SUBSYS-CTRL-2**: The control subsystem shall provide a horizontal force equal to 123 N.
- **REQ-SUBSYS-CTRL-3**: The control subsystem shall provide a vertical force equal to <TBD> of the water expelling force.
- **REQ-SUBSYS-CTRL-4**: The onboard computer shall record 8 channels of data.
- **REQ-SUBSYS-CTRL-5**: The onboard telemetry shall transmit the recorded channels to a ground station continuously during the mission.
- **REQ-SUBSYS-CTRL-6**: The control subsystem shall keep the UAV stable in wind conditions up to 6 Bft.
- **REQ-SUBSYS-CTRL-7**: The control subsystem shall execute a pre-established emergency procedure when a fault is detected.
- **REQ-SUBSYS-CTRL-8**: The control subsystem shall land the UAV autonomously in case of signal loss or motor failure.
- **REQ-SUBSYS-CTRL-9**: The control subsystem shall send an error warning in case of non-critical component faults or failures.
- **REQ-SUBSYS-CTRL-10**: The control subsystem shall have the option of autonomous landing upon operator input.
- **REQ-SUBSYS-CTRL-11** The control subsystem shall keep the UAV stable and controllable with one engine inoperative.
- **REQ-SUBSYS-CTRL-12**: The control subsystem shall be able to override operator input in order to avoid in-flight collisions.
- **REQ-SUBSYS-CTRL-13**: The control subsystem shall keep the UAV stable and controllable during weight and center of gravity location changes.

Owing to the lack of detail in the design at the conceptual stage, some of the requirements were left as <To-Be-Determined>. In the following sections, uncertainties in requirements will be settled considering advancements made in the design of other subsystems. Also, the compliance matrix is correspondingly shown at the end of the chapter, filled in with supporting justifications for the current or planned fulfillment of each requirement.

8.2. Preliminary Selection

Given these requirements, the following elements of the control subsystem were chosen based on Design Option Trees and established trade-offs in the mideterm report [3]:

- In-flight control law: Augmented flight;

Direct control of the UAV is left to the operator, but some procedures and operations are automated. This was considered to be the only viable option, as the customer requires an operator-controlled UAV, while completely manual control might be complex during certain maneuvers. The augmentations will be detailed in the following subsections.

- Control Variable: Motor rotational rate;

  This was compared to other options, such as controlling the propeller pitch or the motor axis direction. This was chosen as it is the most straightforward and is the standard for modern multicopters. The other options require complicated mechanisms, which increase the overall weight and lead to reliability concerns. Therefore, controlling the rotational rate was adopted for this case, with the motors being controlled by Pulse Width Modulation (PWM) signals.

- Emergency procedure: Autonomous landing;

  In case a critical fault is detected on-board the UAV or if the operator chooses to do so, the UAV will immediately return to the landing spot autonomously. This was preferred over the option of having a killswitch and deploying a parachute, since that does not allow for any control over the landing area. The definition of a critical fault and detailing of this emergency procedure is tackled in the following subsection.

- Autonomous landing guidance: GPS guidance;

  The UAV will be capable to 'return to base' and land on its own, requiring the operator to provide a landing spot. This was chosen following a trade-off against the option of guidance using Radio Frequency (RF) beacons. The GPS emerged as the winner especially due to the better accuracy, but also owing to a lower set-up time. This functionality demands accurate GPS sensors, which will be detailed later in this chapter.

- Obstacle Avoidance: RADAR sensors;

  RADAR sensors were chosen following a trade-off against LiDAR (laser) and SONAR (sound waves). LiDAR sensors were considered unsuitable for the UAVs operations mainly because of their limited performance in smoke and fog, which are expected to be encountered during a normal mission. SONAR sensors, on the other hand, were surpassed by the RADAR considering their short range, in the order of a few meters. In the following subsections, a RADAR system is detailed.

The high-level decisions made during the conceptual design stage, resulting in the previously mentioned options, do not offer sufficient detail. Therefore, specific components were chosen for the control system.

8.3. Software, Flight Modes and Special Functionalities

Before detailing the physical components that make up the control subsystem, the working modes of the drone need to be addressed first. This includes the software, the flight modes and any special functionalities that the drone should fulfill.

8.3.1. Selected Autopilot Software

Using open-source autopilot software was considered as the only choice taking into account the nature of the UAV's mission and the limited resources of the project. This solution is cost-effective and bypasses the effort and complexity involved in designing an autopilot from the ground up, while enabling augmentations to the code to include new functionalities.

The choice was made between the two most popular open-source flight control software platforms: PX4 [1] and ArduPilot [2]. Their popularity implies that they are tried-and-true options, giving confidence in the safety of the drone's operations. Both autopilots support various UAV configurations, including

[1] `https://px4.io/` [Date Accessed: 10/06/2025]

[2] `https://ardupilot.org/` [Date Accessed: 10/06/2025]

the X8. In general terms, the main difference between the two autopilots is that ArduPilot is oriented more towards hobby applications, with a large supporting community and a focus on ease of use, while PX4 is considered to be more flexible for specialized applications and offers more advanced autopilot features, being more prominent in industry [3]. Licensing is also different between the two, as ArduPilot requires any modifications done to the base code to also be made open-source. Both autopilots, however, are customizable, which make them good choices.

Considering the more specific application of the UAV, which puts the emphasis on the flexibility of the software, but also taking into account the automated features desired by the client, the PX4 Autopilot was selected. While augmenting the software with supplementary features is possible, PX4 already includes functionalities that are considered important for the mission of the drone, such as support for various flight modes, as explained in in the following section. The full documentation of the software can be found on the PX4 website. Nevertheless, a high-level block diagram displaying the main functionalities of the software as well as interrelations can be seen in the Software Block Diagram.

8.3.2. Flight Modes and Phases

The mapping from the control input of the ground operator to the change in control variables make the object of the flight modes. They can be tailored to each mission phase and many autopilots including PX4, come with configured manual or autonomous modes.

An example of flight mode is one that takes stick inputs for roll or pitch and outputs roll or pitch angles, as shown in Figure 8.1. Another flight mode may output position instead of rotational angles, making it more comfortable for an unexperienced operator but less maneuverable for an experienced one. To match the level of experience expected from a ground operator of a commercial drone, a relatively flexible manual flight mode will be considered.

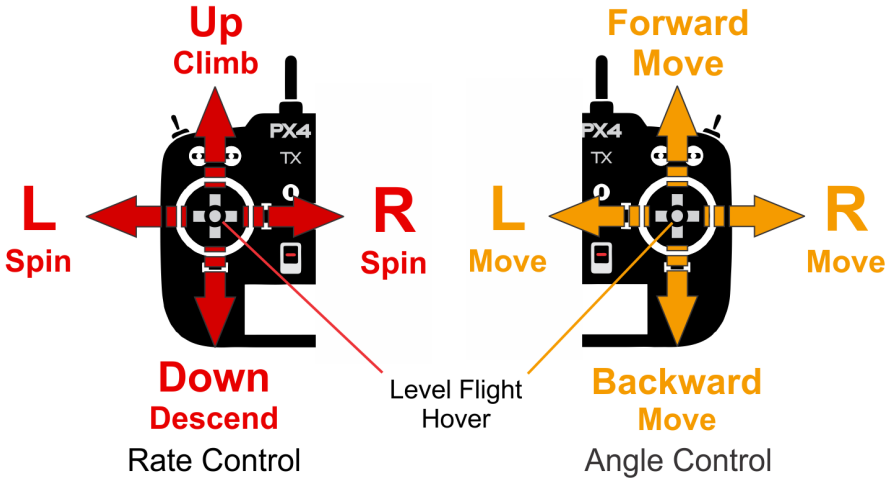

Figure 8.1: Control mapping of the Stabilized flight mode used within PX4

Specifying the suitable flight modes first requires a definition of the flight phases that the drone will operate throughout a typical mission. A typical mission is composed of the phases presented in Section 5.3. Moreover, two emergency phases have also been considered for the types of malfunctions considered in Section 8.7:

- Emergency return to take-off spot - in case of non-critical malfunctions;
- Emergency landing on present position - in case of critical malfunctions.

[3] `https://www.thedroningcompany.com/blog/px4-vs-ardupilot-choosing-the-right-open-source-flight-stack` [Date Accessed: 10/06/2025]

Communications \ Data Handling Block Diagram

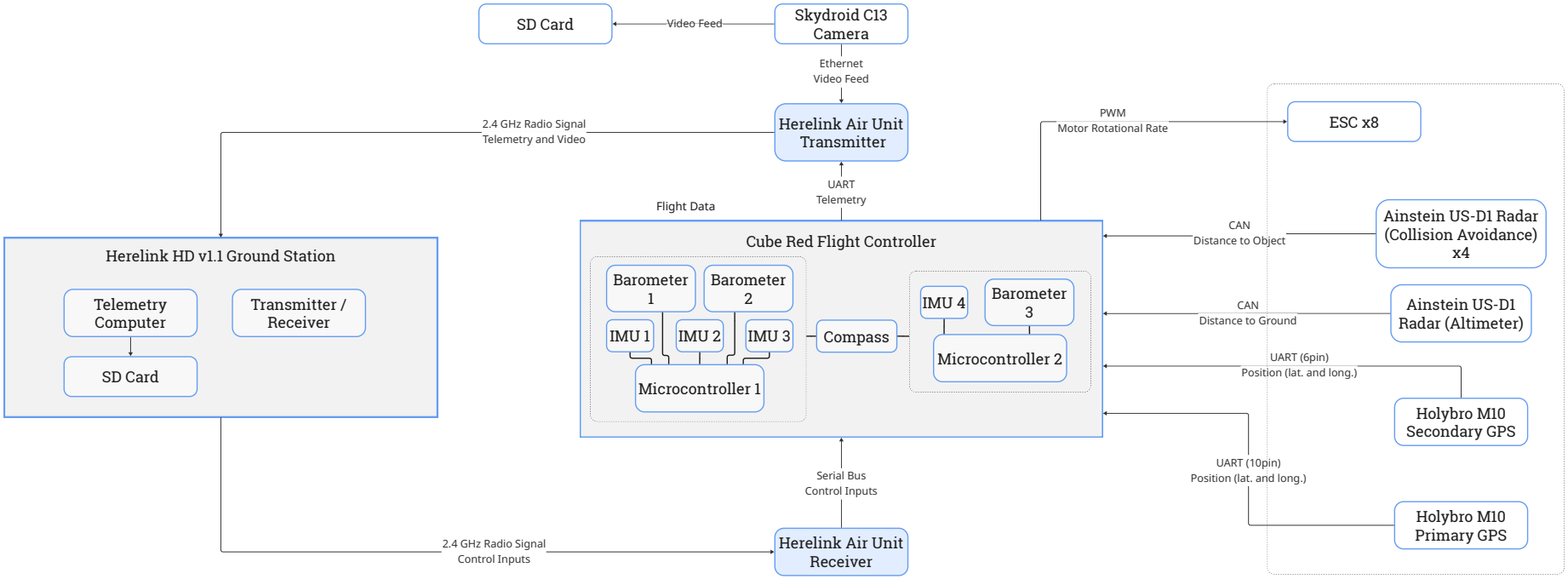

Software Diagram

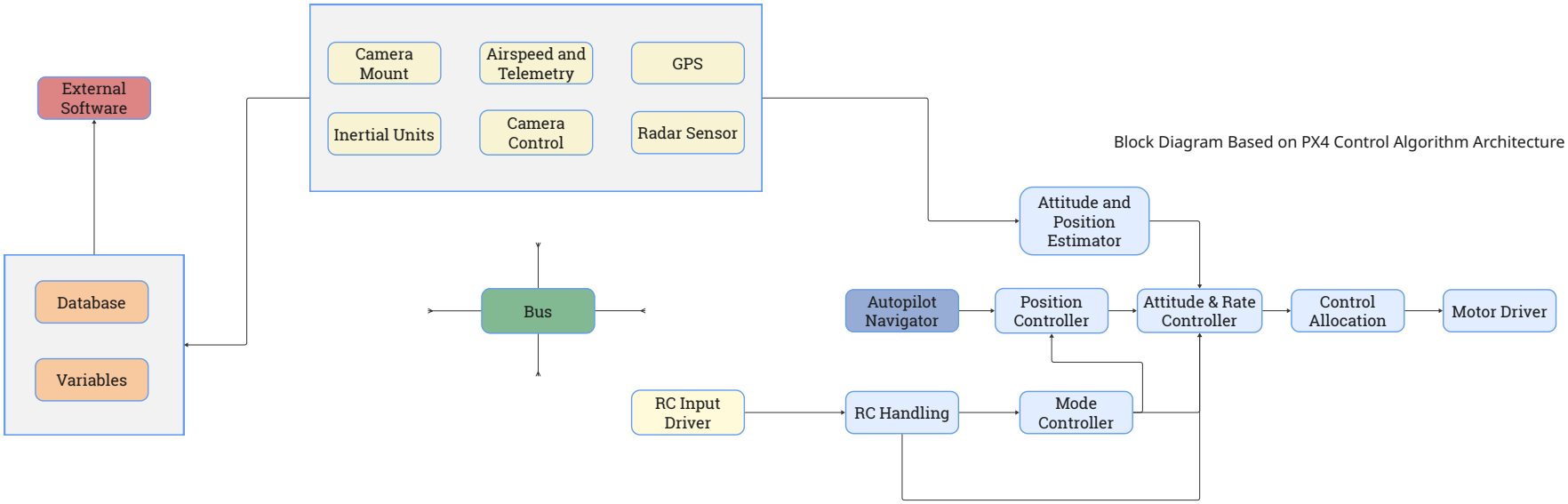

With the flight phases established, the flight modes tasked with taking inputs and outputting a certain maneuver can be discussed. All of the flight modes needed for performing both a normal mission and an emergency procedure are shown below and can be found among the modes that come pre-programmed in the PX4 software.

Manual flight mode
As mentioned at the beginning of this subsection, the selected flight mode sits closer to the difficult end of the manual flight modes. The Stabilized mode[4] takes the throttle, yaw, pitch and roll inputs and outputs rate changes in altitude and yaw, and angles of pitch and roll respectively. The drone will also climb/descent depending on the last received input.

Augmented flight mode
In order to reduce workload for the operator and improve safety, it was decided that a water spraying or dropping maneuver should be accompanied by an augmentation from the flight computer. For this purpose, the Hold mode[5] of the PX4 has been selected. This mode simply maintains the drone's altitude (based on a barometer reading) and horizontal position (based on GNSS), under external forces. As long as the drone is controllable (analysis shown in Section 8.4), it is assumed that the onboard flight controller is able to perform the required maneuver with the available thrust. Any operator input will disengage this mode and revert to the manual flight mode.

Fully-autonomous mode
Two emergency flight modes have been assessed to match the distinction made in Section 8.7: the Return mode[6] which would activate in case of non-critical faults. Once activated (automatically or manually), the drone will be maneuvered towards the take-off position and land fully-autonomously. In case of control-critical faults, the Land mode[7] takes over and autonomously lands the drone while keeping it still in space. From its definition, a critical fault endangers the drone's ability to be controlled, hence landing immediately may be desired over maneuvering to the take-off spot.

Any input from the ground controller is passed through a PID (Proportional, Integral, Derivative) controller that converts the input to an output for each motor according to the set flight law. Without such controller, small disturbances would make the drone unstable and would make for a vehicle hard to control for ground operators. PID controllers are set-up automatically by the PX4 software, but can also be fine-tuned to better tailor the vehicle to the desired control characteristics [8].

8.4. Controllability and Stability Characteristics

The controllability of an aircraft is defined as the ability to perform the desired maneuver, while stability is defined as the ability for the aircraft to return to a balanced flight after being subjected to a force or moment disturbance. Unlike fixed-wing aircraft which can be designed to be stable depending on sizing and positioning of the wing, fuselage, engines and empennage, rotorcraft and multicopters are naturally unstable. Without a flight management computer inputting control commands or significant intervention from the pilot, a hovering aircraft will not return to an equilibrium state given by hovering with no angular speed around its axes [16].

The controllability of a multicopter is highly dependent of the selected configuration. More motors allow for finer and more power-efficient maneuvers, through smaller control inputs distributed over a larger number of engines. In general, an increased number of motors is also more fault tolerant, depending of the motor positioning.

This section will delve into the controllability characteristics of the UAV, based on methods for determining multicopter controllability presented by Quan Quan [16] [17]. The controllability is analyzed about an equilibrium (hovering) state, with a few assumptions. These assumptions are:

[4] https://docs.px4.io/main/en/flight_modes_mc/manual_stabilized.html [Date Accessed: 17/06/2025]
[5] https://docs.px4.io/main/en/flight_modes_mc/hold.html [Date Accessed: 17/06/2025]
[6] https://docs.px4.io/main/en/flight_modes_mc/return.html [Date Accessed: 17/06/2025]
[7] https://docs.px4.io/main/en/flight_modes_mc/land.html [Date Accessed: 17/06/2025]
[8] https://docs.px4.io/main/en/config_mc/pid_tuning_guide_multicopter.html [Date Accessed: 18/06/2025

- The center of gravity and moment of inertia coincide;
- The drone is free to rotate around all three axis (X - roll, Y - pitch, Z - yaw) and free to move vertically (Z axis). No maneuvers in the X and Y axes will be analyzed;
- All motions are decoupled, meaning motion in one axis does not cause a force or rotation in or around any other action; this is true for most symmetrical drone designs [16];
- The rotation angles are small and the small angle approximation can be used without a significant loss in accuracy [16];
- No interactions between motors that could reduce thrust occur.

The analysis starts from a linear time-invariant system, in Equation 8.1.

$$\dot{\mathbf{x}} = A\mathbf{x} + B\mathbf{u}, \tag{8.1}$$

Where $\mathbf{x} \in \mathbb{R}^n$ is the state vector and $u \in \mathbb{R}^{n\times n}$ is the control vector, while $A \in \mathbb{R}^{n\times n}$ and $B \in \mathbb{R}^{n\times n}$ are coefficient matrices. For a multicopter in hover, the dynamic model becomes the one represented in Equation 8.2.

$$\dot{\mathbf{x}} = A\mathbf{x} + B(\mathbf{u}_f - \mathbf{g}), \tag{8.2}$$

Where:

$$\begin{aligned}
\mathbf{x} &= [p_{z_e}\ \phi\ \psi\ v_{z_e}\ \omega_{x_b}\ \omega_{y_b}\ \omega_{z_b}]^T \in \mathbb{R}^8 \\
\mathbf{u}_f &= [f\ \tau_x\ \tau_y\ \tau_z]^T \in \mathbb{R}^4 \\
\mathbf{g} &= [mg\ 0\ 0\ 0]^T \in \mathbb{R}^4 \\
A &= \begin{pmatrix} 0_{4\times4} & I_4 \\ 0_{4\times4} & 0_{4\times4} \end{pmatrix} \in \mathbb{R}^{8\times8} \\
B &= \begin{pmatrix} 0_{4\times4} \\ J_f^{-1} \end{pmatrix} \in \mathbb{R}^{8\times4} \\
J_f &= \text{diag}(-m,\ J_{xx},\ J_{yy},\ J_{zz}) \in \mathbb{R}^{4\times4}.
\end{aligned}$$

A and B are coefficient matrices, in which J_f is the diagonal matrix composed of the mass and the mass moments of inertia about the body axes. As for $\mathbf{x}$, it is the state vector composed of the z-position, pitch, roll and yaw angles about the body axes, as well as the pitch, roll and yaw rates.

More background is required on how the force vector $\mathbf{u}_f$, composed of the vertical (z-axis) resultant force f and the resultant pitch, roll and yaw moments *induced by the propellers*, is defined. $\mathbf{u}_f \in \Omega$, where:

$$\Omega = \{\mathbf{u}_f \mid \mathbf{u}_f = B_f\mathbf{f},\ \mathbf{f} \in \mathcal{U}_f\}$$

In this definition, $\mathbf{f} = [T_1 \dots T_n]$ is the propeller thrust, with $T_i \in [0, K_i]$, K_i being the maximum thrust of each motor. It is important to mention that the propellers are assumed to only provide unidirectional thrust, either in the positive or negative z-axis direction (in this case - negative z direction). The set $\mathcal{U}_f$ is the infinite cartesian product of all the intervals $[0, K_i]$. As for the matrix $B_f \in \mathbb{R}^{4\times m}$, it is referred to as the *control effectiveness matrix*. In parametrized form, it is:

$$B_f = \begin{pmatrix} \eta_1 & \dots & \eta_n \\ -\eta_1 d_1 \sin\varphi_1 & \dots & -\eta_n d_n \sin\varphi_n \\ \eta_1 d_1 \cos\varphi_1 & \dots & \eta_n d_n \cos\varphi_n \\ \eta_1 k_\mu \sigma_1 & \dots & \eta_n k_\mu \sigma_n \end{pmatrix} \tag{8.3}$$

in which the $\eta_i \in [0,1]$ are parameters used to take into account the wear or failure of each motor, $k_\mu = C_M/C_T$ is the ratio between the reaction torque generated by the motors and their thrust, d_i are distances from the center of gravity to the UAV to the propellers and φ_i are the angles between the coordinate system y axis and the radii extending to the propellers. The angles and distances can be seen in Figure 8.2, with the mention that r_m is equivalent with d_m in the figure. Therefore, by taking the product of the motor thrust vector $\mathbf{f}$ with the control effectiveness matrix, the vertical force as well as the pitch, roll and yaw moments generated by the propellers are obtained in the vector $\mathbf{u}_f$. Moreover, the difference $\mathbf{u}_f - \mathbf{g}$ represents the control vector $\mathbf{u}$ from Equation 8.1.

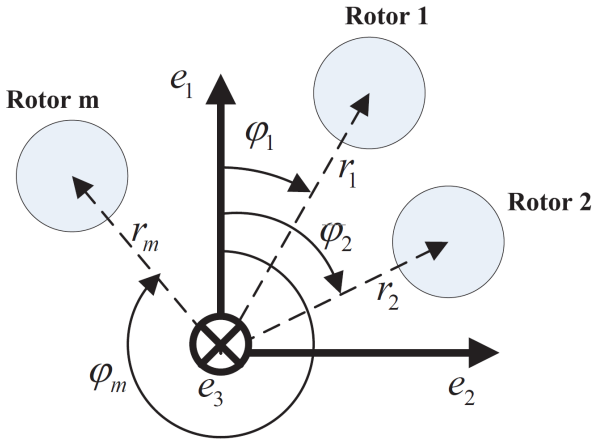

Figure 8.2: Geometry definition used for the controllability model [17]

From theory [16], the controllability matrix pertaining to the system Equation 8.2 can be defined as:

$$C(A,B) = [B \; AB \dots A^{n-1}B] \tag{8.4}$$

The theory of *classic controllability* states that the system depicted in Equation 8.2 is controllable if and only if the controllability matrix C is of full rank: $\text{rank}\, C(A,B) = n$. However, this criterion was proven to be necessary, but not sufficient to describe the complete controllability of a multicopter. It was shown by Guang-Xun Du [18] that, in spite of the controllability matrix being of full rank, a standard configuration hexacopter was uncontrollable after one rotor had failed.

As a more suitable alternative to the classic framework, a *positive* controllability theory is proposed by Quan Quan [17]. The theorem obtained is that "the following conditions are necessary and sufficient for the controllability of the system":

(i) Rank $C(A,\ B) = 8$, where $CA,\ B = [B \; AB \dots A^7 B]$

(ii) There is no real eigenvector $\mathbf{v}$ of A^T satisfying $\mathbf{v}^T B\mathbf{u} \leq 0$ for all $\mathbf{u} \in \mathcal{U}$"

In this theorem, $\mathcal{U} = \{\mathbf{u} \,|\, \mathbf{u} = \mathbf{u}_f - \mathbf{g}, \mathbf{u}_f \in \Omega\}$, where Ω is the set of all force vectors $\mathbf{u}_f$.

However, testing for the condition above is not practically possible, since one would have to test point (ii) for all possible values of $\mathbf{u}$. Another condition, equivalent with (ii), which can be tested for easier, can be formulated by defining the following measure:

$$\rho(\mathbf{a}, \partial\Omega) \triangleq \begin{cases} \min\{\|\mathbf{a}-\mathbf{b}\| : \mathbf{a} \in \Omega, \mathbf{b} \in \partial\Omega\} \\ -\min\left\{\|\mathbf{a}-\mathbf{b}\| : \mathbf{a} \in \Omega^C, \mathbf{b} \in \partial\Omega\right\} \end{cases} \tag{8.5}$$

Where $\delta\Omega$ is the boundary of the set Ω and Ω^C is the complementary set of Ω. This is called Available Control Authority Index (ACAI). It is a unitless parameter dependent on the mass, moments of inertia, position of c.g., arm length, motor positioning, motor thrust, motor-induced moment and disturbances in the form of Z forces or X, Y, Z moments. This parameter is used to determine whether the drone is controllable, which is the case if and only if:

$$\rho(\mathbf{g}, \partial\Omega) > 0$$

The measure $\rho(\mathbf{g}, \partial\Omega) = \min\{||\mathbf{g} - \mathbf{u}_f||, \mathbf{u}_f \in \delta\Omega\}$, which is the radius of an enclosed sphere with the center at $\mathbf{g}$, can be interpreted as the maximum control thrust or moment that can be generated in all directions. Therefore, it can be used to measure the available control authority of the system *after the disturbance* $\mathbf{g}$ is compensated for.

The algorithm for obtaining the ACAI is described in detail by Quan Quan [17]. This procedure was implemented in a Python script which would take all of the above-mentioned parameters as input and output the ACAI.

Verification of the code at a system level was conducted by directly comparing the results obtained through implementation of the algorithm to the results presented by Quan Quan [17] in the case of a **hexacopter** with equidistant and equiangular motors arranged in two configurations: *PNPNPN* and *PPNNPN*, where *P* denotes an anti-clockwise rotation and *N* denotes a clockwise rotation of the motor.

Having verified the algorithm, it can be applied to the present configuration of X8. The ACAI of the drone will be tested under multiple situations: simply hovering, flying with a speed of 15 m/s and spraying water, thus having to stabilize an imposed moment around the X or Y axis, and finally hovering with a shift in center of gravity, representing the situation when water has been released.

It is known from Section 9.2 that the spraying action causes a moment given by the force at the nozzle exit with a value of:

$$M_y = F \cdot d = \dot{m} \cdot v \cdot d = 150 \, \frac{\text{L}}{\text{min}} \cdot 8.13 \, \frac{\text{m}}{s} \cdot 0.66 \text{ m} = 13.4 \text{ Nm} \tag{8.6}$$

Where $\dot{m}$ is the mass flow rate of the water, v is the velocity of the water at the nozzle exit and d is the arm-length, taken from the nozzle exit to the top of the drone to assume a worst-case scenario where the c.g. is the furthest away from the spray of water. In Section 5.3 the drag force is also simulated for different approximations of drone shape. The worst result of 103 N is given by simulating the drag of a cube with 4 arms of the same dimensions of the drone. The moment disturbance is then given by:

$$M_y = F \cdot d = 103 \cdot 0.9 \text{ Nm} = 92.7 \text{ Nm} \tag{8.7}$$

Once again Summing the two results, the moment disturbance that should be counteracted by a stable drone is ≈ 106 Nm. This value around the X or Y-axis will be considered for the ACAI analysis.

8.4.1. Inoperative Engine Redundancy

An important consideration regarding controllability is the behavior of the UAV if one or more motors fail. A motor or rotor failure can occur due to an electrical or motor fault, but can also be caused by debris from the fire hitting the drone or by collisions. Therefore, it is expected that the UAV will deal with inoperative motors in flight during its lifetime. It is thus important to consider the ACAI with different combinations of motors non-operational and check whether the UAV is still controllable. The ACAI values are presented in Table 8.1, with the subscripts i of μ_i corresponding to the motor numbering in Figure 6.1:

Table 8.1: ACAI results using own implementation with no disturbance and a moment disturbance M_x

Case Nr.	Configuration	ACAI (no disturbance)	ACAI (M_x or M_y disturbance)
1	No failures	100.4	99.81
2	$\mu_{1...8} = 0$	54.16	45.64
3	μ_1, $\mu_6 = 0$	0	0
4	μ_1, $\mu_4 = 0$	54.16	45.64
5	μ_1, $\mu_7 = 0$	0	0
6	μ_1, $\mu_3 = 0$	8.040	8.040
7	μ_1, $\mu_8 = 0$	0	0
8	μ_1, μ_2, μ_3, $\mu_4 = 0$	7.989	0

Owing to symmetry, only a part of the total possible cases need to be analyzed: for example, motors 1 and 6 being inoperative is the same case as turning off motors 4 and 7.

In cases 2 and 4, the UAV is not completely controllable any longer. Even though there are 6 motors still available, with enough thrust over weight ratio to maintain the UAV in the air (1.5975), the layout of the remaining motors does not allow for complete control. More exactly, there exists a desired force vector $\mathbf{u}_f$ for which there is no combination of thrust values of remaining motors $\mathbf{f}$ to obtain it.

In spite of this, it can be still possible to land the UAV safely, by means of *relaxing the control constraints*: while a mapping from the vector $\mathbf{f}$ to the full vector $\mathbf{u}_f = [f \ \tau_x \ \tau_y \ \tau_z]$ may not exist, disregarding one of the elements of $\mathbf{u}_f$ might make the mapping possible. As stated by Mark W. Mueller [19] it was proven through simulations and, partially, through experiments, the capability of a quadcopter to reduce position error and maintain *position* stability even with only one motor functional, by giving up yaw, pitch and roll authority, progressively.

The same procedure can be applied to the UAV being designed. In case two, when the motors on the same arm fail, the situation is equivalent to a quadcopter with one failed motor. Therefore, yaw authority can be abandoned in order to be able to control the vertical force, pitch and roll. The UAV would spin about the z-axis, but would be able to change its position and descend vertically to land. Regarding case four, with motors failing on adjacent arms but different layers, an imbalance in reaction torques is created, as more motors will spin in one of the two possible directions. This indicates that yaw authority is also easiest to renounce, as well as being convenient.

According to the results of Mark W. Mueller [19], it is possible to control the position of the UAV even when more than two motors have failed on different layers. However, this case was not considered, as the failure of this many motors would be very improbable or would imply a severe collision, such that the structural integrity of the UAV itself and the ability to salvage it would become questionable.

8.4.2. Center of Gravity Excursion

Another important aspect of the controllability of the drone is its allowed c.g. excursion, both under normal conditions and one engine inoperative conditions. To find this, the c.g. was assumed to be in the middle of the X-Y plane as shown in Figure 6.2, with any excursion taken around this point. The results illustrate c.g. values at MTOW that would allow the drone to be controllable with no engine inoperative and one engine inoperative respectively.

No engine inoperative

C.g. excursion has been tested within the outline the body of the drone (excluding arms and water nozzles), which is ≈ 700x700 mm in size as seen from the XY plane. Thus x and y values are allowed to vary according to $(x, y) \in [-350, 350]$ x $[-350, 350]$ mm. With all engines operative, the plot in Figure 8.3 are obtained. Having in mind that the batteries and the water tank are placed symmetrically in the XY-plane, c.g. excursions close to the limit have no purpose other than testing the continuity of the curve, as the c.g. position is very unlikely to occur in such an extreme place.

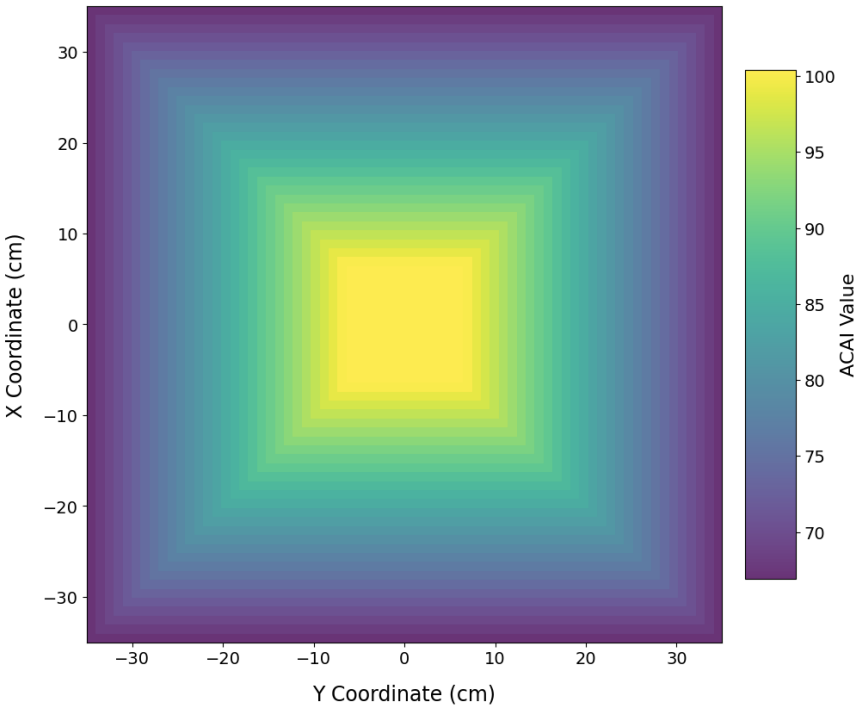

Figure 8.3: ACAI as a function of the center of gravity position in the XY plane with all engine working

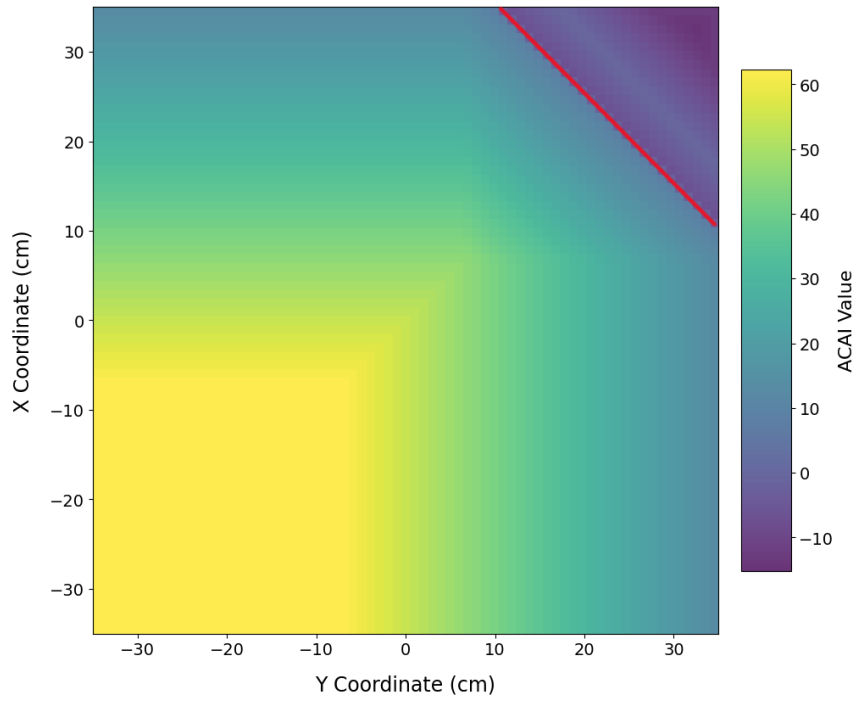

Figure 8.4: ACAI as a function of the center of gravity position in the XY plane with engine no. 1 inoperative

One engine inoperative

One inoperative engine will naturally result in a less controllable drone, but the c.g. position heavily influences the controllability, with a lower ACAI obtained for a c.g. that is closer to the inoperative engine. This bias is explained by the fact that the affected arm has less thrust authority for keeping the drone in air. Moreover, any imbalance in Z-moment caused by the working engine on the affected arm has to be counteracted by the remaining engines, decreasing the potential total efficiency. These ACAI results for this scenario can be found in Figure 8.4.

The figure clearly shows a few things: the easiest to understand is perhaps the decrease of ACAI along the $X = Y$ line, which is consequence of the inability to control the mass concentrated close to one engine. After a certain line, illustrated in red, the ACAI dips suddenly under zero, meaning that the drone is no longer controllable with the c.g. situated in the violet region. Another takeaway from the figure is that the ACAI reaches a plateau when the c.g. is moved far enough from the inoperative motor. This plateau has a smaller value than was the case for the scenario of all working engines. This is most likely due to having a reduced amount of total thrust, together with the limitation imposed by the asymmetric moment distribution, limiting the amount of thrust that can be produced by the remaining engines.

8.5. Hardware Component Selection

In the preliminary selection conducted in the midterm review [3], choices were made on a conceptual level. It is now possible to make choices for actual subsystem components and fit them together.

Flight Controller and Carrier Board

The flight controller, considered the "brain" of a drone, is a circuit board that contains a central processor, tasked with running the autopilot, but also various sensors, such as Inertial Measurement Units (IMUs) or a compass, and even communication modules.

Because the flight controller incorporates all the functionalities of the drone, it is connected to other sensors, as well as the ESCs and controls for the payload. The control interface is provided by the carrier board. If an analogy to a personal computer is made, the carrier boards represents the motherboard on which the processor (flight controller) and other components are mounted.

There are various flight controllers that support the PX4 autopilot. Because the drone is expected to operate in a harsh environment, with high temperatures that may affect sensors or even the processor itself, a flight controller with a high degree of redundancy is desired. Consequently, the Cube Red Flight Management Unit was chosen [9]. It is a professional flight management unit (FMU) manufactured by CubePilot, aimed at industry or military applications. The Cube Red was chosen for the following functionalities, specified by the manufacturer:

- Dual microprocessors: the Cube Red is marketed as a dual FMU. It houses two microcontrollers, separated into a primary and a secondary. In spite of the secondary microprocessor having fewer interfaces, it is capable of control of the UAV in case the primary suffers a failure. The microprocessors also support ambient temperatures of up to 125 degrees Celsius;
- Quadruple IMU Redundancy: the first microprocessor is linked to three IMUs, while the fourth IMU is linked to the second microprocessor;
- Compass and three barometers: two barometers are associated to the primary microprocessor and one is linked to the secondary microprocessor.

[9] `https://docs.cubepilot.org/user-guides/autopilot/cube-red`[Date Accessed: 02/06/2025]

Figure 8.5: Cube Red

The full specifications of the Cube Red flight controller can be found on the CubePilot manufacturer website [10]. Together with the flight controller, a compatible carrier board must also be chosen. Due to the dual DF-17 interface, the choice was limited to the Cube Red Standard Carrier Board [11], also manufactured by CubePilot. The board boasts a large number of interfaces, including, among others, two GPS ports and three CAN ports useful for the RADAR system. The board's pinout is available on the manufacturer's website and the board, together with the Cube Red mounted on it, can be seen in Figure 8.5. The combination of Cube Red flight controller and Cube Red Standard Carrier Board is also available for purchase as the Cube Red Pro Standard Set [12].

Transmitter, Remote Controller and Ground Station

The next components to be chosen is the RC transmitter/receiver, as the flight controller does not account for ground communication, but also the ground station for telemetry and the UAV remote control. There are many options on the market for these components, while the following features are desired:

- Integrated control, camera and telemetry;
- A high number of transmission channels or configurable buttons: four channels are required for additional controls, one for flight mode selection and two more for the payload;
- A low latency of data transmission with a high transmission power. A strong signal allows for a reliable connection even when the line-of-sight is temporarily broken by small objects.
- Flexible firmware: since the UAV will have additional controls for the payload which are not typical for drones, it is expected that the new controls need to be integrated with the firmware;

These being considered, the Herelink v1.1 [13] system was selected for this purpose. Like the Cube Red[14], it is manufactured by CubePilot and it is described by the manufacturer as "an integrated remote controller, ground station and wireless digital transmission system designed to be used with Cube Autopilot, Ardupilot or PX4". The Herelink consists of a controller and an onboard transmitter called an "airunit".

The transmission frequency band is 2.4 GHz, with a bandwidth of 20 MHz. The maximum unobstructed transmission distance is 20 km. The controller integrates a 5.46 inch touchscreen that can be used for telemetry and displaying HD video, but also for additional controls. The controller also has six configurable physical buttons, which can be used for payload controls. Full specifications are available

[10] https://docs.cubepilot.org/user-guides/autopilot/cube-red/specifications[Date Accessed: 02/06/2025]

[11] https://docs.cubepilot.org/user-guides/~/changes/mvMsnRI8xnoKpbe3XhLK/carrier-boards/cube-red-standard-carrier-board-pinout[Date Accessed: 02/06/2025]

[12] https://irlock.com/products/cube-red-standard-set-beta-version?srsltid=AfmBOoqE-qcqhiMC6BUvVvsqry_mTKH3CSTSXXAPiWDxLRrHLCv8SIQC[Date Accessed: 02/06/2025]

[13] https://docs.cubepilot.org/user-guides/herelink/herelink-overview[Date Accessed:02/06/2025]

[14] https://www.airbot-systems.com/produit/cube-red-pro-standard/?lang=en#1711023598426-ef4ea08e-2ec3[Date Accessed:02/06/2025]

on the CubePilot website[15].

GPS Sensors

For positioning, it has been determined that Global Positioning System (GPS) sensors are used. Multiple GPS sensors are desired in the design for instance for redundancy. Moreover, multiple sensors would mitigate the problem of signal jamming through sensor fusion [20]. This is especially critical during maneuvers where obstacles could block the signal.

The model chosen which fit the characteristics above while being lightweight is M10 GPS from Holybro [16] which can be used for the four main Global Navigation Satellite System (GNSS) constellations: GPS, Galileo, GLONASS, and BeiDou opening the drone for other countries' markets. Two units can be used: one is a 10-pin model that includes a light and a buzzer for the purposes of relaying information about the system and a 6-pin model that simply works as a GPS sensor.

Figure 8.6: M10 GPS

The M10 GPS also has a high operating temperature of 80ºC. The total weight of one GPS module is 32 g. With dimensions of 50 mm in diameter and 14.4 mm in height. Also, the power consumption is small, as it operates with 200 mA at 5 V. The full list of specifications is available on the manufacturer's website. The GPS module can be seen in Figure 8.6.

RADAR Sensor System

The final hardware component to be chosen is the RADAR system, used for collision avoidance as well as determining the altitude. There are various options for RADAR altimeters on the market. For collision avoidance, on the other hand, most available systems consist of LiDAR, with few RADAR options and even fewer for which prices or quotes are available.

At the same time, the difference between RADAR altimeters and RADAR collision avoidance sensors is on the level of firmware, which is modifiable. Therefore, it was assumed that is is possible to use RADAR altimeters also for collision avoidance, with appropriate firmware modifications. This simplifies the problem and enables searching for only one RADAR sensor model.

When searching for a sensor, the characteristics considered desirable are:

- Large Field-of-View: this is especially advantageous for collision avoidance, since fewer sensors can be used, translating to a less complex design, a smaller weight and a smaller power consumption. The problem of enough ports on the carrier board must also be considered;

[15] `https://docs.cubepilot.org/user-guides/autopilot/cube-red/specifications`[Date Accessed: 02/06/2025]

[16] `https://holybro.com/products/m10-gps?srsltid=AfmBOoo9Bp2S7zQI2Vz3Y6felThZfpe-DiEAqGOHI9WE9_sP0Aa1GppI` [Date Accessed:05/06/2025]

- Large range: a range in the order of 100 meters allows for a prompt response of the collision avoidance system and thus the UAV can fly at higher speeds;
- High update rate: this is a characteristic that is relevant for fast maneuvers but also the detection of any potential debris flying towards the drone. An ideal refresh rate starts from 20 HZ.

Consequently, the Ainstein US-D1 RADAR altimeter [17] was selected. The manufacturer specifies a 50 meter maximum operating altitude (thus range), with a 43° horizontal field-of-view and a 30° vertical field-of-view. The update rate is 100 Hz and it is waterproof, with an IP67 rating. The full list of specifications can be found on the manufacturer website and a depiction of the product can be seen in Figure 8.7.

Figure 8.7: Ainstein US-D1 RADAR

Given the FOV of one unit, eight radars would be used in the horizontal plane of the drone, totaling to 344° making use of the wider dimension, falling a little short of 360° coverage. Due to the limited sensors of this type compatible, choosing other, better performing radars is hardly an option, while adding another sensors to cover the entire surroundings would raise difficulties in placement on the drone. As it stands, four sensors are placed on the motor mount, with enough clearance ensured between the FOV angle and propeller tips, with the other four placed on the body. The remaining radar is placed on the bottom of the body with sufficient clearance from the ground and functions as a radio altimeter.

There are some technical incompatibilities generated by the large number of RADAR sensors used. Firstly, each Ainstein US-D1 uses UART or CAN interfaces. However, the carrier board includes only three CAN ports, two of which are dedicated to the primary microcontroller and one to the secondary. There are also two UART interfaces, but they are used for telemetry. Therefore, there is a shortage of ports. To solve this, it is possible to order CAN splitter connectors and connect multiple sensors to each splitter. It was decided to connect the RADAR sensors to splitters from the primary micro-controller CAN ports. This also implies that should the primary microcontroller fail, the collision avoidance capability is lost. Procedures considered in case this event occurs are detailed in Section 8.7.

There is an additional issue regarding power consumption. As per manufacturer specifications, each RADAR consumes 2 W. Having nine radars means a power consumption of 18 W, while the carrier board is only rated for a power of 14 W. Therefore, the RADAR sensors themselves already draw more than the rated power for the board, without even taking into account the other peripherals.

The solution proposed in this case makes use of the CAN bus pinout, which consists of 4 pins[18]:

- VCC_5V OUT: Power supply wire;
- CAN_H IN/OUT: Data transmission wire;
- CAN_L IN/OUT: Data transmission wire;

[17] `https://ainstein.ai/us-d1-all-weather-radar-altimeter/`[Date accessed: 27/05/2025]
[18] `https://cdn.sparkfun.com/assets/e/9/4/6/8/Pixhawk4-Pinouts.pdf`[Date Accessed: 24/06/2025]

- GND: Ground cable.

To circumvent the power problem, it is possible to strip the VCC_5V wire and only connect the remaining three wires to the carrier board. This wire can be routed, along with a ground cable, to a separate PDB directly connected to the batteries.

8.6. Component Setup. Electrical Hardware Diagram

With the hardware components of the control system having been established, they must be properly connected to one another. To illustrate the interrelations between the components as well as all the required connections, a Hardware Diagram was constructed, which can be seen at the end of this chapter. A split was made between electric and electronic components on one side and load-bearing components on the other side. While the focus of the Electrical Hardware Diagram is on the control subsystem, it also contains power and propulsion subsystem components. The diagram is thus comprehensive and encompasses multiple aspects of the drone.

At the core lies the Flight Management Unit (FMU, colored in red), acting as the computer of the drone: it is mainly tasked with processing and executing commands from the ground operator, based on sensor readouts. The FMU is directly connected to the carrier board (colored in black with beige ports), which connects to the sensors, ESCs, servos, accessories, receivers and transmitters.

Each sensor uses a certain connection type to the flight computer board, given the complex nature of the system. This section will explain each connection type and any modifications to an otherwise standard pin-out of the connection.

Power lines

The PDBs distribute the vast amount of power to the ESCs and then to the motors, while passing smaller amount of energy to accessories and servos through the BECs. Since the carrier board is a more critical component, power to the board is ensured by means of two separate power connections, from two separate PDBs.

Signal lines

Lines that link the carrier board to the ESCs carry PWM signal for motor modulation. They are accompanied by ground cables in order for the entire system to have a common ground [19]. Another type of cable carries digital signal in the form of serial bus. This is the case for the cable between the receiver/transmitter and the RC IN port of the carrier board. This is also the case for any other servos that connect to the AUX OUT ports, namely the camera gimbal and the three relays, each receiving a digital signal.

Transmitter/Receiver connection

The receiver/transmitter chosen has an input voltage of 7-12V, in excess of the 5V that can be outputted by the carrier board. Therefore, separate power lines have been used to power this component. Same situation applies to the camera, which accepts 7.2-72V [20]. Because the Herelink Unit is also able to transmit telemetry, it is connected to the assigned TELEM1 port and the connection between the camera + gimbal ensemble and receiver is achieved through Ethernet, achievable with a 2-in-1 cable.

Sensors and auxiliaries

GPS units connect to their dedicated ports, while lights and buzzers connect to a universal connector I2C. The most important modification compared to a standard connection arises in the case of the Radar sensors, where the power wires need to be stripped from the signal cables and connected to a separate, smaller PDB.

Mass and Cost Budgeting

The batteries that have been chosen in Section 7.3 are arranged in pairs connected in series. Since they will be connected together during their whole life cycle including charging, so, they will be

[19] `https://ardupilot.org/copter/docs/common-powering-the-pixhawk.html`[Date Accessed: 18/06/2025]
[20] `https://www.worldronemarket.com/skydroid-c13-user-manual/`[Date Accessed: 18/06/2025]

soldered together. The battery comes with a QS10 male connector includes therefore the PDB will require a QS10 female connector [21]. One connector would be needed per pair of batteries therefore four connectors are required totaling to 184g and 55.80€.

The PDB distributes the power to several components, for instance to the ESCs. The cables to connect these two is about 300mm and this connection will be bolted together (included in PDB weight). Furthermore, to connect the ESCs and the motors a further 700mm of cable is required and two pairs of compatible connectors. The wires would have to same diameter as the motor wire which is 7mm. Therefore a 1 AWG Gauge Insulated Copper Building Wire was chosen from Paladin Distribution [22], it weighs 470g/m and costs 7.81€/m [17/06/2025]. Since a ground wire is required when distributing, this means that it would require 2m (700mm + 300mm) x 2 of cable for the power and the ground connections. The same logic is applied to the connectors. There are eight motors therefore 16m of cable totaling 7.52kg and 124.96€ [17/06/2025]. Consequently, two pair of connectors per motors means 16 pairs of connectors. The connection between the ESC and the motors will have connectors to ease maintenance, the connectors chosen were the Amass AS150 7mm Gold Bullet Anti Spark Connector [23]. These weigh 24g cost 9,20€ [17/06/2025] per pair. For all connectors it would be 384g and 147.41€.

The PDB will also distribute power to other components such as the flight controller or the pump. These will require a lower voltage than that distributed by the PDB hence a series of step down coverters is required. The camera, the transmitter and the RADARs require 12V so a Step-Down Power regulator Module from Avizar[24] is used which weighs 75g and costs 16€, four of them would be needed. Furthermore, a fitting cable would be required, hence a 22 AWG cable would be required according to the guide provided by the distributor[25]. Therefore, a possibility would be provided by the droneshop [26] since it has a weight of about 6g/m this would be negligible. To connect the flight controller, further step down converters are required since going from 88.8V to 5V directly is quite complicated, therefore a 12-5V 8A Step-Down Power regulator Module from Avizar[27] will be used after the 12V one. These weigh 35g and cost 8€, two of them will be required for redundant power. Wires will also be needed to carry the power, these would be 24 AWG from the droneshop[28] but these are quite inexpensive and very light weight.

Moreover, the PDB will also distribute to components that require 24V such as the door-lock system for the vertical release of water. To do so therefore a step down converter from 100V to 24V is required. This would be 100V to 24V at 10A the from LLCUJVVR[29]. This converter would weigh 50g and cost 153.24€ [17/06/2025], two of them would be needed. To carry the current wires would be needed with 20 AWG, the droneshop would provide these[30]. They are very cheap and light weight therefore they will not be accounted for. The water-pump will require 17V as stated in Section 9.2, therefore, it shall be lowered slightly. Since step down converters for such specific voltage are not easily available a resistor was opted for since the pumps will only operate for 20 seconds. The resistor chosen was the wrapped resistor with a resistance of one ohm [31], it weighs 17g and costs 5.69€. Since there are two pumps, two resistors will be required. The wires that would be used have already been stated, the 20 AWG wires from the droneshop but again would have a negligible effect on the mass and cost budgets.

[21] https://www.progressiverc.com/products/qs10-connectors-1-pair [Date Accessed:17/06/2025]

[22] https://www.paladindistribution.com/shop/1-awg-gauge-stranded-copper-building-wire-thhn-thwn-2-600-volt-ul-listed-cut-to-length-black/ [Date Accessed:17/06/2025]

[23] https://www.flyingtech.co.uk/product/amass-as150-7mm-gold-bullet-anti-spark-connector/ [Date Accessed:17/06/2025]

[24] https://www.ercmarket.com/dc-dc-in-26-100v-to-out-12v-8a-step-down-power-regulator-module/ [Date Accessed:17/06/2025]

[25] https://oscarliang.com/wires-connectors/ [Date Accessed:17/06/2025]

[26] https://droneshop.nl/22-awg-siliconen-kabel-zwart [Date Accessed:17/06/2025]

[27] https://www.ercmarket.com/dc-dc-in-6-25V-to-Out-5V-8A-Step-Down-Power-regulator-Module/ [Date Accessed:17/06/2025]

[28] https://droneshop.nl/24-awg-siliconen-kabel [Date Accessed:17/06/2025]

[29] https://www.amazon.com/Converter-Voltage-30-120V-Output-Current/dp/B0DKBBZDCM?th=1 [Date Accessed:17/06/2025]

[30] https://droneshop.nl/20-awg-siliconen-kabel [Date Accessed:17/06/2025]

[31] https://www.allekabels.nl/weerstand/7366/1065846/resistor.html [Date Accessed:17/06/2025]

For the electronics it was decided that no fuses were necessary since the system is made to withstand large peak powers. Therefore, if the current were to spike the system would be able to withstand it for a short period. On the other hand, if fuses were in place and they break the battery would be shut off and so two motors would lose power and force an emergency landing. Furthermore, the drone would be decommissioned until it undergoes proper maintenance so the mission would be a failure.

8.7. Emergency Decisions and Procedures

Because the UAV participates in emergency firefighting operations, it is reasonable to expect that difficulties such as technical faults, signal loss or operator errors will happen throughout its operational life. The customer requirements state that the UAV shall be able to land autonomously in case of signal loss and that it shall have a fault tolerant control design, in order to land safely with OEI. These requirements can be expanded upon with extra procedures and features, to improve the safety of the drone operations.

Two types of malfunctions were considered: critical and non-critical. A critical malfunction is one that directly affects the UAV's ability to fly. On the other hand, a non-critical malfunction does not hinder the flight of the drone so it can perform a routine return to the landing spot or even keep fighting the fire.

At this stage in the design, some non-critical and critical malfunctions were considered, with associated contingency procedures where possible. A non-critical malfunction can be:

- A leak or defect in the water tank: this fault is non-detectable by the UAV;
- A fault in one of the pumps or a hose: send warning; control to operator; mission may be continued;
- A failure of a RADAR collision sensor: send warning; control to operator; mission may be continued;
- A non-functional GPS sensor: send warning; switch to primary GPS; control to operator; mission may be continued;
- Malfunction in the camera gimbal: send warning, control to operator; mission may be continued;
- One of the batteries is under a state of charge of less than 10%: send warning; head back to deployment spot autonomously;
- Failure of the primary microcontroller in the Cube Red: send warning; control to operator; mission not recommended to be continued;

Conversely, if the failure is critical, severely affecting the UAV. A critical malfunction can be:

- A malfunction in the camera array, making the visual camera unusable: autonomously return to deployment spot;
- Failure of both GPS sensors: send warning; leave control to operator; instruct operator to land immediately at the nearest open location;
- Loss of Remote Control (RC) signal: autonomously return to deployment spot;
- Compromise of structural integrity: this fault is not detectable;
- An electrical failure leading to one or more inoperative motors: stabilize and autonomously land at the nearest open location, immediately;
- Collision leading to one or more damaged rotors: stabilize and autonomously land at the nearest open location, immediately; present the option of dumping the water to the operator.

Combining both critical and non-critical malfunctions, the decisions can be summarized in a Decision Tree Diagram, indicating the best course of action in case a malfunction is detected. It can be seen in Figure 8.8. In the diagram, each decision is made based on mutually exclusive cases: either "Yes / No" situations or, in case of motor failures, based on the number of motors that have failed. The

reconfigurations of the engine control mapping are done based on controllability characteristics with inoperative engines presented in subsection 8.4.1.

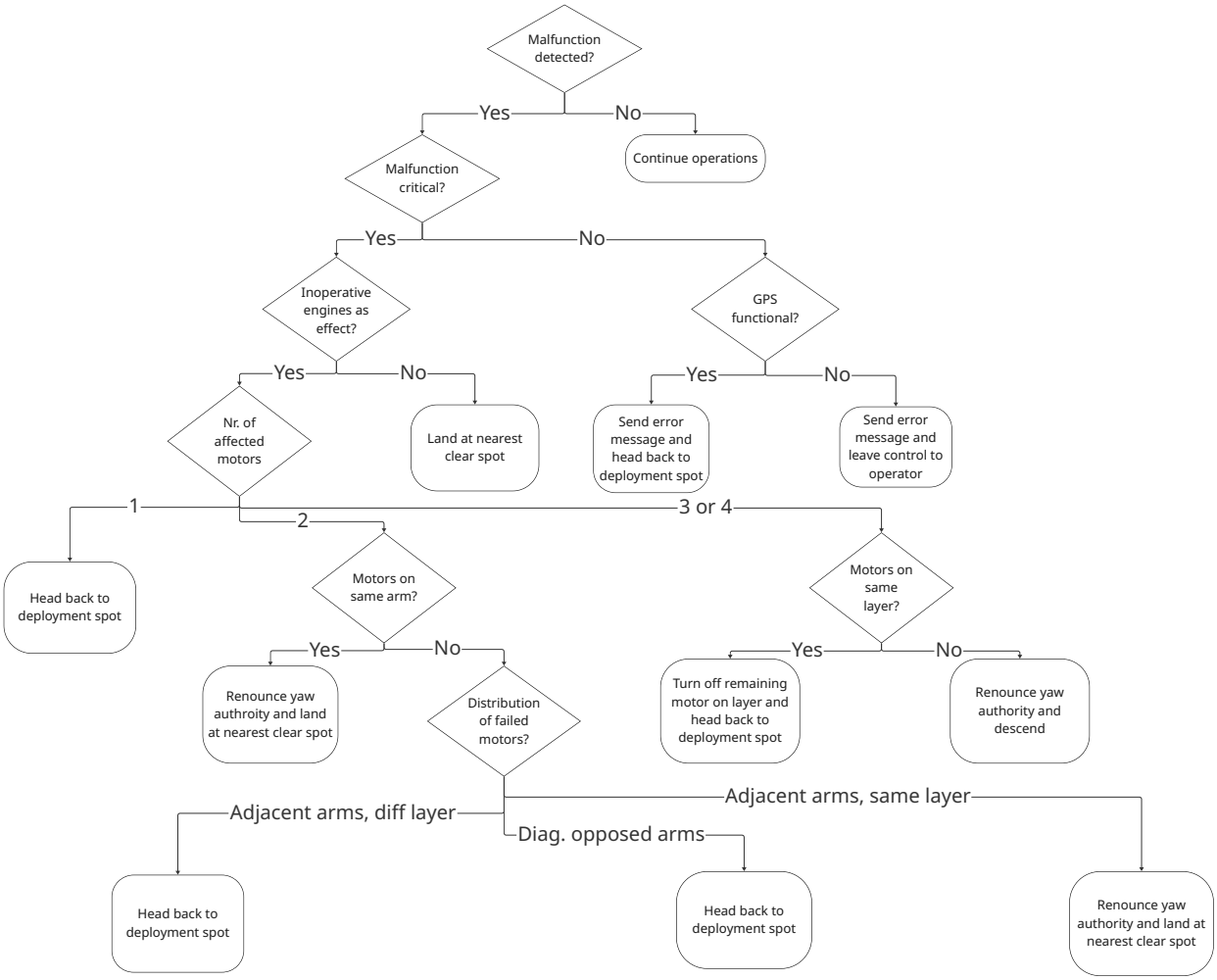

Figure 8.8: Decision procedure diagram

8.8. Control Subsystem Budgeting

Table 8.2: Control Budgets

Component	Mass [kg]	Cost [€]	Power Required [W]
Autopilot	0.324	1050	14
Receiver	0.095	1098.99	4
GPS (x2)	0.032	38.09	2
RADAR (x9)	0.11	519.46	2
Step down 100V to 24V (x2)	0.05	155	N/A
Step down 100V to 12V (x4)	0.075	16	N/A
Step down 12V to 5V (x2)	0.035	8	N/A
Resistor 24V to 16V (x2)	0.017	5.69	N/A
Cable (250A, 1000V)	7.52	143.70	N/A
Bullet connector (16 pairs)	0.024	9.21	N/A
Total	9.881	7592.75	40

Table 8.3: Compliance Matrix Control System

Identifier	Requirement Description	Check	Justification	Method	Reference
REQ-SUBSYS-CTRL-1	The control subsystem shall keep the UAV stable when expelling fire retardant.	**P**	According to ACAI, the drone has enough control authority to counteract the moment disturbance caused by water spraying. Testing this in real life would confirm this result and would be a necessary test.	Test	Section 8.4
REQ-SUBSYS-CTRL-2	The control subsystem shall provide a horizontal force equal to 123 N.	**P**	The ACAI results found the drone to be controllable under this vertical force	Test	Section 8.4
REQ-SUBSYS-CTRL-3	The control subsystem shall provide a vertical force equal to <TBD> of the water expelling force.	✗	This requirement is no longer needed, as the nozzles were fitted perfectly horizontal, thus only causing a horizontal force	Inspection	Chapter 9
REQ-SUBSYS-CTRL-4	The onboard computer shall record 8 channels of data.	✔	The chosen transmitter/receiver is capable of receiving up to 16 channels on the S.BUS connection.	Inspection	[32]
REQ-SUBSYS-CTRL-5	The onboard telemetry shall transmit the recorded channels to a ground station continuously during the mission.	✔	The chosen transmitter/receiver has the ability to continuously transmit to a ground station. This capability should also be demonstrated.	Demonstration	[33]
REQ-SUBSYS-CTRL-6	The control subsystem shall keep the UAV stable in wind conditions up to 6 Bft.	**P**	It was shown that in a wind disturbance corresponding to 6 Bft the drone is perfectly controllable around the X and Y axes	Test	Section 8.4
REQ-SUBSYS-CTRL-7	The control subsystem shall execute a pre-established emergency procedure when a fault is detected.	**P**	The onboard software is programmable and can automatically initiate an autonomous landing and initiate other procedures in the form of sending warning messages and automatically expelling excess water	Test	Section 8.3
REQ-SUBSYS-CTRL-8	The control subsystem shall land the UAV autonomously in case of signal loss or motor failure.	**P**	The onboard software is equipped with autonomous flying modes, including immediate land and return-to-base functions	Test	Section 8.3
REQ-SUBSYS-CTRL-9	The control subsystem shall send an error warning in case of non-critical components faults or failures.	✔	This can be programmed in the autopilot software and controller interface	Demonstration	Section 8.7

[32] `https://discuss.cubepilot.org/t/herelink-channels/8472`[Date Accessed: 18/06/2025]
[33] `https://docs.cubepilot.org/user-guides/herelink/herelink-overview`[Date Accessed: 18/06/2025]

Identifier	Requirement Description	Check	Justification	Method	Reference
REQ-SUBSYS-CTRL-10	The control subsystem shall have the option of autonomous landing upon operator input.	✔	This is a functionality provided by the PX4 autopilot.	Demonstration	Section 8.3
REQ-SUBSYS-CTRL-11	The control subsystem shall keep the UAV stable and controllable with one engine inoperative.	✔	The X8 configuration, together with a high T/W ratio and automatic emergency procedures, allows the UAV to be controlled with even more than one engine inoperative.	Demonstration	Section 8.7
REQ-SUBSYS-CTRL-12	The control subsystem shall be able to override operator input in order to avoid in-flight collisions.	✔	Collision avoidance is a feature provided by the PX4 autopilot and the software can be augmented with the override.	Demonstration	[34]
REQ-SUBSYS-CTRL-13	The control subsystem shall keep the UAV stable and controllable during weight and center of gravity location changes.	✔	This was demonstrated through a CG excursion analysis. The CG is not expected to deviate significantly during flight, even when the water is emptied.	Analysis	Section 8.4

[34] https://docs.px4.io/main/en/computer_vision/collision_prevention.html[Date accessed: 18/06/2025]

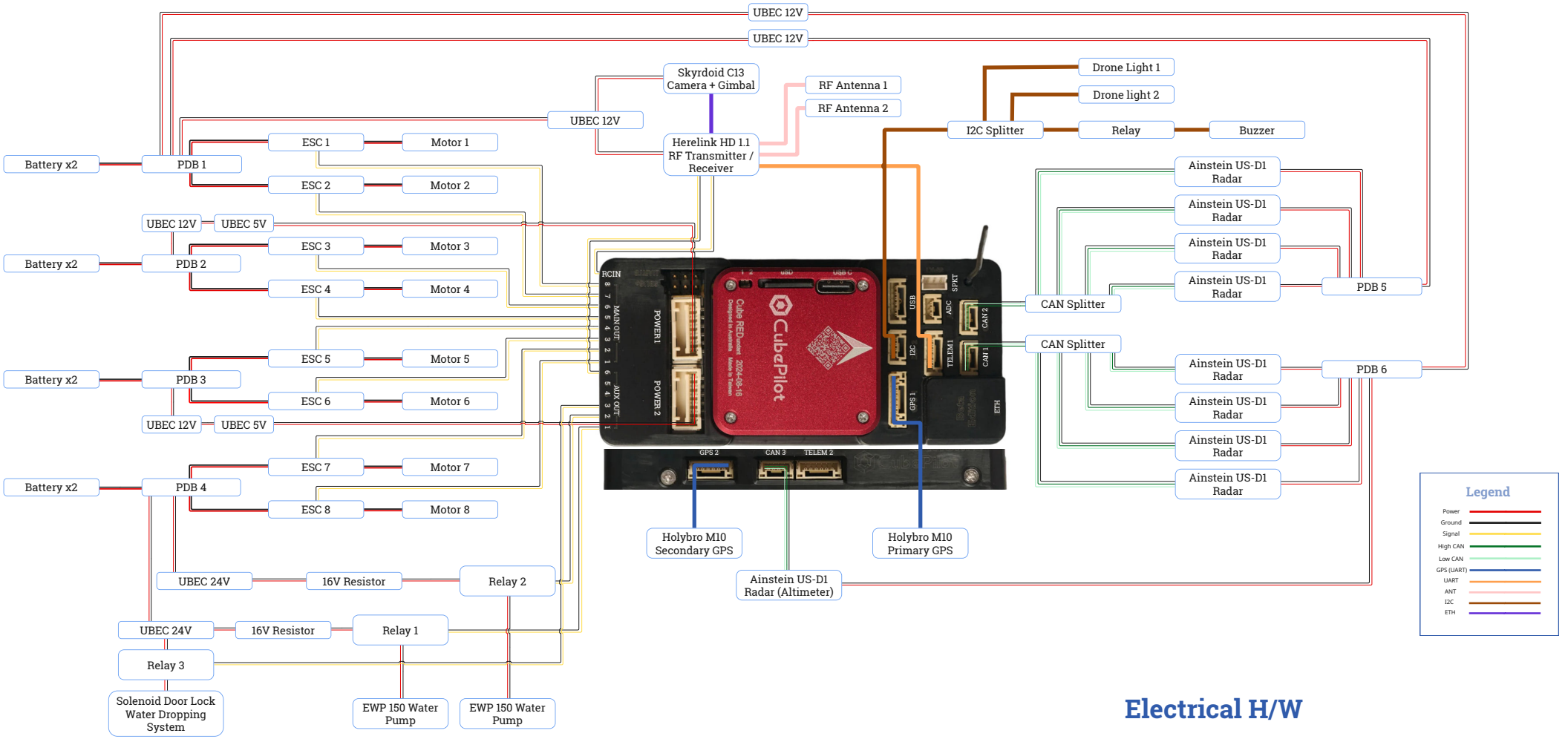

Electrical H/W

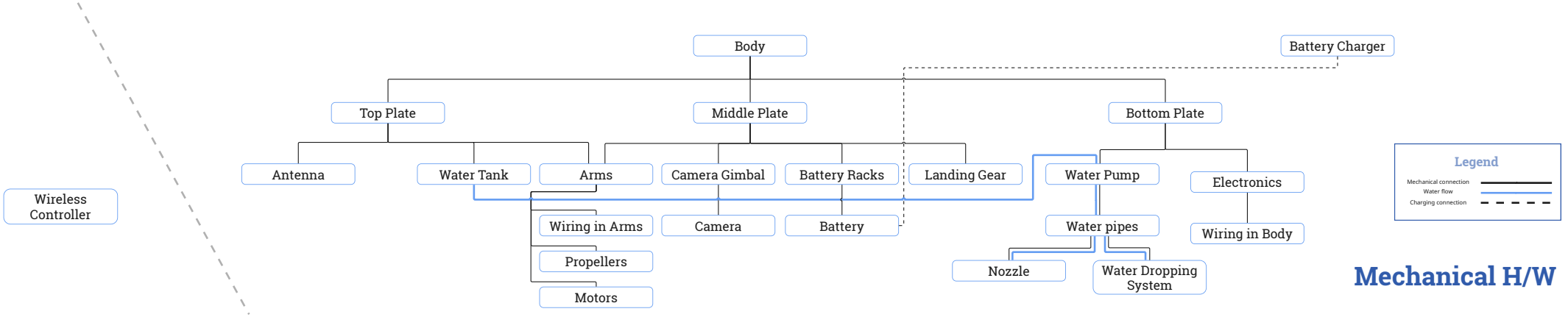

Mechanical H/W

9. Payload Subsystem

The payload subsystem contains the most important components used for the firefighting operations: the water tank, the water-release mechanism, the nozzle, the pump, the cameras, and the visual and acoustic signals system.

9.1. Requirements Assessment

Since the payload system contains the firefighting mechanisms, most of the requirements were set by the client, Gezamenlijke Brandweer. Others were derived during the design process to ensure optimal performance. The final list of the payload system requirements can be seen below:

- **REQ-SUBSYS-PLD-1**: The tank shall have a minimum capacity of 50 L.
- **REQ-SUBSYS-PLD-2**: The pump shall have a minimum flow rate of 150 L/min.
- **REQ-SUBSYS-PLD-3**: The firefighting system shall support water jet and water dropping capabilities.
- **REQ-SUBSYS-PLD-4**: The water jet shall have a throw of at least 6 m.
- **REQ-SUBSYS-PLD-5**: The firefighting system shall have an accuracy of at least 5 cm.
- **REQ-SUBSYS-PLD-6**: The UAV shall be equipped with visual and acoustic signals.
- **REQ-SUBSYS-PLD-7**: The UAV shall carry at least one thermal camera and one visual light camera.
- **REQ-SUBSYS-PLD-8**: The payload shall operate for temperatures of up to 60 degrees.
- **REQ-SUBSYS-PLD-9**: The tank shall accommodate refilling using a C-type hose.
- **REQ-SUBSYS-PLD-10**: The tank shall be designed such that the sloshing effect is minimized.
- **REQ-SUBSYS-PLD-11**: The camera assembly shall be water-resistant.

The compliance matrix is correspondingly shown at the end of the chapter, filled in with supporting justifications for the current or planned fulfilment of each requirement.

9.2. Final Subsystem Design

Based on the list of requirements shown above, a selection of the payload components was made, including a trade-off analysis. The final choices are presented below:

9.2.1. Tank Design and Water-release Mechanism

The tank is an integral part of the UAV, given its larger dimensions dictated by the required capacity of 50 liters. In order to minimize the effect of the change of the center of gravity location during water release, the tank will be mounted centrally. Furthermore, the design should address the water-release or spraying capabilities, refilling, and maintenance procedures.

In order to account for all these, a circular, 'mushroom-shaped' tank was chosen. This design will ensure the necessary access for refilling and maintenance, while being easy to manufacture and providing the needed structural strength [1]. This design features 2 sections: a wider one on top accommodating a hose connection for refilling and a longer, narrower one on the bottom, which accommodates 2 pump connections and an orifice for the water-release capabilities. In addition, the flanges feature a slanted bottom to allow a better flow of water. The dimensions of the water tank can be seen in Table 9.1:

[1] https://dennerik.com/2024/04/17/round-vs-rectangular-choosing-the-right-water-tank-for-your-application/ [Date Accessed: 12/06/2025]

Table 9.1: Water Tank Dimensions

	Component	Dimension
Top Section		
	Radius (Exterior)	250 mm
	Height (Exterior)	100 mm
	Volume (Interior)	16.97 L
	Pump Connection Hole Radius	19 mm
	Refilling Connection Hole Radius	25 mm
Bottom Section		
	Radius (Exterior)	180 mm
	Height (Exterior)	400 mm
	Volume (Interior)	37.52 L
	Water-release Semicircular Orifice Radius	160 mm
Entire Tank		
	Wall Thickness	5 mm
	Volume (Interior)	54.59 L

By having these dimensions, the tank can hold 54.59 liters of water, more than the minimum required capacity of 50 liters. This accounts for any possible empty space left after refilling, ensuring that the minimum capacity is reached at all times. The geometry of the tank can be visualized in Figure 9.1:

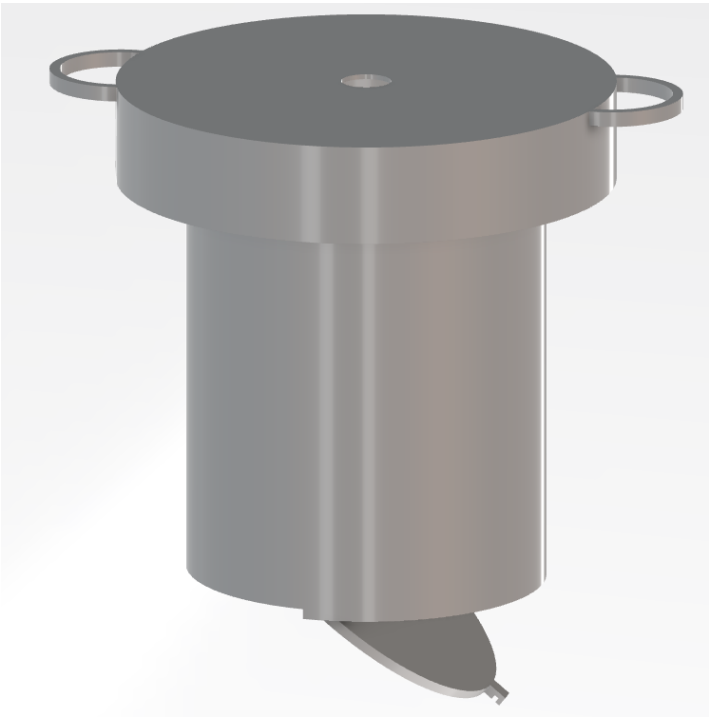

Figure 9.1: Water Tank Geometry

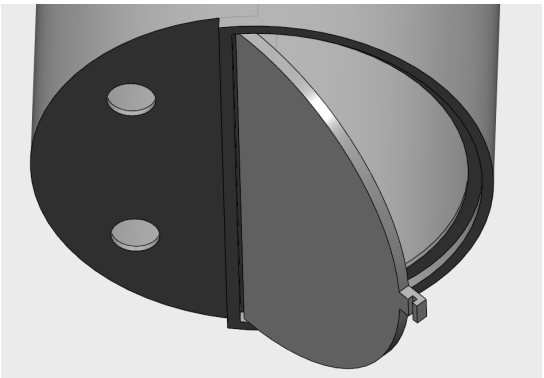

Figure 9.2: Water-release Door

Figure 9.3: Solenoid Door Lock

An important part of the tank geometry is the water-release mechanism. The water-release door is highlighted in Figure 9.2, while the actual release mechanism is a solenoid lock showcased in Figure 9.3 [2]. The whole system works as follows: it features a hinged door at the bottom of the tank, which can be released by the solenoid lock when activated. In order to ensure that no water leaks, a rubber seal

[2] `https://www.kendrion.com/en/products-services/door-locking-systems/solenoid-door-locks` [Date Accessed 16/06/2025]

is applied between the door and the tank edge, while a pre-loaded spring compresses this rubber, providing a water-tight seal. However, a calculation has to be performed in order to make sure the lock can hold the door closed and that it has enough compression force to seal the opening. Thus, the total force that needs to be supported by the door lock is:

$$F = F_{\text{door}} + F_{\text{seal}} \tag{9.1}$$

where F is the total force, F_{door} is the force supporting the weight of the door and the water above it, while F_{seal} is the compression force needed to maintain the water seal.

In the case of the force needed to support the door, a conservative approach is chosen, considering the weight of the door and the total weight of the water multiplied by the area ratio of the orifice. This force also has to be multiplied by the load factor, and because the hinges on the other side of the release door support this weight as well, the final result will be divided by 2:

$$F_{\textbf{door}} = (m_{\text{door}} + V_{\text{water}} \cdot \rho_{\text{water}}) \cdot g \cdot n \cdot 0.5 \tag{9.2}$$

where F_{door} is the force supporting the weight of the door and the water above it, m_{door} is the mass of the door, V_{water} is the water volume, ρ_{water} is the density of water ($997\,\text{kg/m}^3$), g is gravitational acceleration ($9.81\,\text{m/s}^2$), and n is the load factor.

In the case of the compression force needed to seal the door, the first step is calculating the hydrostatic pressure on the sealing surface:

$$p_{\text{water}} = \rho_{\text{water}} \cdot g \cdot h_{\text{tank}} \tag{9.3}$$

where ρ is the density of water, g is gravitational acceleration, and h_{tank} is the height of the tank (0.5 m). This pressure acts on the rubber gasket, which generates frictional forces resisting sliding and potential leakage. Since the rubber gasket interfaces with both the tank door and the tank wall, the total friction force is shared across both surfaces. Therefore, only half of the total frictional force is provided by each interface, leading to a required force F_{seal} applied by the spring to compress the gasket, computed as:

$$F_{\text{seal}} = \frac{p_{\text{water}} \cdot A_{\text{gasket}}}{2\mu} \tag{9.4}$$

where p_{water} is the water pressure, A_{gasket} is the area of the rubber gasket exposed to the water ($0.0041\,\text{m}^2$, considering a gasket thickness of 5 mm), and μ is the friction coefficient. For the friction coefficient μ, empirical data for neoprene against HDPE is limited. However, based on available data for rubber against smooth plastic surfaces, a conservative value of $\mu = 0.5$ is adopted [3].

These 2 forces are calculated and added to determine the loads in the 2 limiting cases: the ascending (load factor = 2.1) and hovering (load factor = 1) phases. The results are presented in Table 9.2:

	Ascending Phase	Hovering Phase
F_{door} [N]	105.47	221.48
F_{seal} [N]	40.23	40.23
F [N]	105.47	221.48

Table 9.2: Loads Acting on Water Door During Operation

Given the operational limit of 400 N set by the manufacturer of the door lock [2], it is clear from Table 9.2 that the loads experienced by the lock during water-release operations are well below this limit, even when experiencing the maximum load factor.

[3] `https://www.engineeringtoolbox.com/friction-coefficients-d_778.html` [Date Accessed 13/06/2025]

Another important aspect that needs to be determined is the time it takes for the water to be released. As the water-release system has to be operable in case of emergency, it is crucial that the water is released as soon as possible. In order to calculate the flow of water dropping through the bottom orifice, the following equation can be used [21]:

$$Q = C_d \cdot A \cdot \sqrt{2 \cdot g \cdot h} \tag{9.5}$$

where Q is the flow rate, C_d is the discharge coefficient, A is the area of the orifice, g is the gravitational acceleration, and h is the height of the water above the orifice. For a plate with sharp edges, the value of C_d is 0.61 [4] [21]. Considering an area of 0.0402 m^2, the gravitational acceleration of 9.81 m/s^2, and a height of 0.5 m, the flow rate is equal to 0.0768 m^3/s. The time to empty the tank can be computed using:

$$t = \frac{V}{Q} \tag{9.6}$$

where t is the time to empty the tank, V is the water volume inside the tank, and Q is the flow rate. Since the volume is equal to 0.05449 m^3, the time to empty the tank is 0.7095 s. This very small value can be explained by the large size of the opening and the simplistic calculation employed. To estimate the time even better, a CFD analysis is performed using the Ansys Fluent program. Figure 9.4 showcases some images from the analysis:

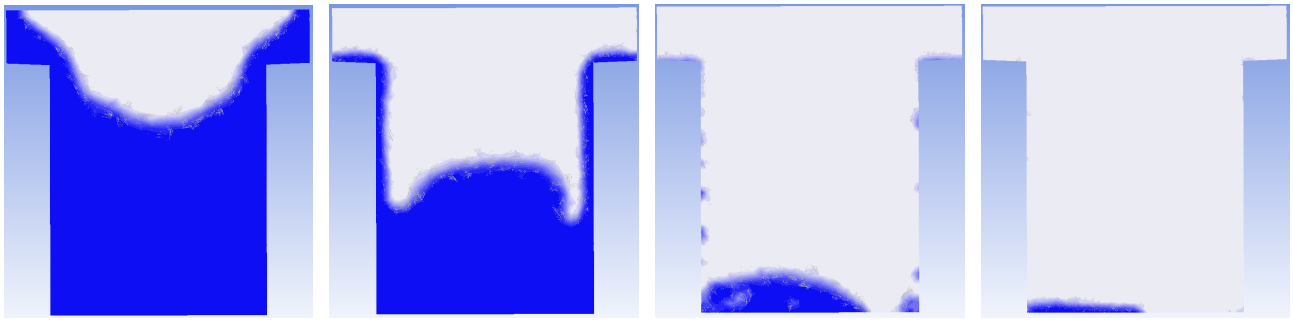

(a) Water Volume at 0.25 s **(b)** Water Volume at 0.5 s **(c)** Water Volume at 1 s **(d)** Water Volume at 1.5 s

Figure 9.4: CFD Simulation of Water-release Scenario

As seen above, the time to release the water is slightly larger than the first estimation. This can be explained by the effect of the geometry on the water flow. After 1 s, a considerable amount of water has been dropped, while at 1.5 s, only a small amount of water is left in the tank, in the area of the pump connections. The CFD analysis still contains limitations, like neglecting the wall friction, but the accuracy of the time calculation is deemed acceptable at this stage in the design phase. More accurate results can be obtained after testing the UAV, during the verification and validation process.

When it comes to the material the water tank is made of, a trade-off was made between aluminium, thermoplastics (HDPE), and carbon fiber. The best choice was deemed the high-density polyethylene (HDPE), given its excellent mass performance (a density of only 0.93 - 0.97 g/cm^3 [5]), great manufacturability [6], corrosion resistance [7], and reduced costs (only €1.1–1.5/kg [8]). The only drawback is the limiting maximum operational temperature of ≈ 82°C [9], however, this is within the constraint set by REQ-SUBSYS-PLD-8.

[4] https://wiki.sustainabletechnologies.ca/wiki/Flow_through_an_orifice [Date Accessed 16/06/2025]

[5] https://plasticseurope.org/plastics-explained/a-large-family/polyolefins/ [Date Accessed: 09/05/2025]

[6] https://plastimex.mx/es_mx/how-are-hdpe-containers-manufactured/ [Date Accessed: 09/05/2025]

[7] https://www.tapplastics.com/image/pdf/HDPE_CRCWB.pdf?srsltid=AfmBOopUGkNw6NOy9_sIohsoZ1dgF1VlvgJUtdijm-G-QaIjrKo52kXf [Date Accessed: 09/05/2025]

[8] https://businessanalytiq.com/procurementanalytics/index/hdpe-price-index/ [Date Accessed: 09/05/2025]

[9] https://www.piedmontplastics.com/blog/mechanical-plastic-temp-limits?srsltid=AfmBOorBxrg2634tfCa5dwh2fgdhwTtTV7-noo9bqk9N82jI3j94e7FG [Date Accessed: 09/05/2025]

The last consideration for the water tank regards the costs. For the material used for the water tank and release door, the HDPE has a very low cost of only €7.7 [8] [17/06/2025], considering a weight of 5.5 kg. The chosen solenoid door lock does not have a set price; however, upon contacting the manufacturer, the offered price was €96.95. Other additional components like the hinges, the spring, and the rubber gasket are conservatively estimated to weigh 0.5 kg and cost €100.

9.2.2. Pump and Nozzle System Design

A key requirement for the pumping system is the ability to suppress fires through a water jet at a horizontal reach of at least 6 meters, as stated by REQ-SUBSYS-PLD-4. Correspondingly, the amount of water that is reaching the fire, i.e., the flow rate, ought to be at least 150 L/min for effective suppression. The pumping system consists of three components, namely a pump, a hose, and a nozzle. An impression of the system is depicted in Figure 9.5, for which the upcoming analysis is done for hose 2 specifically. The number of pumps is yet to be determined.

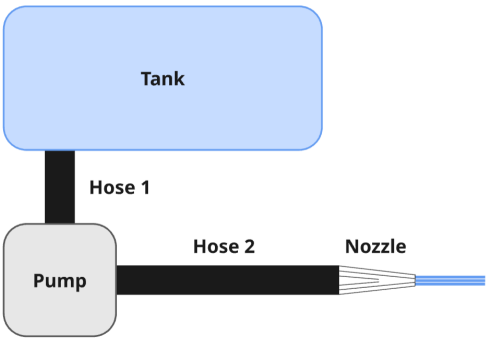

Figure 9.5: Schematic view of pump system

In order to estimate the necessary pump characteristics, the Bernoulli equation for steady, incompressible flow can be employed [21]. Equation 9.7 expresses the Bernoulli equation in terms of heads, where H_{pump} is the useful pump head delivered to the fluid, H_{losses} is the head loss due to friction, v_1 and v_2 are the respective average velocities at sections 1 and 2, ρ is the density, g is the gravitational acceleration, $z_1 - z_2$ is the relative height, and $P_1 - P_2$ represents the static pressure drop across the flow sections. This expression is convenient because it allows for visualization of the individual terms in units of height.

$$\frac{P_1}{\rho g} + \frac{v_1^2}{2g} + z_1 + H_{\text{pump}} = \frac{P_2}{\rho g} + \frac{v_2^2}{2g} + z_2 + H_{\text{losses}} \tag{9.7}$$

Both the tank and nozzle will be open to atmospheric pressure, which simplifies the equation by setting $P_1 = P_2 = P_{\text{atm}}$, eliminating the pressure terms. Equation 9.8 re-expresses the equation as a function for head pressure, where the individual contributions are denoted.

$$H_{\text{pump}} = \underbrace{\frac{v_2^2 - v_1^2}{2g}}_{\text{Velocity head}} + \underbrace{z_2 - z_1}_{\text{Elevation head}} + H_{\text{losses}} \tag{9.8}$$

Although the versatility and simplicity of the Bernoulli equation make it a valuable tool, its limitations and restrictions must be acknowledged. The first limitations assume steady, inviscid (frictionless) flow. In this case, the short hose length and constant flow rate justify these assumptions in most parts of the system. However, because the nozzle introduces substantial frictional effects, a head loss term H_{losses} is included to account for this. Other assumptions are incompressible adiabatic conditions, meaning no heat is added or removed from the fluid. These assumptions are valid due to the constant density of the water. Lastly, the equation is strictly speaking only valid along a streamline, however, when

considering irrotational flow, it becomes valid across streamlines as well, and can then be applied throughout the entire flow field.

To evaluate the required pump head pressure, an iterative approach was adopted due to the presence of multiple free variables: the flow rate, the nozzle exit area, the horizontal reach, and vertical height above the fire from which the water is expelled. To relate these variables and estimate the required exit velocity at the nozzle, a simplified projectile motion model was applied. This approach assumes that the water jet behaves like a point mass under constant gravitational acceleration, without the influence of air resistance or wind. Even under high wind, these assumptions are valid due to their short horizontal travel distance and brief flight time of the water jet, making the aerodynamic impact relatively limited compared to gravitational effects. Furthermore, the drone can be positioned such that it faces into the wind direction, minimizing any lateral deflection of the water and further reducing the sensitivity of the trajectory to wind disturbances.

With a horizontal reach of at least $\Delta s = 6$ m and a given jet height Δh, the required nozzle exit velocity $v_{\text{exit,req}}$ can be estimated using the following relation, derived from classical projectile motion:

$$v_{\text{exit,req}} = \frac{\Delta s}{\Delta t} = \frac{\Delta s}{\sqrt{\frac{2\Delta h}{g}}}$$

where g is the gravitational acceleration. This relation was used as a baseline to iteratively determine a suitable height and corresponding nozzle diameter that meets both the flow rate and pressure constraints imposed by the pump selection.

In contrast to the required exit velocity, the estimated exit velocity can be found by fixing the flow rate and nozzle exit diameter. The nozzle inlet velocity is computed by Equation 9.9

$$Q = A \cdot v \quad \Rightarrow \quad v = \frac{Q}{A} \tag{9.9}$$

where, Q is the volumetric flow rate, A is the cross-sectional area, and v is the flow velocity. Then, using the continuity equation for incompressible flow ($\rho_1 = \rho_2 =$ constant) as

$$A_1 v_1 = A_2 v_2 \Rightarrow \quad v_{\text{exit}} = \frac{A_{\text{inlet}}}{A_{\text{outlet}}} v_{\text{inlet}} \tag{9.10}$$

results in the corresponding exit velocity for set values of exit diameter and flow rate. The objective is to ensure the required and estimated exit velocities are in line, while guaranteeing sufficient pump head pressure at that flow rate. The velocity head in Equation 9.8 is now found, but recall that the elevation head and head losses are also required to find the head pressure.

The head losses through the system are modeled in two segments; first the hose, then the nozzle. The pressure losses in the hose are estimated by the Darcy-Weisbach equation, an empirical relation that relates the head loss due to friction along a pipe to the fluid flow of an incompressible fluid. Equation 9.11 describes this relation with ρ, the density of the fluid, V, the average velocity in the pipe, L, the length of the pipe, D, the diameter of the pipe, and f_D the Darcy friction factor.

$$\Delta p = f_D \frac{\rho V^2}{2} \frac{L}{D} \tag{9.11}$$

Equation 9.12 estimates the friction factor of the hose by the Blasius correlation[21], which approximates the hose as a smooth pipe with a low relative roughness. It is dependent on the Reynolds number, a dimensionless quantity that predicts the flow regime.

$$f_D = \frac{0.3164}{Re^{0.25}} \tag{9.12}$$

Equation 9.13 expresses the Reynolds number in terms of flow speed $\mathcal{V}$, characteristic length L and kinematic viscosity ν. Note that for the hose the characteristic length is the diameter, not the length. The flow speed equals the nozzle inlet velocity.

$$\mathrm{Re} = \frac{\mathcal{V}L}{\nu} \tag{9.13}$$

The nozzle, on the contrary, mainly contributes to the head pressure by inducing a velocity change, as denoted by the velocity head in Equation 9.8. However, based on the shape and contraction angle, a certain considerable amount of friction can also be present. This loss is expressed in terms of the loss coefficient K_L, defined in Equation 9.14

$$K_L = \frac{2h_L g}{V^2} \tag{9.14}$$

where h_L is the additional irreversible head loss caused by the insertion of the component, defined as $h_L = \Delta P_L/\rho g$. V is the flow velocity and g the gravitational acceleration. In [22] it was shown that for a conical nozzle with a contraction angle of 10 degrees, $K_L = 0.08$. For an accurate performance estimate, this type of nozzle will be chosen. Rewriting Equation 9.14 yields an expression for the head loss, h_L, due to the friction in the nozzle.

The described methods now allow for a relatively accurate estimate of the pump requirements. In brief, the iterative approach for pump selection can be outlined as follows:

1. Fix the nozzle inlet area, A_{inlet}, corresponding to the pump outlet and , $z_2 - z_1$, the relative height of tank with pump.
2. Choose a flow rate, Q, horizontal reach, Δs, nozzle exit area, A_{outlet}, and spray height, Δh.
3. Intermediate results for the spraying time Δt, hose flow velocity, v_{inlet}, nozzle exit velocity, v_{outlet}, and required exit velocity, $v_{\text{exit,req}}$, are then found.
4. Ultimately, the specified flow rate and corresponding head must be verified against the pump performance curve to ensure that the required pressure is achieved at the given flow rate.

A conservative case where the tank is almost empty, hence the lowest hydrostatic pressure, was considered. Integration of the pumping system with the drone body thus necessitated a beneficial elevation head of approximately 10 cm, paired with a hose length of 70 cm. The hose length is chosen for operational needs, clarified at the end of this section. The analysis showed that no commercially available pump could deliver the combination of a 150 L/min flow rate with sufficient pressure. However, a dual-pump configuration allowed for a wider range of pumps.

As final configuration, two centrifugal pumps were selected, each delivering a flow rate of 75 L/min at a pressure of 5 psi, equivalent to 34.5 kPa [10]. This setup was deemed optimal, as the spraying distance is optimized for the required flow rate. This is beneficial in high wind scenarios. To minimize vibrational effects and simplify mounting, a rigid aluminium pipe was chosen instead of a flexible hose that was referred to earlier. The nozzle will be conically contracting from 3.8 cm to 1.4 cm at an angle of 10 degrees. Note that the pump systems are parallel to each other and will not be mechanically coupled to avoid flow interference and pressure imbalances.

Table 9.3 shows the complete set of system properties. Note that the diameters are derived from the circular definition of the hose and nozzle geometry. The specifications of the corresponding pump can be found in Table 9.5. For clarity and confirmation, a pressure distribution along the pump system has also been generated. Figure 9.6 aligns with the assumptions of the analytical approach. For instance, the pressure drop along the hose due to frictional effects is purely static. Furthermore, converting the resultant dynamic pressure at the end of the nozzle yields indeed the required exit velocity, thus

[10] `https://daviescraig.com.au/product/ewp150-remote-electric-water-pump-12v-8160` [Date Accessed: 20/05/2025]

showing the consistency of the iteration. Also note that the static pressure before the pump is nonzero due to the negative elevation of the pump with respect to the tank, positively contributing to the pressure requirements.

Table 9.3: Pump System Performance Specifications

Specification	Value	Specification	Value
Nozzle inlet diameter	38 mm	Darcy friction factor, f_D	0.0221
Elevation head, $z_2 - z_1$	-15 cm	Loss coefficient, K_L	0.08
Hose length	70 cm	Pump Head Pressure	34.5 kPa
Flow rate, Q	75 L/min	Hose Frictional Pressure Loss	246.7 Pa
Horizontal reach, Δs	6.36 m	Nozzle Frictional Pressure Loss	2.64 kPa
Jet height, Δh	3 m	Nozzle Velocity Head Loss	32.4 kPa
Required exit velocity, $v_{\text{exit,req}}$	8.13 m/s		
Nozzle inlet velocity, v_{inlet}	1.10 m/s		
Nozzle exit diameter	14 mm		
Nozzle exit velocity, v_{outlet}	8.13 m/s		
Nozzle contraction angle	10 deg		

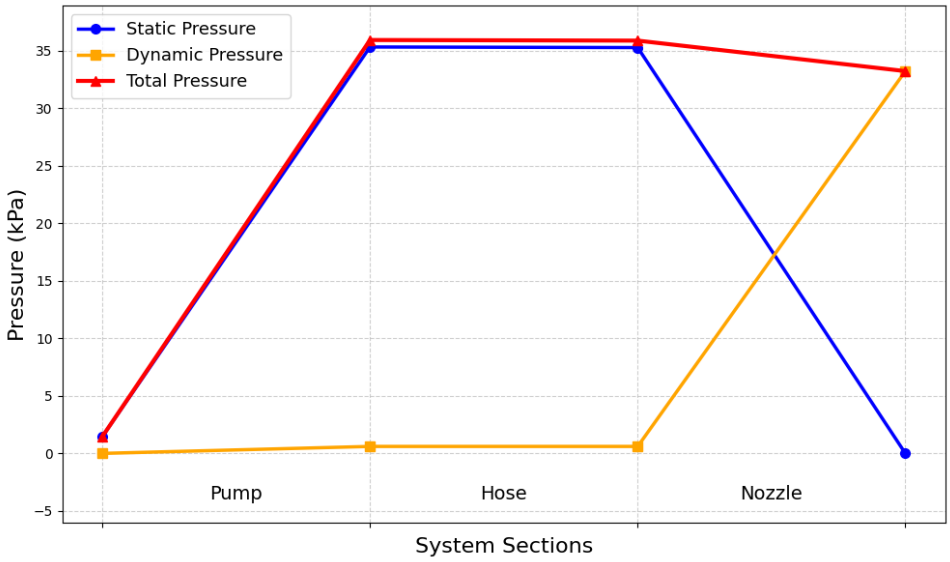

Figure 9.6: Pressure Transformation in Pump-Hose-Nozzle System

While the pump system performance parameters have been defined now, the specific dimensions and materials of the components also need to be established. Table 9.4 contains all the structural aspects of the system, most importantly the mass. The pipe thickness is chosen with respect to manufacturing considerations and structural integrity. A simple hoop stress calculation, assuming a thin-walled structure calculates the thickness as shown below [23]. The lowest bound of yield strength, σ_{hoop}, of pure HDPE[11] is selected for this calculation, since commercially manufactured pipes typically have higher yield stresses. Note that P denotes the static pressure.

$$\sigma_{\text{hoop}} = \frac{P \cdot r_{\text{inner}}}{t} \quad \Rightarrow \quad t = \frac{P \cdot r_{\text{inner}}}{\sigma_{\text{hooop}}} = \frac{35.94\ \text{kPa} \cdot 19\ \text{mm}}{11\ \text{MPa}} = 62\ \mu\text{m}$$

The chosen thickness is more than sufficient. The equality $10 \cdot t = 0.62\ \text{mm} \leq 38\ \text{mm}$ justifies the use

[11] https://www.matweb.com/search/datasheet_print.aspx?matguid=fce23f90005d4fbe8e12a1bce53ebdc8[Date Accessed: 16/06/2025]

of the thin-walled hoop stress equation. The higher thickness also considers the allowance of potential manufacturing imperfections.

Hose 1 will be a 1.5-inch red rubber water hose [12], cut to a custom length of 10 cm. This hose was chosen for its durability, compatibility with the pump's requirements, and suitability for firefighting operations. It features an internal diameter of 38.1 mm and an external diameter of approximately 51.6 mm, matching the specifications required by the pump inlet. To ensure a secure and leak-free connection, Clamp Size 28 [13] is selected. This stainless steel clamp is designed to fit hose outer diameters between 35 mm and 57 mm, making it well-suited for the selected hose dimensions.

Table 9.4: Pump System Structural Specifications

	Hose 1	**Hose 2 + Nozzle**	**Pump**	**Clamp**
Length [cm]	10	70 (hose 2) + 8.8 (nozzle)	N/A	N/A
Thickness [mm]	6.7	1.0	N/A	N/A
Material	Reinforced EPDM rubber	HDPE	N/A	Stainless steel
Mass [kg]	0.19	0.12	1.17	0.027 (est.)

Table 9.5: Electric Water Pump Specifications [10]

Specification	**Value**
Model No.	8160 (EWP150)
Voltage Range	3–15 V DC
Maximum Flow Rate	150 L/min
Max Current Draw	10 A
Operating Temperature	−40°C to +130°C
Weight	1170 g
Material	Aluminium
Maximum Head Pressure	0.5 bar
Burst Pressure	5 bar
Hose Connection Size	38–39 mm
Connector Type	AN16
Height	90 mm
Outer Diameter	125 mm
Cost	€ 150.15 [18/06/2025]

The operational procedures of the mission can be optimized by considering a variable horizontal reach. An investigation was done on the effect of nozzle length on the horizontal spraying distance, measured from the nozzle exit. Table 9.6 shows this correlation, but in addition to that, it also defines a certain effective reach, i.e. the sum of pipe length, nozzle length, and reach. The flow rate was kept constant at 150 L/min to optimize for the reach. It can be concluded that the increase in pipe length greatly contributes to the horizontal reach, despite the associated increase in static pressure drop along the extended length. The nozzle exit area remained within 0.21% of the designed 14 mm, and the reach only decreases by 7 cm compared to 0.50 and 1.5 m. Hence, the effective reach can be set by the user through the use of different lengths. This might be important in scenarios where the drone operates close to a building with high chances of collision. A sufficiently long nozzle would function as a safety measure, ensuring the nozzle hits the wall first instead of any propeller blade. A length of 70 cm is settled on, meaning the nozzles are extended 10 cm longer compared to the propellers.

[12] https://www.factorydirecthose.com/products/1-5-red-rubber-water-hose-purchase-by-the-foot-air-water-light-chemical[17/06/2025]

[13] https://www.aftfasteners.com/hose-clamp-size-chart/[17/06/2025]

Table 9.6: Effective Reach for Different Pipe Lengths

Pipe length [m]	Reach [m]	Effective Reach [m]
0.15	6.38	6.62
0.50	6.37	6.96
0.70	6.36	7.15
0.75	6.36	7.19
1.0	6.35	7.44
1.5	6.3	7.89

9.2.3. Camera Array

To provide visual assistance and thereby guidance to the drone operator, a visual camera could be used. In case the smoke were to block the view of the operator, a thermal camera should also be included. To minimize the system's complexity, the camera should include both of these.

The chosen camera was the Skydroid C13 Three-Light Gimbal [14] and can be observed in Figure 9.7. It includes a 500W-pixel visible light camera, a 640 thermal imaging camera, and a laser rangefinder. The Skydroid C13 has a 30x zoom to clearly view details if necessary. In addition, the thermal imaging camera has a wide field of view.

To increase the video quality, the camera must be stabilized, which is done through a camera gimbal, which provides three-axis stabilization, in turn making footage smoother even during abrupt turns [15]. The camera is attached to the gimbal at all times. Moreover, the main body of the camera attaches to the main drone through some screws. An additional feature of a memory card slot is also included, which means that the footage can be reviewed in case of failure or for mission improvement. The camera would cost 1420€ [05/06/2025] and weigh 0.85 kg.

Figure 9.7: Skydroid C13 Three-Light Gimbal

9.2.4. Visual and Acoustic Signaling

According to the FAA, there are regulations in place to signal to the citizens nearby where the drone is. The drone must be visible from at least three miles away [16] to be able to operate at night. To make the system able to operate indefinitely and with short turnaround times, the visual signaling was connected to the main battery rather than to its own. The STROBON v2 Navigation Light[17] meets all of the aforementioned requirements. The light weighs 1.5g without cables, operates at 6V, and costs 7.79€ [17/06/2025]. Four lights were chosen, one for each of the arms.

[14] https://www.worldronemarket.com/product/skydroid-c13-three-light-gimbal/[Date Accessed: 05/06/2025]

[15] https://www.xdynamics.com/uncategorized/what-is-a-gimbal/[Date Accessed: 05/06/2025]

[16] https://www.ecfr.gov/current/title-14/chapter-I/subchapter-F/part-107/subpart-B/section-107.29[Date Accessed:12/06/2025]

[17] https://store.flytron.com/products/strobon-v2-navigation-light?variant=32120645779587[Date Accessed:12/06/2025]

The drone must also provide acoustic signaling to indicate its location. This was done through the use of a buzzer. Since the drone's noise emissions should also be minimized as much as possible and cannot exceed 80 dB due to acceptable labor conditions [18], the buzzer should also fit these restrictions. Therefore, a buzzer that can fulfill these requirements while being lightweight would be the SFM-27-I buzzer [19]. The buzzer weighs 22.67g, operates at 3 - 24 V, and 4 pieces cost 5.19€ [12/06/2025]. Moreover, the buzzer will be connected to a relay so that it can be turned on and off. With the buzzer and the strobe lights, the drone will fulfill the FAA requirement and thereby REQ-SUBSYS-PLD-6.

9.3. Payload Subsystem Budgeting

In Table 9.7, the mass, cost, and power budgets for the payload subsystem are presented. Note that the cost only includes the raw material costs in the case of custom components.

Table 9.7: Payload Budgets

Component	Mass [kg]	Cost [€]	Power required [W]
Pump (2x) [10]	1.17	150.15	130
Hose Clamp for Pump Inlet (2x) [13]	0.027	2.18	N/A
Outlet Fitting 1.5" Barb to -16AN O-Ring (2x) [20]	0.05	13.86	N/A
Hose 1 (rubber) (2x) [12]	0.19	5.42	N/A
Hose 2 + Nozzle (HDPE) (2x)	0.12	0.17	N/A
Full Tank + Release Door [8]	5.50	7.70	N/A
Solenoid Door Lock [2]	0.15	96.95	36
Hinges, Spring, Rubber Gasket	0.50	100.00	N/A
Skydroid C13 Camera [14]	0.85	1420.00	4
Visual Signaling (4x) [17]	0.0015	7.79	5
Acoustic Signaling [19]	0.023	5.19	0.72
Total	10.143	2004.56	320.72

[18] https://business.gov.nl/regulation/harmful-noise-levels/[Date Accessed: 12/05/2025]

[19] https://www.amazon.com/dp/B0DVT1Q9NK/ref=sspa_dk_hqp_detail_aax_0?psc=1&sp_csd=d2lkZ2V0TmFtZT1zcF9ocXBfc2hhcmVk[Date Accessed:12/06/2025]

[20] https://www.anhosefittings.com/1-5-inch-hose-barb-16-o-ring-adapter-fitting.html?srsltid=AfmBOoo61EcCu4yK3VnYDMQ6yPvidMhnXR9uLnO7vTRcSzNiT7xZxwDr [16/06/2025]

Table 9.8: Compliance Matrix Payload System

Identifier	Requirement Description	Check	Justification	Method	Reference
REQ-SUBSYS-PLD-1	The tank shall have a minimum capacity of 50 L.	✔	The custom design of the tank has a volume of 54.59 L.	Inspection	Table 9.1
REQ-SUBSYS-PLD-2	The pump system shall have a minimum flow rate of 150 L/min.	✔	The model chosen for the pumps can deliver up to 150 L/min each, but the flow rate will be limited to 75 L/min to achieve the required throw of water.	Demonstration	Table 9.3
REQ-SUBSYS-PLD-3	The firefighting system shall support water jet and water dropping capabilities.	✔	The tank design features 2 pump connections and a water-release door.	Demonstration	Figure 9.2
REQ-SUBSYS-PLD-4	The water jet shall have a throw of at least 6 m.	✔	By limiting the flow rate of each pump to 75 L/min, the throw of 6.38 m can be achieved from a jet height of 3 m.	Demonstration	Table 9.3
REQ-SUBSYS-PLD-5	The firefighting system shall have an accuracy of at least 5 cm.	**P**	The nozzle accuracy needs to be tested to demonstrate that this requirement is fulfilled.	Test	
REQ-SUBSYS-PLD-6	The UAV shall be equipped with visual and acoustic signals.	✔	The UAV features both navigation lights and a buzzer for acoustic signaling.	Inspection	Subsection 9.2.4
REQ-SUBSYS-PLD-7	The UAV shall carry at least one thermal camera and one visual light camera.	✔	The chosen camera array model includes both a visual and a thermal camera.	Inspection	Subsection 9.2.3
REQ-SUBSYS-PLD-8	The payload shall operate for temperatures of up to 60 degrees.	✔	The custom-made tank and nozzle can withstand this temperature, given information from manufacturers, but the temperature resistance of other components like the camera array and the visual and acoustic signaling needs to be demonstrated.	Demonstration	Business Analitiq [9]
REQ-SUBSYS-PLD-9	The tank shall accommodate refilling using a C-type hose.	✔	The opening at the top of the tank accommodates the dimensions of a C-type hose.	Inspection	Table 9.1
REQ-SUBSYS-PLD-10	The tank shall be designed such that the sloshing effect is minimized.	**P**	The tank design was changed to a circular one to account for and minimize the sloshing effect. The full impact of it has to be analyzed further.	Analysis	
REQ-SUBSYS-PLD-11	The camera assembly shall be water-resistant.	**P**	This needs to be tested later since no information is given by the manufacturer.	Test	

10. Structure Subsystem

The design of the structural subsystem addresses the configuration of all load-carrying elements, while also accounting for subsystem interfaces, component positioning, and accessibility to internal parts. Consequently, this chapter will also discuss aspects related to the layout of specific elements of each subsystem. Structural choices will be accompanied by stress, deformation, and vibration analyses to prove the efficacy of the final subsystem plan.

10.1. Requirements Assessment

The requirements for the structure were previously formulated to ensure operational integrity throughout the drone's lifetime. Some are also derived from the mission's needs, such as the limitation imposed by the transport van's dimensions.

- **REQ-SUBSYS-STRUC-1:** The UAV arms shall be collapsible.
- **REQ-SUBSYS-STRUC-2:** The UAV arms shall not expand more than 1000 mm.
- **REQ-SUBSYS-STRUC-3:** The UAV landing legs shall withstand a stress in excess of 700 MPa.
- **REQ-SUBSYS-STRUC-4:** The UAV arms shall be perforated.
- **REQ-SUBSYS-STRUC-5:** The displacement tolerance of the extended arm shall be less than 5 mm.
- **REQ-SUBSYS-STRUC-6:** The displacement tolerance of the extended arm shall be less than 1 deg.
- **REQ-SUBSYS-STRUC-7:** The arms shall resist a bending moment of 900 Nm.
- **REQ-SUBSYS-STRUC-8:** The loads in the structure shall not exceed 80% of the yield stress during normal operation.
- **REQ-SUBSYS-STRUC-9:** The drone structure shall withstand all operational loads, including lift, thrust, payload, and impact forces, with a minimum safety factor of 1.5.
- **REQ-SUBSYS-STRUC-10:** The drone structure shall withstand corrosion from water.
- **REQ-SUBSYS-STRUC-11:** The drone structure shall withstand temperatures in excess of 50 .
- **REQ-SUBSYS-STRUC-12:** The drone structure materials shall be resistant to galvanic corrosion.

These requirements will be discussed and explored throughout this chapter, supported by in-depth computations will be performed. Also, the compliance matrix is correspondingly shown at the end of the chapter, filled in with supporting justifications for the current or planned fulfillment of each requirement.

10.2. Component Selection

Given these requirements, the design of various structural elements can be discussed. In comparison to previous subsystems, the structure will employ the use of many custom parts, requiring analyses to derive characteristics based on the drone's targets and limitations.

Arm Selection

The main considerations behind the design of the arms are sizing limitations (REQ-SUBSYS-STRUC-1, 2), load-carrying capabilities (REQ-SUBSYS-STRUC-3, 7, 8, 9), and functionality for the motors (REQ-SUBSYS-STRUC-4).

The forces acting on the arms are usually expected during regular operations. Apart from the components' weights, only the propulsive force generated by the motors will apply a load on the arms. This aspect enables a detailed design, incorporating both analytical and computational sizing

derivations. Given this aspect, combined with the high stiffness-to-weight ratio it provides, CFRP is considered the best option for the arms. This design option has also been argued in earlier steps [3].

It was previously chosen to include a rotating joint hinge in order to comply with REQ-SUBSYS-STRUC-1. This rotating mechanism proved to perform best in comparison with similar choices for collapsing the drone [3]. The chosen hinge design incorporates the following parts:

- Arm-hinge interface: It is a metal component that is meant to be fixed to the CFRP arms on one side and provide a hole on the other side through which a rotation bolt can run.
- Bracket: It acts as the main carrier of load from the arms to the main body. It will take the shape of an aluminium block with a circular cutout through which the carbon fiber rod runs. For assembly purposes, it will be cut transversely, and two bolting points will be added between the two resulting parts. One of them will be fixed in place between the plates, while the other half will be permanently adhered to the rods. This design allows the arms to fold while maintaining high strength during regular operations.
- Rotation bolt: It is a cylindrical bolt that is fixed to the top face of the top plate and the bottom face of the middle plate. It will act as the arm's rotation axis.

The last aspect to consider is the length of the arms. This aspect depends primarily on the propeller size as given in Table 6.4. These determined the required minimum clearance between the tip of the blades and the drone body. The length can already be set as the minimum possible dimension in order to decrease mass contributions. Based on the size of the propellers, an arm length of at least 0.7 m is needed.

Main Body Plates

As previously mentioned, the arms will distribute the lifting forces that the arms carry in a circular pattern, separated in 90° quadrants. The connections between the arms and the plates concentrate in two places, the bracket and the rotation bolt.

The plates are designed to accommodate the water tank easily, while providing enough clearance for the arms to freely rotate during folding and unfolding. The main body also needs to fit multiple components from other subsystems.

The first dimension comes from the water tank. The center hole needs to be at least as large as the water tank (r_{hole} = 18 cm, Table 9.1). The other dimensions can be set based on the arm assemblies.

The preliminary design idea for the main body is to have two plates with similar dimensions. The arm assembly will run through them, and all bending forces will be transferred only into them. The higher one will also accommodate the water tank, while the lower one will have the legs and other components attached to it.

Landing Legs

The landing legs introduce a huge critical point in the design. They need to hold the entire weight of a fully loaded drone, plus additional impact loads. Several factors need to be considered, such as tip-over conditions, providing enough height and clearance for operational purposes, while adhering to sizing limitations.

First, the legs will be designed to have high rigidity and low deflection under static loading, which assumes a fully loaded drone with all motors turned off. As an assumption, the drone can be prone to sudden drops, and the maximum dropping height shall be 0.5 m. It is worth noting that this value was set arbitrarily, and further iterations can be performed to increase it. Calculations will be done to ensure the structural integrity of the drone for such a drop.

10.3. Material Study

As many parts in the structure are custom-made, a proper material study is necessary to determine the best choices in each case.

Aluminium Alloys

Aluminium is the most versatile metal for production. It brings great stiffness, great durability, and it is easy to machine. It was previously argued that incorporating aluminium alloys in the design is really necessary for many parts [3].

The temper designation is a description of how the alloys are manufactured to understand what physical properties are conserved, added, or hindered [1]. Usually, the T6 temper designation provides the best strength for each specific alloy due to the way the material is treated.

Table 10.1 covers the most used aluminium alloys in the aerospace industry. They are chosen based on density, stiffness, resistance to temperature, corrosion levels, and other significant properties. The displayed values are the only ones relevant for this design phase.

Table 10.1: Aluminium Alloys

Alloy	**Density** ρ [kg/m^3]	**Young's Modulus** E [GPa]	**Yield Strength** σ_{yield} [MPa]	**Source**
6061-T6	2700	68.9	310	[2]
6063-T6	2700	68.9	241	[3]
7010-T6	2820	70	530	[4]
7075-T6	2810	71.7	572	[5]
7475-T6	2810	70	490	[6]

From Table 10.1 can be seen that the most useful material choices are 6063-T6 and 7075-T6. They bring great strength and stiffness given their densities, helping with mass optimizations.

Carbon Fibers

Carbon Fiber Reinforced Polymers (CFRPs) are widely used in aerospace and UAV applications due to their high specific strength and specific stiffness — that is, strength and stiffness per unit weight. This makes them ideal for structural components where weight minimization is critical, such as arms and landing legs of drones. CFRPs are composite materials made of a carbon fiber fabric (the reinforcement) and a polymer matrix (the binder), typically an epoxy resin. Their performance depends heavily on the type of fiber used (e.g., standard, intermediate, or high modulus), the matrix type, and the fiber orientation (e.g., unidirectional vs. woven). CFRPs are typically specified by fiber type, layup, and resin system. The prepreg form (pre-impregnated fibers with resin) is common for high-performance applications.

Carbon fibers [7] are manufactured from polyacrylonitrile (PAN) precursors through a multi-stage thermal and chemical process designed to align and crystallize the polymer chains, which directly impacts the fiber's mechanical properties. The main steps are shown in Figure 10.1. The first stage involves polymerization and spinning, where PAN is stretched to align its molecular chains along the filament axis — a critical step in achieving the final fiber strength. These filaments then undergo oxidation at 200–300 °C under tension to make them non-flammable while preserving chain alignment.

Next, the fibers are carbonized at temperatures around 1,500 °C in an inert environment. For high-modulus fibers, a secondary heat treatment above 2,000 °C is required. This significantly increases the degree of crystalline alignment — and thus the modulus — but also adds to processing time, energy demands, and cost. After thermal treatment, the fibers are surface-treated through controlled

[1] https://www.matweb.com/reference/aluminumtemper.aspx [Date Accessed: 24/06/2025]
[2] https://asm.matweb.com/search/specificmaterial.asp?bassnum=ma6061t6 [Date Accessed: 24/06/2025]
[3] https://asm.matweb.com/search/SpecificMaterial.asp?bassnum=MA6063T6 [Date Accessed: 24/06/2025]
[4] https://www.makeitfrom.com/material-properties/7010-T6-Aluminum [Date Accessed: 24/06/2025]
[5] https://asm.matweb.com/search/specificmaterial.asp?bassnum=ma7075t6 [Date Accessed: 24/06/2025]
[6] https://www.makeitfrom.com/material-properties/7475-T6-Aluminum [Date Accessed: 24/06/2025]
[7] https://toray-cfe.com/en/what-is-carbon-fiber/ [Date Accessed: 24/06/2025]

electrochemical processes. Finally, a sizing agent is applied to improve fiber handling and matrix compatibility during layup and curing.

These complex and tightly controlled processes, particularly at higher temperatures for high-modulus grades, directly influence cost, availability, and handling characteristics, all of which are relevant for the manufacturing of the UAV.

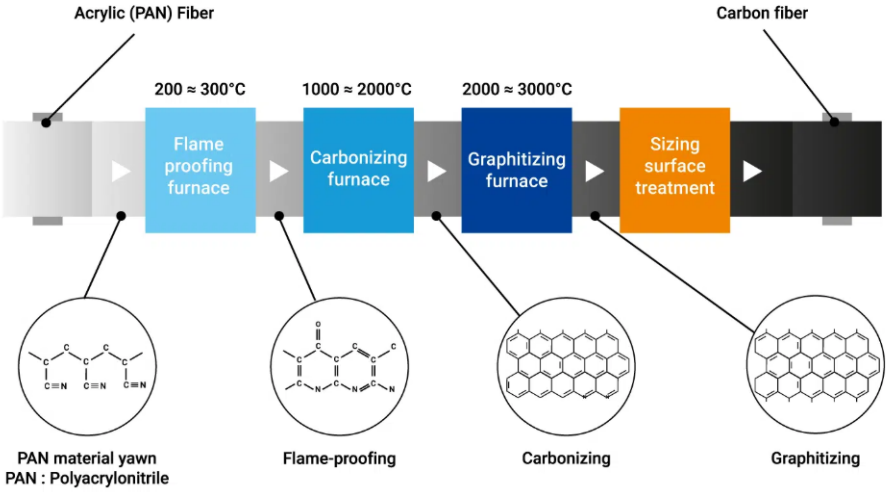

Figure 10.1: Typical Manufacturing Procedures for CFRP [8]

Table 10.2: Comparison of European-Produced Carbon Fibers [9]

Fiber	Strength [GPa]	Modulus [GPa]	Density [g/cm^3]
T400H (Standard)	4.41	250	1.80
T830H (Intermediate)	5.34	294	1.81
M46J (High)	4.20	436	1.84

Table 10.2 provides the main material properties for three selected fibre types produced by Toray [9], each representing a different class of elastic modulus. Carbon fibers are developed and manufactured globally, but for supply chain resilience and easier procurement, this comparison focuses on fibers that are available through Toray's European operations, making them more practical choices for UAV builders operating in Europe.

Although M46J stands out for its extremely high stiffness (Young's Modulus = 436 GPa), it is more brittle and expensive, requiring autoclave curing and stricter quality control. T830H, in contrast, offers a strong balance of moderate weight, high strength (5.34 GPa), and manageable processing. For general-purpose structural parts where cost, impact resistance, and ductility matter most, T400H remains an attractive and accessible option.

Iron Alloys

Some parts need additional strength. As a compromise to increasing the size of the drone, some parts can be made from iron alloys, specifically steel. However, it should be kept in mind that steel densities are much greater in comparison with aluminium ones, therefore, its use should be limited.

The most common choice of steel in an aerospace environment is AISI 4130 [10]. Its density is 7850 kg/m^3,

[8] https://toray-cfe.com/en/what-is-carbon-fiber/ [Date Accessed: 24/06/2025]
[9] https://www.toraycma.com/products/prepreg/#prepreg-aerospace [Date Accessed: 24/06/2025]
[10] https://www.matweb.com/search/DataSheet.aspx?MatGUID=e1ccebe90cf94502b35c2a4745f63593 [Date Accessed: 24/06/2025]

the Young modulus is 205 GPa, and the yield strength is $\sigma_{\text{yield}} = 435$ MPa.

10.4. Structural Loading Analysis

Some initial sizing calculations need to be performed to have a preliminary design that can be further iterated using analytical, computational, or empirical methods.

10.4.1. Arm Loading

The arm assembly serves as the connection between the body assembly and the motor assembly. As such, the upward thrust produced by the motor assembly is the critical load that acts on the arm. This is best represented by a point-load applied at the end of the beam. As the beam is connected to the main body assembly through a clamp and a bolt, they both create moments, as well as forces in the vertical direction. These are shown in Figure 10.2. Note that the horizontal force created by the bolt is not shown, since it is equal to 0.

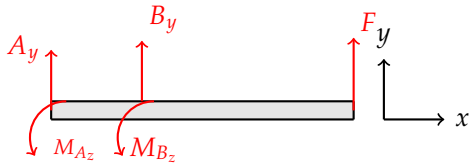

Figure 10.2: Free-Body Diagram of Arm Assembly

In this FBD, the reaction forces created by the C-bracket are denoted by B_y and M_{B_z}, while the reaction forces at the pin joint are denoted by A_y and M_{A_z}. These are meant to counteract the load created by the thrust of the motors, F. This load is equal to:

$$F = 2 \cdot g \cdot T_{\text{motor in kg}}$$

where g is the gravitational constant and $T_{\text{motor in kg}}$ is the thrust of the maximum thrust of the motor in kilograms, as given in Chapter 6. For a $T_{\text{motor in kg}} = 40$ kg, a force of $F = 392$ N is yielded. It is assumed that the relieving moment caused by the weight of the arm assembly is ignored, which results in a conservative loading of the arm.

From the FBD in Figure 10.2, it can be deduced that this is a statically indeterminate problem since there are four support reactions and only two equilibrium equations, namely the force equilibrium in the Z-direction and the moment equilibrium about the Y-axis, given in Equation 10.1. Therefore, two more equations are needed to solve for all of the unknowns, and these are the compatibility equations. Before applying them, however, the method of superposition is applied to separate the complex problem into several sub-problems and apply universal deflection formulas. The sub-problems are shown in Figure 10.3.

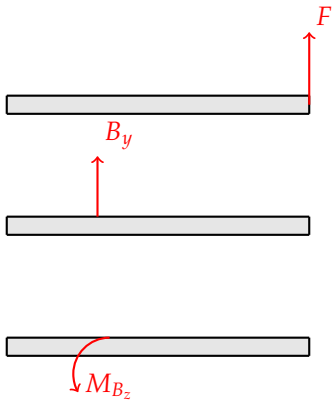

Figure 10.3: Superposition of loading cases: Force F, internal force B_y, and internal moment M_{B_z}

$$\begin{aligned} \sum F_y^{\uparrow} &: 0 = B_y + A_y + F \\ \sum M^{\circlearrowleft} &: 0 = M_{A_z} + M_{B_z} + B_y \cdot x_B + F \cdot L \end{aligned} \tag{10.1}$$

The first compatibility equation to use is the deflection of the beam due to loading. It is imposed that, at the location x_B, the deflection is null. This means that the resulting deflections due to the moment, the upward point load applied at the end, as well as the reaction at point B, result in zero upward displacement. Similarly, the slope of the beam is assumed at that location to be zero which gives Equation 10.2 and Equation 10.3.

$$v_B = \delta_{M_B} + \delta_{B_y} + \delta_F = 0 \tag{10.2}$$

$$\theta_B = \delta_{M_B} + \delta_{B_y} + \delta_F = 0 \tag{10.3}$$

where δ and θ indicate deflection and slope, respectively, due to the specified case. Using the solutions for beam deflection [11] given by Hibbeler [24], Equation 10.2 can be written as Equation 10.4.

$$\frac{F}{6EI} \cdot x_B^2 \cdot (3L - x_B) + \frac{B_y \cdot x_B^3}{3EI} + \frac{M_0 \cdot x_B^2}{2EI} = 0 \tag{10.4}$$

where EI is a material and cross-sectional property but as it is a common denominator, it can be discarded. The slope can also be written as Equation 10.5.

$$\frac{M_B \cdot x}{EI} + \frac{F}{2EI} x_B (2L - x_B) + \frac{B_y}{2EI} x_B^2 = 0 \tag{10.5}$$

This system of two equations can be solved iteratively for various positions of the bracket, as well as for various arm lengths. For a bracket position of $x_B = 0.15L$ and $L = 0.70$m, the clamp reactions are $M_B = -431.2$ Nm and $B_y = -784$ N, respectively. Note that this provides a critical engineering insight: Due to the clamp, the fixed end with the bolt, carries no load. Physically, this is not possible as deformations and load transfer in the main body plates will inevitably lead to forces in the bolt. Nevertheless, with these values obtained, it is possible to create the internal shear force and moment diagrams using the relations shown by Hibbeler [24].

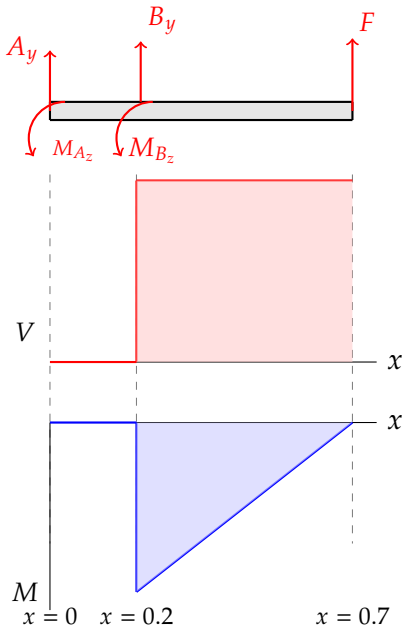

Figure 10.4: Internal Force Diagrams for Shear and Moment

[11] `https://mechanicalc.com/reference/beam-analysis` [Date Accessed: 18/06/2025]

With the loading diagrams generated, it is possible to compute both the tensile and shear stresses in the arms. To do so, Equation 10.6 will be used, assuming that no axial loads are present.

$$\sigma = \frac{My}{I} \tag{10.6}$$

where M is the moment at a particular location, y is the distance from the neutral axis of the rod to the point where stress is to be calculated, and I is the area moment of inertia around the neutral axis. The maximum moment is found at $x = 0.2$ m and, to calculate the maximum stress, the point on the rod that needs to be considered is the point furthest away from the neutral axis, so $y = r_{\text{outer}}$. Only the moment of inertia I has to be computed, and this is done by subtracting the inner moment of inertia as given in Equation 10.7 [12].

$$I = \frac{1}{4} \cdot \pi \cdot \left(r_{\text{outer}}^4 - r_{\text{inner}}^4\right) \tag{10.7}$$

Additionally, as the arms are hollow rods, it is possible to calculate their resulting mass by using Equation 10.8.

$$m = \rho \cdot L \cdot \pi \cdot \left(r_{\text{outer}}^2 - r_{\text{inner}}^2\right) \tag{10.8}$$

It is now possible to optimize the design of the arm by changing the total radius of the rod, as well as the inner radius, with the goal of minimizing stress while also minimizing the mass. Considering the following dimensions: $r_{\text{outer}} = 50$ mm, $t = 2$ mm, a resulting $r_{\text{inner}} = 48$ mm and a length of $L = 0.7$ m, the reaction force at the clamp is 784 N, and the reaction moment is 392 Nm, with the second moment of area equal to $7.395 \cdot 10^{-7}$ m^4 and an average Young's modulus of 101 GPa. The resulting maximum stress occurs at the clamp and using Equation 10.6, a tensile stress of 29.1 MPa is obtained. This tensile stress, depending on the Carbon Fiber composite used, is significantly below the yield strength of such composites which is on average 965 MPa[13]. The resulting material safety factor is in excess of 33, which indicates an over designed arm. Nevertheless, the total deflection of the arm, which can be calculated using Equation 10.9 [24], is found to be less than 1 mm.

$$v_{\text{max}} = \frac{PL^3}{3EI} \tag{10.9}$$

Additionally, the shear strength of the rod has to be taken into account, but is not expected to be a critical parameter. The shear stress can be calculated using Equation 10.10.

$$\tau = \frac{VQ}{It} \tag{10.10}$$

where V is the shear force at a given location, Q is the first moment of an area about the neutral axis, I is the second moment of area of the entire cross-sectional area, and t is the width of the member's cross section.

Computing the sectional properties as shown by Hibbeler [24], the shear stress is found to be 1.73 MPa. Once again, this is significantly below the average shear strength of the CFRP of 89.4 MPa.

With all values calculated, the most limiting parameter for the arm is the axial stress.

10.4.2. Top Plate Loading

The top plate, given that it carries the water tank and most forces from the arms, is the limiting design element included in the main body. As the plate's dimensions are significantly large, the thickness needs to be properly optimized in order to remain within mass budgeting margins. A preliminary

[12] https://www.engineeringtoolbox.com/area-moment-inertia-d_1328.html [Date Accessed: 18/06/2025]

[13] https://www.matweb.com/search/datasheet.aspx?matguid=39e40851fc164b6c9bda29d798bf3726 [Date Accessed: 18/06/2025]

sizing method was used to obtain an initial thickness of the plate from which further iterations can be performed. Analytically, it is impossible to determine an exact solution for plate loadings, especially for rectangular ones. A common solution is to assume a simply supported Kirchhoff plate, which implies the incorporation of the following assumptions [25]:

- straight lines normal to the mid-surface remain straight and normal to the mid-surface after deformation;
- the thickness of the plate does not change during a deformation.

The arm assembly was set to 0.7 m in length, with 0.2 m between the rotation bolt and the bracket. Based on the system sizing requirements ($3.0 \times 3.0 \times 1.38$ m^3 in combination with the size of the arms with unfolded blades (radius of 0.5 m), the plate can be at most 1 m. However, the initial calculations were done with a size of $740 \times 740 \times 3$ mm^3 as this provides enough space for the arm assembly and the water tank to be mounted to the main body.

Given the specifications previously described in Section 10.2 and the arm assembly calculations in subsection 10.4.1, Figure 10.5 shows the sketch of the forces applied on the top plate. It includes two normal forces, applied in the bracket and in the bolt, and a bending moment in the bracket. It should be noted that the force in the bolt is calculated to be zero, but it was added in the algorithm in case any forces are modeled. Additionally, the weight of the water tank was modeled as a uniform pressure. The value was determined by dividing the weight by the area on which the tank sits:

$$p = \frac{55.5\ [\mathrm{N}] \cdot 9.81\ [\mathrm{m/s^2}]}{\pi\,(0.25^2 - 0.18^2)\ [\mathrm{m^2}]} = 5757.65\ \mathrm{N/m^2}.$$

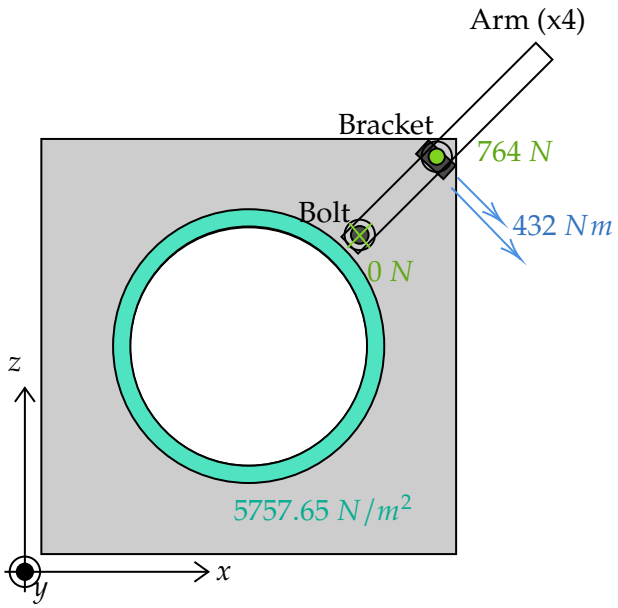

Figure 10.5: Plate Loading Sketch

Given the coordinate system defined in Figure 10.5, the deformation axes are x and z. The Navier Solution is a method that determines the deflection of rectangular plates subjected to out-of-plane loads by using a Fourier series representation. The equations and procedure are taken from Kelly's Lecture Notes [26]. First, a sinusoidal solution for the deflection is assumed. Its formulation is given by Equation 10.11.

$$w(x,z) = \sum_{m=1}^{\infty}\sum_{n=1}^{\infty} A_{\mathrm{mn}} \sin\left(\frac{m\pi x}{L}\right) \sin\left(\frac{n\pi z}{L}\right) \tag{10.11}$$

The derivatives of the function can be obtained easily, and is given in Equation 10.12.

$$\begin{aligned}\frac{\partial^2 w}{\partial x^2} &= \sum_{m=1}^{\infty}\sum_{n=1}^{\infty}\left(-\frac{m^2\pi^2}{L^2}\right)A_{\text{mn}}\sin\left(\frac{m\pi x}{L}\right)\sin\left(\frac{n\pi z}{L}\right)\\ \frac{\partial^2 w}{\partial z^2} &= \sum_{m=1}^{\infty}\sum_{n=1}^{\infty}\left(-\frac{n^2\pi^2}{L^2}\right)A_{\text{mn}}\sin\left(\frac{m\pi x}{L}\right)\sin\left(\frac{n\pi z}{L}\right)\end{aligned} \tag{10.12}$$

It is necessary to bound the system with boundary conditions. They limit the actual values and the second-order derivatives in order to comply with the assumptions, and are written in Equation 10.13.

$$\begin{aligned}w(x,0) = w(x,L) = w(0,z) = w(L,z) = 0\\ \frac{\partial^2 w}{\partial x^2}(x,0) = \frac{\partial^2 w}{\partial x^2}(x,L) = \frac{\partial^2 w}{\partial x^2}(0,z) = \frac{\partial^2 w}{\partial x^2}(L,z) = 0\end{aligned} \tag{10.13}$$

It can be noticed that the deflection equation (Equation 10.11) uses a coefficient, A_{mn}. This term is specific to each loading point, and its actual formula can be obtained analytically, stemming from the boundary conditions and the orthogonality condition. As Kelly deduces [26], the coefficients are given by Equation 10.14, where D represents the flexural rigidity, seen in Equation 10.15, and $q(x,z)$ is the applied load. It shall be considered that, in the case of discrete, independent loads, the integrals in the coefficient's formula disappear, leaving a simple summation.

$$A_{\text{mn}} = -\frac{1}{\pi^4 D}\frac{4}{L^2}\left(\frac{m^2+n^2}{L^2}\right)^{-2}\int_0^L\int_0^L q(x,z)\sin\left(\frac{m\pi x}{L}\right)\sin\left(\frac{n\pi z}{L}\right)dxdy \tag{10.14}$$

$$D = \frac{t^3 E}{12(1-\nu^2)} \tag{10.15}$$

The applied loads adhere to Figure 10.5. However, the Navier solution doesn't allow for a moment load application. Given the bracket dimensions, the moment can be divided in two coupled forces, divided by the thickness of the bracket, 20 mm. The needed force is given by the equivalence equation:

$$\begin{aligned}M_{\text{bracket}} = 432\,[\text{Nm}] = 2\cdot\frac{0.020\,[\text{m}]}{2}\cdot F = 0.020\,[\text{m}]\cdot F \implies\\ \implies F = 21600\,\text{N}.\end{aligned}$$

The modelled forces are illustrated in Figure 10.6, where the plate is shown in profile. It shall be noted that the loads are applied four times, once for each arm assembly, in their equivalent positions. The points of application, with their coordinates and their respective forces, are presented in Table 10.3. The locations are based on the distance between the bracket and the bolt determined earlier in Section 10.2. The arm assemblies were positioned such that enough clearance from the center hole is provided, while still giving the brackets enough surface area for transferring the forces.

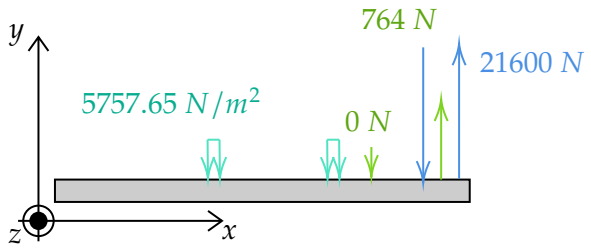

Figure 10.6: Sketch of Plate Loading in Profile

Table 10.3: Applied Loads and Coordinates of Application Locations

Applied Load **P** [N]	x-Coordinate $\mathbf{x_P}$ [m]	z-Coordinate $\mathbf{z_P}$ [m]
0	0.170	0.170
0	0.570	0.170
0	0.170	0.570
0	0.570	0.570
26100	0.008	0.008
26100	0.732	0.008
26100	0.008	0.732
26100	0.732	0.732

(a) Part 1

Applied Load **P** [N]	x-Coordinate $\mathbf{x_P}$ [m]	z-Coordinate $\mathbf{z_P}$ [m]
-26100	0.022	0.022
-26100	0.718	0.022
-26100	0.022	0.718
-26100	0.718	0.718
764	0.014	0.014
764	0.726	0.014
764	0.014	0.726
764	0.726	0.726

(b) Part 2

The pressure application given by the water tank also needs a discretization method to comply with the Navier solution. The grid bounded by the radius of the hole (inner radius) and the tank's radius (outer radius) was separated into many sub-surfaces, on which the loads equivalent to that specific area can be applied as independent forces. The equivalent force was obtained by multiplying the pressure by the unit surface, while the pressure is given by the total weight of the tank divided by the entire disc grid. The list made out of the equivalent forces and their respective polar coordinates transformed to rectangular coordinates was, therefore, appended to Table 10.3 in order to complete the loading method.

Through the calculated deflections at each point across the discretized plate, the following procedure, explained in Kelly's notes [26], can be followed to obtain the stresses at all points. Firstly, from geometry and from the initial conditions implied by the assumptions, the flexural strains can be expressed, as seen in Equation 10.16.

$$\varepsilon_{xx} = -y\frac{\partial^2 w}{\partial x^2}, \quad \varepsilon_{zz} = -y\frac{\partial^2 w}{\partial z^2} \tag{10.16}$$

Considering the plate is assumed thin, therefore the stress in the thickness axis (y axis) is null, the stresses can be written as functions of the strains. Combined with Equation 10.16, the stresses become a function of the deflections. They are given in Equation 10.17.

$$\begin{aligned} \sigma_{xx} &= -\frac{E}{1-\nu^2} y \left(\frac{\partial^2 w}{\partial x^2} + \nu \frac{\partial^2 w}{\partial z^2} \right) \\ \sigma_{zz} &= -\frac{E}{1-\nu^2} y \left(\frac{\partial^2 w}{\partial z^2} + \nu \frac{\partial^2 w}{\partial x^2} \right) \end{aligned} \tag{10.17}$$

Equation 10.12 can be replaced in Equation 10.17, and, together with the formulas for the A_{mn} coefficients seen in Equation 10.14, the final form of the stresses is obtained in the form of Equation 10.18. It is important to note that, in the case of stress calculations, y will be equal to half of the thickness, i.e. $y = t/2$. This stems from the definition of the stress resulting from bending, where the y coordinate is given as distance from the neutral axis. For thin plates, it will always be the line equally separated from both faces.

$$\begin{aligned} \sigma_{xx} &= \frac{E}{1-\nu^2} \frac{t}{2} \frac{\pi^2}{L^2} \sum_{m=1}^{\infty} \sum_{n=1}^{\infty} \left(m^2 + \nu n^2 \right) A_{\text{mn}} \sin\left(\frac{m\pi x}{L} \right) \sin\left(\frac{n\pi z}{L} \right) \\ \sigma_{zz} &= \frac{E}{1-\nu^2} \frac{t}{2} \frac{\pi^2}{L^2} \sum_{m=1}^{\infty} \sum_{n=1}^{\infty} \left(\nu m^2 + n^2 \right) A_{\text{mn}} \sin\left(\frac{m\pi x}{L} \right) \sin\left(\frac{n\pi z}{L} \right) \end{aligned} \tag{10.18}$$

An important factor in the plate's design is the large hole in the center, meant to hold a fully loaded water tank. Therefore, no stress can be carried in that region. Unfortunately, the Navier solution is limited in modelling this specific design characteristic. However, it is common to compute the usual loads, and, in the vicinity of the hole, a stress concentration factor (SCF) is considered. This value is usually chosen based on the present geometries. In the case of a thin rectangular plate with a circular extrusion, a factor of $SCF = 3$ can be assumed [27]. The buffer is set to 0.05 m from the edge of the circle outwards.

Finally, the total stress can be obtained using the von Mises stress estimations [28]. For a biaxial-loaded plate, with no stress in the thickness direction (y axis), the von Mises stress is given by Equation 10.19.

$$\sigma_{\text{von Mises}} = \sqrt{\sigma_{xx}^2 + \sigma_{zz}^2 - \sigma_{xx}\sigma_{zz}} \tag{10.19}$$

The algorithm for the stress estimation is now set. Based on the yield stresses of suitable materials, a practical thickness can be obtained to assure structural integrity in the top plate. A few iterations showed that a thickness of $t = 3$ mm is enough for withstanding the loads the arms and the water tank provide for a plate made out of aluminium, specifically the 7075-T6 alloy, seen in Table 10.1. The generated figures can be seen in Figure 10.7.

It can be seen that the stress values in the bracket locations are greatly surpassing the strength of aluminium, even 7075-T6 (Table 10.1), visible in Figure 10.7a and Figure 10.7b. However, it is evident that the stress exceeds the yield strength only in the locations of the brackets. This is expected as the moment was discretized as two coupled forces instead of a distributed load. In reality, the stresses around those points will be different as the entire bracket will distribute the local loads better. Also, the brackets will act as stiffeners as they will connect the two plates, increasing local strength. The actual physical properties of the assembled main body, however, cannot be properly calculated without Finite Element Methods.

Figure 10.7c shows the total stress in all points. Apart from the maximum values seen in the brackets, which can be ignored as discussed previously, the highest stress value is around 360 MPa. It is particularly seen around the hole, where a conservative stress concentration factor was considered. Given the yield strength, a safety factor for the top plate of around $SF = 1.5$ is obtained, which corresponds with REQ-SUBSYS-STRUC-9.

Figure 10.7d shows the deflection of the plates. Given that the boundary conditions set the deflection to zero on the edges, the deflections are given in reference to the edges. It can be seen that the tank bends the plate by about 1 cm. This is a significant consideration that necessitates the inclusion of other specific components, which will be discussed later.

Nonetheless, Figure 10.7c shows many points that do not necessarily carry a lot of stress and can, therefore, be cut to save mass. The stresses are concentrated around the center hole and the corner lines. The proposed design is seen in Figure 10.8. The total dimensions are approximately $850 \times 850 \times 3\,\text{mm}^3$ in order to increase the stiffness in the flanges. Unfortunately, the Navier solution doesn't provide the possibility of modelling such cuts in the plates. Verifying their integrity can, therefore, only be done using Finite Element Methods.

10.4.3. Landing Legs Loading

The landing legs have to withstand the static load of the drone on the ground, as well as impact loading in case of hard landings. Furthermore, they have to provide stability on the ground to ensure that the drone does not tip over in case of a moment disturbance.

The primary design constraint is constituted by impact loading. As such, this problem is going to be approached using the energy method, where it is assumed that the drone free-falls from a certain height. This method assumes that the entire gravitational potential energy of the drone is converted into kinetic energy and then elastic potential energy. To compute the potential energy, Equation 10.20

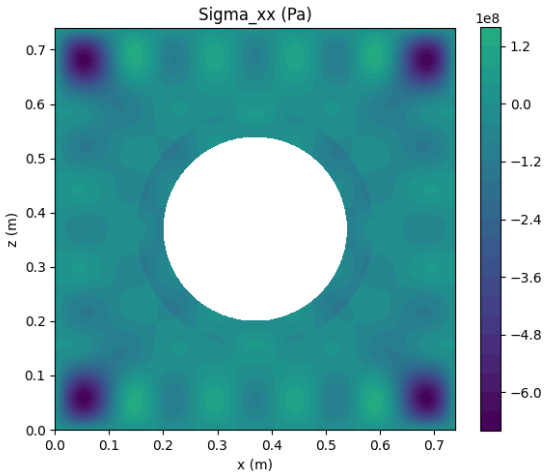

(a) x axis Stress σ_{xx}

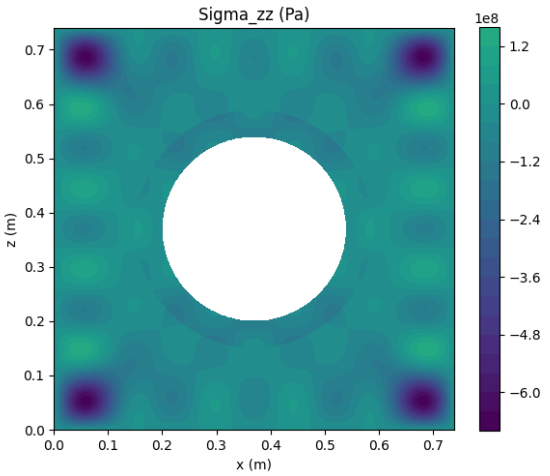

(b) z axis Stress σ_{zz}

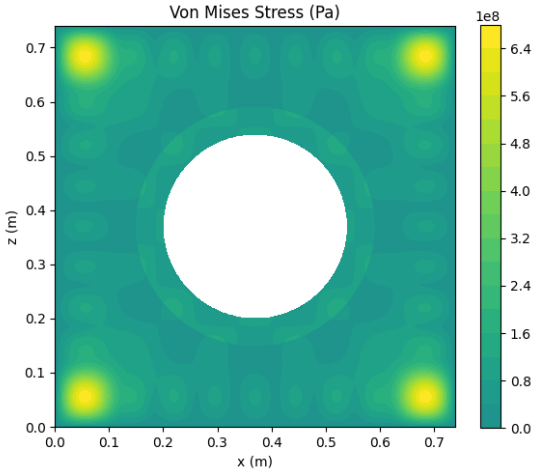

(c) Von Mises Stress $\sigma_{\text{von Mises}}$

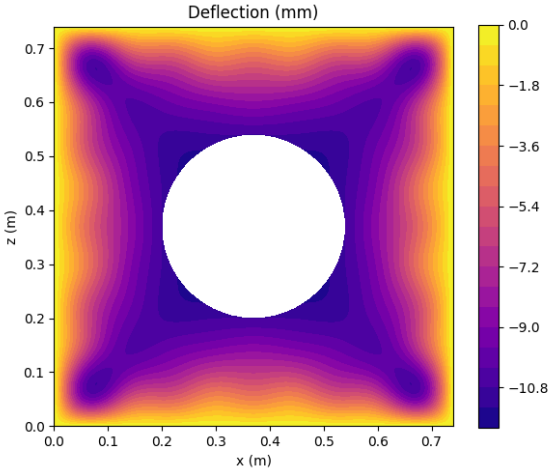

(d) Deflection $w(x, z)$

Figure 10.7: Stress and deflection distributions in the plate: (a) σ_{xx}, (b) σ_{zz}, (c) von Mises stress, (d) deflection.

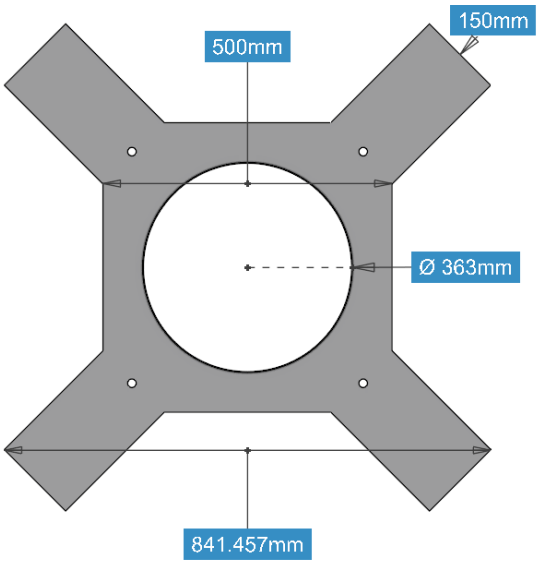

(a) Main Body Higher Plate

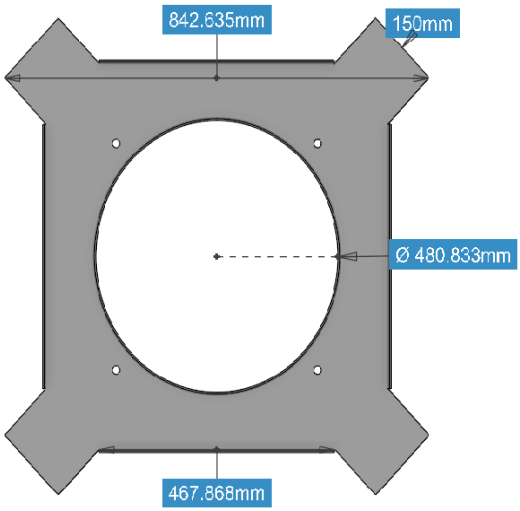

(b) Main Body Lower Plate

Figure 10.8: Initial Design of the Main Body Plates with Dimensions

is used, where MTOM is the maximum take-off mass or 150 kg for the worst-case scenario, g is the gravitational acceleration and h is the height of the fall.

$$PE = \text{MTOM} \cdot g \cdot h \tag{10.20}$$

All the potential energy of the drone has to be absorbed by the legs, which are going to be angled to allow the operators to access batteries. As such, the total potential energy of the fall will have to be absorbed through the bending of the legs, as well as their axial compression. To visualize this, Figure 10.9 is created.

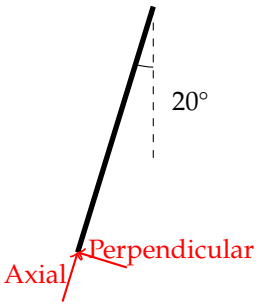

Figure 10.9: Leg loading with axial and perpendicular force components

Now, while energy is a scalar, it can be divided in components as given in Equation 10.21.

$$\begin{aligned} PE_{\text{axial}} &= PE\cos^2(\theta) \\ PE_{\text{perpendicular}} &= PE\sin^2(\theta) \end{aligned} \tag{10.21}$$

These can later be divided in axial and perpendicular deflections as shown in Equation 10.22:

$$\begin{aligned} PE_{\text{axial}} &= \frac{1}{2}k_{\parallel}\delta_{\parallel}^2 \\ PE_{\text{perpendicular}} &= U_{\text{elastic},\perp} \end{aligned} \tag{10.22}$$

Now, the axial strain energy is given by Equation 10.23, where $k_{\parallel}$ is the elastic constant and δ is the deformation of the landing legs, in an axial direction.

$$PE_{\text{axial}} = \frac{1}{2}k_{\parallel}\delta^2 \tag{10.23}$$

To obtain the elastic constant in the axial direction, Equation 10.24 can be used, where E is Young's modulus of the legs in Pascals, A is the cross-sectional area in m^2 and L is the length of the part in meters.

$$k_{\parallel} = \frac{EA}{L} \tag{10.24}$$

To obtain the axial stress, Equation 10.23 can be equated to the axial component of the potential energy given in Equation 10.22. This will yield the deformation, which, if multiplied by $k_{\parallel}$, will give the axial force in the arm. Finally, the resulting axial stress is obtained by dividing this force by the cross-sectional area of the rod.

For the transversal or perpendicular loading, the elastic strain energy is given by Equation 10.25, where P is the point load applied transversely, L is the length of the rod in meters and E is Young's modulus and I is the second moment of area.

$$U_{\text{elastic},\perp} = \frac{P^2L^3}{6EI} \tag{10.25}$$

From this equation, a point load can be obtained and, finally, to get the bending load of the legs, Equation 10.26.

$$\sigma = \frac{P \cdot L \cdot y}{I} \tag{10.26}$$

The cross-sectional area of a hollow rod, given by Equation 10.27 and the second moment of area is given by Equation 10.7.

$$A = \pi \cdot (r_{\text{outer}}^2 - r_{\text{inner}}^2) \tag{10.27}$$

Now, values can be plugged in, to get values for the stress experienced by a landing leg during a hard landing from a height of 0.5m. With $r_{\text{outer}} = 0.025$m and $r_{\text{inner}} = 0.020$m, a Young's modulus E of 107 GPa, the following axial and bending stresses are obtained:

$$\sigma_{\text{axial}} = 572.5 \text{ MPa}$$
$$\sigma_{\text{bending}} = 563.7 \text{ MPa}$$

These stresses can then be added to obtain a total stress of 1136.3 MPa, meaning that the landing legs require one of the stronger CFRPs.

10.5. Structural Computational Design

All design decisions so far have been made using analytical methods, yielding predictable and understandable outcomes. However, the previous models have limitations in their assumptions. Finite Element Methods (FEM) can be performed to verify the calculations done in Section 10.4. It is worth noting that, even though Finite Element Analyses provide great flexibility related to irregular shapes, force applications, and interactions between different parts, they still bring limitations in the results. Several other parameters need to be considered, such as mesh dimensions, and connections between components must be idealized. Nevertheless, it provides great interpretability for the parts subjected to computational loadings.

In all cases, the von Mises stress is used to describe the stresses in the components. Even though this parameter is actually an estimation of the actual stress component at each specific point, it is usually the most conservative way of showing the stresses of a FEM representation [14]. Ideally, stress tests should still be performed on actual prototypes of the design to validate the results given in this section.

10.5.1. Arm Assembly FEM Analysis

The actual loading of the arms is straightforward enough. subsection 10.4.1 provides the analytical deflection and stress values without any major assumptions, the arms being simple cantilever beams. Therefore, it is rather more relevant to discuss stress concentrations under loading with the actual brackets and rotation hinges installed.

Figure 10.10 shows the tip of the arm deflecting upwards by 1.85mm. While this is larger than the hand-calculated deflection in subsection 10.4.1, it is still under the required 5mm displacement tolerance for controllability.

Figure 10.11 shows the von Mises stress and a stress concentration at the location of the clamp. As expected, the finite element model highlights an uneven stress distribution over the surface of the beam, but the largest difference appears at the bolt that facilitates the rotation of the arm. At this location, due to the boundary conditions imposed on the bolt, there are unexpected stresses. While the calculations have shown that the clamp sustains the entire load, the analysis predicts further stress at the bolt. Due to the deformation of the plates during normal operation, this is plausible. Nevertheless, the stresses presented are still under the yield strength of all of the materials that are used in the arm assembly.

[14] https://www.simscale.com/docs/simwiki/fea-finite-element-analysis/what-is-von-mises-stress/ [Date Accessed: 24/06/2025]

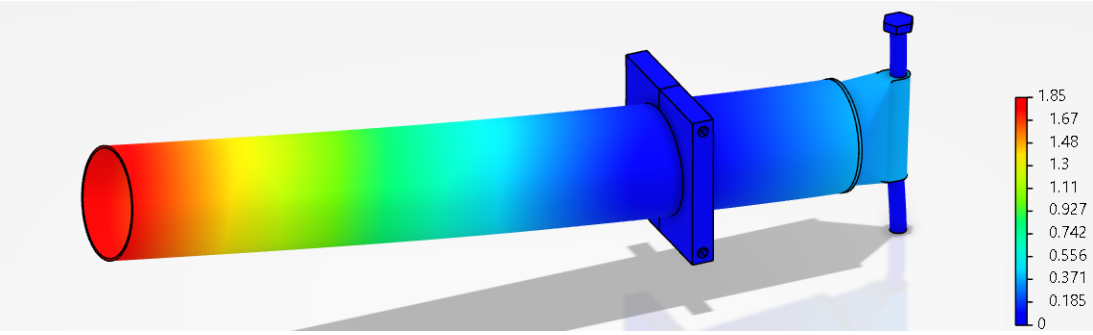

Figure 10.10: Arm Displacement [mm]

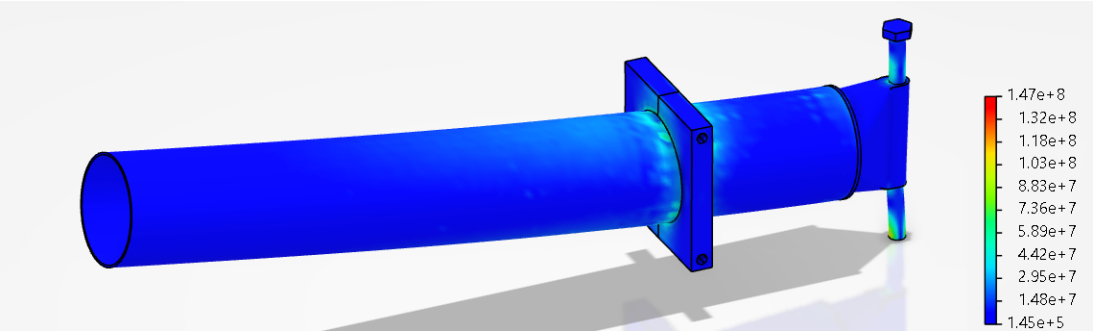

Figure 10.11: Arm von Mises Stresses [Pa]

10.5.2. Main Body FEM Analysis

As presented in subsection 10.4.2, the plates are cut according to Figure 10.8b and Figure 10.8a. As such, the mass of the plates are 1.14 kg for the top plate and 2.98 kg for the bottom plate. This would yield a relatively light main body. Therefore, the plates require many verification steps as their integrity is crucial for a safe flight.

Figure 10.12 shows the loaded plates under regular operations, with the force being assumed to be the maximum thrust the motors can provide (approximately 800 N per arm). The loading points are in the extremities of the plate flanges, as the actual distribution of the load from the clamps is hard to model.

Figure 10.12b shows few stress concentration points. This is an indication that the design of the lower plate can be further cut in order to save mass. Figure 10.12a, however, shows a maximum stress value of 350 MPa, which, for the 7075-T6 alloy (its properties can be seen in Section 10.3), a safety factor of around 1.5 is assured. This stands to verify the results obtained in subsection 10.4.2 and fulfills REQ-SUBSYS-STRUC-9.

10.5.3. Landing Legs FEM Analysis

As previously discussed in subsection 10.4.3, further parameters were obtained analytically for an impact force generated by a 0.5 m drop. This has been achieved using energy methods, which have not yet been replicated in FEM algorithms. Rather, a force was imposed on the landing structure until a deflection similar to the theoretical one was obtained.

The analysis only considered the legs separated from the whole structure. As a replacement, the end connections of the legs were set to a clamp boundary condition, which limits any type of displacement in that specific point (both translational and rotational). The force was divided into three components: two symmetrical point forces, placed in the corners of the legs (the transitions from the vertical to the horizontal sections), and a distributed force on the horizontal section. The magnitudes were divided as follows: 45% for each point force and 10% for the distributed component. This decision was made based on the idea that, upon impact with the ground, the corners will provide more stiffness to the legs, thereby maximizing their actual contact with the ground.

The theoretical displacement was found to be around $d = 25$ mm. Through multiple iterations on

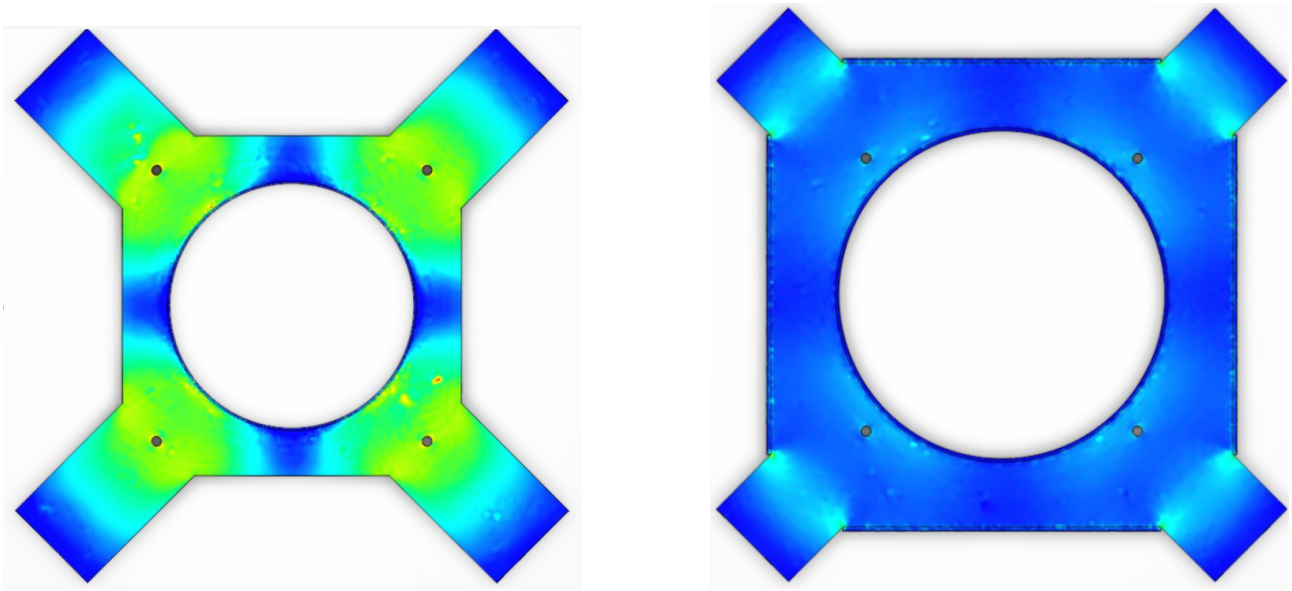

(a) Main Body Higher Plate
Max. Stress: 350 MPa

(b) Main Body Lower Plate
Max. Stress: 280 MPa

Figure 10.12: Initial Design of the Main Body Plates with Dimensions

the 3D design of the landing legs, a deflection of 27.3 mm was obtained for a force of 40000 N (the equivalent of around 4.1 tonnes). This force value is logical in the context a drop from a height of 0.5 m given how heavy and dense the UAV is.

Figure 10.13 shows the FEM representation of the legs, with two displayed parameters: displacement, in Figure 10.13a (scale is in [mm]), and von Mises stress, in Figure 10.13b (scale is in [Pa]). As can be seen, a maximum stress value of around 585 MPa is obtained in this case, contradictory to the result of 1136.3 MPa obtained in subsection 10.4.3. This can be explained by the fact that the impact stresses were calculated on a single vertical section of the legs, whereas now the entire leg is assumed, with two vertical sections acting as load carriers. It can be observed that, by doubling the obtained stress, a value of 1170 MPa is obtained. This parameter is much closer to the analytically determined value.

Looking at Figure 10.13b, it can be seen that most stresses are concentrated very close to the clamp. This raises the need for a detailed design of the connection between the legs and the main body.

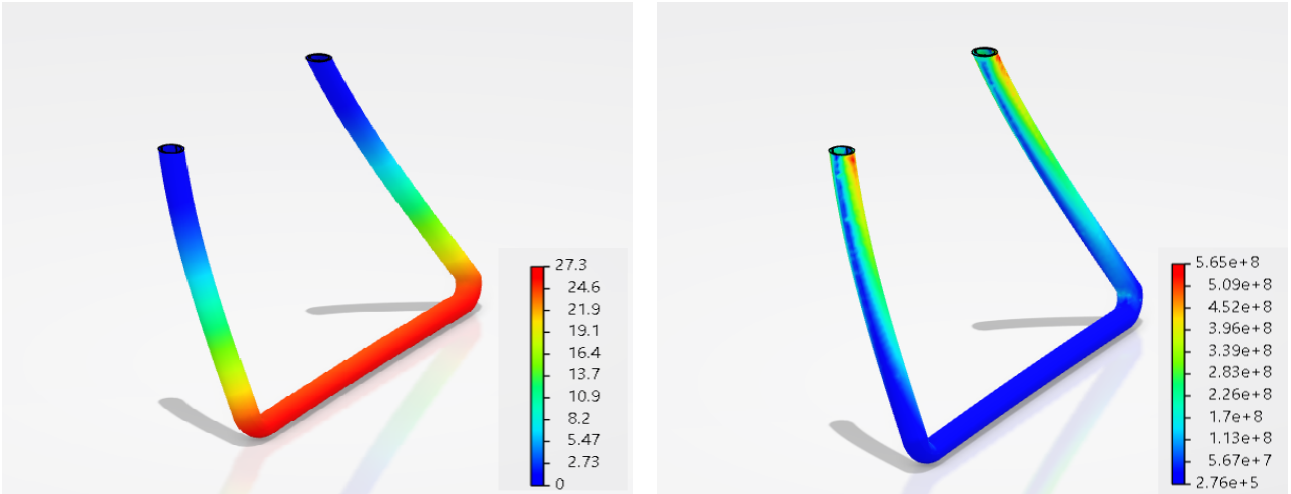

(a) Leg Displacement [mm]

(b) Leg von Mises Stresses [Pa]

Figure 10.13: FEM Analysis on the Landing Legs

10.6. Additional Structural Components

So far, all load-carrying parts have been discussed. Multiple other components are needed, though, such as the plate carrying the batteries, the pumps, the electronics. As proposed in Section 10.4, the main body plates require further reinforcements, specifically around the center hole. All supplementary components will be discussed in this section.

Bottom Plate

The main body is formed by two offset plates. As the pumps need to sit lower than the tank, an additional is necessary very low in the assembly. Therefore, the main body plates will become the top and middle plates, while the lowest one will be named the bottom plate. It will carry most non-structural components, mainly the battery packs and the water pumps.

The sizing of the plate stems as a result of the clamping methods. The plate is hinged to the assembly in two ways. First, clamps are attached to the legs that carry most of the plate's weight. Given the static forces applied to this plate, the contribution on the leg stresses won't be significant. Second, a simple truss structure was designed to help distribute the forces along the assembly. It is connected to the main body in points close to the landing legs fixing mechanisms in order to help the middle plate keep upward bending loads during flight under control.

Cylindrical Plate

The reinforcement between the main body plates is designed as a cylindrical plate fixed between them. It is placed close to the center hole location in order to limit displacements in the top plate when the water tank is filled. It also acts as shielding for the water tank, especially for the upper part of the tank's shape.

10.7. Assembled Structure

Finally, all structural elements have been described. Figure 10.14 shows all components brought together.

Figure 10.14: Assembled Structure

10.8. Vibrational Analysis

An additional analysis into the vibration of the entire structure is required. While not exhaustive, it does provide an important insight into the resistance of the structure to vibrational loads that the drone will experience during normal operation. The study was done only on the load-carrying parts of the structure.

The main sources of vibrations in the structure are the motors and the propellers. The motors induce

vibrations through the RPMs it generates. It was seen in Chapter 6 that a peak RPM of 6400 was to be expected, which is equal to 106.67 Hz. The BPF (blade passing frequency) is a direct function of the RPMs which indicates how many times the blades pass the arm, inducing overall vibrations. It can be easily calculated as the RPM value times the number of blades per axle. In this design case, this value is 4 due to the coaxial setup of the two-bladed propellers. Therefore, the BPF is 426.67 Hz.

Figure 10.15 shows the only modal resonance with the aforementioned values, mode 19, with a frequency of 106.5 Hz. It can be observed, however, that such a mode is unlikely, especially with the added components discussed in Section 10.6, which act as stiffeners and/or dampeners.

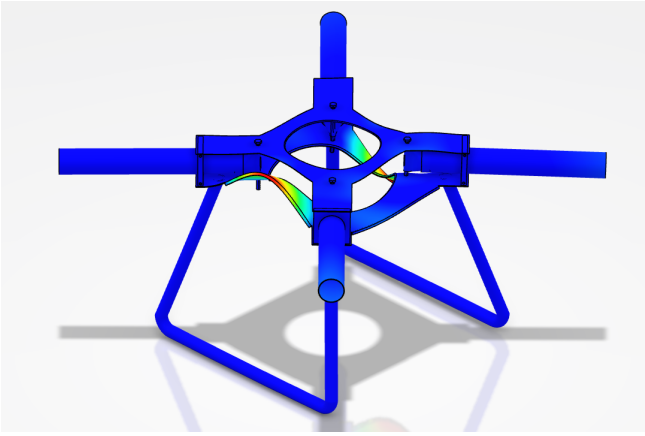

Figure 10.15: Mode 19 Vibration

10.9. Structure Budgeting

The structures subsystem budget is outlined in Table 10.4.

Table 10.4: Structural Budgets

Component	Mass [kg]	Cost [€]	Power required [W]
Body (Aluminium)[15]	7.32	18.3	N/A
Top Plate	1.144	2.86	N/A
Middle Plate	2.976	7.44	N/A
Bottom Plate	3.2	8	N/A
Cylindrical	0.6	1.5	N/A
Arm Assembly	12.312	189.74	N/A
Arm (Carbon Fiber) [16] (x4)	0.70	168	N/A
Motor connector (Aluminium)[15] (x4)	1.0	10	N/A
C clamp (Aluminium) [15] (x8)	0.289	5.78	N/A
Pin (Steel) (x4)	0.30	0.96	N/A
Pin connector (Aluminium)[15] (x4)	0.50	5	N/A
Legs (Carbon Fiber)[16] (×2)	4.10	492	N/A
Total	**28.432**	**700.00**	N/A

[15] `https://markets.businessinsider.com/commodities/aluminum-price` [Accessed: 17/06/2025]
[16] `https://www.easycomposites.co.uk/carbon-fibre-tube` [Accessed: 17/06/2025]

Table 10.5: Compliance Matrix Structure System

Identifier	Requirement Description	Check	Justification	Method	Reference
REQ-SUBSYS-STRUC-1	The UAV arms shall be collapsible.	✔	The structure includes a rotation bolt for the arms, allowing them to rotate such that the drone's dimensions are decreased.	Demonstration	Section 10.4
REQ-SUBSYS-STRUC-2	The UAV arms shall not expand more than 1000 mm.	✔	The 3D model is within bounds, and the drone can be measured once assembled.	Inspection	Section 10.4
REQ-SUBSYS-STRUC-3	The UAV landing legs shall withstand a load in excess of 700MPa.	✔	The legs were designed to withstand such loads.	Inspection	Section 10.4
REQ-SUBSYS-STRUC-4	The UAV arms shall be perforated.	✔	The arms were chosen to fulfil this requirement, and the arms can be checked when bought.	Inspection	Section 10.4
REQ-SUBSYS-STRUC-5	The displacement tolerance of the extended arm shall be less than 5 mm.	**P**	Tolerance measurements can be done after the drone is assembled.	Test	Section 10.4
REQ-SUBSYS-STRUC-6	The displacement tolerance of the extended arm shall be less than 1 deg.	**P**	Tolerance measurements can be done after the drone is assembled.	Test	Section 10.4
REQ-SUBSYS-STRUC-7	The arms shall resist a bending moment of 900 Nm.	✔	Analytically, the arms were designed to resist such bending. Static loading experiments can be performed on the assembled drone.	Demonstration, Analysis	Section 10.4
REQ-SUBSYS-STRUC-8	The loads in the structure shall not exceed 80% of the yield stress during normal operation.	✔	Analytically, the drone is designed to ensure that 80% of the yield stress is not exceeded for any of the materials	Analysis	Section 10.4
REQ-SUBSYS-STRUC-9	The drone structure shall withstand all operational loads, including lift, thrust, payload, and impact forces, with a minimum safety factor of 1.5.	✔	The drone was designed to withstand 1.5 times the operational loads encountered during normal operation	Demonstration, Analysis	Section 10.4
REQ-SUBSYS-STRUC-10	The drone structure shall withstand corrosion from water.	✔	The metallic (aluminium) parts will be anodized. Tests can be conducted in high-humidity and salty environments.	Demonstration	Section 10.4
REQ-SUBSYS-STRUC-11	The drone structure shall withstand temperatures in excess of 50 $^{\circ}C$.	✔	The assembled drone can be put into a temperature-varying chamber to inspect for heat damage.	Demonstration	Section 10.4
REQ-SUBSYS-STRUC-12	The drone structure materials shall be resistant to galvanic corrosion.	✔	All connections between carbon fiber and aluminium are treated with proper corrosion protectors.	Demonstration	Section 10.4

11. Subsystem Integration and Review

11.1. Compatibility Study

In the conceptual phase, a decentralized approach to subsystem design was adopted. Rather than developing several integrated designs to a conceptual level and performing the trade-off between them, each subsystem was considered separately, while the selection of the overall configuration was also disconnected. This gives rise to the justified concern that incompatibilities between the selected subsystem concepts may go unnoticed. However, this approach was considered advantageous in this situation due to the more conventional design considered for the mission.

Owing to the nature of the UAV operations, as well as the requirements imposed by the client and EU regulations, it was decided that the UAV configuration itself is the most important factor in the design. Moreover, not choosing a configuration first would mean that some subsystem-level concepts may be treated unfairly in eventual trade-offs. The use of the UAV in emergency operations supports the selection of tried-and-true options rather than experimental designs, such that the configurations selected for the trade-off in the Design Option Tree were, to a certain extent, conventional. This makes subsystem integration easier, which allows treating them separately during the conceptual design.

It is first necessary to ensure that the selected subsystem concepts are compatible from a conceptual standpoint. To visualize this, it is convenient to build an N2 diagram, which showcases the dependencies between subsystems during the design phase and helps in the identification of potential incompatibilities or bottlenecks. The N2 diagram presented in the baseline report[1] was thus expanded by splitting each subsystem into its respective high-level components. The updated N2 chart can be found below.

N2 Diagram

Propeller	Propeller Rotational Speed											Propeller Dimensions
Propeller Diameter	Motor	Motor Rotational Speed, Current, Voltage	Motor Power, Motor Voltage									Motor Weight, Layout, Maximum Thrust
		ESC		ESC Voltage	ESC Drivers							
Battery Weight			Battery	Battery Voltage						Battery Shape, Weight, Dimensions		Battery Weight
				Power Distribution Board / Voltage Regulators						PDB Position		
				Computer Voltage	On-board Computer							
			Sensor Power		Sensor Drivers	Sensors, IMU, GPS				Sensor Positions		
			Camera Power	Camera Voltage			Camera Array			Camera Shape, Dimensions, Field of View		
Tank Weight								Water Tank	Tank Connection Point	Tank Shape, Weight, Dimensions	Tank Weight	Tank Weight
Pump Weight			Pump Power	Pump Voltage	Pump Actuation Procedure				Water Pump	Pump Shape, Weight, Dimensions	Pump Weight	Pump Weight
Structural Weight			Battery Placement					Tank Placement	Pump Placement	Body Structure and Shape	Structural Weight, Joint Design	Arm Attachment Points
										E-Modulus, Allowable Manufacturing Methods, Density	Materials	E-Modulus, Allowable Manufacturing Methods
Arm Length, Position, Weight											Shape, Folding Mechanism	Arms

Propulsion | Power | Control | Payload | Structure

By analyzing the N2 chart, several important dependencies between subsystems, as well as individual components of a subsystem, can be observed. It is in these cases that compatibility between conceptual design options is most critical and must be discussed. The dependencies are:

- **Payload - Structure:** They display the strongest coupling, which necessitates close coordination between departments during the design process. It is possible to integrate the water tank with the structure through attachment points and even make the tank modular, while the same is done for the camera by using a gimbal. The structure is thus built around the payload.
- **Payload - Power:** The coupling in the design of these two subsystems is generated by the differences in component voltage, which need to be accounted for. They are possible to manage, however, through a PDB or, in more extreme cases, through step-up or step-down voltage regulators. These solutions are commonly used in current multicopter UAVs.
- **Propulsion - Structure:** The integration of the motors, ESCs, and Propellers in the structure represents the challenge in this case. Since the structure consists of arms on which the motors and propellers are mounted, the arms are designed such that they house the motors, while their length should be such that enough clearance for the propellers is provided.
- **Propulsion - Power:** Just as for Payload and Power, the coupling between these subsystems is determined by the voltages required by the motors, as well as the power draw of the ESCs. This is tackled through the appropriate sizing and configuration of the ESCs and PDBs, as these components are also commonly used in UAVs.

11.2. Final Engineering Budgets

This section presents the finalized mass, cost, and power consumption budgets for each major subsystem of the UAV. These values reflect the outcome of all design trade-offs, component selections, and integration decisions made throughout the project. The budget provides a comprehensive overview of the drone's resource distribution and serves as the foundation for verifying compliance with regulatory constraints, such as the maximum take-off weight and total power availability.

Table 11.1: Final Engineering Budgets

Subsystem	Mass [kg]	Cost [€]	Power Required [W]
Propulsion	29.36	9727.20	68000.00
Power	29.89	18876.64	-
Control	9.88	7592.75	40.00
Payload	10.14	2004.56	320.72
Structure	27.83	700.00	-
Total	**107.1**	**38901.15**	**68360.71**

Mass Limitation Note: The current total system mass, excluding water, is approximately 107.1 kg. Considering the legal maximum take-off weight (MTOW) of 150 kg imposed by European UAV regulations, this leaves a margin of roughly 42.9 kg for water, operator-specific mounting equipment, and unaccounted minor components. The original requirement specified a minimum payload of 50 L of water, which corresponds to approximately 50 kg. However, this exceeds the remaining allowable mass and would cause the UAV to violate MTOW constraints. Therefore, to comply with regulatory limits, the operational water payload has been adjusted to 40 L (approximately 40 kg), ensuring that the fully equipped UAV remains within the 150 kg MTOW threshold while still meeting the mission's firefighting objectives with acceptable effectiveness. This is in accordance with discussions that the group had with the main stakeholder of the mission, the Dutch Fire Brigade. Thus, the original REQ-STK-1.1.2 was not fulfilled in the end, but it was adapted dynamically according to negotiation with the customer and the evolution of the UAV design.

The other two aspects, cost and power, are well within the budget of the project, as the total vehicle cost was set to 75000 EUR and the estimated value is just a bit more than half (considering only component

prices, without manufacturing costs and other aspects, described in more detail in the cost breakdown chapter), while the selected batteries can handle a peak power output of about 117 kW (for a short period), which is well above the estimated peak consumption.

11.3. System Layout

Now that all subsystems have been designed, the components can be laid out throughout the structure.

The propulsion subsystem includes the motors, paired with the propellers and their respective ESCs. They are, of course, put in the special harnesses that the arm ends provide. The ESCs are glued inside the arms to limit wire mass. The positioned parts are seen in Figure 11.1.

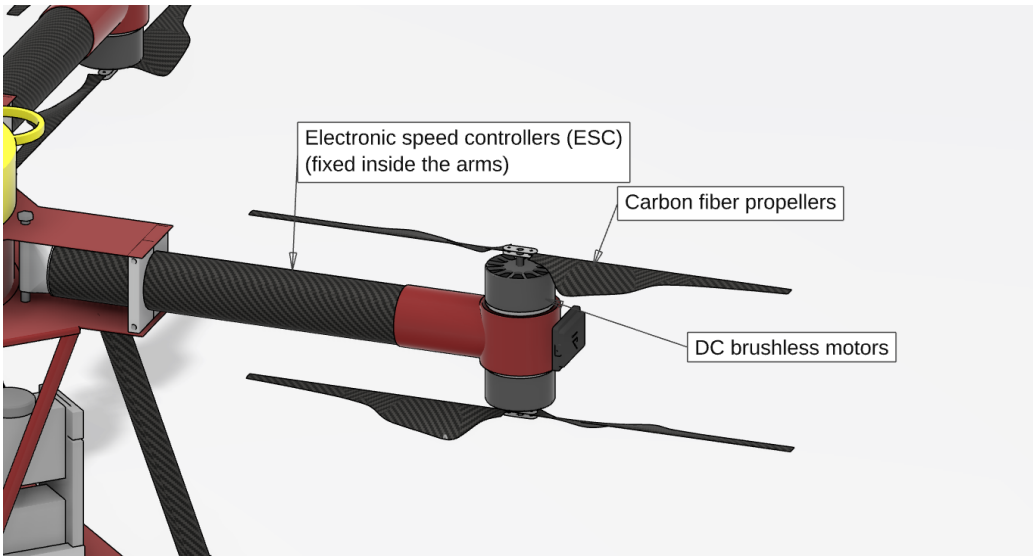

Figure 11.1: Layout of the Propulsion Subsystem

The power subsystem manages the battery assemblies and the PDBs. They are positioned such that they can be easily replaced during a turnaround. The layout is seen in Figure 11.2.

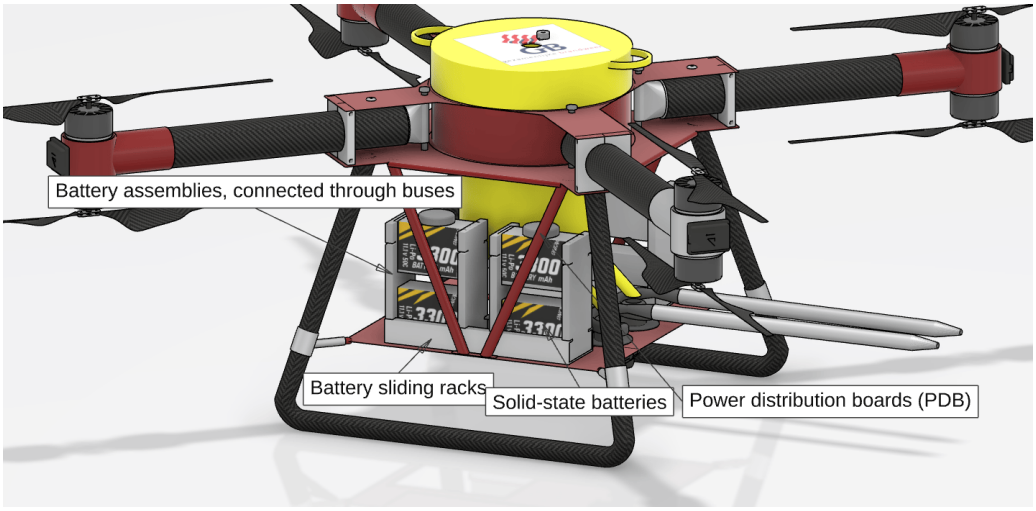

Figure 11.2: Layout of the Power Subsystem

The control subsystem incorporates most components, from the sensors and autopilot modules to the voltage stepdowns and wires. The positioning of various elements is seen in Figure 11.3.

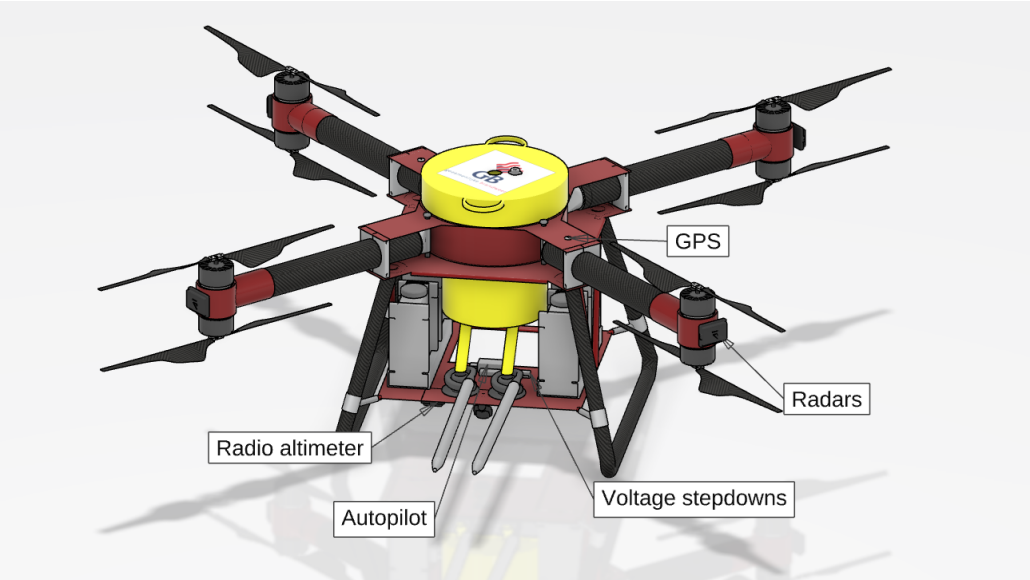

Figure 11.3: Layout of the Control Subsystem

Finally, the payload subsystem is seated in the structure. The positioning of the payload components is given by Section 11.4.

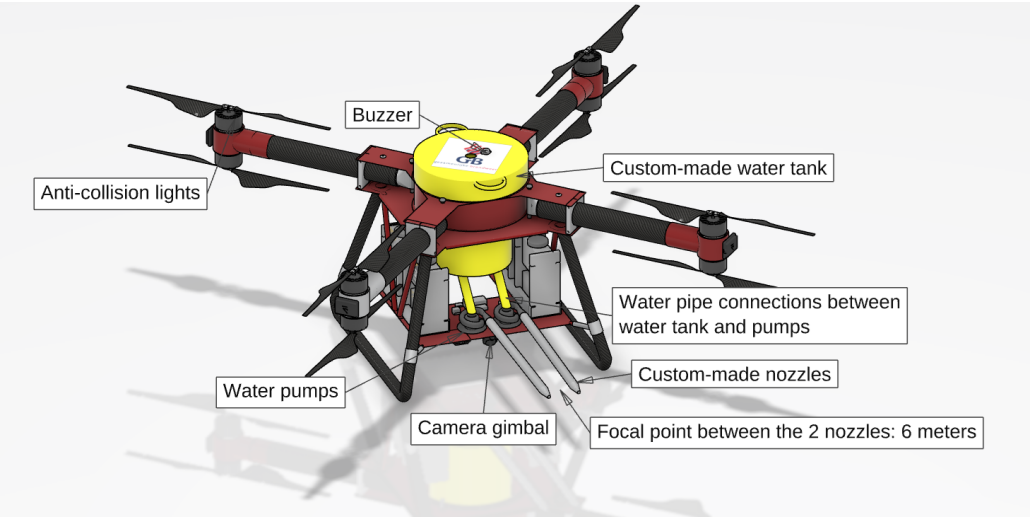

Figure 11.4: Layout of the Payload Subsystem

As a result of the placement of all the components, the CG locations are: 0.068 mm along X, 11.818 mm along Y, and −140.349 mm along Z, respectively. These are referenced with respect to the center of the tank and are important for the control subsystem tuning.

The current design can also fold to be easily transported between missions. Figure 11.5 and Figure 11.6 show the dimensions of the drone in both unfolded and folded states. It should be mentioned again that the nozzles are removable, so the dimensions for the folded design could be smaller.

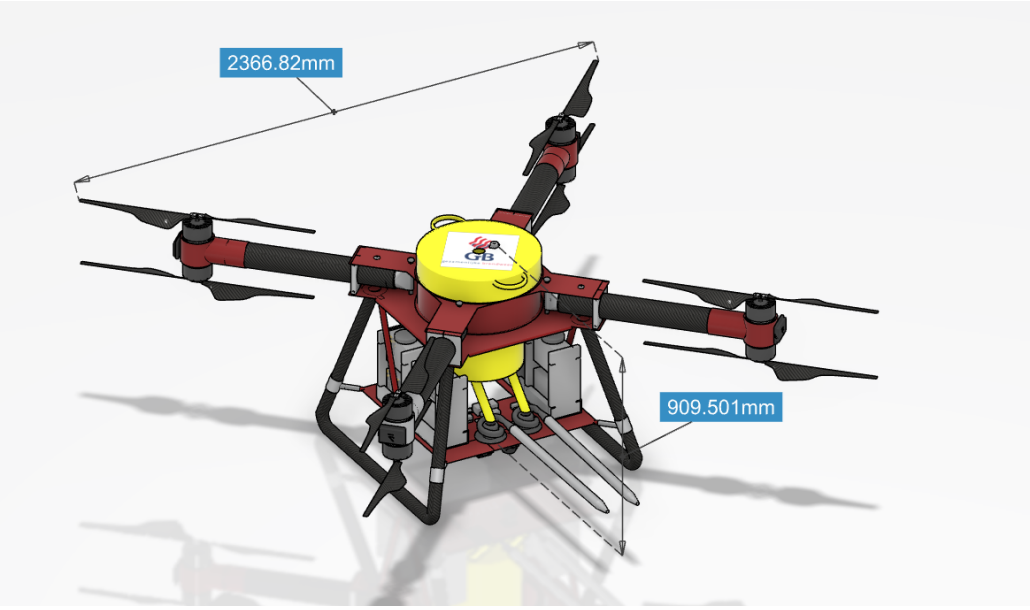

Figure 11.5: Unfolded View with Dimensions

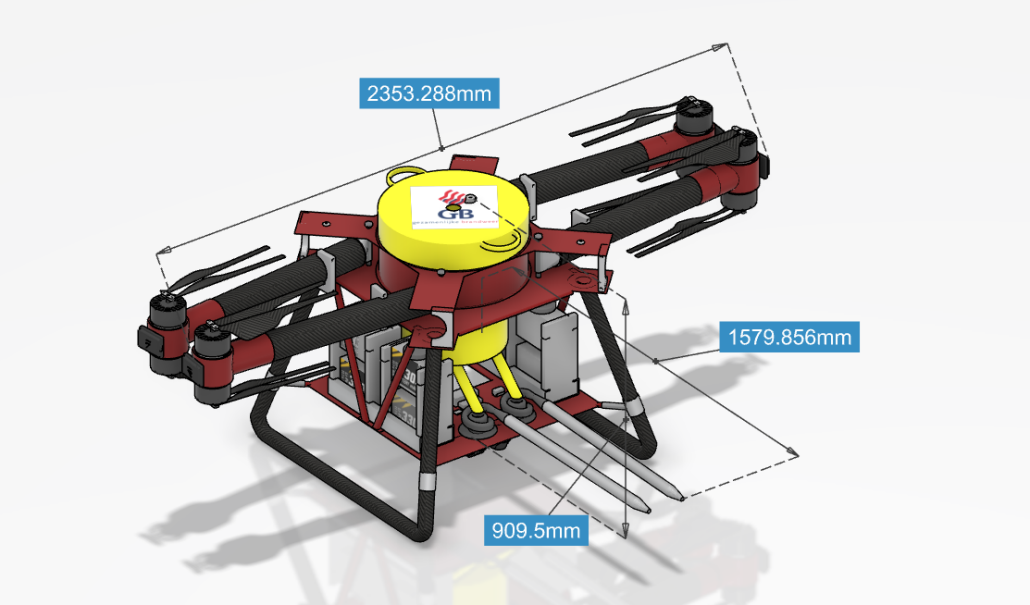

Figure 11.6: Folded View with Dimensions

11.4. Design Sensitivity Analysis

To assess the robustness and adaptability of the UAV design, a sensitivity analysis was performed by evaluating how specific design changes affect key system characteristics. Unlike the one in the trade-off analysis, this sensitivity analysis investigates how the final design responds to some variations in technical assumptions, design decisions, or component substitutions. These changes were chosen based on realistic manufacturing, performance, or operational constraints that may arise during development or deployment.

For each change, the UAV was qualitatively and semi-quantitatively assessed, based on the impact on subsystem mass, power consumption, and overall feasibility. This approach does not rely on numerical simulations or parametric tools but instead leverages engineering reasoning and known dependencies from the existing sizing and performance calculations.

Evaluation of Sensitivity Cases

1. 4 Larger Motors Instead of 8 Coaxial

Switching to four larger motors reduces component count and wiring complexity. While motor efficiency may slightly improve, each motor must generate double the thrust, increasing propeller diameter and structural loads on each arm. As a quick sizing comparison, new motors that would fulfill the thrust requirements, such as the larger options offered by Furious Motors [1], would weigh 5.9 kg each, giving an overall motor mass increase of 4.4 kg, or 15% of the current propulsion system mass. Then, they require longer propellers [2], of 47 inches, which could pose problems for the overall dimensions in flight or during transportation, or at least impose significant structural changes that can affect mass even more. Larger ESCs would also be needed to keep them compatible with the 300 A current capability suggested by the manufacturer of the new motors. Another mass increase would come from the batteries, which shall sustain a power draw of 18 kW from four motors, compared to 8.5 kW from eight motors before, and this will also propagate to the wiring mass, as it will have to sustain higher currents and thus weigh more. Last but not least, losing a motor during flight for the quadcopter version would be much more critical compared to the current propulsion and control system design, which accounts for safety as a top priority. Considering the tight mass budget and the fact that this change does not bring significant operational improvements, its feasibility is quite low.

2. Full Aluminium Frame

Replacing CFRP with aluminium increases structural weight by an estimated 18%, depending on geometry, since the arm mass increases from 0.7 kg to 1.2 kg, while the leg mass increases from 4.1 kg to 5.6 kg. This is equivalent to a 5 kg mass increase, which is not desirable at all in the context of the payload capability, which was already reduced to 40 L, as these five additional structural kilograms will equate to an additional water quantity decrease. While cost and manufacturability improve, total MTOW approaches or surpasses regulatory limits, requiring performance sacrifices or redesign, thus making this material change would not be beneficial overall.

3. Lower Thrust-to-Weight Ratio (TWR)

Reducing TWR reduces total motor and battery mass, potentially improving endurance and decreasing power demand, and leaving some margin for the payload mass. However, responsiveness during aggressive maneuvers or emergency recovery (e.g., one-motor-out) degrades, as well as resistance to stronger wind gusts. Due to the operational considerations of the mission, it was deemed that it is more important to ensure safe flight during hard conditions (smoke, wind, collision avoidance, OEI scenarios) than to deliver 10 more liters of water per ascent, because this last aspect can be mitigated well by having a good turn-around time and efficient ground operations.

4. Increased Arm Length

Longer arms improve control authority and allow a lower thrust-to-weight ratio, reducing power needs and possibly battery mass. However, they add structural weight and complexity, especially for folding mechanisms. Increased arm length also raises aerodynamic drag and vibration risks, which can affect efficiency and sensor performance. Additionally, the water nozzles must be positioned further out to avoid obstruction by the propellers, requiring an additional structure. Practical limits on drone size for transport and deployment restrict how long the arms can be.

[1] https://furiousmotor.com/products/zero-g-154-120

[2] https://furiousmotor.com/products/ah-47

Table 11.2: Design Sensitivity Overview

Change	**Motivation**	**Mass**	**Power**	**Other impacts**	**Feasibility**
4 Larger Motors	Fewer ESCs, simpler wiring	↑	↑	↓ safety (OEI)	Low
Aluminium Frame	Cheaper, easier to make	↑	–	↑ thrust needed	Low–Med
Decrease thrust-to-weight ratio	Mass reduction, payload increase	↓	↓	↓ agility and safety	Low
Longer Arms	More control authority	–	↓	↓ compactness, ease of transport	Medium

12. Technical Risk Assessment

Risk analysis starts with a risk register, stating the event and its corresponding subsystem, its type, its impact, its likelihood, its consequence, and its risk. A responsible person is assigned to evaluate the risk during the project constantly. It is outlined in Table 12.1. Likelihood is the probability of occurrence of an event, ranked from 1 to 5 as follows: 1 - rare, 2 - unlikely, 3 - moderate, 4 - likely, 5 - very likely. The consequence is the severity of the event in case it occurs, ranked from 1 to 5 as follows: 1 - insignificant, 2 -minor, 3 - moderate, 4 - major, 5 - extreme. The risk is the product of likelihood and consequence.

Based on this point system, the risk map can be constructed in Figure 12.1, first for general risks for the system as a whole. The risks are divided into three categories, colored in green for scores 1-5, in yellow for scores 6-14, and in red for scores 15-20. Green denotes a minor risk, yellow stands for a moderate risk, while red indicates a major risk.

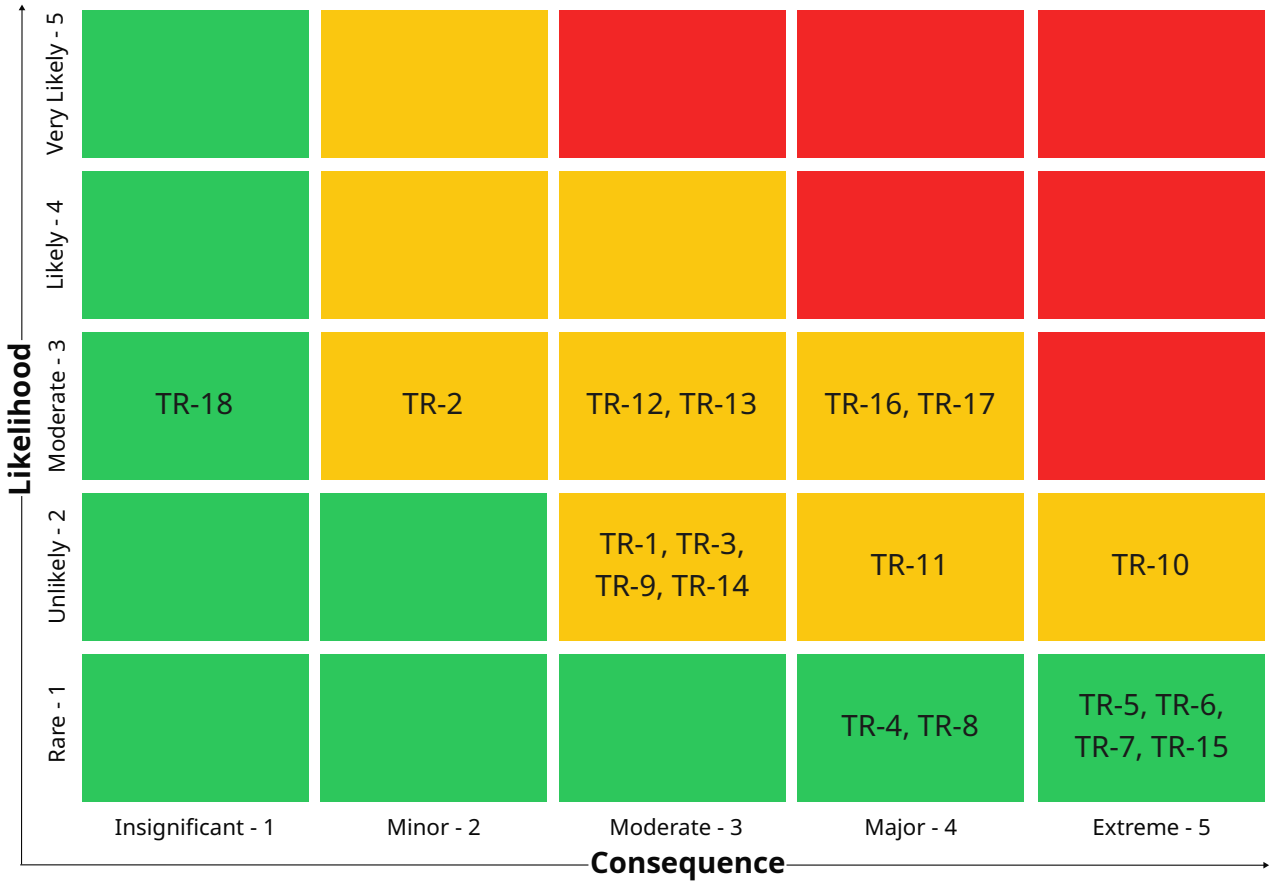

Figure 12.1: Technical Risk Map

Table 12.1: Technical Risk Register for Firefighting UAV

ID	Event	Impact	Likelihood	Consequence	Risk	Responsible
TR-1	Manufacturing defects/errors present in the product	Possible mission failure, certification issues, delays due to remanufacture	2	3	6	Vlad
TR-2	Failure of one or more certification tests	Redesign, delays in development/production, higher cost	3	2	6	Andres
TR-3	Product damaged during transportation	Time lost for replacement, increased cost for repairs	2	3	6	Andres
TR-4	Start-up mechanisms/software not functioning properly	Mission is delayed until reboot; mission abortion possible if error persists	1	4	4	Eduard
TR-5	Failed take-off or landing	Safety hazard, product destruction, mission delay	1	5	5	Stefan
TR-6	Failed or unresponsive maneuvering	Target missed, control issues, potential damage	1	5	5	Radu
TR-7	Failed stabilization measures	Tip-over, collisions, aiming failure	1	5	5	Laura
TR-8	Sudden rotor(s) failure	Loss of control, crash risk, mission failure	1	4	4	Arun
TR-9	Failure of fire-detection devices	Reduced situational awareness, missed fire target	2	3	6	Hugo
TR-10	Failure of fire-extinguishing system	Mission delay or failure due to need to return to base	2	5	10	Andres
TR-11	Recharge/refill/replacement faults on ground	Turnaround delays, failure risk without redundancy	2	4	8	Vlad
TR-12	Operator error during operation	Structural integrity compromised, cumulative damage risk	3	3	9	Laura
TR-13	Prolonged exposure to fire/hostile environments	Gradual damage, reduced mission performance	3	3	9	Radu
TR-14	Loss of communication signal	Mission aborted or delayed by auto-landing	2	3	6	Arun
TR-15	Failure to initiate emergency landing	Unsafe landing, risk to UAV and surroundings	1	5	5	Alexandra
TR-16	Improper software maintenance	In-flight errors, mission failure	3	4	12	Andres
TR-17	Improper hardware maintenance	Degraded performance, critical failures	3	4	12	Hugo
TR-18	Unsustainable end-of-life procedures	Environmental harm, waste of materials	3	1	3	Gijs

Table 12.2: Mitigation and Contingency Planning for Selected Technical Risks

ID	Event	Impact	Preventive Measures / Mitigation	Contingency Plan	Post-management Risk
TR-10	Failure of fire-extinguishing system	Mission delay or failure due to the need to return to base	Frequent functional tests at base; nozzle cleaning before deployment; use of filtering system for water	Use of dual-pump system for redundancy; return to base for fixing	3
TR-11	Recharge/refill/ replacement faults on ground	Turnaround delays, failure risk without redundancy	Have redundant batteries which are modular; tank carefully refilled, and a level sensor to avoid spillage	Use a backup UAV to avoid mission delays	3
TR-12	Operator error during operation	Structural integrity compromised, cumulative damage risk	Mandatory operator training, use of multiple sensors to avoid collisions	Autonomous landing after detecting abnormal behavior	4
TR-13	Prolonged exposure to fire/hostile environments	Gradual damage, reduced mission performance	Heat-resistant coatings with enclosed electronics	Autonomous landing for inspection when excessive temperature is detected	4
TR-16	Improper software maintenance	In-flight errors, mission failure	Automated version control, pre-flight software diagnostics	Reboot to backup firmware; autonomous landing if UAV does not recover	6
TR-17	Improper hardware maintenance	Degraded performance, critical failures	Frequent part inspections; maintenance tracking	Return to operator to prevent safety risks; replace with backup parts, if unavailable, deploy alternate UAV to continue mission	3

After identifying the critical risks, risk management can be performed. Table 12.2 outlines the highest-risk events. The mitigation represents a preventive measure of reducing the occurrence of the risk, therefore decreasing the likelihood, while the contingency plan ameliorates the situation in case the event occurs [29]. In Figure 12.2, the post-mitigation risk map is showcased.

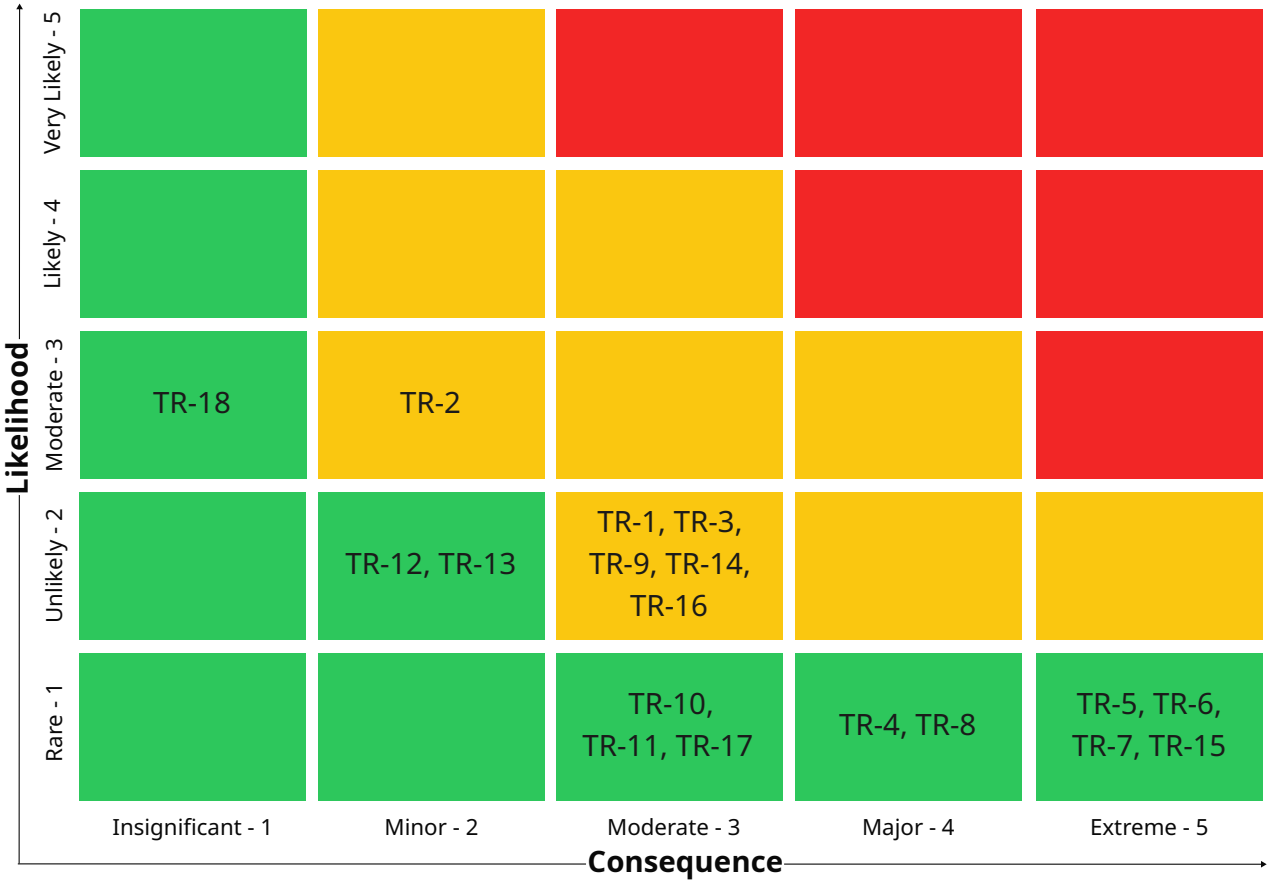

Figure 12.2: Post-management Risk Map

It can be seen that there are fewer events causing risks in the yellow category and many of them have made the transition to the green category. The risks in the yellow category should be constantly monitored.

Next, based on the subsystem design, risks at subsystem level are defined in Table 12.3 and illustrated on a risk map in Figure 12.3. The mitigation strategy is then explained in Table 12.4 and the post mitigation risk map is shown in Figure 12.4.

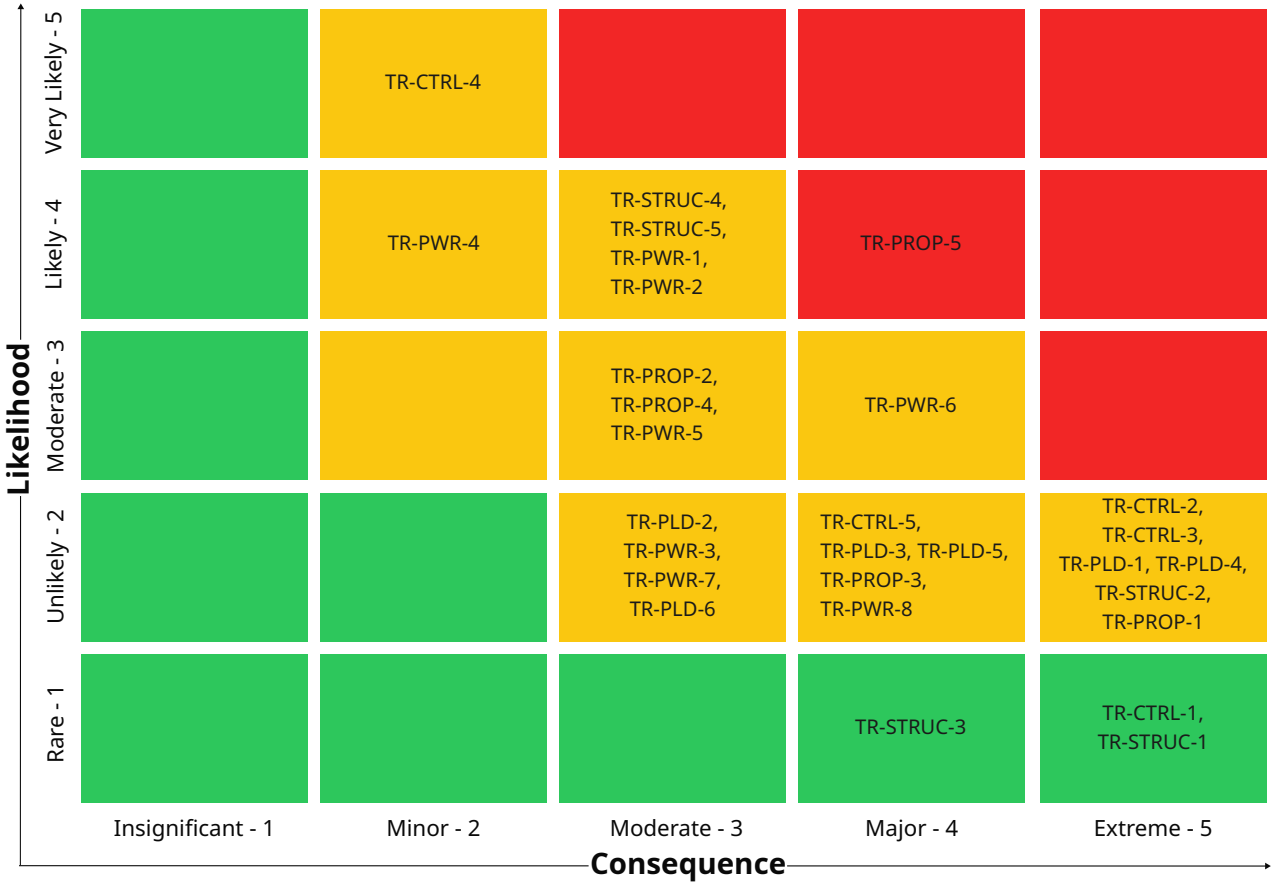

Figure 12.3: Technical Risk Map at Subsystem Level

Table 12.3: Technical Risk Register for Firefighting UAV

ID	Event	Impact	Likelihood	Consequence	Risk	Responsible
TR-PLD-1	The tank sustains damage due to transport/heat/impact with foreign objects	Water could leak, leading to mission abortion	2	5	10	Radu
TR-PLD-2	Tank opening mechanism jams or warps	Failure to release payload when needed	2	3	6	Alexandra
TR-PLD-3	Pump clogging from particulates or scale	Decreased extinguishing reach and pressure	2	4	8	Alexandra
TR-PLD-4	Hose rupture or detachment during spraying	Interruption of flow and reduced suppression efficiency; mission has to be aborted	2	5	10	Radu
TR-PLD-5	Camera inoperable due to fogging or overheating	Reduced thermal imaging clarity or misreading of hotspots	2	4	8	Alexandra
TR-PLD-6	Water release mechanism leaks or opens by mistake during flight	Payload loss, refill required, possible controllability problems due to unexpected water drop	2	3	6	Radu
TR-PWR-1	Battery degradation over time	Reduced endurance and less reliable, increases down-time frequency	4	3	12	Hugo
TR-PWR-2	Battery overheating	Decrease battery life, release toxic gases, short circuits and component melting, battery replacement delays	4	3	12	Hugo
TR-PWR-3	Moisture absorption during mission	Causes electrical short circuits, corrosion, or complete failure in wet environments	2	3	6	Hugo
TR-PWR-4	Connector failure or corrosion	Partial or total power loss, could lead to failure or increased resistance	4	2	8	Gijs
TR-PWR-5	Incorrect battery mounting/vibrations	Damage to connector or cells, unexpected heating, sparks	3	3	9	Gijs
TR-PWR-6	Too high peak current	Damage components, loss of thrust	3	4	12	Gijs
TR-PWR-7	Electromagnetic interference	Disruption of control/communication signals	2	3	6	Hugo
TR-PWR-8	Remaining energy storage insufficient for finishing mission, during flight	Possible loss of flight capabilities or mission abortion	2	4	8	Hugo

ID	Event	Impact	Likelihood	Consequence	Risk	Responsible
TR-PROP-1	8 motors demand high instantaneous current during aggressive maneuvers or takeoff	Overloading the power distribution board or wires can lead to fire or malfunction	2	5	10	Andres
TR-PROP-2	Heat buildup in stacked/coaxial motor pairs	Overheating, efficiency loss, motor or ESC burnout	3	3	9	Laura
TR-PROP-3	Centralized power/signal distribution to 2 motors on an arm fails	Both motors on one arm can be lost	2	4	8	Andres
TR-PROP-4	Mismatch in motor KV or ESC calibration	Uneven thrust, oscillations, or loss of control	3	3	9	Laura
TR-PROP-5	Dust, water, or soot accumulates in/on motors/ESCs (common in firefighting UAVs)	Short circuits, degraded motor performance, corrosion	4	4	16	Andres
TR-CTRL-1	RADAR sensors cause electromagnetic interference	Failure to process commands, stuck controls, imminent crash	1	5	5	Vlad
TR-CTRL-2	Main power supply to the autopilot board fails in-flight	Imminent crash	2	5	10	Vlad
TR-CTRL-3	Autopilot software bugs due to insufficient testing	Collision avoidance system malfunctions, control commands unexecuted, drone crashes	2	5	10	Vlad
TR-CTRL-4	Flight instability induced by uncertain fire environment	Flight law augmentation delivers suboptimal flight stabilization during spraying	5	2	10	Vlad
TR-CTRL-5	One RADAR sensor fails	Collision avoidance performance is degraded	2	4	8	Vlad
TR-STRUC-1	Arm structure fails	Thrust imbalance, imminent crash	1	5	5	Eduard
TR-STRUC-2	Joint between arm and body structure fails	Arm folds, thrust imbalance, imminent crash	2	5	10	Eduard
TR-STRUC-3	Vibrations resonate with the natural frequency of the structure	Component failure	1	4	4	Arun
TR-STRUC-4	Repeated exposure to high temperatures causes creep	Deformation, drone immobilization	4	3	12	Arun
TR-STRUC-5	Multiple mission cycles can propagate fatigue	Drone immobilization	4	3	12	Arun

Table 12.4: Mitigation and Contingency Planning for Selected Technical Risks

ID	Event	Preventive Measures / Mitigation	Contingency Plan	Post-Likelihood	Post-Consequence	Risk
TR-PLD-1	Tank sustains damage in operation	Thin aluminium shielding, internal reflective coating, robust mounting	Check the integrity of the tank as soon as possible; patch/replace the tank	1	4	4
TR-PLD-4	Hose ruptures during spray	Use braided hose, avoid tight bend radius	Monitor pressure drop; shut off pump, return to base	1	4	4
TR-PWR-1	Battery degradation over time	Use batteries with high cycles, schedule replacements, limit discharge, plan routine battery checks	Use replacement batteries, use degraded batteries for training, alert operator	3	2	6
TR-PWR-2	Battery overheating	Efficient cooling system, safe battery composition choice	Sensors to cut off power, emergency landing, alert operator	3	2	6
TR-PWR-6	Too high peak current	Limit current and thrust, use batteries with a high C-rate, use high current motors, avoid strong maneuvers, have a current limiter	Reduce thrust, let stabilize drone by hovering, land if necessary	2	3	6
TR-PROP-1	8 motors demand high instantaneous current during aggressive maneuvers or takeoff	Overspec the PDB and wiring for peak current, simulate worst-case electrical load during design	Trigger automated throttle reduction if voltage drops below safe threshold, Allow ESCs to shut down motors gracefully if overheating occurs	1	4	4
TR-PROP-5	Dust, water, or soot accumulates in/on motors/ESCs (common in firefighting UAVs)	Prefer inrunner motors (sealed or semi-enclosed)	Run post-flight cleaning protocol (compressed air, isopropyl wipes), swap affected components between sorties	2	3	6

ID	Event	Preventive Measures / Mitigation	Contingency Plan	Post-Likelihood	Post-Consequence	Risk
TR-CTRL-2	Main power supply to autopilot board fails in-flight	Use an extensively tested, dual-path power module with voltage monitors	Use the backup, secondary power supply	1	4	4
TR-CTRL-3	Autopilot software bugs in-flight	Extensive autopilot testing under high load conditions; preflight diagnostics	Failsafe to autonomous landing mode or reboot to backup firmware	1	4	4
TR-CTRL-4	Flight instability induced by uncertain fire environment	Have passive/active wind/turbulence rejection mechanisms to increase stability	Stop spraying to better balance the drone, abort, and land if necessary	4	1	4
TR-STRUC-2	Joint between arm and body structure fails	Use high-strength fasteners, redundant brackets or cross-links to distribute load	Set automatic throttle cut-off and enter controlled descent mode if sensor detects rapid arm movement, limit folding range to prevent complete collapse	1	4	4
TR-STRUC-4	Repeated exposure to high temperatures causes creep	Use heat-resistant materials (like carbon fibre) in load-bearing parts, thermal insulation to arms near hot components or external heat sources	Monitor frame temperature with onboard sensors, land and ground drone, if warping exceeds tolerance	3	2	6
TR-STRUC-5	Multiple mission cycles can propagate fatigue	Design structural components using fatigue-rated materials (e.g.carbon fiber), establish mission life-cycle limits, and perform periodic non-destructive testing	Inspect key joints and arms at regular maintenance intervals, retire or replace structural components before reaching fatigue life	3	2	6

As a conclusion, there are no events causing risks in the red category, and fewer events are causing risks in the yellow category. However, the risks that still belong to the yellow category shall be monitored continuously by the responsible members and mitigated when possible, in order to ensure they do not become critical over time.

Figure 12.4: Post-mitigation Technical Risk Map at Subsystem Level

Additional requirements are generated in order to accomplish the mitigation procedures, as following:

- **REQ-SYS-RISK-1**: The payload system pump system shall have more than one pump for redundancy.
- **REQ-MIS-RISK-1**: The water refill system on the ground shall filter the water.
- **REQ-MIS-RISK-2**: The turnaround routine shall have redundant batteries.
- **REQ-MIS-RISK-3**: The turnaround routine tank refill shall avoid spillage.
- **REQ-MIS-RISK-4**: The UAV shall land autonomously at the nearest clearing in case of degraded performance.
- **REQ-MIS-RISK-5**: The UAV maintenance department shall perform frequent part inspections.

13. Production Plan

Because the UAV is expected to be produced in small numbers, it will be assembled manually. In this chapter, the Production Plan of the UAV is described, from the gathering of the materials to the final assembly.

13.1. Description of the Assembly

The structure of the UAV consists of a main body and four motor arms. The main body supports the water tank and is made of a top plate, a middle plate, and a bottom plate. The top and middle plates are the most important parts of the structure and are load-bearing. They are also used for wiring and to mount certain electrical components, such as the PDBs. The bottom plate, on the other hand, is not an integral part of the structure and is used to mount the batteries, the pumps, the autopilot, and voltage regulators.

The assembly will be done in such a way as to provide strength to the structure. The full assembly consists of the main body assembly and the four arm assemblies, which are put together separately. Moreover, the main body can be split into multiple sub-assemblies, one consisting of a top plate-middle plate combination and one made of a bottom plate and landing legs.

13.2. Tool List

The successful assembly of the UAV requires a well-defined set of tools and safety equipment to ensure precision, repeatability, and safety throughout the production process. The following lists outline the necessary items categorized into safety gear, measurement instruments, and assembly tools, all of which are essential for handling aluminium and CFRP components, performing accurate cuts and drillings, and mounting both mechanical and electronic parts.

Measurement Instruments

- Metal ruler (50 cm) with level, for measuring short distances and checking level surfaces;
- Measuring tape (200 cm), for measuring longer distances;
- Pencil, for temporary markings;
- Permanent marker, for permanent markings and annotations;
- Try square, to measure right angles.

Assembly Tools

- Milling machine/CNC machine;
- Sheet metal bending press;
- Welding kit;
- Cutting die/hacksaw with carbide tooth blade, to cut aluminium plates to size;
- Hand reamer, for deburring of the plates;
- Battery-powered drill, for drilling holes into aluminium plates;
- Center punch, to make indents in points marked for drilling;
- Drill bit set;
- Deburring drill bit, for hole deburring;
- Wrench set, for tightening nuts;
- Hot glue pistol, for mounting circuit boards and small electrical components.

Assembly Materials

1. Aluminium-aluminium adhesives;
2. Aluminium-CFRP adhesives (with galvanic corrosion resistance);
3. Anti-corrosive treatments (for example, electrolyte bath for anodizing aluminium).

13.3. Material and Component List

Here, all the necessary materials and components to assemble the UAV are listed. The cables are listed separately. The required materials are:

- 2x $850 \times 850 \times 3$ mm^3 7075-T6 Aluminium alloy plate - for the top and middle plates;
- 1x $750 \times 750 \times 3$ mm^3 7075-T6 Aluminium alloy plate - for the bottom plate;
- 1x $1000 \times 1000 \times 1$ mm^3 7075-T6 Aluminium alloy plate - for the cylindrical plate;
- 4x 700 mm CFRP tube - for the arms;
- 1x $200 \times 200 \times 100$ mm^3 7075-T6 Aluminium alloy block - for the brackets (to be cut in four $180 \times 180 \times 20$ mm^3 blocks);
- 4x AISI 4130 steel pins - for the rotation bolts;
- 4x $200 \times R20$ mm^2 7075-T6 Aluminium tubes - for the truss structure;
- 1x $100 \times 100 \times 1$ mm^3 7075-T6 Aluminium sheet - for various additions;
- 4x $100 \times 100 \times 100$ mm^3 6063-T6 Aluminium alloy block - for the arm-rotation bolt connectors in the hinges.

The required components are:

- 2x CFRP landing legs (custom-made);
- 8x 350 Wh/kg Series Semi-Solid State High Energy Density Battery Pack, TARBG3526312S10X from Grepow;
- 8x 12070 40 kg BLDC Furious Motor for VTOL/UAV Heavy Lift Drone;
- 8x Furious Motor 24S 150A High Compatibility ESC for Multi Rotor Drones;
- 8x FA 36.2 inch Diameter, 11.8 inch Pitch Foldable Prop - 2 pcs/pair;
- 6063-T6 Aluminium tube head motor connectors (custom-made);
- 2x Davies Craig EWP150 Pump;
- 1x Skydroid C13 Three-Light Gimbal;
- 2x Water nozzle (custom-made);
- 2x Water hose (custom-made);
- 1x Water tank (custom-made);
- 1x Kendrion Solenoid Door Lock;
- 2x 6063-T6 Aluminium battery rails (custom-made);
- 2x Holybro M10 GPS;
- 9x Ainstein US-D1 RADAR;
- 1x Herelink v1.1 Air Unit receiver;
- 1x Cube Red flight controller + Cube Red standard carrier board;
- 2x Mateksys SVPDB-8S Power distribution board;
- 4x Avizar PDB-1000 Power distribution board;
- 8x Voltage regulator / Battery eliminator circuit;

- 4x SFM-27-I buzzer;
- 4x STROBON v2 Navigation Light;
- Bolts and rivets; specifying their types was considered outside the scope of this project.

13.4. Preparation

Until the assembly can be started, a safe workplace must be ensured before starting work, and components need to be prepared.

Safety

1. A workplace coat, long trousers, work boots, and safety glasses must be worn at all times;
2. Hair must be tied;
3. The workplace must be kept clean and orderly;
4. During sawing of material, drilling and deburring using the battery drill, long sleeves must be worn;
5. During sawing of the material, hearing protection must be worn;
6. During welding of the material, the necessary safety equipment provided by the kit's producer must be worn;
7. The workplace must be cleaned after finishing work.

Cutting Plates to Size

1. Take the aluminium sheet;
2. Make pencil cutout markings according to the *Top Plate Technical Drawing*;
3. Check markings for correctness and go over pencil with permanent marker;
4. Make cuts with the milling machine;
5. Use hand reamer to deburr edges;
6. Make pencil markings for bolt holes according to the *Top Plate Technical Drawing*;
7. Check markings for correctness and go over pencil with permanent marker;
8. Use battery-powered drill to drill holes;
9. Use a deburring drill bit to deburr hole edges.

Bending the Cylindrical Plate

1. Take the aluminium sheet cut to the needed dimensions;
2. Use the bending press to bend the plate to a cylindrical shape;
3. Bend ends as flanges;
4. Use hand reamer to deburr edges;
5. Make pencil markings for rivet holes according to the *Cylindrical Plate Technical Drawing*;
6. Check markings for correctness and go over pencil with permanent marker;
7. Use battery-powered drill to drill holes;
8. Use a deburring drill bit to deburr hole edges.

Welding the Truss Structure

1. Take the spare aluminium sheet;
2. Make pencil cutout markings according to the *Truss Structure Plate Technical Drawing*;
3. Check markings for correctness and go over pencil with permanent marker;
4. Repeat steps 1-3 for each added plate (3 in total);

5. Place the tubes in the positions indicated in the *Truss Structure Technical Drawing*;
6. Weld the tubes to the plates;
7. Use hand reamer to deburr edges.

Treat for Corrosion

1. Anodize the aluminium parts by submersing them in acid electrolyte baths;
2. Treat aluminium faces that will be in contact with CFRP with galvanic corrosion preventive substances;
3. Treat aluminium faces that will be in contact with other aluminium parts with anti-corrosive substances.

13.5. Assembly of the Main Body

The plates of the main body and the landing legs are assembled and joined.

Bottom Plate Assembly

Required components: bottom plate, 2x water pump, 2x battery rails, flight controller + carrier board, camera, 4x PDB, 1x RADAR.

1. Take bottom plate;
2. Mark holes/standoffs with corresponding components that will be mounted;
3. Mark positions of components in pencil according to the bottom plate assembly technical drawing;
4. Check markings for correctness and go over pencil with permanent marker;
5. Use hot glue gun to install the carrier board + flight controller in its marked position;
6. Use a wrench to install the water pumps in their marked position;
7. Use a wrench to install the battery rails in their marked position;
8. Use a wrench to install the camera in its marked position.

Middle Plate and Landing Legs Assembly

Required components: 2x landing legs, middle plate, 4x aluminium leg end plates, 2x truss structure.

1. Take first landing leg;
2. Insert two end plates into the free ends of the landing leg, one for each free end;
3. Clamp down the end plates;
4. Join middle plate with landing legs and insert screws through the common standoffs;
5. Repeat steps 1-4 for the second landing leg and the remaining two end plates;
6. Join both truss structures with both the middle and bottom plates;
7. Tighten screws.

Connecting the Bottom Plate

Required components/sub-assemblies: middle plate and landing legs assembly, bottom plate assembly.

1. With the landing legs assembly on flat ground (use level), measure 170 mm from the ground;
2. Mark the 170 mm level with permanent marker on each end;
3. Slide the bottom plate assembly under the landing leg assembly and tighten the corner clamps at the 20 cm level;
4. Use a level ruler to check that the bottom plate is level with the ground;

13.6. Assembly of the Arms

Required components: 4x arm, 4x aluminium arm end caps, 8x motor, 4x pin, 8x aluminium bracket halves, 4x arm-hinge aluminium connectors.

1. Take arm;
2. Insert arm into end cap;
3. Tighten end cap clamp;
4. Place the first motor on top of the end cap;
5. Pull motor cable through the hollow center of the arm;
6. Screw down motor;
7. Place the first motor on the bottom of the end cap, holding it in position;
8. Pull motor cable through the hollow center of the arm;
9. Screw down motor;
10. Check motors and end caps for any play;
11. Fix the arm-hinge interface to the arm.

13.7. Complete Assembly

With the sub-assemblies completed, they can be joined in the complete assembly.

Joining the Arms to the Body

Components/sub-assemblies required: landing legs, bottom and middle plate assembly, 4x arm assembly, top plate, 8x steel pins, 4x aluminium bracket half-piece.

1. Take landing legs, bottom plate, and middle plate assembly;
2. Screw down aluminium bracket half-pieces in corresponding standoffs in the corners of the middle plate;
3. Take the top plate and set it on the screwed-down aluminium bracket half-pieces;
4. Screw down top plate to aluminium bracket half-pieces in corresponding standoffs;
5. Take the arm assembly and steel pin;
6. Join together the middle plate bracket half-piece to the arm-attached bracket half-piece and manually hold the arm in place;
7. Insert steel pin into its corresponding stand-off;
8. Repeat steps 5-7 for the remaining three arm assemblies.

Final assembly

Required components: Body-arms assembly, water tank, 8x propellers, 8x RADAR, 2x GPS, 1x buzzer, 4x anti-collision lights.

1. Add water tank to its pocket in the main body;
2. Glue the RADARs in their intended positions;
3. Glue the GPS components in their intended positions;
4. Glue the buzzer to its intended position;
5. Glue the anti-collision lights to their intended positions;
6. Attach the propellers to the motors.

14. Technical Sustainability Plan

The Life Cycle Sustainability Assessment (LCSA) approach divides sustainability into three connected themes [30]:

- Environmental Life Cycle Assessment (ELCA);
- Life Cycle Costing (LCC);
- Social Life Cycle Assessment (SLCA).

The framework is depicted in Figure 14.1, where LCA is equivalent for ELCA. The first theme needs to be focused on for technical analysis purposes. This category considers the recyclability, emissions, and energy consumption of the design. These aspects have directly been translated into requirements to promote sustainability into the design.

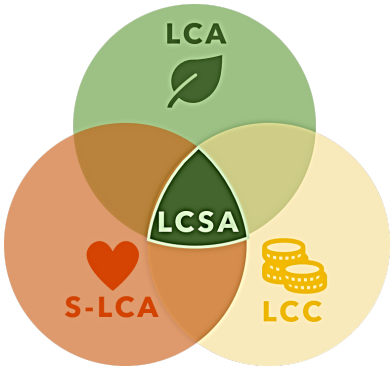

Figure 14.1: Life Cycle Sustainability Assessment Framework

Table 14.1, Table 14.2 and Table 14.3 show an overview of the sustainability assessment procedure. Each theme has its corresponding metrics and requirements (targets). This overview has a dynamic nature, because it was continuously updated throughout the design process. The Sustainability Manager was responsible for the ELCA and LCC categories, while the HR & Legal Manager carried the responsibility of social sustainability. Note that only the Sustainability Manager has the mandate to enforce design decisions.

Some target metrics have already been determined with preliminary research or design decisions. Others were planned to be set at a later stage in accordance with the stakeholders. However, since contact was not possible, the values are set as deemed reasonable. The toxic material content, for instance, should be zero, as set by law. For environmental purposes, the life span of the product shall be at least 5 years. Noise emissions should also be minimized as much as possible and cannot exceed 80 dB due to acceptable labor conditions [1]. A design goal is to use at least 60% of recyclable material, and to have a high work satisfaction (4/5). The carbon footprint is aimed to be lower than 171 g CO_2/min, to be lower than the average diesel car per minute, assuming an average speed of 60 km/h[2]. The operational energy consumption is preferred to be less than 2000 Wh to be lower than the production of two average 1 kW solar panels[3]. Lastly, by new regulations, the package material should be recyclable for at least 65% by the end of 2025, but the aim will be at least 75%[4] to be compliant with possible constraints in the future. The LCC-related targets are, as mentioned earlier, based on estimated values with regards to the stakeholders. Given the relatively simple structure and

[1] https://business.gov.nl/regulation/harmful-noise-levels/ [Date Accessed: 02/05/2025]
[2] https://www.bbc.com/news/science-environment-49349566 [Date Accessed: 19/05/2025]
[3] https://nenpower.com/blog/how-much-electricity-does-a-1-kw-solar-panel-generate [Date Accessed: 19/05/2025]
[4] https://eur-lex.europa.eu/legal-content/EN/TXT/?uri=legissum:l21207 [Date Accessed: 19/05/2025]

recyclable components of the drone, disposal costs are assumed to remain below or equal to the annual maintenance costs. The annual recurring maintenance costs per year shall be maximum €2,625, as estimated by the average world-class standard for Replacement Asset Value (RAV) benchmark of 3.5%[5]. Disposal costs are therefore also limited to a maximum of €2,625. To ensure financial viability, the drone's end-of-life recycling value should at least cancel out the disposal costs, implying a minimum recycling value of €2,625. The manufacturing cost shall be less than €75,000, directly stemming from REQ-MIS-COST-2.2.1. Regarding the SLCA goals, a teamwork satisfaction survey will be done throughout the project. It is aimed to achieve at least 4.0/5.0.

There is a distinction between sustainability goals and sustainability requirements. During the design process, the sustainability requirements had to be complied with, whereas the sustainability goals only needed to be maximized without compromising the operational performance. The specific requirements correspond with the system requirement list [1], where the identifiers can also be linked to prior reports.

The requirements given in the list indirectly affect sustainability. For instance, there will certainly be a battery incorporated into the design, necessitating responsible end-of-life management. This includes the use of recyclable battery materials, clear disassembly instructions, and safe disposal procedures.

A representative example of how sustainability was involved in the design choices was seen in the power subsystem. There, all three categories are implemented. The trade-off between solid-state and lithium-ion batteries considered the energy extraction values (ELCA). Also, between the anode materials, silicon received an extra high score because of sustainability and thus leading the design.

With the final design in place, the current values for the requirements have been fully determined. They are all compliant, meaning that the design can be considered technically sustainable. Note that the requirements themselves will also be presented in the final compliance matrix, including justification and reference. This is found in Table 17.1.

The design goals also have been determined. The estimations are generally done based on Equation 14.1. The operational estimations were based on two 30-minute missions per week. The average equivalence of 98 g/kWh[6] is used to estimate the carbon footprint per minute.

$$\text{Total} = \sum \left(\text{Component Mass} \cdot \text{Recyclability Fraction}\right) \tag{14.1}$$

Components with a high recyclability are the plates of the structure, the batteries and the water tank. The plates of the structure are made out of aluminium which is traditionally a material with a high recovery rate (more than 90%) across all industries and the vast majority of alloys[7]. The batteries, although a novel technology, are also highly recyclable due to the ability of splitting them into anode and cathode, which both have high recovery rates in the region of 80-90% [31, 32]. Finally, processing the HDPE tank at end-of-life will recover almost all of the raw material, as is the case for many types of polymers [33]. The same analysis is performed for the remaining components.

At this stage, not all goals can be assigned a value, for instance, the ELCA packaging waste recyclability. This is left as pending (**P**) to be further analyzed during the manufacturing process and shipping processes.

[5] https://upkeep.com/learning/budget-for-equipment-maintenance/ [Date Accessed: 10/06/2025]

[6] https://www.nowtricity.com/country/netherlands/ [Date Accessed: 24/06/2025]

[7] https://mogensen.es/wp-content/uploads/2023/05/MOGENSEN-GSort-Alminium-Recycling.pdf [Date Accessed: 24/06/2025]

Table 14.1: SLCA Sustainability Assessment

Theme	Metric	Target	Current Value	Assigned To	Status
GOALS					
SLCA	Team work satisfaction (1–5 survey score)	≥ 4.0	4.1	HR & Legal Manager	On target
SLCA	Hours/week per team member (avg hr/wk)	≤ 40 hr	40	HR & Legal Manager	On target

Table 14.2: ELCA Sustainability Assessment

Theme	Metric	Target	Current Value	Assigned To	Status
REQS					
ELCA	Toxic material content (g)	0 g	0 g	Sustainability Manager	On target
ELCA	Noise emissions (dB)	< 80 dB	< 80 dB	Sustainability Manager	On target
ELCA	Product life span (years)	> 5 yr	> 5 yr	Sustainability Manager	On target
GOALS					
ELCA	Mass % of recyclable material used	$\geq 60\%$	$> 78\%$	Sustainability Manager	On target
ELCA	Estimated total carbon footprint (g CO_2e/min)	< 171	0.66	Sustainability Manager	On target
ELCA	Operational energy consumption (kWh/year)	$\leq 2,000$	1,943	Sustainability Manager	On target
ELCA	Packaging waste recyclability (%)	$\geq 75\%$	**P**	Sustainability Manager	To be calculated

Table 14.3: LCC Sustainability Assessment

Theme	Metric	Target	Current Value	Assigned To	Status
REQS					
LCC	Maintenance cost (EUR/year)	$\leq 2,625$	2,412	Sustainability Manager	On target
GOALS					
LCC	Manufacturing cost (EUR)	$\leq 75,000$	$\leq 40,000$	Sustainability Manager	On target
LCC	End-of-Life disposal cost (EUR)	$\leq 2,625$	**P**	Sustainability Manager	To be calculated
LCC	Recycling value (EUR recouped)	$\geq 2,625$	**P**	Sustainability Manager	To be calculated

15. RAMS Characteristics

Reliability, Availability, Maintainability, and Safety (RAMS) are performance indicators for a design that make sure that it can function effectively, be always accessible, be easily repaired, and operate without causing harm [1].

15.1. Reliability

Reliability refers to the probability that a system performs its intended function without failure for a specified period under defined conditions. This section explores how design decisions, failure analysis, and redundancy strategies contribute to building a robust and dependable firefighting UAV.

Determining reliability for each subsystem requires breaking down the drone system into series and parallel networks. These are shown in Figure 15.2.

- **Payload**: In the payload context, high reliability means the water delivery system, tank, pump, and targeting sensor will operate fault-free throughout emergency missions.
- **Power**: For the power subsystem, the battery is the only component that can fail. The life cycle for a solid-state battery with a silicon anode with an NMC cathode is about 1200 cycles before the capacity drops to 80% [2].
- **Propulsion**: For the propulsion subsystem, which primarily includes the electric motor, the Electronic Speed Controller (ESC), and the propeller. The mean time between failures for an electric motor is found to be around 1000 hours [3]. This translates into a failure probability of 0.001 per hour. The electronic speed controllers have a failure rate of around $5.4 \cdot 10^{-6}$ [34]. For the propeller, as it is a purely structural component, it is not expected to spontaneously fail, but due to the harsh operating conditions, it may not resist the multiple loading cycles.
- **Control**: The control subsystem, made up of only electrical components, has a high failure rate at first, which then decreases and then increases again with time. This is shown in Figure 15.1 [4].
- **Structures**: In the context of the structure, high reliability means that the structure will perform as required during its defined life cycle, under the expected loads and the expected environmental conditions, while undergoing minimal degradation. Currently, the failure rate for the structure cannot be quantified since structures cannot fail spontaneously after a certain time, and they are highly dependent on the conditions they operate in.

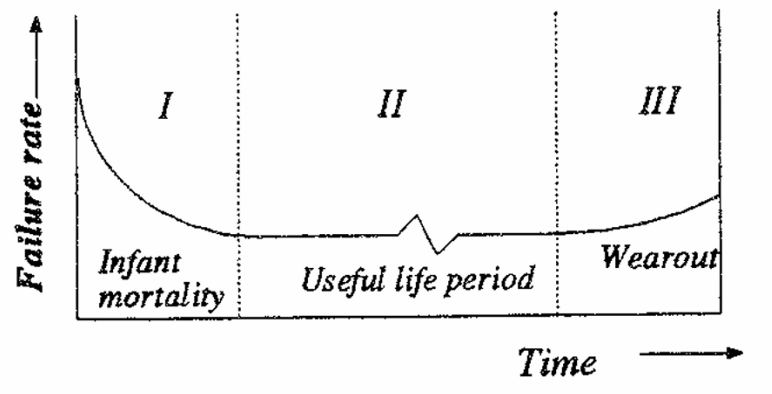

Figure 15.1: Failure Rates [4]

[1] https://zoidii.com/glossary-post/rams-framework[Date Accessed: 24/06/2025]

[2] https://www.grepow.com/semi-solid-state-battery/350wh-kg-series-high-energy-density-battery-pack.html [Date Accessed: 19/05/2025]

[3] https://store.tmotor.com/product/u15-v2-motor-u-power-kv80.html [Date Accessed: 19/05/2025]

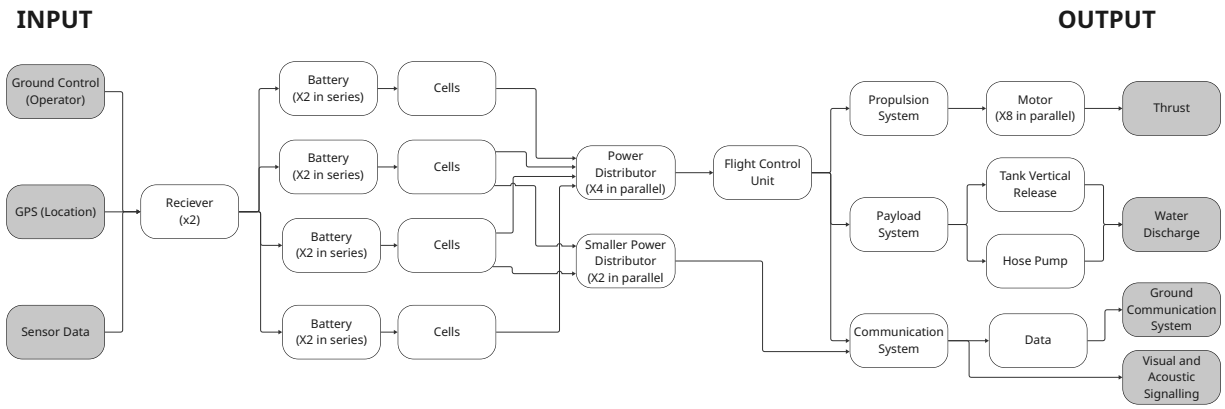

Figure 15.2: Reliability Block Diagram

Figure 15.2 displays the components that operate in series and in parallel. If a component were to fail, the other components connected to it in series would also fail. Therefore, it can be observed that the flight control unit is a crucial component.

15.2. Maintainability

Maintainability refers to the ease, speed, and resources required to inspect, service, or repair a UAV system to keep it in operational condition. It includes both preventive and corrective maintenance actions. The goal is to ensure that failures can be anticipated or quickly rectified with minimal downtime, especially critical with these mission requirements, where turnaround time must remain under five minutes.

15.2.1. Corrective Maintenance

Table 15.1: Corrective Maintenance Task Overview [4]

Task	Time (min)	Frequency (year)
Replace propeller blades	10	4
Replace faulty motors	50	0
Replace ESC(s)	50	2
Replace individual wires if ripped/damaged	20	3
Replace water tank if damaged	5	1
Replace broken camera lenses	20	1
Unclog the water pump	20	26
Realign the nozzles	5	26
Replace gimbal dampers	20	3
Clean the drone of dirt, soot, debris	15	104
Realign or replace bent landing gear	15	5
Realign or replace arms	50	2
Replace batteries after 1200 cycles	5	0

[4] https://www.duncan-parnell.com/blog/88/guide-to-drone-maintenance?srsltid=AfmBOopgKNkC1oOUW65I_unZhm0zglEhIWHKAF3kmrDgK_LqhcNlmZ-0 [Date Accessed: 21/02/2025]

For propeller blades, impacts can occur frequently. As such, only a few cases per year are expected to require full replacement, typically following a significant collision. Faulty motor replacement is considered unnecessary on a yearly basis due to the mean time to failure of 1000 cycles, and an estimated 52 hours of annual flight time (3 flights × 2 missions × 52 weeks × ≈15 min), the likelihood of failure remains below 5%. ESCs are more vulnerable due to electronics, and with two 4-in-1 modules in the system, an estimation of two replacements per year was made. This maintenance has been made into an easier process through the use of bullet connectors between the motors and the ESCs. The total cost for four blade replacements and two ESCs would be 2405€ [18/06/2025].

Individual wire replacements are not frequent but can arise due to heat or mechanical stresses. This involves reconnecting subsystems and recalibrating systems, especially in the control subsystem, hence the moderately high task duration. The water tank, made of HDPE, is designed for fast replacement. However, HDPE's thermoplastic nature means it softens under heat, making an annual replacement likely; replacement would cost 7.70€. Camera lens damage is rare if careful transport protocols are followed and a protective case is applied to the lens, but impact or exposure to debris can still require replacement occasionally.

Water pump clogging, although it can be mitigated by filtering or purifying water, can still occur after a couple of weeks due to particulate buildup. With the use of two pumps, small impacts may cause misalignment of the pumps, resulting in unbalanced coverage and inconsistent reach therefore, adjustments are required frequently. Cleaning the drone after every mission is also essential, given exposure to dust. Gimbal dampers can fail during hard landings or significant impacts and usually can be replaced; the task itself is short.

Structural tasks include replacing or simply realigning bent landing gear, an easy swap due to its mechanical independence from internal electronics. Landing gear is expected to require at least realignment every 20 flights due to impacts on landing. Replacing the arms, however, requires full system recalibration since the ECS wiring passes through them. Solid-state batteries typically endure 1,200 charge cycles, which covers the number of annual missions.

In total, corrective maintenance accounts for roughly 46 hours of maintenance per year. The cost for component replacement would be 2412€ without taking into account cleaning or realigning, which could be performed by the maintenance team and would come at no additional cost.

15.2.2. Preventive Maintenance

Tasks that should be performed between missions and that contribute to preventing failures are grouped under preventive maintenance. These are further broken down into two subcategories: superficial inspection, easily done by a single person, within a short time frame, and detailed inspection, which requires disassembling to verify the internals of the drone or highly specialized devices. These tasks are showcased in Table 15.2.

Table 15.2: Preventive Maintenance Task Overview

Superficial Inspection	Detailed Inspection
Check propellers for damage	Check state of wiring and solder joints
Check motors are free-spinning	Perform firmware updates (autopilot, remote controller, telemetry software)
Inspect antennae	Calibrate IMU, GPS, other sensors
Check camera lens for cleanliness	Check for rupture in water tank
Check landing gear condition	Check gimbal dampers
Inspect for loose screws	Check battery (voltage, capacity)
Check body condition	Check charger station
Verify folding hinges	Check nozzle aims are properly calibrated

Added up, all superficial tasks total to roughly one hour of maintenance done daily, equating to seven hours a week. In the case of detailed inspection, maintenance is done on a weekly basis and should take in the order of two hours. This way, preventive maintenance adds up to **9 hours of maintenance per week**. Approximating maintenance time and intervals is relevant for approximating the overall availability of the UAV.

Measures taken during the design that take maintainability into account are few. Some physical components are already designed with modularity in mind (batteries and water tank), while others are made easily accessible for disassembly (arm hinges), making the servicing and replacing of said components easier. Furthermore, given the required dimensions of the drone (≈3x3x1.68m), the system is already adapted for human-scale interactions with no accessibility issues (e.g., need for ladders, lifts). Very little can be done about making the drone maintainable, since drones, even of this size, are easy to work with.

15.3. Availability

Availability measures a system's readiness to be operational when needed, reflecting the combined effect of reliability and maintainability. This section examines how design support concepts ensure the UAV remains ready for firefighting missions with minimal downtime. The relation between the availability of the UAV, the mean maintenance time, and the mean time between maintenance is:

$$\text{Availability} = \frac{\text{MTBM}}{\text{MTBM} + \text{MMT}}$$

Where MTBM is the Mean Time Between Maintenance and MMT is the Mean Maintenance Time. Over the span of a year, the availability of the drone, as computed with the formula stated above, is 94%, meaning that with the imposed maintenance from the previous section, the availability of the drone over a period of one year is given by:

$$\text{Availability} = \frac{365 \cdot 24 - (9 \cdot 52 + 40)}{365 \cdot 24} = 94\%$$

15.4. Safety

Safety is the system's ability to operate without causing harm to users, the environment, or equipment. This section highlights how risk analysis, protective measures, and fault-tolerant design ensure safe UAV operation even in hazardous firefighting environments.

- **Payload:** The most safety-critical payload component is the visual and acoustic signals system. By including these on the UAV, possible human injuries during operation can be avoided. Furthermore, by employing mitigation strategies from Chapter 12, like shielding the water tank or using braided hoses, the risk of debris falling from the UAV is reduced, thus, increasing safety.
- **Power:** The safety of the power subsystem can be improved by making sure the batteries are operating within their limits, avoiding potential battery fires/explosions. This can be achieved by constantly monitoring the temperature of the batteries and providing frequent maintenance.
- **Propulsion:** To guarantee a safe environment, the X8 layout was chosen, minimizing the number of arms needed. Furthermore, a thorough cleaning procedure will be performed after every sortie, so no dust/soot accumulation is present, maintaining safety operations.
- **Control:** The control subsystem will make sure that the UAV does not collide with obstacles, preventing unsafe situations. This is done by employing a radar system that will override the operator in case of imminent collision. Furthermore, an automatic landing sequence is initiated in case of signal loss/ engine failure.
- **Structures:** The safety of the structures comes from the minimum safety factor of 1.5 set in place for all structural components. Furthermore, frequent maintenance checks will make sure that any potential defects are observed in a timely manner, improving the safety of the UAV.

16. Verification & Validation

The current approach follows the V diagram method. The system can be verified in multiple ways, through test, analysis, demonstration, and inspection according to NASA [35]. For testing, a controlled experiment shall be performed to measure the performance of the system and then compare this with the requirements. Analysis is done through the use of mathematical models or simulations to predict how the system will perform and again compare to the requirements. Demonstration is a more informal sort of testing where the system is observed to perform as required under specific conditions. Inspection confirms visually or through physical measurements that the system fits the design specifications.

Table 16.1: Verification Procedures

Requirement ID	Verification Method	Verification Description	Equipment/ Facility
REQ-SUBSYS-PLD-1	Inspection	Fill the water tank, empty it and measure the amount of water	Measuring container
REQ-SUBSYS-PLD-2	Demonstration	The firefighting system is turned on for exactly 1 minute, and the amount of expelled water is measured.	Measuring container
REQ-SUBSYS-PLD-3	Demonstration	The firefighting system is turned on and used with both capabilities.	Fire in a controlled environment
REQ-SUBSYS-PLD-4	Demonstration	The firefighting system is turned on, and the water jet length is measured.	Measuring tape
REQ-SUBSYS-PLD-5	Testing	Colored water is used, and the jet is aimed at a target. The outline of the first impact is measured against the target.	Measuring tape, tint, calipers
REQ-SUBSYS-PLD-6	Inspection	The visual and acoustic signal system is turned on.	Test crowd to check drone awareness
REQ-SUBSYS-PLD-7	Inspection	The UAV is powered on, and the camera feeds are checked. Identify seat of fire, embers	Fire in a controlled environment
REQ-SUBSYS-PLD-8	Demonstration	Fly the drone into a fire, measuring temperatures constantly. Check the drone for damages	Fire in a controlled environment; thermometer
REQ-SUBSYS-PLD-9	Demonstration	Try the compatibility of the tank refilling mechanism with different hose types	Different hose types
REQ-SUBSYS-PLD-10	Analysis	Model the tank and run software analysis to simulate sloshing effect	Computational Fluid Analysis (CFD) software
REQ-SUBSYS-PLD-11	Demonstration	Spray the camera with water, simulating rain/mist conditions	Water spraying equipment

REQ-SUBSYS-PWR-1	Inspection & Test	Inspect the wiring. Test the behavior after a failure by simulating the loss of a path.	Test bench, multimeter
REQ-SUBSYS-PWR-2	Test & Analysis	Test or simulate the failure of a cell and measure whether the system still has power.	Test bench, multimeter
REQ-SUBSYS-PWR-3	Inspection & Test	Verify from the wiring that the voltage regulators are independent. Test the regulators are independent by removing one and measuring if unchanged.	Electrical test bench
REQ-SUBSYS-PWR-4	Demonstration	Run the system and verify that the operator receives the required alerts and data.	Ground station, controller
REQ-SUBSYS-PWR-5	Demonstration	Measure time to get from zero to nominal voltage while charging.	Battery charger (including multimeter), timer
REQ-SUBSYS-PWR-6	Test & Inspection	Discharge a fully charged battery at a constant known current from nominal voltage to cut-off voltage, measure how long it takes to do so. Energy will be the voltage x current x time. Review the components' data sheets and confirm they fit the energy storage requirements.	Multimeter, timer, load receiver or battery analyzer
REQ-SUBSYS-PWR-7	Demonstration	Fire-brigade team performing full battery swap	Stopwatch, replacement battery
REQ-SUBSYS-PWR-8	Demonstration	Connect the battery to the fire truck system and verify that it is charging properly	Fire truck with charger
REQ-SUBSYS-PWR-9	Test	Measure peak current of battery	Multimeter
REQ-SUBSYS-PWR-10	Test	In a chamber, test the battery with simulated mission loads and measure the temperature	Temperature sensors, test chamber
REQ-SUBSYS-PROP-1	Testing	Perform static thrust test of full UAV on thrust stand. Record total thrust and weight to compute thrust-to-weight ratio.	TU Delft propeller test rig
REQ-SUBSYS-PROP-2	Testing	Mount one arm only (before final assembly, motor+propeller) to the thrust rig. Ramp to full throttle. Measure peak thrust per motor.	TU Delft propeller test rig
REQ-SUBSYS-PROP-3	Testing	Use same rig; set thrust at hover power (e.g. 50–60% throttle) and confirm hover requirement.	TU Delft propeller test rig

REQ-SUBSYS-PROP-4	Inspection	Check shaft diameter, bolt pattern, and RPM match between propeller and motor.	Calipers
REQ-SUBSYS-PROP-5	Inspection	Physically measure the diameter of each propeller	Ruler / tape
REQ-SUBSYS-PROP-6	Inspection & Demonstration	Confirm each coaxial pair contains CW + CCW rotors using labels or by recording a test	Visual check
REQ-SUBSYS-PROP-7	Demonstration	Activate full system, observe direction of rotation of opposing arms. Verify symmetry.	TU Delft CyberZoo
REQ-SUBSYS-PROP-8	Analysis	Create CFD/CSD simulation for rotors, spin each motor to peak RPM. Study aeroelastic loads	Combined CFD-structural model simulation
REQ-SUBSYS-PROP-9	Inspection & Testing	Check datasheet for material temperature resistance. Optionally heat propellers to realistic near-fire temperatures and inspect for warping.	TU Delft MAM Lab
REQ-SUBSYS-PROP-10	Analysis	Check ESC rated continuous current against motor's max draw; confirm 20% margin.	Datasheet check
REQ-SUBSYS-PROP-11	Analysis	Confirm ESC and motor voltage rating exceeds full battery charge voltage.	Datasheet check
REQ-SUBSYS-CTRL-1	Testing	Conduct dynamic stability tests while expelling fire retardant	UAV Outdoor Testing Area
REQ-SUBSYS-CTRL-2	Analysis	Calculate counteracting horizontal force	Python
REQ-SUBSYS-CTRL-3	Analysis	Calculate counteracting vertical force	Python
REQ-SUBSYS-CTRL-4	Demonstration	Demonstrate logging of the required number of data channels.	TU Delft CyberZoo
REQ-SUBSYS-CTRL-5	Demonstration	Demonstrate telemetry transmission to the ground station	Telemetry test setup
REQ-SUBSYS-CTRL-6	Demonstration	Conduct dynamic stability tests in 6bft wind gusts conditions	TU Delft Open Jet Facility
REQ-SUBSYS-CTRL-7	Demonstration	Cause a fault and check the emergency response	TU Delft CyberZoo
REQ-SUBSYS-CTRL-8	Demonstration	Simulate signal loss or motor failure and check autonomous landing procedure	TU Delft CyberZoo
REQ-SUBSYS-CTRL-9	Demonstration	Simulate water pump malfunctions, tank ruptures, radar sensor failure, camera malfunctions, telemetry antenna malfunctions, and check error warning	Python

REQ-SUBSYS-CTRL-10	Demonstration	Give autonomous landing input and check performance.	TU Delft CyberZ00
REQ-SUBSYS-CTRL-11	Demonstration	Simulate motor failure	TU Delft CyberZoo
REQ-SUBSYS-CTRL-12	Demonstration	Override operator input and check compliance with commands.	TU Delft CyberZoo
REQ-SUBSYS-CTRL-13	Demonstration	Perform dynamic stability tests when the center of gravity constantly shifts due to water tank emptying	UAV Outdoor Testing Area
REQ-SUBSYS-CTRL-14	Inspection	Check on-board computer data sheet.	Datasheet Check
REQ-SUBSYS-STRUC-1	Demonstration	Manually fold and unfold all arms, confirm they lock in place securely	-
REQ-SUBSYS-STRUC-2	Inspection	Fully extend arms and measure added length from stored state	Calipers or tape
REQ-SUBSYS-STRUC-3	Inspection	Mount UAV with weights or hydraulic press to simulate vertical impact, ensure no yielding or fracture	Force sensors, structural test stand
REQ-SUBSYS-STRUC-4	Inspection & Demonstration	Check wind holes are placed correctly, test UAV flight with wind conditions	TU Delft Open Jet Facility
REQ-SUBSYS-STRUC-5 & 6	Test	Mount extended arm and apply lateral load, measure tip displacement/ angular rotation	Loading frame, displacement gauge, inclinometer
REQ-SUBSYS-STRUC-7	Demonstration & Analysis	Apply known bending moment to a test arm using weights or a loading jig, compare displacement vs calculated yield	Structural test stand
REQ-SUBSYS-STRUC-8	Analysis	Simulate normal operational loads and check deflection and yield	CAD
REQ-SUBSYS-STRUC-9	Analysis & Demonstration	Load a mock-up structure till failure to check the ultimate loads	Structural test stand
REQ-SUBSYS-STRUC-10	Demonstration	Expose structure connections between CFRP and metal (galvanic interaction) to salt spray or mist for 72h, inspect for pitting, oxidation	Insulated container, sprays
REQ-SUBSYS-STRUC-11	Demonstration	Heat the drone structure to the highest temperature that will be encountered during normal operation	Structural test stand
REQ-SUBSYS-STRUC-12	Analysis	Perform non-destructive drone materials compatibility check	Structural test stand

Validation Procedure

System validation ensures that the UAV performs its intended firefighting mission reliably and effectively under realistic operational conditions.

Fire Simulation and Payload Validation

To validate fire detection and extinguishing effectiveness, controlled fires are simulated using heat sources and flame tables with certified firefighting training facilities. Radiometric validation is conducted by measuring the UAV's thermal sensor output while hovering 5–15 meters above controlled flame sources of varying intensities. Surface temperatures are monitored with thermocouples to confirm the thermal mapping accuracy of the sensor. The water-dispensing mechanism is then tested by deploying the drone over the fires. Extinguishing efficiency is then determined by measuring temperature reduction using IR cameras.

Wind Disturbance and Aerodynamic Stability

To simulate operational wind conditions, tests are conducted in a large-scale wind tunnel or, alternatively, in an outdoor environment with controlled fan arrays or wind tunnel generating wind speeds between 5 and 15 m/s. These tests evaluate the UAV's ability to maintain position and orientation during hover and forward flight.

Thermal Stress and Component Durability

To test material and system response to elevated temperatures, the UAV is placed in a thermal chamber where ambient temperatures reach 60°C, simulating proximity to fires. Sensors, electronics, and the HDPE tank are monitored for deformation, electrical failure, or thermal drift. Functional tests are repeated every 15 minutes for a one-hour test to verify proper thermal resistance. Additionally, camera modules are evaluated for thermal lens fogging and image clarity is scored against a standardized test image placed within the field of view. The thermoplastic tank is visually inspected to detect early-stage deformation.

Redundancy and Emergency Scenarios

To validate fault-tolerance, motor failure is simulated mid-flight by disabling one motor remotely. The coaxial X8 configuration should automatically redistribute thrust. Attitude stabilization and altitude hold are monitored using onboard flight logs and video analysis. In a separate test, battery failure is mimicked by cutting power to one power distribution line, verifying emergency descent.

Operational Duration and Battery Performance

Endurance is validated by fully charging the UAV and flying a mission-representative flight profile including hover, transition, and high-thrust segments. The UAV must sustain at least 15 minutes of flight time under full payload for successful validation. A cooldown period is implemented between repetitions, and over-discharge cutoffs are enabled to prevent cell damage.

17. Requirement Compliance Check

As a final check after defining all the subsystem characteristics and selecting components, a compliance matrix is used to check whether all requirements are met. A compliance matrix indicates the requirement identifier and description, followed by the status of the requirement verification procedure, its justification and the method used. Requirements can be checked through through inspection, analysis, demonstration and testing. A checked status is marked with ✔, a pending status is marked with **P** and a not implemented status is marked with ✗. At this stage of the project, inspection and analysis procedures are completed, whereas demonstration and testing procedures are pending.

The compliance matrix for the stakeholder and mission requirements is presented in Table 17.1 and the one for the system requirements is outlined in Table 17.2.

Table 17.1: Compliance Matrix

Identifier	Requirement Description	Check	Justification	Method	Reference
REQ-STK-1.1.1	The extinguishing mechanism shall have a minimum flow rate of 150 L/min.	✔	The model chosen for the pumps can deliver up to 150 L/min each, but the flow rate will be limited to 75 L/min to achieve the required throw of water.	Demonstration	Table 9.3
REQ-STK-1.1.2	The minimum amount of water transported shall be 50 L.	✗	The payload was reduced to 40 L.	Inspection	Section 11.2
REQ-STK-1.3.1	The UAV shall be able to fly at least 70 m from the ground.	✔	The climb profile allows for a constant climb rate of 3 m/s for approximately 38 s, which is sufficient for reaching 70m from the ground.	Analysis	Chapter 5
REQ-STK-2.1.1	The UAV dimensions during transport shall not exceed 1.38 x 3.00 x 1.63 m (w/l/h).	✔	The CAD drawings for the folded UAV have been checked.	Inspection	
REQ-STK-2.4.1	The Maximum Take-Off Weight of the UAV shall be less than 150 kg.	✔	The MTOW has been checked based on datasheet specifications and mass budgets.	Inspection	Table 11.1
REQ-STK-2.4.2	The maximum span of the UAV when operating shall be 3.0 x 3.0 m.	✔	The CAD drawings for the unfolded UAV have been checked.	Inspection	
REQ-STK-2.5.1	Sustainable materials shall be promoted without compromising operational capabilities.	✔	Sustainable materials have been promoted in the trade-off tables.	Inspection	Chapter 4
REQ-STK-MKT-1	The drone shall be untethered, operating without any ground connection	✔	The drone is powered using batteries.	Inspection	Chapter 7
REQ-STK-MKT-2	The drone shall have a modular payload allowing changes depending on the situation.	✔	The UAV can accommodate different tanks, pumps, and nozzles, based on the mission. The only limitation is the dimensions of the cutout for the tank and the MTOW limit.	Demonstration	REFERENCE LAYOUT FIGURE
REQ-STK-MKT-3	The UAV shall have a status display to indicate when a refill or battery replacement is required.	✗	Not fulfilled due to MTOW constraints	-	-
REQ-STK-MKT-4	The UAV shall run a self-diagnostic before beginning a mission.	**P**	The autopilot software is going to be tested.	Testing	Section 8.3
REQ-MIS-FF-1.1.3	The throw length of the water jet shall be at least 6 m.	✔	By limiting the flow rate of each pump to 75 L/min, the throw of 6.38 m can be achieved from a jet height of 3 m.	Demonstration	Table 9.3

Identifier	Requirement Description	Check	Justification	Method	Reference
REQ-MIS-CTRL-1.4.1	The UAV shall fly in windy conditions up to 6 bft.	**P**	The control system capabilities will be tested under 6 bft wind conditions using a wind tunnel.	Testing	Chapter 8
REQ-MIS-POW-1.5.1	Hover endurance for one flight shall be at least 15 min.	✔	It has been checked that the battery specifications meet the power requirements needed for the 15 minutes endurance.	Analysis	Table 7.3
REQ-MIS-LOG-2.1.4	The drone shall have a 5 min turnaround time.	**P**	A practice mission will time the battery replacement and tank refill procedures.	Analysis, Demonstration	Section 5.4
REQ-MIS-SAF-2.3.3	The UAV shall have fault-tolerant control to land safely when one engine is inoperative.	**P**	It will be assessed whether the UAV safely lands based on the control system's inoperative engine redundancy considerations.	Demonstration	Section 8.4
REQ-MIS-SAF-2.3.4	The UAV shall autonomously land at the nearest clearing if signal loss occurs.	**P**	It will be assessed whether the UAV safely lands based on the control system's inoperative engine redundancy considerations.	Demonstration	Section 8.4
REQ-MIS-SAF-2.3.1	The UAV shall have a redundant collision avoidance system operable in smoke and high temperatures.	**P**	Sensors maximum operating temperature was taken into account in the mission profile and their performance in these conditions will also be tested.	Testing	Section 8.3
REQ-MIS-SAF-2.3.2	The UAV shall be equipped with visual and acoustic signals.	✔	The UAV features both navigation lights and a buzzer for acoustic signaling.	Inspection	Subsection 9.2.4
REQ-MIS-COM-1.2.1	The UAV shall carry at least one thermal camera and one visual light camera.	✔	The chosen camera array model includes both a visual and a thermal camera.	Inspection	Subsection 9.2.3
REQ-MIS-SUS-2.5.2	The UAV shall operate using battery power.	✔	Batteries were selected and their integration has been checked in CAD.	Inspection	Table 7.3
REQ-MIS-FF-1.1.4	The payload mechanism shall be able to drop water while hovering above the target area.	✔	The tank's water-dropping capabilities were simulated in ANSYS.	Analysis	Figure 9.4
REQ-MIS-COST-2.2.1	The cost of a single vehicle shall not exceed 75000 EUR.	✔	Based on the budget tables, the total cost is below 40000 EUR.	Analysis	Table 11.1
REQ-MIS-COST-2.2.2	The maintenance cost of a single vehicle shall not exceed 2625 EUR.	**P**	Analysis is performed based on components' cost and maintenance procedures in subsection 15.2.1.	Analysis	Table 14.3
REQ-MIS-SUS-2.5.1	The toxic material content shall be 0 g.	✔	No toxic material is used in the structure, or any of the other components.	Inspection	Table 14.2

Identifier	Requirement Description	Check	Justification	Method	Reference
REQ-MIS-SUS-2.5.4	The noise emissions shall not be greater than 80 dB during normal operation.	✔	The buzzer does not exceed this limit.	Inspection	Section 9.2
REQ-MIS-SUS-2.5.5	The product life span shall be at least 5 years.	✔	Based on maintenance procedures, the life span of at least 5 years is fulfilled.	Analysis, Demonstration	Table 14.2, Chapter 19
REQ-MIS-RISK-1	The water refill system on the ground shall filter the water.	✗	Not implemented	-	-
REQ-MIS-RISK-2	The turnaround routine shall have redundant batteries.	✔	There is one spare set of eight batteris available.	Inspection	Chapter 5
REQ-MIS-RISK-3	The turnaround routine tank refill shall avoid spillage.	**P**	Water spillage will be assessed during the practice mission.	Demonstration	Chapter 5
REQ-MIS-RISK-4	The UAV shall land autonomously at the nearest clearing in case of degraded performance.	**P**	It will be assessed whether the UAV safely lands in case of failure detection.	Demonstration	Chapter 8
REQ-MIS-RISK-5	The UAV maintenance department shall perform frequent part inspections.	✔	Part inspections are part of the turnaround procedures.	Inspection	Chapter 5

Table 17.2: Compliance Matrix for UAV System Requirements

Identifier	Requirement Description	Check	Justification	Method	Reference
REQ-SYS-FF-1.1.5	The firefighting system shall have an accuracy of at least 5 cm.	**P**	The nozzle accuracy will be tested.	Testing	Chapter 9
REQ-SYS-COM-1.2.2	The delay between control command and drone movement shall be less than 200 ms.	✔	The RC control has a response time of 110 ms.	Demonstration	[1]
REQ-SYS-PROP-1.3.2	The drone shall produce a thrust in excess of 30.9 kN.	**P**	The motor performance has been checked, based on the data sheets and will be tested.	Testing	Section 6.3

[1] `https://www.unmannedtechshop.co.uk/product/herelink-controller-unit/?srsltid=AfmBOopSJTEZLO6n3mTsOW__9w7UARrIHy9OumsEsUhAxz-ePvmnpysq` [Date Accessed: 18/06/2025]

Identifier	Requirement Description	Check	Justification	Method	Reference
REQ-SYS-PROP-1.3.3	The drone shall have a climb rate of at least 1 m/s.	✔	Based on the climb profile analysis, a climb rate of 3 m/s is achieved.	Analysis	Chapter 5
REQ-SYS-CTRL-1.4.2	The drone shall be able to adjust to weight loss.	✔	An analysis regarding the center of gravity excursion is performed.	Analysis	Section 8.4
REQ-SYS-POW-1.5.2	The drone shall have an energy storage of at least 9.23 kWh.	✔	The battery's datasheet has been checked.	Inspection	Table 7.3
REQ-SYS-STRUC-1.6.1	The drone shall be able to withstand temperatures of at least 50 ° C.	**P**	Materials' resistance to this temperature will be tested	Testing	Chapter 10
REQ-SYS-STRUC-1.6.2	The drone structure shall carry the propulsive forces of the motors.	✔	A load analysis has been performed in CATIA.	Analysis	Chapter 10
REQ-SYS-LOG-2.1.2	The onboard computer of the UAV shall log and store flight data.	✔	The RF receiver includes an SD card slot.	Inspection	Chapter 8
REQ-SYS-LOG-2.1.3	The deployment of the drone shall take less than 10 minutes.	**P**	The deployment time will be checked during the practice mission.	Demonstration	Chapter 5
REQ-SYS-LOG-2.1.5	The battery recharge time shall be maximum 30 minutes.	**P**	The battery charging characteristics specify a charge rate of 2C, equivalent to 30 minutes. A demonstration will also be done to further verify this.	Demonstration, Inspection	Table 7.1
REQ-SYS-LOG-2.1.6	The UAV system shall be operated by fewer than 3 people.	**P**	A practice mission will be performed to check the feasibility of the operational procedures.	Demonstration	Chapter 5
REQ-SYS-SAFE-2.3.5	The UAV shall detect battery overheating and notify the operator.	✗	Not fulfilled due to MTOW considerations	-	-
REQ-SYS-LEG-2.4.4	The drone shall not reach an altitude above 120 m.	**P**	It will be tested that the user receives a message when the control system detects an altitude higher than 120m.	Testing	Section 8.3
REQ-SYS-LEG-2.4.5	The drone shall stay within the line of sight of the operator.	**P**	It will be tested that the user receives a message when the UAV is out of the line of sight based on the power signal.	Testing	Section 8.3
REQ-SYS-LEG-2.4.6	The UAV shall be at a maximum distance from the operator of 500 m.	**P**	It will be tested that the user receives a message when the UAV is more than 500 m away based on the power signal.	Testing	Section 8.3
REQ-SYS-SUS-2.5.3	At EOL, the UAV shall have a high degree of recyclability.	**P**	End-of-life analysis will be performed.	Analysis	Chapter 5
REQ-SYS-RISK-1	The payload system pump system shall have more than one pump for redundancy.	✔	It has been checked in the CAD drawings that the payload consists of two pumps.	Inspection	Chapter 9

18. Cost Breakdown Structure

The cost break down diagram displays what components will be bought or made. It is divided into subsystems and can be seen in Figure 18.1.

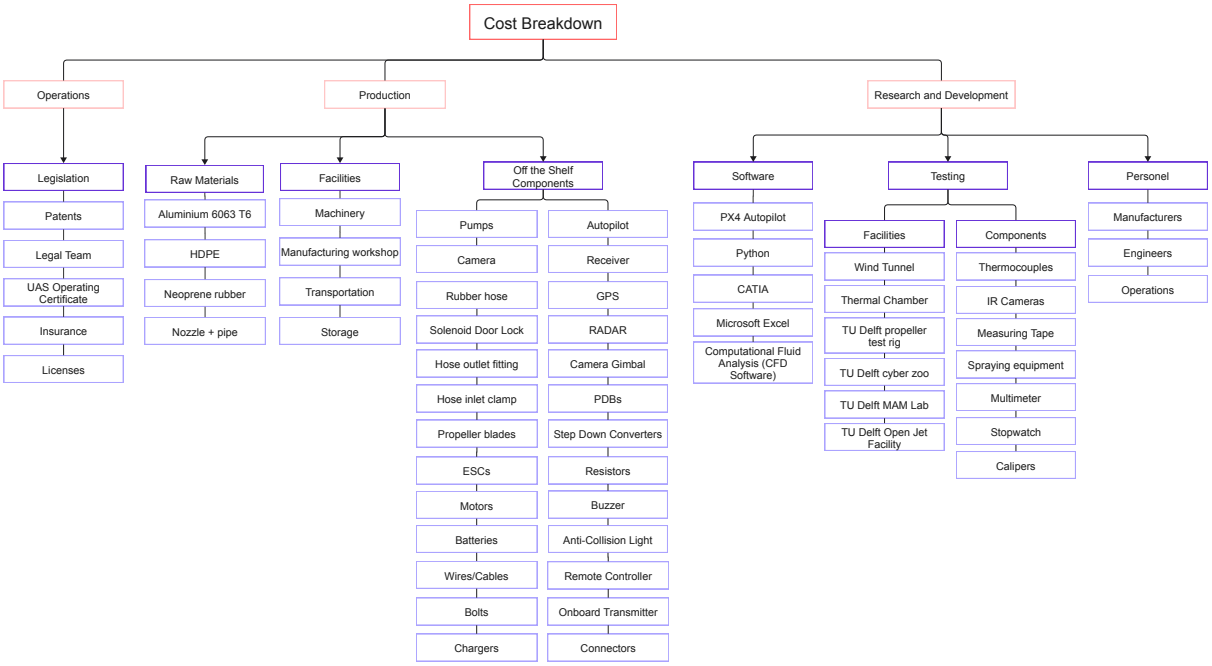

Figure 18.1: Cost Breakdown Diagram

18.1. Raw Cost of UAV

The requirement REQ-MIS-COST-2.2.1 sets a maximum budget for the raw cost of one vehicle. The raw cost includes the materials for custom components, as well as the off-the-shelf components. A margin was also applied to account for any uncertainties regarding the cost. The value of the margin ranges from 5 to 50%, based on the risk of additional costs. The value of 50% is only present for the chargers, as the client suggested more chargers might be needed, based on the operational performance of the Flame Aegis UAV.

Table 18.1: Detailed Cost Breakdown of the Prototype Development by Subsystem and Component

Subsystem	Component	Cost [€]	Margin [%]	Cost including Margin [€]
Payload (Table 9.7)	Pumps	300.30	5%	315.32
	Water Tank	7.7	10%	8.47
	Camera	1420.00	5%	1491.00
	Hoses, Outlets	43.26	20%	51.91
	Water-release Mechanism	196.95	20%	236.34
	Visual & Acoustic Signaling	36.35	5%	38.17
Propulsion (Table 6.5)	Motors	2400	10%	2640.00
	ESCs	3600	10%	3960.00
	Propeller Blades	3727.2	10%	4099.92
Power (Table 7.6)	Batteries	12620.16	10%	13882.18
	Chargers	4846.40	50%	7269.60
	PDBs	1410	15%	1621.50
Control (Table 8.2)	Autopilot	1050	5%	1102.50
	GPS	76.18	15%	87.61
	RADAR	4675.14	15%	5376.41
	Receiver	1098.99	20%	1318.79
	Resistors	11.38	30%	14.80
	Step Down Converters	390	20%	468.00
	Wires / Cables	143.70	15%	165.26
	Connectors	147.36	30%	191.57
Structures (Table 10.4)	Body	18.30	20%	840.00
	Arm Assembly	189.74	20%	227.69
	Legs	492	20%	590.4
Total		**38901.11**	**18.24%**	**45997.44**

18.2. Additional Costs

There are several ways in which the actual cost of producing the drone will increase. Manufacturing and assembling the drone itself will not be free, therefore the professionals doing so will have to be paid. Moreover, the creation of custom parts like the structure will not only be the raw material cost but also the production costs from using the special machines and professional workers.

Licenses cost

To create the design several student licenses are in place. If the project were to be pursued in a professional manner these licenses would stop being free. The 3DExperience Innovator license costs 3276€ per person but it will be assumed that three people will be allocated accounts. This means a total of 9828€[1]. On the other. there are also free licenses in place for Python or Github. Moreover, the PX4 Autopilot and the Herelink HD air unit have open-source code which can be easily adapted. Microsoft 365 standard business license for 10 people costs 1404€ [2], this will be necessary for presentations or tables. To perform Computation Fluid Dynamics an Ansys license is required, this will cost between 10,000 and 50,000€ [3]. Therefore, for licenses, it is estimated a total cost of about 60,000€ to be necessary per year.

[1] `https://my.3dexperience.3ds.com/welcome/compass-world/3dexperience-industries/transportation-and-mobility/bid-to-win/mechanical-engineering/3d-innovator/buy/offer`[Date Accessed:18/06/2025]

[2] `https://www.microsoft.com/es-es/microsoft-365/business/microsoft-365-plans-and-pricing`[Date Accessed:18/06/2025]

[3] `https://blog.ozeninc.com/industry-applications/ansys-pricing`[Date Accessed:18/06/2025]

Design Labor Cost

Current labor costs for designing the drone have been 0€ since the drone design was not performed as a money-making scheme. But, by taking the average annual wage in the Netherlands which is 25.32€/hour[4] and having 10 people work for 8 hours during 10 weeks this would be a total of €101,280. Assuming the full development takes a further two years which would be 102 weeks this would be 1,033,056. This is only for the research team excluding the manufacture labor. So, it is estimated that design labor will cost about 500,000€ yearly.

Manufacture

Performing test and applying for certifications will also create additional costs. Moreover, to create the first prototype a very large additional cost will be generated since it would be almost like generating the final drone. Faulty parts or parts that do not meet the data sheet shall also be replaced. To create the arms from CFRP they would be provided by Rocket West [5] since they allow for custom lengths. Therefore, for four tubes with a 50mm outer diameter and a 46mm inner diameter. Taking a price of 136.29€/m this would be €381.61 [17/06/2025] for the four pieces. For the custom made landing gear it is harder to find an estimate for its price. Gill et al. [36] analyzed the costs involved in manufacturing carbon fiber based elements. Although the conclusion that manufacturing costs can be reduced by about 50% was reached, it was estimated that the market cost is around 20 $/kg in the European sector. A preliminary value will be set by considering a tripling in manufacturing cost (i.e. 60 $/kg), but a large contingency percentage will be set. With a carbon fiber landing gear weight of 9kg this means 540€. Furthermore, for the Aluminium plates it can be estimated that the price is doubled for their manufacture. This would mean an additional 50€. Taking assembly workers to get paid 26.67€/hour [4] with four workers completing the assembly in two days that would mean 1706.88€. This means that the total additional manufacturing cost is about 3000€.

Delivery

Delivery of the completed drone shall also be taken into account which will be taken as 1.45€/kg [17/06/2025] for the European Union [37], since the drone will weigh about 150kg this would mean about 217.5€ in shipping. Due to the fragility of the drone it is more likely to be moved by truck or be delivered in a more expensive and safer package which would increase the price. A further 1000€ is estimated for the parts to arrive at the assembly point, totaling roughly 2000€ for deliveries.

Operation and End-of-life

During operation it is likely that the drone will have to undergo maintenance due to broken or damaged parts. The reparation or replacement of these parts will come at an additional cost, moreover, someone inspecting and repairing the drone will also incur some cost. There will also be some expenses when recycling the drone. Since these costs occur after the start of operation they will be omitted. Also, it has been assumed that the drone operators are trained professionals which have their own operating license, so, it does not need to be accounted for. The maximum yearly maintenance cost was estimated to be 2625€ as mentioned in Chapter 14.

Therefore, including all of the additional costs mentioned above, it can be estimated that the yearly cost for the project will be about 570,000€. A further margin of 10% can be applied to this so about 630,000€ would be the additional cost budget.

[4] https://www.statista.com/statistics/538707/average-hourly-wage-in-the-netherlands-by-sector/[Date Accessed:18/06/2025]

[5] https://www.rockwestcomposites.com/pbrt-4650.html[Date Accessed:17/06/2025]

19. Project Design And Development Logic

From Figure 19.2 the Project Design And Development Logic Diagram can be observed. The development is divided into stages which are colored green, these are made up of multiple main tasks, these are orange, which in turn are usually made of multiple smaller sub tasks which are blue.

Create Final Design

The created design has been under development for 10 weeks, but the design has not been fully developed. There are further steps such as designing and adapting the software or further structural optimization to be performed. Therefore, it is estimated that this process will take a further six months. Delays in main tasks would mean about one month.

Create prototype

A prototype will be built to validate the design. Each components must undergo a quality control test before being integrated into the prototype to confirm proper manufacturing. If a part does not pass the test this would be about a month of delay. It must also integrate the software created to be able to test the whole design later on, delays when integrating the software could take up to two months depending on the severity of the problem. All information and data gathered through the process shall also be logged to not repeat any mistakes. This is expected to take about six months.

Perform Verification and Validation

To confirm that the system performs as required multiple set of tests will occur. This means tests for individual subsystems first and then for the whole system. When testing the whole system it will then include tests when there are one or multiple engine failures occurring. This is necessary to confirm the drone is controllable at all times. In addition, certain requirements will need to verified through demonstration such as the turn around time. Also, other components that are not the drone shall be tested such as the ground controller. This is expected to take about six months.

Drone Certification

For the drone to be able to become commercially available and for it to be able to take flight it must be certified by its corresponding EASA category. If the design were to be rejected the drone would have to return to the designing phase which could mean a delay of up to six months. To minimize how long this process takes most of the already generated data shall be reused. This stage is quite vital for the development of the drone since once it gets certified it can be manufactured and sold. The certification will take about three months assuming no delays are in place.

Manufacturing

To construct the final system the necessary components shall be bought and tested individually. The drone shall be set-up the drone taking into account what was learned while building the prototype. The software must also be uploaded when the drone has been built to make it operational. For the itself drone to get individually certified it must undergo acceptance tests. This process should take about four months.

Maintenance

After every mission the drone shall undergo a checkup to make sure that the drone has not sustained any damages. If it has the maintenance procedures shall be followed. Moreover, if a part is damaged it shall be repaired if possible or replaced if necessary. The drone has been designed with modularity taken in mind to ease maintenance. This shall occur during all of the operational life of the drone,

estimated at 5 years in this present work.

End of Life

When the drone can no longer be repaired it shall be recycled. It is likely that a large amount of the components can be reused or repurposed. First, the drone shall be separated into components. Each component shall be inspected individually and an approximation of how much life time they have left could be performed. The batteries are likely to have few cycles left unless the have been replaced recently. The electronics which are still in a good state could be donated to a school or learning institution to experiment. The carbon fiber is harder to recycle and comes at a large cost but it can return 90% of its properties [38]. The aluminium as has been previously mentioned, can also be recycled. Therefore, the components that cannot be repurposed or reused shall be disposed of accordingly. Like for instance following the disposal of radioactive materials standard procedures.

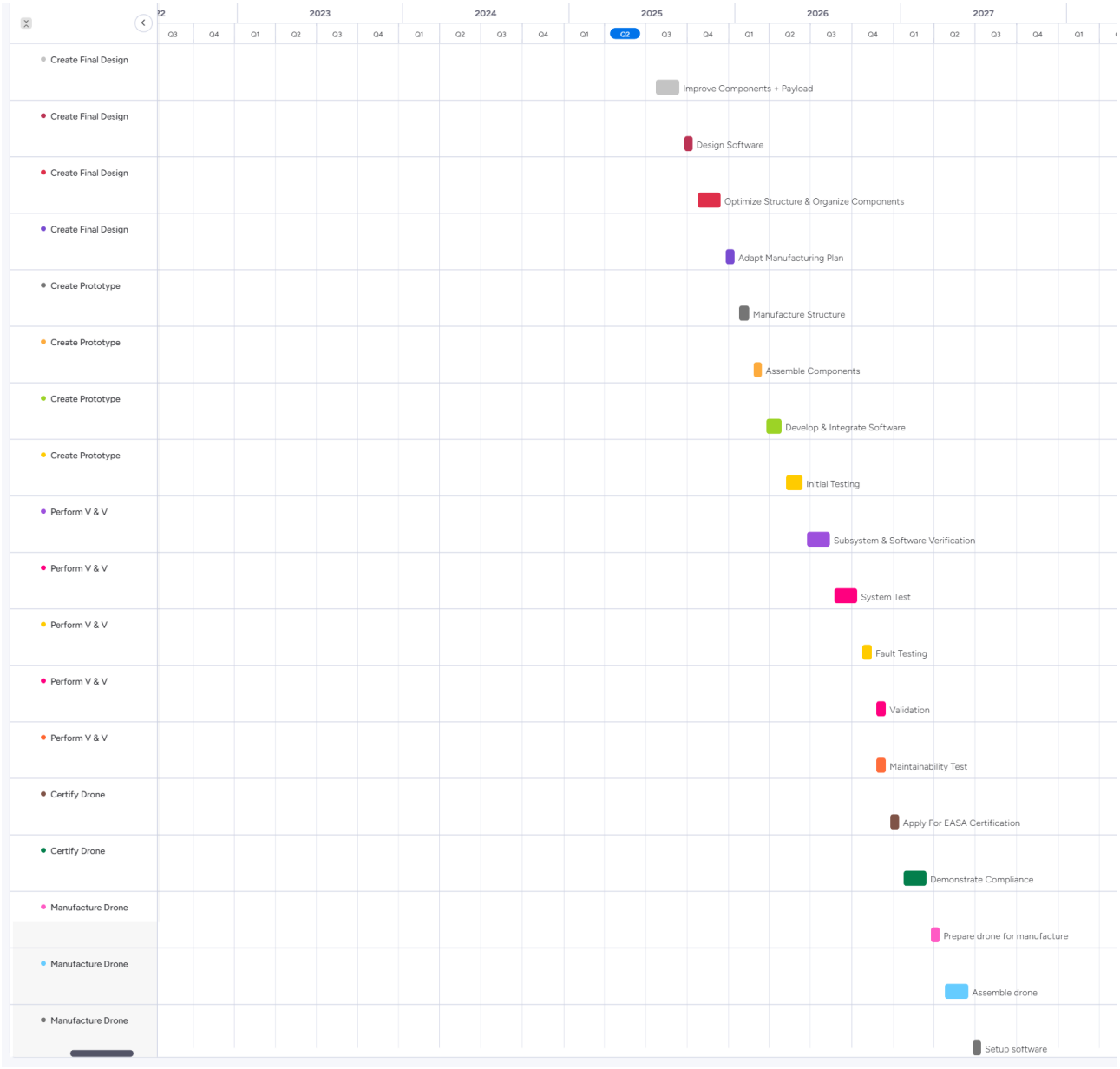

Figure 19.1: Project Gantt Chart (Post-DSE)

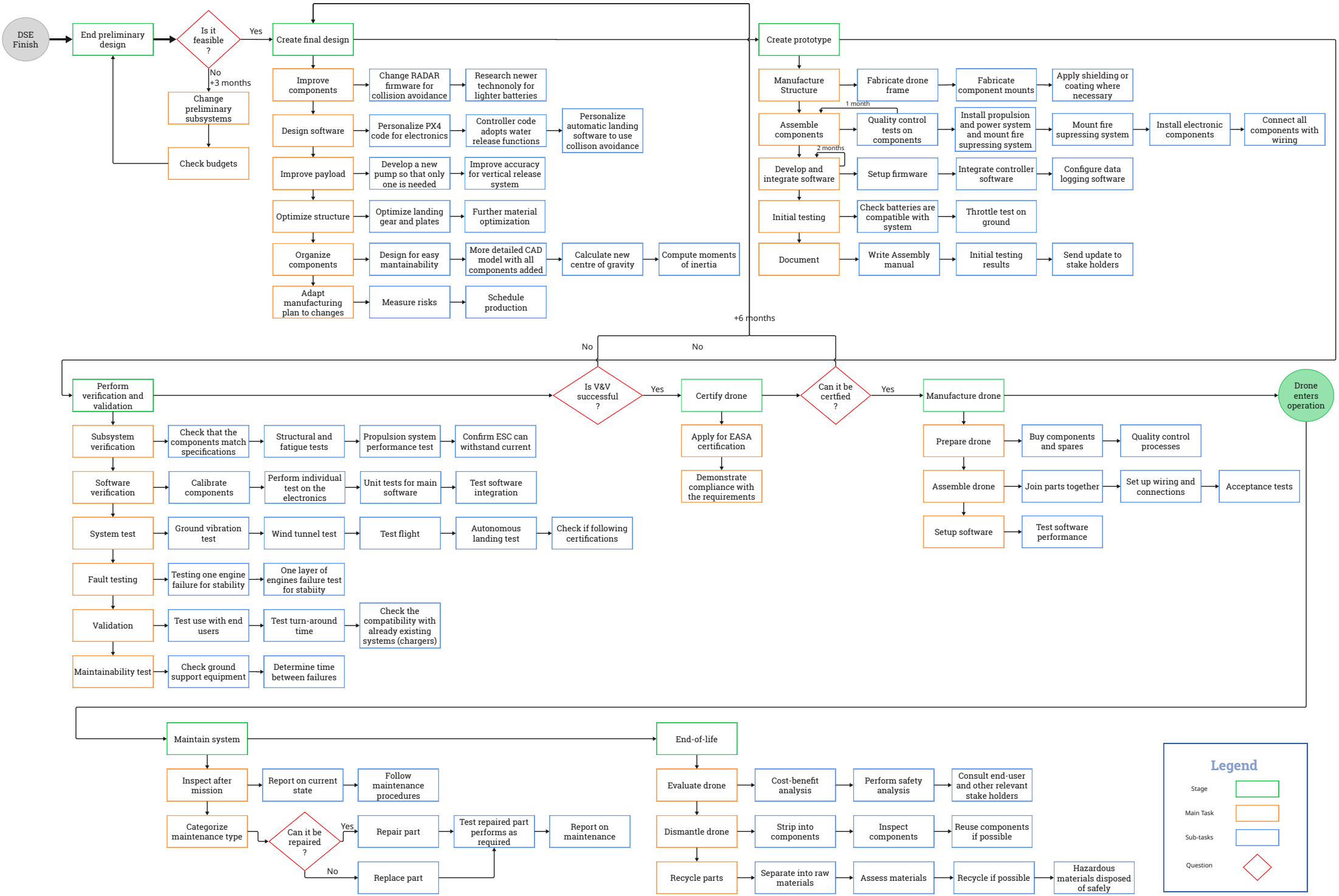
DSE Finish
End preliminary design
Is it feasible ?
Yes
No
+3 months
Change preliminary subsystems
Check budgets
Create final design
Improve components
Change RADAR firmware for collision avoidance
Research newer technonoly for lighter batteries
Design software
Personalize PX4 code for electronics
Controller code adopts water release functions
Personalize automatic landing software to use collison avoidance
Improve payload
Develop a new pump so that only one is needed
Improve accuracy for vertical release system
Optimize structure
Optimize landing gear and plates
Further material optimization
Organize components
Design for easy mantainability
More detailed CAD model with all components added
Calculate new centre of gravity
Compute moments of inertia
Adapt manufacturing plan to changes
Measure risks
Schedule production
Create prototype
Manufacture Structure
Fabricate drone frame
Fabricate component mounts
Apply shielding or coating where necessary
Assemble components
1 month
Quality control tests on components
Install propulsion and power system and mount fire supressing system
Mount fire supressing system
Install electronic components
Connect all components with wiring
Develop and integrate software
2 months
Setup firmware
Integrate controller software
Configure data logging software
Initial testing
Check batteries are compatible with system
Throttle test on ground
Document
Write Assembly manual
Initial testing results
Send update to stake holders
+6 months
No
No
Perform verification and validation
Is V&V successful ?
Yes
Certify drone
Apply for EASA certification
Demonstrate compliance with the requirements
Can it be certfied ?
Yes
Manufacture drone
Prepare drone
Buy components and spares
Quality control processes
Assemble drone
Join parts together
Set up wiring and connections
Acceptance tests
Setup software
Test software performance
Drone enters operation
Subsystem verification
Check that the components match specifications
Structural and fatigue tests
Propulsion system performance test
Confirm ESC can withstand current
Software verification
Calibrate components
Perform individual test on the electronics
Unit tests for main software
Test software integration
System test
Ground vibration test
Wind tunnel test
Test flight
Autonomous landing test
Check if following certifications
Fault testing
Testing one engine failure for stability
One layer of engines failure test for stabiity
Validation
Test use with end users
Test turn-around time
Check the compatibility with already existing systems (chargers)
Maintainability test
Check ground support equipment
Determine time between failures
Maintain system
Inspect after mission
Report on current state
Follow maintenance procedures
Categorize maintenance type
Can it be repaired ?
Yes
No
Repair part
Replace part
Test repaired part performs as required
Report on maintenance
End-of-life
Evaluate drone
Cost-benefit analysis
Perform safety analysis
Consult end-user and other relevant stake holders
Dismantle drone
Strip into components
Inspect components
Reuse components if possible
Recycle parts
Separate into raw materials
Assess materials
Recycle if possible
Hazardous materials disposed of safely
Legend
Stage
Main Task
Sub-tasks
Question

20. Conclusion & Recommendations

Flame Aegis is a fire-fighting drone designed to combat high-rise building fires in urban areas. This product has been requested by the Gezamenlijke Brandweer, and certain stakeholder requirements have been imposed. There are further regulatory constraints at both national and European levels. A 150 kg drone with a capacity of 40 L of water was designed in the end. The water can be delivered by spraying at a rate of 150 L/min through a nozzle or by dropping the contents of the tank within 2 seconds. The drone is able to perform a 15-minute mission with a 5-minute turnaround time. A visual representation of the drone can be seen in Figure 20.1.

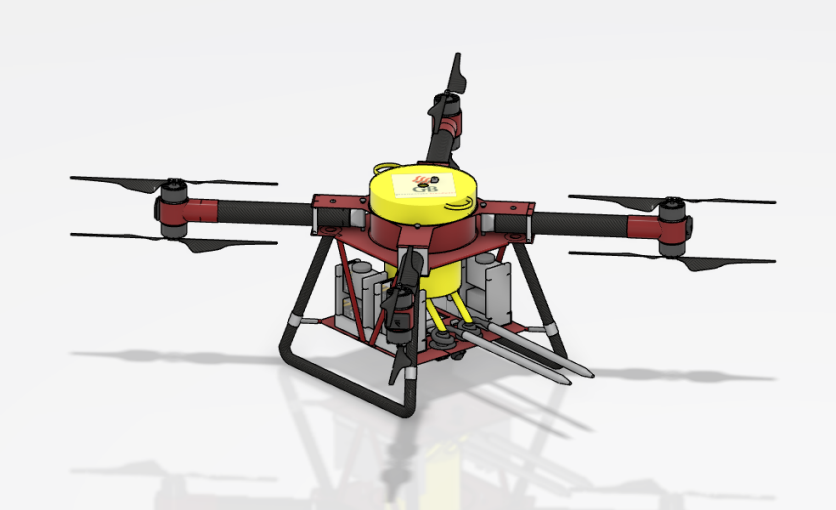

Figure 20.1: View of the Full Drone

The drone is a coaxial octocopter configuration, with four arms and two coaxial motors per arm. It is designed in a modular manner to allow for fast turnaround times and easy maintenance. Moreover, the design includes sustainable techniques such as easily recyclable materials. Further down the development process, software will also be implemented by adapting the firmware and software of the autopilot and controller, in spite of these components being open source and off-the-shelf.

The payload subsystem has a 54.6-liter HDPE water tank with a limitation of 40 L due to EU regulations, two centrifugal pumps, each capable of delivering 75 L/min, and a camera gimble containing a visual and a thermal camera.

The propulsion system has eight brushless motors, each paired with a two-bladed propeller. Together, the motors are able to provide a thrust-to-weight ratio of 2.1 for the drone. When paired with the control system, the drone is able to maintain stability when one motor becomes inoperable or, in some cases, even when two or more motors fail. The control subsystem is also responsible for applying the manual inputs from the operator as well as outputting the telemetry and video from the sensors and camera. It also provides visual and acoustic signaling to follow the drone regulations.

The drone is battery-powered, with state-of-the-art solid-state batteries made with a silicon anode and a nickel-manganese-cobalt cathode. They are able to meet the power and energy requirements provided by the other components with an added margin on top.

The structure needs to support all of the components and loads as well as allow easy maintenance, while minimizing weight. The drone is made of Carbon Fiber Reinforced Polymer (CFRP), Aluminium 7075-T6, Aluminium 6063-T6, and steel. The sustainability of the materials has been taken into account, as well as weight-specific performance.

Recommendations

After consulting the customer, several insights were obtained about possible project changes that could be made. Since the drone is able to take off around the full perimeter of the building, it should be able to take-off close the fire source. This means that the drone operator can observe and analyze the building to locate the most critical area. In the future the precise location and altitude of the attack position could be stored in order to autonomously operate the drone from take-off to landing.

The requirement on the Maximum Take-off Weight of 150 kg is not negotiable due to legislation in force. Therefore, the water tank shall not be filled with 50 L of water and instead, it should be filled up until the Maximum Take-off Weight is achieved. Since this is not optimal, ways of reducing the empty weight should be sought out. Further research could be performed on the batteries for instance in search of lighter ones. If the weight cannot be reduced, the tank shall be redesigned for the new volume of water. This in turn means resizing the structure, which would lower the weight. Several iterations can be performed around this.

There are further improvements that can be made to the design that are not focused solely on weight. The RADAR system could be implemented fully so that the system automatically intervenes in autonomous or manual operation. This would mean the implementation of the relevant software to coordinate multiple components including RADAR, the camera and other sensors. This would be the collision avoidance software, it would measure the location and speed of the drone if it is too close to an object it will automatically come to a stop. This is very useful for automatic landings. In addition, the drone currently has a static nozzle which makes it hard for aiming. The implementation of a movable nozzle could help fix this issue. Furthermore, in the current design there is no way to check the battery status like its temperature or how much energy is left so this is something that definitely should be implemented in the final design. Since batteries have no connection of this sort, a series of sensors should be implemented. In the current auto-pilot board there are not enough ports so a new one should be searched or another form of wireless communication should be implemented.

Even though the drone mission is currently limited by how much water it can carry and the battery life, the project would still be able to create a prototype which can be improved. Moreover, the drone mission could also be adjusted to coordinate multiple drones to ensure that the fire is constantly being suppressed by the water. In the future the use of drones for firefighting in cities could become a vital asset.

References

[1] Garaiman, A. R., Iacob, E. T., Ion, S., Madrid Gutierrez, H., Osman, A., Pereira Matias Teles Teixeira, A., Pop, R. I., Reurekas, G., Stoica, V. M., and Tanasiciuc, L. C., "Baseline Report: AE3200 Design Synthesis Exercise," May 2025. Faculty of Aerospace Engineering, Delft University of Technology.

[2] Wang, K., Yuan, Y., Chen, M., Lou, Z., Zhu, Z., and Li, R., "A Study of Fire Drone Extinguishing System in High-Rise Buildings," *Fire*, Vol. 5, 2022.
https://www.doi.org/10.3390/fire5030075

[3] Garaiman, A. R., Iacob, E. T., Ion, S., Madrid Gutierrez, H., Osman, A., Pereira Matias Teles Teixeira, A., Pop, R. I., Reurekas, G., Stoica, V. M., and Tanasiciuc, L. C., "Midterm Report: AE3200 Design Synthesis Exercise," May 2025. Faculty of Aerospace Engineering, Delft University of Technology.

[4] Hamann, R. and van Tooren, M., "Systems Engineering Technical Management Techniques Part II," Lecture Notes, Jan. 2006.

[5] Erdil, N. O. and Arani, O., "Quality function deployment: more than a design tool," *International Journal of Quality and Service Sciences*, Vol. 11, 2018.
https://www.doi.org/10.1108/IJQSS-02-2018-0008

[6] Kim, W., Choe, J., Jung, T., and Kim, D., "Design and control of a central-rotor type pentacopter design and implementation capable of contacting to and moving on wall surface," *International Journal of Advanced Robotic Systems*, Vol. 21, 2024.
https://www.doi.org/10.1177/17298806241278167

[7] Suprapto, B. Y., Heryanto, M. A., Suprijono, H., Muliadi, J., and Kusumoputro, B., "Design and development of heavy-lift hexacopter for heavy payload," 2017, pp. 242–247.
https://www.doi.org/10.1109/ISEMANTIC.2017.8251877

[8] Yoon, D., Na, K.-M., Lee, J. D., Lee, C.-H., and Bang, H., "Practical fault-tolerant control allocation based on attainable control set analysis for a coaxial dodecacopter," *Control Engineering Practice*, Vol. 156, 2025, pp. 106235.
https://doi.org/10.1016/j.conengprac.2024.106235

[9] Vedrtnam, A., Negi, H., and Kalauni, K., "Materials and Energy-Centric Life Cycle Assessment for Drones: A Review," *Journal of Composites Science*, Vol. 9, No. 4, 2025.
https://doi.org/10.3390/jcs9040169

[10] Fontes, T. F. V. P., *Conceptual Design and Performance Analysis Tool for Rotorcraft Systems*, Master's thesis, Instituto Superior Técnico, University of Lisbon, 2021, Supervisor: Prof. Filipe Szolnoky Ramos Pinto Cunha.

[11] Pollet, F., Delbecq, S., Budinger, M., and Moschetta, J.-M., "Design optimization of multirotor drones in forward flight," *32nd Congress of the International Council of the Aeronautical Sciences*, Shanghai, China, Sept. 2021.

[12] Fire Dynamics Simulator Team, "Approaches to Fire Modelling," 2023. Accessed: 2025-06-02.

[13] Baaij, S., de Witte, L., Hofman, R., Huizer, E., Molenaar, J., and Weewer, R., *Handboek Gebouwbrandbestrijding*, Nederlands Instituut Publieke Veiligheid (NIPV), Arnhem, Nederland, 2023.

[14] Biczyski, M., Sehab, R., Whidborne, J. F., Krebs, G., and Luk, P., "Multirotor Sizing Methodology with Flight Time Estimation," *Journal of Advanced Transportation*, Vol. 2020, 2020.
https://doi.org/10.1155/2020/9689604

[15] Wu, A., "Grepow battery inquiry reply," May 2025. Personal communication.

[16] Quan, Q., *Introduction to Multicopter Design and Control*, Springer Singapore, Singapore, Jan. 2017.
https://www.doi.org/10.1007/978-981-10-3382-7

[17] Du, G.-X., Quan, Q., Yang, B., and Cai, K.-Y., "Controllability Analysis for Multirotor Helicopter Rotor Degradation and Failure," *Journal of Guidance, Control, and Dynamics*, Vol. 38, 5 2015, pp. 978–985.
10.2514/1.G000731

[18] Du, G.-X., Quan, Q., and Cai, K.-Y., "Controllability Analysis and Degraded Control for a Class of Hexacopters Subject to Rotor Failures," *Journal of Intelligent & Robotic Systems*, Vol. 78, 4 2015, pp. 143–157.
10.1007/s10846-014-0103-0

[19] Mueller, M. W. and D'Andrea, R., "Relaxed hover solutions for multicopters: Application to algorithmic redundancy and novel vehicles," *The International Journal of Robotics Research*, Vol. 35, 7 2016, pp. 873–889.
10.1177/0278364915596233

[20] Yoo, C.-S. Y. C.-S. and Ahn, I.-K. A. I.-K., "Low cost GPS/INS sensor fusion system for UAV navigation," *Digital Avionics Systems Conference, 2003. DASC '03. The 22nd*, Indianapolis, IN, USA, 2003, pp. 8.A.1–8.1–9 vol.2.
10.1109/DASC.2003.1245891

[21] Çengel, Y. A. and Cimbala, J. M., *Fluid Mechanics: Fundamentals and Applications*, McGraw-Hill Series in Mechanical Engineering, McGraw-Hill, New York, 1st ed., 2006.

[22] Xian'an, C., Kai, W., Jiangfei, S., and Yu, S., "Numerical Analysis of Nozzles' Energy Loss Based on Fluent," *Proceedings of the 2nd International Workshop on Materials Engineering and Computer Sciences (IWMECS 2015)*, Atlantis Press, Nanjing, China, 2015, pp. 756–760.

[23] Megson, T., *Aircraft Structures for Engineering Students*, Butterworth-Heinemann Inc, Oxford, 7th ed., 2021.

[24] Hibbeler, R., *Mechanics of Materials*, Pearson, 2018.

[25] Reddy, J., "Theory and Analysis of Elastic Plates and Shells," *CRC Press*, 2006.
https://www.doi.org/10.1201/9780849384165

[26] Kelly, P., *Lecture Notes: An Introduction to Solid Mechanics*, 2025.
https://pkel015.connect.amazon.auckland.ac.nz/SolidMechanicsBooks/Part_II/index.html

[27] Hudramovich, V., Hart, E., and Terokhin, B., *Stress Concentration Around a Circular Hole in Thin Plates and Cylindrical Shells with a Radially Inhomogeneous Inclusion*, Springer Nature Switzerland, Cham, 2024, pp. 249–264.
https:/www.doi.org/10.1007/978-3-031-54063-9_18

[28] Jones, R., *Deformation Theory of Plasticity*, Bull Ridge Pub., 2009.
https://books.google.nl/books?id=kiCVc3AJhVwC

[29] Hamann, R. and van Tooren, M., "Systems Engineering Technical Management Techniques Part I," Lecture Notes, Sep. 2006.

[30] Muthu, S. S., *Life Cycle Sustainability Assessment (LCSA)*, Springer, Singapore, 2021. https://www.doi.org/10.1007/978-981-16-4562-4

[31] Wang, Y., He, S., Jia, Y., Chen, J., Zhang, S., Wang, L., and Han, J., "Efficient recovery of valuable components from lithium battery cathode and silicon carbide waste based on a synergistic roasting-magnetic separation process," *Journal of Environmental Chemical Engineering*, Vol. 13, No. 3, 2025. https://doi.org/10.1016/j.jece.2025.116991

[32] Clyde, D. A., Tan, K. Y., Yiang, W. J., Poh, W. S., Tiu, J., Wang, J., Li, J.-t., Huang, N. M., Chen, B., and Foo, C. Y., "Upscaled Recycling of Lithium Nickel Manganese Cobalt Oxide (NMC) Cathode Using an Automated Electrochemical System towards Low-Carbon Utilization of Waste Lithium-Ion Battery (LIB)," *ACS ES&T Engineering*, Vol. 5, No. 4, 2025, pp. 979–990. 10.1021/acsestengg.4c00744

[33] Li, X., Mahadas, N. A., Zhang, M., DePodesta, J., Stefik, M., and Tang, C., "Sustainable high-density polyethylene via chemical recycling: From modification to polymerization methods," *Polymer*, Vol. 295, 2024, pp. 126698. 10.1016/j.polymer.2024.126698

[34] D'Arpino, M., Rizzoni, G., Justin, C., Patel, S., Verberne, J., Gladin, J., and Ozcan, M., "NASA Reliability and Safety Assessment of Urban Air Mobility Concept Vehicles," March 2021. https://www.doi.org/10.13140/RG.2.2.33486.38722

[35] NASA, "NASA Systems Engineering Handbook," 2023. Date Accessed: 15/05/2025. https://www.nasa.gov/reference/5-3-product-verification

[36] Gill, A., Visotsky, D., Mears, L., and Summers, J., "Cost Estimation Model for PAN Based Carbon Fiber Manufacturing Process," *Journal of Manufacturing Science and Engineering*, Vol. 139, 09 2016. https://www.doi.org/10.1115/1.4034713

[37] Slattery, M. J., Dunn, J. B., and Kendall, A., "Transportation of electric vehicle lithium-ion batteries at end-of-life: A literature review," *Resources, Conservation and Recycling*, Vol. 169, 2021, pp. 105526. 10.1016/j.resconrec.2021.105526

[38] Isa, A., Omar, M. F., and et al., N. N., "A Review on Recycling of Carbon Fibres: Methods to Reinforce and Expected Fibre Composite Degradations," *Materials (Basel)*, 2022. 10.3390/ma15144991